



National Library
of Canada

Acquisitions and
Bibliographic Services Branch

395 Wellington Street
Ottawa, Ontario
K1A 0N4

Bibliothèque nationale
du Canada

Direction des acquisitions et
des services bibliographiques

395, rue Wellington
Ottawa (Ontario)
K1A 0N4

Vous le reconnaîtrez

Vous le reconnaîtrez

NOTICE

The quality of this microform is heavily dependent upon the quality of the original thesis submitted for microfilming. Every effort has been made to ensure the highest quality of reproduction possible.

If pages are missing, contact the university which granted the degree.

Some pages may have indistinct print especially if the original pages were typed with a poor typewriter ribbon or if the university sent us an inferior photocopy.

Reproduction in full or in part of this microform is governed by the Canadian Copyright Act, R.S.C. 1970, c. C-30, and subsequent amendments.

AVIS

La qualité de cette microforme dépend grandement de la qualité de la thèse soumise au microfilmage. Nous avons tout fait pour assurer une qualité supérieure de reproduction.

S'il manque des pages, veuillez communiquer avec l'université qui a conféré le grade.

La qualité d'impression de certaines pages peut laisser à désirer, surtout si les pages originales ont été dactylographiées à l'aide d'un ruban usé ou si l'université nous a fait parvenir une photocopie de qualité inférieure.

La reproduction, même partielle, de cette microforme est soumise à la Loi canadienne sur le droit d'auteur, SRC 1970, c. C-30, et ses amendements subséquents.

UNIVERSITY OF ALBERTA

Analysis and Failure of Laminated Fiber Reinforced Composites

by

Hany A. El Kadi



A thesis
submitted to the Faculty of Graduate Studies and Research in partial fulfillment
of the requirements for the degree of

Doctor of Philosophy

Department of Mechanical Engineering

Edmonton, Alberta

Fall, 1993



National Library
of Canada

Acquisitions and
Bibliographic Services Branch

395 Wellington Street
Ottawa, Ontario
K1A 0N4

Bibliothèque nationale
du Canada

Direction des acquisitions et
des services bibliographiques

395, rue Wellington
Ottawa (Ontario)
K1A 0N4

Yours truly / Votre dévoué(e)

Cheerfully / Avec reconnaissance

The author has granted an irrevocable non-exclusive licence allowing the National Library of Canada to reproduce, loan, distribute or sell copies of his/her thesis by any means and in any form or format, making this thesis available to interested persons.

The author retains ownership of the copyright in his/her thesis. Neither the thesis nor substantial extracts from it may be printed or otherwise reproduced without his/her permission.

L'auteur a accordé une licence irrevocable et non exclusive permettant à la Bibliothèque nationale du Canada de reproduire, prêter, distribuer ou vendre des copies de sa thèse de quelque manière et sous quelque forme que ce soit pour mettre des exemplaires de cette thèse à la disposition des personnes intéressées.

L'auteur conserve la propriété du droit d'auteur qui protège sa thèse. Ni la thèse ni des extraits substantiels de celle-ci ne doivent être imprimés ou autrement reproduits sans son autorisation.

ISBN 0-315-88235-2

Canada

UNIVERSITY OF ALBERTA
RELEASE FORM

Name of Author: **Hany A. El Kadi**

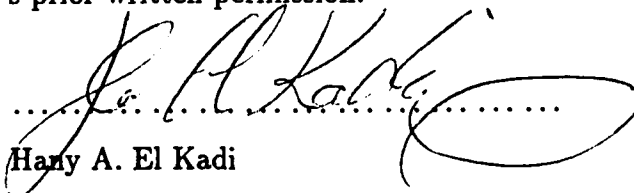
Title of Thesis: **Analysis and Failure of Laminated Fiber
Reinforced Composites**

Degree: **Doctor of Philosophy**

Year this degree granted: **Fall 1993**

Permission is hereby granted to The University of Alberta Library to reproduce single copies of this thesis and to lend or sell such copies for private, scholarly or scientific research purposes only.

The author reserves all other publication and other rights in association with the copyright in the thesis, and except as hereinbefore provided neither the thesis nor any substantial portion thereof may be printed or otherwise reproduced in any material form whatever without the author's prior written permission.

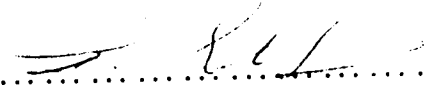


Hany A. El Kadi
604 D Michener Park
Edmonton, Alberta
Canada
T6H 5A1

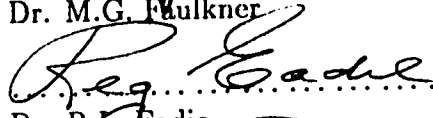
Date : *September 3rd 1993*

UNIVERSITY OF ALBERTA
FACULTY OF GRADUATE STUDIES AND RESEARCH

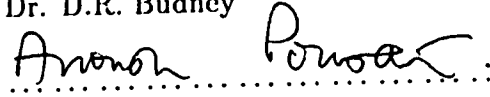
The undersigned certify that they have read, and recommend to the Faculty of Graduate Studies and Research for acceptance, a thesis entitled **Analysis and Failure of Laminated Fiber Reinforced Composites** submitted by **Hany A. El Kadi** in partial fulfillment of the requirements for the degree of **Doctor of Philosophy**.


.....
Dr. F. Ellyin (Supervisor)


.....
Dr. M.G. Faulkner


.....
Dr. R.L. Eadie


.....
Dr. D.R. Budney


.....
Dr. A. Poursartip

Date : *Sept. 2, 1993.*

TO MY WIFE MANAL

Acknowledgements

The author wishes to express his deep gratitude and appreciation to Dr. F. Ellyin for his supervision, guidance, suggestions and financial support during the course of this research.

I would also like to thank Dr. M.G. Faulkner, past Chairman of the Mechanical Engineering Department at the University of Alberta, for his continuous advice as well as Dr. R.L. Eadie for his comments on this work.

Acknowledgements are also due to Dr. D. Kujawski and Dr. Z. Xia for many fruitful discussions during the course of this study.

Many thanks are also due to Mr. Allan Muir, Machine Shop Supervisor at the Mechanical Engineering Department, and his very capable crew: Mr. Max Schubert; Mr. Don Fuhr; Mr. Tony VanStraten and Mr. Albert Yuen, for their help in the preparation of the specimens and the modifications of the testing apparatus.

Thanks are also due to Mr. Tom Villett, past Technicians Supervisor; Mr. Brian Cielin, Technicians Supervisor at the Mechanical Engineering Department, and his creative crew: Mr. Bernie Faulkner for his continuous help throughout the experimental investigation; Mr. Ian Burtar for writing the computer code controlling the testing machine; Mr. John Foy and Mrs. Tuula Hilvo for their preparation of the photographic material included in this work.

Last but not least, I would like to thank the Mechanical Engineering Department at the University of Alberta, Canada for providing me with financial support for the duration of my studies; the Natural Sciences and Engineering Research Council of Canada and The Defence Research Establishment at Valcartier Québec, for funding several parts of this work.

Abstract

Composite materials are replacing conventional materials in various engineering applications. The damage of these materials is considered in this work.

The strain energy can be used as a fatigue failure criterion for unidirectional fiber reinforced composite materials. The relation between the strain energy and the number of reversals to failure was found to be of a power law type which applies to different material types. To include the effect of the stress ratio in the formulation, a non-dimensional form of the strain energy is used. This parameter correlates fairly well with the experimental data obtained for five different fibers orientation angles under three different values of the stress ratio.

The strain energy may also be used as a criterion to predict crack growth direction in a lamina under static off-axis and in-plane mixed-mode loading. Comparison of experimental results with different established criteria from the literature indicates that the present criteria lead to more consistent results.

To extend the use of the strain energy criterion to laminates, an existing theory of isotropic laminated elastic plates is extended to include the effect of anisotropy. This theory satisfies all the interlaminar interface tractions and displacements continuity conditions as well as the zero traction condition on the lateral surfaces. The only restriction would be that the boundary conditions are satisfied in an average manner. The results obtained using this method are presented and the problems arising from the use of thick laminates with high anisotropy are discussed. These results are also compared to those obtained using the three dimensional finite element analysis.

Contents

Chapter 1

Introduction	1
1.1 Introduction	1
1.2 Definition and Classification of Composites	2
1.2.1 Particle-Reinforced Composites	3
1.2.2 Fiber-Reinforced Composites	5
1.3 Scope of the Thesis	7

Chapter 2

Damage in Composite Materials	10
2.1 Introduction	10
2.2 Tensile Failure Modes in Unidirectional Fiber Reinforced Composites	10
2.3 Compressive Failure Modes in Unidirectional Fiber Reinforced Composites	13
2.4 Fatigue Damage Mechanisms in Composite Materials	17
2.4.1 Debonding	18
2.4.2 Matrix Cracking and Local Fiber Breakage	18
2.4.3 Delamination	20
2.4.4 Effect of the Frequency of Cyclic Loading	21

2.4.5	Stiffness Analysis	22
2.4.6	Compression Fatigue	22
2.4.7	Effect of Biaxial Loading	24
2.4.8	Effects of Environmental Conditions	25
2.5	Phenomenological Approach	26

Chapter 3

A Fatigue Failure Criterion for Unidirectional Fiber Reinforced Composite Laminae		29
3.1	Introduction	29
3.2	Stress-Strain Relation for Composite Laminae	31
3.3	Critical Strain Energy Criterion	34
3.4	Comparison with Experimental Data ($R \approx 0$)	36
3.5	Normalization of the Results	54
3.6	Effect of the Stress Ratio, R	54
3.6.1	Experimental Results	58
3.6.2	Negative Stress Ratios	59
3.7	Concluding Remarks	67

Chapter 4

Predicting Crack Growth Direction in Unidirectional Fiber Reinforced Composite Laminae		68
4.1	Introduction	68
4.2	Anisotropic Elasticity Analysis of Crack Tip Stress Fields	69
4.3	Criteria for Predicting Direction of Crack Growth	77
4.3.1	Tensor Polynomial Criterion	77

4.3.2	Minimum Strain Energy Criterion (MSE)	77
4.3.3	Normal Stress Ratio Criterion (NSR)	79
4.3.4	Critical Strain Energy Method - Present Criterion (CSE) . .	81
4.4	Analysis of Off-Axis Unidirectional Tensile Coupons	82
4.5	Unidirectional Laminae Subjected to Mixed-Mode Loading	90
4.6	Limitations of the Normal Stress Ratio Criterion	96
4.7	Concluding Remarks	98

Chapter 5

	Theory of Symmetric Anisotropic Laminated Elastic Plates	99
5.1	Introduction	99
5.2	Stress-Strain Relation for an Orthotropic Lamina in the Principal Directions of a Laminate	101
5.3	Analysis of Stress and Deformation in a Homogeneous Layer	103
5.4	Stretching Solution for a Lamina	116
5.5	Bending Solution for a Lamina	116
5.6	Laminate Geometry	116
5.7	Solution of the Two-Dimensional Classical Thin Plate Theory - The Equivalent Plate	119
5.7.1	The Equivalent Plate	119
5.7.2	The Stretching Case	119
5.7.3	The Bending Case	120
5.8	Three Dimensional Theory for Laminates - Stretching Deformations	120
5.8.1	Two-Dimensional Solution	122
5.8.2	First Approximation	123
5.8.3	Second Approximation	124

5.8.4	Third Approximation	127
5.8.5	Fourth Approximation	128
5.8.6	Determination of σ_{zz}	132
5.9	Three Dimensional Theory for Laminates - Bending Deformations .	134
5.9.1	First Approximation	135
5.9.2	Second Approximation	137
5.9.3	Third Approximation	138
5.9.4	Determination of σ_{zz}	142
5.10	Limitation of the Present Method	143
5.11	Concluding Remarks	145

Chapter 6

Applications		146
6.1	Introduction	146
6.2	Reduction to the Isotropic Case	146
6.2.1	First Order Solution ($n = 1$)	148
6.2.2	Second Order Solution ($n = 2$)	149
6.2.3	Third Order Solution ($n = 3$)	151
6.2.4	Fourth Order Solution ($n = 4$)	153
6.3	Stretching of an Anisotropic Plate Containing a Traction-Free Circular Hole	154
6.3.1	The Equivalent Plate Solution	154
6.3.2	Reduction to the Isotropic Case	157
6.3.3	Solution of the Isotropic Laminated Plate Problem	158
6.3.4	Solution of the Anisotropic Laminated Plate Problem	160

6.3.5	Comparison of the Present Solution and the Three-Dimensional Finite Elements Method Solution	193
6.4	Concluding Remarks	199
 Chapter 7		
	Conclusion	200
 References		
		203
 Appendix A		
	Experimental Investigation	216
A.1	Introduction	216
A.2	Material	216
A.3	Specimen	217
A.3.1	ASTM Standards	217
A.3.2	Specimen Design	218
A.4	Grips	222
A.4.1	Two-part Grips	223
A.4.2	Modified Tension Grips	223
A.5	Specimen Manufacturing	227
A.6	Experimental Apparatus and Results	229
 Appendix B		
	Experimental Data	242

List of Tables

4.1	Comparison Between Different Criteria and Experimental Results for Off-Axis Unidirectional Coupons	83
4.2	Comparison Between Different Criteria for Off-Axis AS4/3501-6 Unidirectional Coupons	89
4.3	Comparison Between Different Criteria for Off-Axis GRP Unidirectional Coupons	89
4.4	Comparison Between Different Criteria and Experimental Results for Unidirectional Laminae Subjected to Mixed-Mode Loading	91
6.1	Mechanical Properties of Different Materials Under Consideration .	162
6.2	Material properties of the Graphite/Epoxy Composite Used by Lucking et al.	193
A.1	Mechanical Properties at Various Stress Angles	217
B.1	Uniaxial Fatigue Results for 0° Specimens at $R = 0.5$	243
B.2	Uniaxial Fatigue Results for 0° Specimens at $R = 0$	244
B.3	Uniaxial Fatigue Results for 0° Specimens at $R = -1$	245
B.4	Uniaxial Fatigue Results for 19° Specimens at $R = 0.5$	246
B.5	Uniaxial Fatigue Results for 19° Specimens at $R = 0$	247
B.6	Uniaxial Fatigue Results for 19° Specimens at $R = -1$	248
B.7	Uniaxial Fatigue Results for 45° Specimens at $R = 0.5$	249
B.8	Uniaxial Fatigue Results for 45° Specimens at $R = 0$	250
B.9	Uniaxial Fatigue Results for 45° Specimens at $R = -1$	251
B.10	Uniaxial Fatigue Results for 71° Specimens at $R = 0.5$	252
B.11	Uniaxial Fatigue Results for 71° Specimens at $R = 0$	253
B.12	Uniaxial Fatigue Results for 71° Specimens at $R = -1$	254

B.13 Uniaxial Fatigue Results for 90° Specimens at $R = 0.5$	255
B.14 Uniaxial Fatigue Results for 90° Specimens at $R = 0$	256
B.15 Uniaxial Fatigue Results for 90° Specimens at $R = -1$	257

List of Figures

1.1	Classification of Composite Materials	4
1.2	Thesis Outline	8
2.1	Possible Tensile Failure Modes in a Unidirectional Fiber Reinforced Composite	12
2.2	Compression Failure Modes in a Unidirectional Fiber Reinforced Composite	14
2.3	Kink Band	16
3.1	Positive Rotation of Principal Material Axes from Arbitrary xy Axes	33
3.2	Definition of Cyclic Strain Energy for Positive Stress Ratios (a) $R = 0$ (b) $R = 0.5$	37
3.3	Correlation of the Strain Energy ΔW with the Experimental Data for Glass/Epoxy, Experimental Data from [48]	40
3.4	Variation of α with the Fibers Orientation Angle θ for the Glass/Epoxy Composite	41
3.5	Variation of κ with the Fibers Orientation Angle θ for the Glass/Epoxy Composite	42
3.6	Comparison of Predicted Values with Experimental Results for Glass/Epoxy, Experimental Data from [48]	44
3.7	Correlation of the Strain Energy ΔW with the Experimental Data for Boron/Aluminum, Experimental Data from [51]	45
3.8	Variation of α with the Fibers Orientation Angle θ for the Boron/Aluminum Composite	46
3.9	Variation of κ with the Fibers Orientation Angle θ for the Boron/Aluminum Composite	47

3.10	Comparison of Predicted Values with Experimental Results for Boron/Aluminum, Experimental Data from [51]	48
3.11	Correlation of the Strain Energy ΔW with the Experimental Data for Graphite/Epoxy, Experimental Data from [53]	50
3.12	Variation of α with the Fibers Orientation Angle θ for the Graphite/Epoxy Composite	51
3.13	Variation of κ with the Fibers Orientation Angle θ for the Graphite/Epoxy Composite	52
3.14	Comparison of Predicted Values with Experimental Results for Graphite/Epoxy, Experimental Data from [53]	53
3.15	Normalized Strain Energy Curve for the Glass/Epoxy Composite, Experimental Data from [48]	55
3.16	Normalized Strain Energy Curve for the Boron/Aluminum Composite, Experimental Data from [51]	56
3.17	Normalized Strain Energy Curve for the Graphite/Epoxy Composite, Experimental Data from [53]	57
3.18	Variation of κ with the Fiber Orientation Angle, θ , for Positive Stress Ratios	61
3.19	Normalized Cyclic Strain Energy vs. Number of Reversals to Failure for Various Fiber Orientation Angles and Positive Values of Stress Ratio	62
3.20	Definition of Cyclic Strain Energy for Negative Stress Ratios with Damage Associated with Tensile Stress Only	63
3.21	Normalized Cyclic Strain Energy vs. Number of Reversals to Failure for Various Fiber Orientation Angles and Stress Ratio of -1 (Only Tensile Loading Causes Damage)	64
3.22	Definition of Cyclic Strain Energy for Negative Stress Ratios with Damage Associated with Compressive Stress Only	65
3.23	Normalized Cyclic Strain Energy vs. Number of Reversals to Failure for Various Fiber Orientation Angles and Different Stress Ratio (Positive and Negative)	66
4.1	Infinite Center Cracked Plate with Far Field Stresses	70
4.2	Infinite Center Cracked Plate Under Biaxial Loading	75

4.3	Transformation and Superposition of Far Field Stresses	
	(a) Total Stresses	
	(b) Singular Stresses	
	(c) Non-Singular Stresses	76
4.4	Normal Stress Ratio Parameters	80
4.5	Variation of Crack Growth Criteria as a Function of ϕ for 30° Off-Axis Graphite/Epoxy Coupons.(case 1)	
	(a) Normal Stress Ratio	
	(b) Minimum Strain Energy	
	(c) Critical Strain Energy (present model)	85
4.6	Variation of Crack Growth Criteria as a Function of ϕ for 15° Off-Axis Graphite/Epoxy Coupons.(case 2)	
	(a) Normal Stress Ratio	
	(b) Minimum Strain Energy	
	(c) Critical Strain Energy (present model)	86
4.7	Variation of Crack Growth Criteria as a Function of ϕ for 15° Off-Axis Graphite/Epoxy Coupons.(case 3)	
	(a) Normal Stress Ratio	
	(b) Minimum Strain Energy	
	(c) Critical Strain Energy (present model)	87
4.8	Variation of Crack Growth Criteria as a Function of ϕ for 15° Off-Axis Graphite/Epoxy Coupons.(case 5)	
	(a) Normal Stress Ratio	
	(b) Minimum Strain Energy	
	(c) Critical Strain Energy (present model)	92
4.9	Variation of Crack Growth Criteria as a Function of ϕ for 15° Off-Axis Graphite/Epoxy Coupons.(case 7)	
	(a) Normal Stress Ratio	
	(b) Minimum Strain Energy	
	(c) Critical Strain Energy (present model)	93
4.10	Variation of Crack Growth Criteria as a Function of ϕ for 15° Off-Axis Graphite/Epoxy Coupons.(case 8)	
	(a) Normal Stress Ratio	
	(b) Minimum Strain Energy	
	(c) Critical Strain Energy (present model)	94

4.11	Variation of Crack Growth Criteria as a Function of ϕ for 15° Off-Axis Graphite/Epoxy Coupons.(case 9)	
	(a) Normal Stress Ratio	
	(b) Minimum Strain Energy	
	(c) Critical Strain Energy (present model)	95
4.12	Infinite Center Plate Under Pure Shear Far-Field Stress	97
5.1	Laminate Geometry and Notation	117
6.1	Plate with an Elliptical Hole Subjected to a Stress P at Infinity . .	155
6.2	Anisotropic Elastic Symmetric Laminated Plate with a Circular Hole Subjected to a Stress P at Infinity	161
6.3	Radial Distribution of σ_{rr} at the Mid-Plane of the $[0/90]_s$ Laminate Around the Hole (Material A)	164
6.4	Radial Distribution of $\sigma_{\theta\theta}$ at the Mid-Plane of the $[0/90]_s$ Laminate Around the Hole (Material A)	165
6.5	Radial Distribution of $\sigma_{r\theta}$ at the Mid-Plane of the $[0/90]_s$ Laminate Around the Hole (Material A)	166
6.6	Radial Distribution of σ_{rr} at the Mid-Plane of the $[0/90]_s$ Laminate Around the Hole (Material B)	167
6.7	Radial Distribution of $\sigma_{\theta\theta}$ at the Mid-Plane of the $[0/90]_s$ Laminate Around the Hole (Material B)	168
6.8	Radial Distribution of $\sigma_{r\theta}$ at the Mid-Plane of the $[0/90]_s$ Laminate Around the Hole (Material B)	169
6.9	Radial Distribution of σ_{rr} at the Mid-Plane of the $[\pm 45]_s$ Laminate Around the Hole (Material A)	171
6.10	Radial Distribution of $\sigma_{\theta\theta}$ at the Mid-Plane of the $[\pm 45]_s$ Laminate Around the Hole (Material A)	172
6.11	Radial Distribution of $\sigma_{r\theta}$ at the Mid-Plane of the $[\pm 45]_s$ Laminate Around the Hole (Material A)	173
6.12	Radial Distribution of σ_{rr} at the Mid-Plane of the $[\pm 45]_s$ Laminate Around the Hole (Material B)	174
6.13	Radial Distribution of $\sigma_{\theta\theta}$ at the Mid-Plane of the $[\pm 45]_s$ Laminate Around the Hole (Material B)	175
6.14	Radial Distribution of $\sigma_{r\theta}$ at the Mid-Plane of the $[\pm 45]_s$ Laminate Around the Hole (Material B)	176

6.15	Radial Distribution of σ_{rz} at the Interlaminar Interface of the $[0/90]_s$ Laminate Around the Hole (Material A)	178
6.16	Radial Distribution of $\sigma_{\theta z}$ at the Interlaminar Interface of the $[0/90]_s$ Laminate Around the Hole (Material A)	179
6.17	Radial Distribution of σ_{zz} at the Mid-Plane of the $[0/90]_s$ Laminate Around the Hole (Material A)	180
6.18	Radial Distribution of σ_{rz} at the Interlaminar Interface of the $[0/90]_s$ Laminate Around the Hole (Material B)	181
6.19	Radial Distribution of $\sigma_{\theta z}$ at the Interlaminar Interface of the $[0/90]_s$ Laminate Around the Hole (Material B)	182
6.20	Radial Distribution of σ_{zz} at the Mid-Plane of the $[0/90]_s$ Laminate Around the Hole (Material B)	183
6.21	Radial Distribution of σ_{rz} at the Interlaminar Interface of the $[\pm 45]_s$ Laminate Around the Hole (Material A)	185
6.22	Radial Distribution of $\sigma_{\theta z}$ at the Interlaminar Interface of the $[\pm 45]_s$ Laminate Around the Hole (Material A)	186
6.23	Radial Distribution of σ_{zz} at the Mid-Plane of the $[\pm 45]_s$ Laminate Around the Hole (Material A)	187
6.24	Radial Distribution of σ_{rz} at the Interlaminar Interface of the $[\pm 45]_s$ Laminate Around the Hole (Material B)	188
6.25	Radial Distribution of $\sigma_{\theta z}$ at the Interlaminar Interface of the $[\pm 45]_s$ Laminate Around the Hole (Material B)	189
6.26	Radial Distribution of σ_{zz} at the Mid-Plane of the $[\pm 45]_s$ Laminate Around the Hole (Material B)	190
6.27	Normalized Stress Components for the $[0/90]_s$ Laminate ($R/t = 10$, $\delta = 90^\circ$, Material A)	192
6.28	Angular Distribution of $\sigma_{\theta\theta}$ Around the Hole for Graphite/Epoxy (a) Finite Element Analysis (b) Present Method	195
6.29	Radial Distribution of σ_{rz} on the Interface Plane Around the Hole for Graphite/Epoxy (a) Finite Element Analysis (b) Present Method	196
6.30	Radial Distribution of $\sigma_{z\theta}$ on the Interface Plane Around the Hole for Graphite/Epoxy (a) Finite Element Analysis (b) Present Method	197

6.31 Radial Distribution of σ_{zz} Near the Midplane Around the Hole for Graphite/Epoxy	
(a) Finite Element Analysis	
(b) Present Method	198
A.1 Variation of Monotonic Strength with Fibers Orientation Angle . .	218
A.2 Initial Specimen Design	219
A.3 Two-Part Grips	220
A.4 Width Waisted Specimen	221
A.5 Final specimen design	222
A.6 Modified Tension Grips	224
A.7 Different Configurations for the Antibuckling Device	225
A.8 Final Configuration for the Antibuckling Device	226
A.9 Mould	228
A.10 Experimental Apparatus	230
A.11 Effect of Loading Frequency on the Fatigue Life of 45° Specimen . .	231
A.12 Failure of a 19° Specimen under Cyclic Loading	232
A.13 Failure of a 45° Specimen under Cyclic Loading	233
A.14 Failure of a 71° Specimen under Cyclic Loading	234
A.15 Failure of a 90° Specimen under Cyclic Loading	235
A.16 Different Failure Modes of a 0° Specimen under Cyclic Loading . .	236
A.17 Variation of Stiffness with Life for a 71° Specimen	237
A.18 Maximum Cyclic Stress vs. Number of Reversals to failure for Specimens with Different Fiber Orientation Angles at $R = 0.5$. . .	239
A.19 Maximum Cyclic Stress vs. Number of Reversals to failure for Specimens with Different Fiber Orientation Angles at $R = 0$	240
A.20 Maximum Cyclic Stress vs. Number of Reversals to failure for Specimens with Different Fiber Orientation Angles at $R = -1$. . .	241
B.1 Maximum Applied Stress vs. Number of Reversals to Failure for 0° Specimens at $R = 0.5$	243
B.2 Maximum Applied Stress vs. Number of Reversals to Failure for 0° Specimens at $R = 0$	244
B.3 Maximum Applied Stress vs. Number of Reversals to Failure for 0° Specimens at $R = -1$	245

B.4	Maximum Applied Stress vs. Number of Reversals to Failure for 19° Specimens at $R = 0.5$	246
B.5	Maximum Applied Stress vs. Number of Reversals to Failure for 19° Specimens at $R = 0$	247
B.6	Maximum Applied Stress vs. Number of Reversals to Failure for 19° Specimens at $R = -1$	248
B.7	Maximum Applied Stress vs. Number of Reversals to Failure for 45° Specimens at $R = 0.5$	249
B.8	Maximum Applied Stress vs. Number of Reversals to Failure for 45° Specimens at $R = 0$	250
B.9	Maximum Applied Stress vs. Number of Reversals to Failure for 45° Specimens at $R = -1$	251
B.10	Maximum Applied Stress vs. Number of Reversals to Failure for 71° Specimens at $R = 0.5$	252
B.11	Maximum Applied Stress vs. Number of Reversals to Failure for 71° Specimens at $R = 0$	253
B.12	Maximum Applied Stress vs. Number of Reversals to Failure for 71° Specimens at $R = -1$	254
B.13	Maximum Applied Stress vs. Number of Reversals to Failure for 90° Specimens at $R = 0.5$	255
B.14	Maximum Applied Stress vs. Number of Reversals to Failure for 90° Specimens at $R = 0$	256
B.15	Maximum Applied Stress vs. Number of Reversals to Failure for 90° Specimens at $R = -1$	257

Chapter 1

Introduction

1.1 Introduction

Composite materials have a long history of usage. Their beginnings are unknown, but all recorded history contains some references to some form of composite materials. For example, plywood was used by the ancient Egyptians when they realized that wood could be rearranged to achieve superior strength and resistance to thermal expansion as well as to swelling owing to the presence of moisture. Medieval swords and armour were constructed with layers of different materials [1].

More recently, early military applications during World War II led to large scale commercial applications, particularly in the marine industry during the late 1940's and early 1950's.

The first widespread use of fiber-and-resin technology took place in the early 1950's, when glass fiber and polyester resins became available. The versatility, and comparatively simple methods of use, of this combination soon led to its appearance in boats, car bodywork, and many other industrial applications.

Recent advances in composite materials technology are largely due to the aerospace industry which found the properties of these materials (for example, high

strength-to-weight and stiffness-to-weight ratios) attractive for their applications.

On the other hand, race-car manufacturers require low weight, high-mechanical-performance components, but do not have to follow specifications as strict as is the case in the aerospace industry. Therefore, they were able to develop techniques at a faster pace.

The versatility of composite technology can be observed in its many applications, ranging from the experimental Spitfire fuselage built in World War II through the much later applications, such as advanced sports equipment, tennis rackets, golf clubs, etc, to advanced aerospace structures and race-car chassis, show the great advances that have been made during the first 35 years of modern composite development.

1.2 Definition and Classification of Composites

Composite materials can be defined as follows [2]:

A Composite Material is a material system composed of a mixture or combination of two or more macroconstituents differing in form and/or material composition and that are essentially insoluble in each other.

Several classification systems have been used to differentiate between different types of composites, including:

- By basic material combinations (metal-organic or metal-inorganic)
- By bulk-form characteristics (matrix system or laminates)
- By distribution of constituents (continuous or discontinuous)

among others. The classification used here is based on the form of the structural constituents (Fig. 1.1) [3]:

1. Particle-Reinforced Composites (particulate composites) which are composed of particles, fillers or thin flakes in a matrix
2. Fiber-Reinforced Composites (fibrous composites) which consist of fibers in a matrix

1.2.1 Particle-Reinforced Composites

A particle, by definition, is non-fibrous and, with the exception of platelets, has generally no elongated dimension. The dimensions of the reinforcement determine its capability of contributing its properties to the composite. Particles of rubber-like substances in brittle polymer matrices improve fracture resistance by promoting and then arresting crazing in the brittle matrices. Other types of particles, such as ceramic, metal, or inorganic particles, produce reinforcing effects in metallic matrices by different strengthening mechanisms. The particles and matrix material in a particulate composite can be any combination of metallic or nonmetallic materials. The choice of a particular combination depends on the desired end properties.

Inorganic fillers are very effectively used to improve various properties of plastics, such as to increase surface hardness, reduce shrinkage and eliminate crazing after moulding, improve fire retardancy, provide colour and improve appearance, modify the thermal and electrical conductivities, and, most importantly, greatly reduce cost without necessarily sacrificing the other desirable properties.

Thin flakes offer attractive features for an effective reinforcement. They primarily have a two dimensional geometry and thus impart equal strength in all directions in their plane compared to fibers that are unidirectional reinforcements. Flakes, when laid parallel, can be packed more closely than fibers or spherical particles.

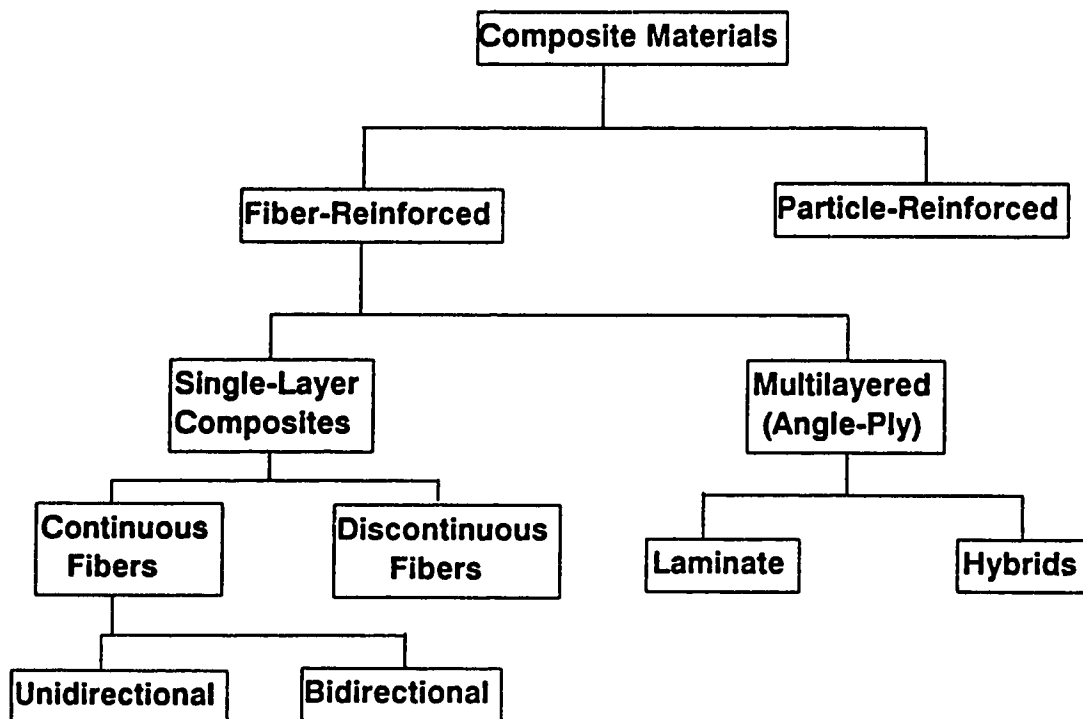


Figure 1.1: Classification of Composite Materials

Although particulate composites form an important class of composite materials, they are not further discussed in this work since discussion is limited to fibrous structural composites.

1.2.2 Fiber-Reinforced Composites

It is well known that the measured strengths of most materials are found to be much smaller than their theoretical strengths. The discrepancy in strength values is believed to be due to the presence of imperfections or flaws in the material. An attempt to minimize or eliminate flaws enhances the strength of a material. Flaws in the form of cracks that lie perpendicular to the direction of the applied loads are particularly detrimental to strength. Therefore, compared with the strength of the bulk material, man-made filaments or fibers of non-polymeric materials exhibit much higher strengths along their lengths since large flaws, which may be present in the bulk material, are minimized because of the small cross-sectional dimensions of the fiber. In the case of polymeric materials, orientation of the molecular structure is responsible for high strength and stiffness.

Fibers, because of their small cross-sectional dimensions, are not directly usable in engineering applications. They are, therefore, embedded in matrix materials to form fibrous composites. The matrix serves to bind the fibers together, transfer loads to the fibers, and protect them against environmental attack and damage due to handling. In discontinuous fiber-reinforced composites, the load-transfer function of the matrix is more critical than in continuous fiber composites. Fibrous composites have become the most important class of composite materials as they are capable of achieving high strengths.

Fibrous composites can be broadly classified as single-layer and multi-layer (angle-ply) composites on the basis of studying both the theoretical and experimental properties. *Single-layer* composites may actually be made from several

distinct layers with each layer having the same orientation and properties, and thus the entire laminate may be considered a *single-layer* composite.

Most composites used in structural applications are *multi-layered*; that is, they consist of several layers of fibrous composites. Each layer or lamina is a single-layer composite, and this orientation is varied according to design. Each layer of the composite is usually very thin, and hence cannot be directly used. Several identical or different layers are bonded together to form a multi-layered composite usable for engineering applications. When the constituent materials in each layer are the same, they are called simply laminates. Hybrid laminates refer to multi-layered composites consisting of layers made up of different constituent materials.

Reinforcing fibers in a single-layer composite may be short or long compared to its overall dimensions. Composites with long fibers are called continuous-fiber-reinforced composites and those with short fibers, discontinuous-fiber-reinforced composites. The continuous fibers in a *single-layer* composite may be all aligned in one direction to form a unidirectional composite. Such composites are fabricated by laying the fibers parallel and saturating them with resinous material, such as polyester or epoxy resin, which holds the fibers in position and serves as the matrix material. Such forms of preimpregnated fibers are called **prepregs**. The unidirectional composites are very strong in the fiber direction but are generally weak in the direction perpendicular to the fibers.

The continuous reinforcement in a single layer may also be provided in a second direction to provide more balanced properties. The bidirectional reinforcement may be provided in a single layer in mutually perpendicular directions as in a woven glass fabric. The bidirectional reinforcement may be such that the strengths in two perpendicular directions are approximately equal.

The orientation of short or discontinuous fibers cannot be easily controlled in a composite material. In most cases the fibers are assumed to be randomly oriented

in the composite. However, in the injection moulding of a fiber-reinforced polymer, considerable orientation can occur in the flow direction.

1.3 Scope of the Thesis

Damage of fiber reinforced composites are considered in this thesis (Fig. 1.2). In chapter 2, the different failure modes for fiber reinforced composites under static tension and compression are reviewed. The fatigue failure mechanisms as well as the factors influencing failure under cyclic loading are then presented. The properties of composites can be determined using two different approaches: phenomenological and mechanistic. At the end of the chapter the two approaches are introduced and compared to one another.

Damage in the form of cracks will initiate in a component made of composite material when it is subjected to cyclic loading. These cracks will generally initiate in the weakest lamina with respect to the direction of the applied load. The first crack initiation in a laminate may be viewed equivalent to the failure of a unidirectional lamina. This lamina will have the same fiber orientation angle as the weakest lamina in the laminate. In chapter 3, a fatigue failure criterion for fiber reinforced laminae under oscillatory states of off-axis loading is developed. This criterion is based on the strain energy. The predictions are compared to experimental data, and are shown to be in good agreement. The effect of the stress ratio ($\sigma_{min}/\sigma_{max}$) is also considered.

A laminated component containing an initial crack in one of its laminae is investigated in chapter 4. This chapter deals with an idealized situation and attempts to predict the crack growth direction in a unidirectional fiber reinforced composite lamina. Comparison between the theoretical prediction of the crack extension direction (also based on the strain energy) and experimental results indicates that the proposed criterion correctly predicts the direction of crack growth

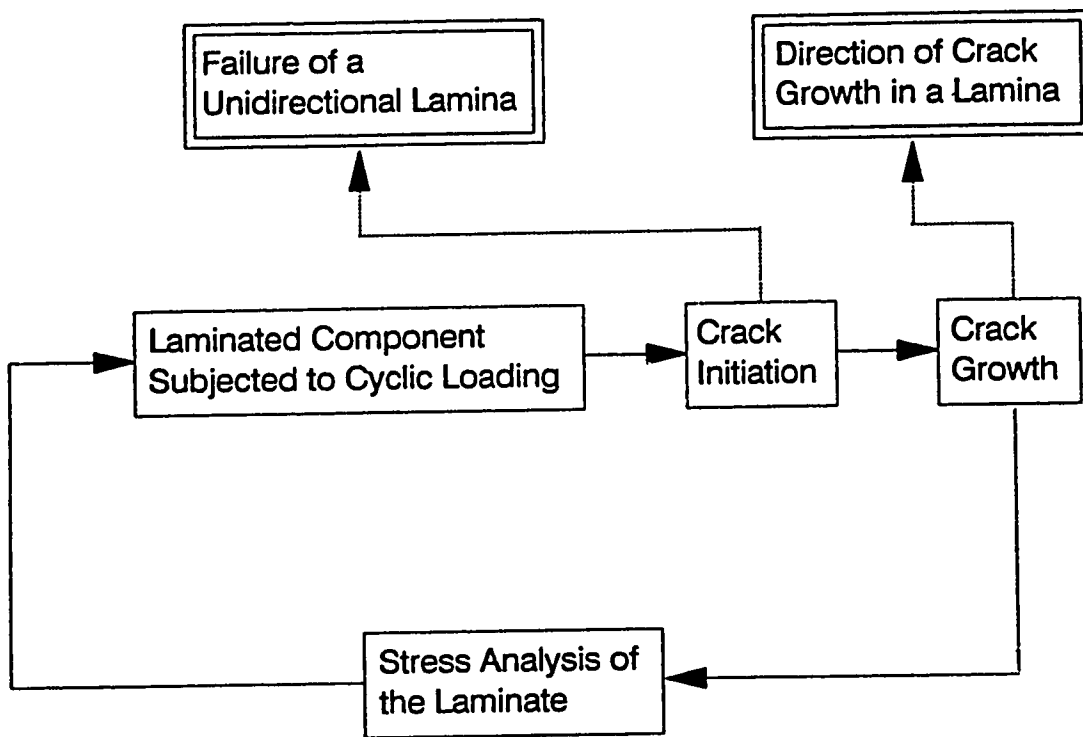


Figure 1.2:Thesis Outline

for the test cases considered.

To analyse the damage in a laminated component, a theory for laminate formulation is required. The *Classical Laminate Theory* is not adequate since it does not provide values for the interlaminar stresses and through-the-thickness stress distribution. In chapter 5, an attempt is made to develop a theory of laminated plates. An approximation involved in this theory is that the edge boundary conditions are satisfied only in an average form.

Verification of the theory of laminates developed in chapter 5 is presented in chapter 6. For the isotropic case, the results obtained are comparable to the isotropic formulation found in the literature. In particular, an isotropic laminated plate with a stress-free circular hole subjected to a uniaxial tension at infinity is studied in details. The similar problem is then considered for the case of an anisotropic laminated plate. For this case, the effects of anisotropy and laminate thickness are addressed. The results are finally compared to those obtained using a three-dimensional finite element analysis and the main differences are presented.

Chapter 2

Damage in Composite Materials

2.1 Introduction

Composite materials are heterogeneous materials and are characterized by the presence of several types of inherent flaws. These are usually broken fibers, voids in the resin, misaligned fibers, resin-rich zones, debonded interfaces, etc. The relative presence of each type of defect depends on the manufacturing process used to make each particular laminate. Therefore, composite materials generally exhibit a variety of failure modes including matrix crazing or microcracking, fiber failures resulting from statistically distributed flaws, debonding, delamination and void growth. In addition, several of these failure modes are generally present at any given time prior to failure.

2.2 Tensile Failure Modes in Unidirectional Fiber Reinforced Composites

The typical sequence of fracture modes leading to tensile failure in unidirectional glass-fiber epoxy is [4]: formation of fiber breaks probably corresponding to the

lower tail of the probability distribution of the strengths of the fibers, development of matrix microcracks beyond a certain initiation stress (these microcracks increase in density as loading proceeds); and, before failure, a rapid increase in fiber failures leading finally to coalescence of fiber breaks by transverse cracking followed by interfacial shearing and failure.

The various modes of fracture in an idealized composite laminate are shown schematically in Fig. 2.1 [4]. Fracture characteristic of brittle fibers in a brittle matrix is shown at 1 while fiber pull-out characteristic of a weak interface is shown at 2. In 3, the main crack has left the fiber intact by crack bridging, and 4 shows additional matrix microcracks bridging fibers; the latter occurs for brittle matrices in which fracture initiation occurs at strains greater than the failure strain of the matrix. The ductile failure of a fiber is shown at 5, while 6 shows fiber fracture at a flaw and the associated plastic strain distribution (or craze) in the matrix. 7 shows the plastic distribution (due to σ_y) at the tip of the main crack, 8 is the plastic shear strain distribution (under influence of τ_{xy}) and 9 is a longitudinal matrix or interfacial crack caused by the influence of the σ_x stress distribution. Finally the dotted outline 10 shows a possible zone of interlaminar shear failure between the ply shown and the adjacent off-axis lamina.

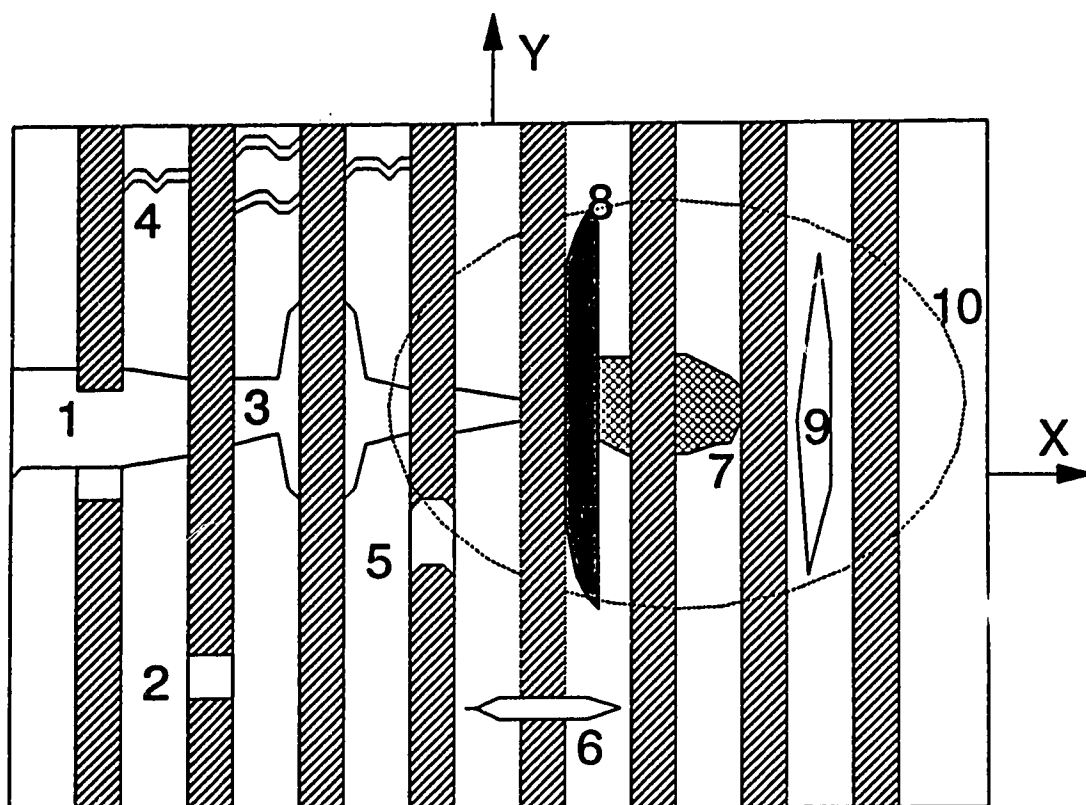


Figure 2.1: Possible Tensile Failure Modes in a Unidirectional Fiber Reinforced Composite

2.3 Compressive Failure Modes in Unidirectional Fiber Reinforced Composites

Compression failure modes in unidirectional fiber reinforced composites can be classified in three groups (Fig. 2.2); failure modes in fibers, failure modes of matrices (or resins) and failure modes of composites as a whole [5].

Fibers fail differently depending on their internal structure. High modulus graphite fibers fracture in shear along a maximum shear plane, while Kevlar fibers, on the other hand, fail in a kink mode because of Kevlar's characteristic weak bond in the radial direction that permits individual fibers to split into fibrils. Both shear failure and fiber kinking are characteristic failure modes for fibers with well-aligned fibrillar structure. The basic mechanism for the two failure modes seems to be the same; that is, they are both the result of aligned fibrillar structure and a weak radial bond. However, the low ductility for graphite fibers leads to fracture while the development of fibrils for Kevlar fibers results in kinking. Brittle fibers with amorphous structure such as glass do not usually fail in the aforementioned failure modes. These fibers can fail in bending, starting from the tension side. Medium to high-strength fibers may also fail in bending. The failure modes strongly depend upon the lateral support provided to the fiber during loading. In the absence of a strong lateral support, all fibers would fail by buckling. As the support stiffness increases, buckling is suppressed and the fiber begins to fail in shear.

Compression tests on bulk resins reveal two types of failure. For ductile resins, plastic flow is frequently observed in a broad band oriented 45-deg to the loading axis. For brittle resins, however, shear banding, namely narrow zones of shear yielding, can precede ultimate failure.

Because of the weakness of the matrix and the fiber/matrix interface compared with the strength of the fibers, unidirectional composites can fracture along the fibers even when loaded by compression. Transverse tensile stresses develop in the

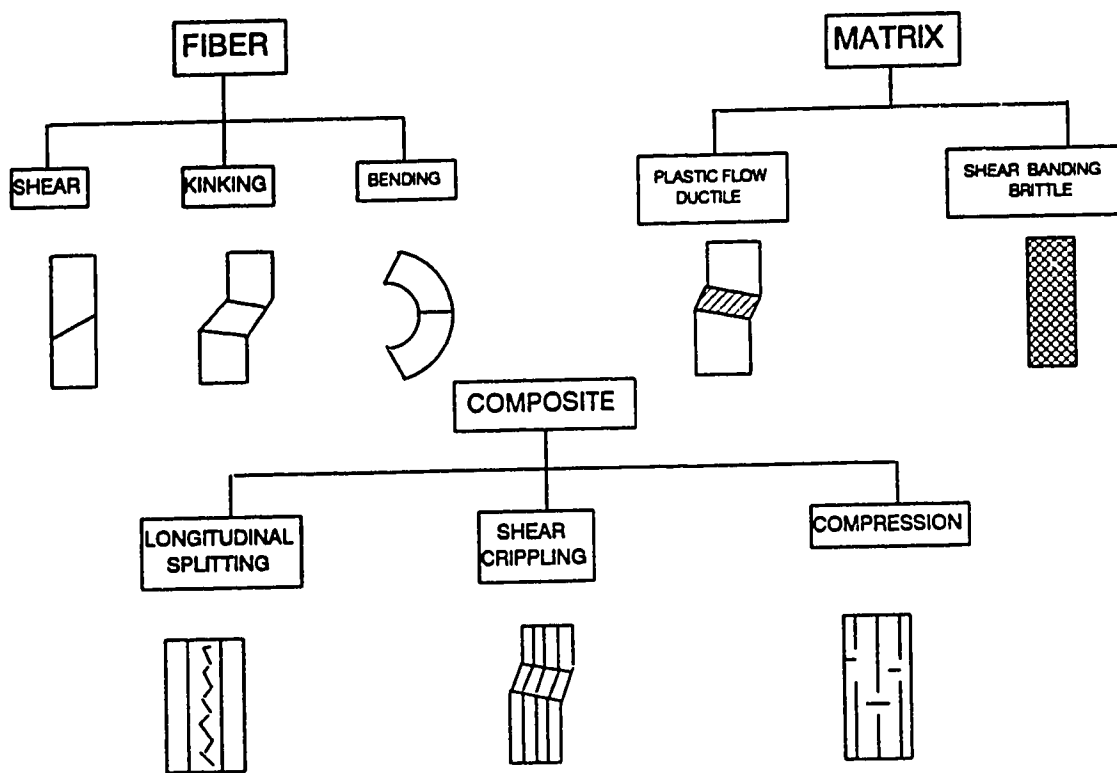


Figure 2.2: Compression Failure Modes in a Unidirectional Fiber Reinforced Composite

matrix due to Poisson's ratio differences between the matrix and fibers, and stress concentrations caused by voids can initiate fracture in the fiber/matrix interface.

If a fiber buckles, the matrix/fiber interface may fracture in shear and lead to ultimate failure. However, if the matrix is ductile and the interface is strong, the fiber can bend without matrix failure and eventually fracture in bending. The eccentricity introduced by such fiber fracture may lead to longitudinal splitting with continued compression loading.

A more likely failure mode of composites associated with fiber buckling and kinking is shear crippling. Macroscopically, shear crippling looks like a shear failure on a plane at an angle to the direction of loading. Microscopic inspection, however indicates shear crippling is frequently the result of kink-band formation (Fig. 2.3).

A third failure mode of composites is associated with pure compression failure of fibers. In this case, the fracture surface is likely to be at an angle, about 45-deg, to loading.

The failure sequence for a composite would likely start with kinking of a few fibers. The kinked fibers disrupt the stability of the neighbouring fibers so that the neighbouring fibers also fail in the kinking mode. This damage propagation process continues until the composite completely fails. In some case, fiber kinking may be initiated at several different locations and eventually converge. The transverse tensile stress in the region where the two advancing kink bands meet may be sufficiently high to cause longitudinal splitting.

Several other failure modes have been distinguished in compression tests on unidirectional specimens [6]. Three of these (transverse, branched transverse, and split transverse) are very similar. Others were brooming, shear failure, shear crippling, etc.

A transverse failure mode is typified by a fracture surface parallel to the thickness direction of the specimen, but typically oriented at an angle in the width direction

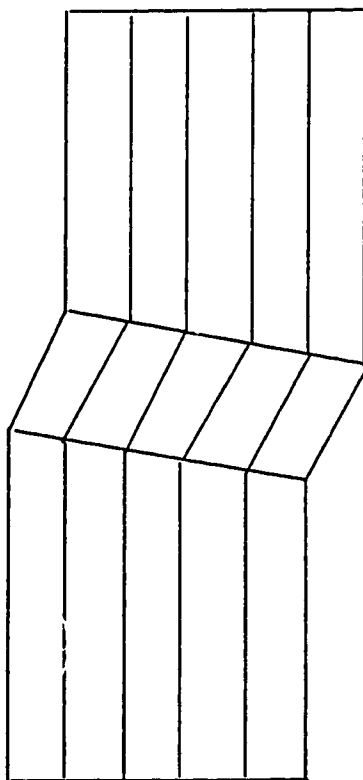


Figure 2.3:Kink Band

of the specimen. The branched transverse failure mode is readily recognizable since a portion of the gauge section will be missing if the two halves of the failed specimen are placed together. The split transverse failure mode is a transverse failure mode with the additional feature of very coarsely spaced splits in the composite parallel to the fiber orientation. That is, the splits are parallel to the axis of compressive loading, perpendicular to the primary failure plane.

The brooming failure mode does not create a distinct failure surface. In this mode the two halves of the failing specimen splay out and then are pushed together since testing machine movement continues slightly as the applied loading is dropping off and the computer control is sensing failure.

The shear failure mode forms at an angle to the normal to the mid-plane. Furthermore, this failure can be parallel to or at an angle to any of the edges of the mid-plane.

The failure modes discussed here depend on various material properties and geometrical parameters. Some properties and parameter values may promote one failure mode while other values may favour another.

2.4 Fatigue Damage Mechanisms in Composite Materials

Fatigue damage mechanisms in composite materials are quite complex and difficult to describe in a general way. The damage state is formed by various combinations of fiber, matrix, and interfacial damage; however, the ways in which these damage components interact and combine govern the fatigue response of composites. The mechanism type, and distribution of damage, depend upon the material system (combination of fiber and matrix materials), stacking sequence of plies, fabrication techniques, geometry of the components, stress state, and the load history. Furthermore, the mechanisms are sensitive to a number of other parameters, including type of loading, frequency of cyclic loading, temperature and moisture.

Fatigue failure modes and the sequence of damage accumulation depend on the stress level [7]. Early in the specimens' life, matrix microcracks between fibers normal to the applied load occur. These microcracks are not deleterious in that they neither trigger fiber failures nor grow bridging the fibers. At medium and high cyclic stresses, degradation in the form of fiber failures is observed. At low stress levels, only matrix microcracks and a few scattered fiber failures are seen.

2.4.1 Debonding

Studies have shown that fatigue damage initiation is associated with interactions of the fibers and matrix at the fiber-matrix interface [8] - [10]. The respective roles which the fibers, matrix, and interface play in the fatigue damage initiation process depend upon the material system, loading mode, and the amplitude of the cyclic stress. In glass fiber reinforced plastics, Owen [8] has observed damage initiation due to debonding between fibers and matrix under tensile loading. The debonds appeared as cracks spreading from one ply interface to the next. Subsequently, the debonds develop by spreading along the ply interface and among the aligned fibers. He also followed the progress of fatigue damage under fully reversed stress and found that it was possible to produce conventional $S - N$ curves for debonding, resin cracking as well as for the final separation of the specimen.

2.4.2 Matrix Cracking and Local Fiber Breakage

Under conditions of high cyclic stress, crack initiation can occur on the first cycle and new cracks develop as loading continues. Dharan [10] noted three regions in the $S-N$ curve for unidirectional glass fiber composites. When the applied cyclic stress is large enough to be within the strength distribution of the fibers, local fiber failures occur on the first cycle. Upon the application of additional cycles, the local failures join together until fracture of the specimen occurs within a few cycles. If

the applied stress is not sufficiently large to cause a large number of fiber fractures, matrix microcracks initiate and propagate during cycling until delamination of the ply interfaces begins. Although some fiber breaks may occur early in the life of the material, they do not appear to have a major influence on the fatigue response. If the applied stress level is below that required to initiate matrix microcracks, fatigue lives greater than one million cycles can be obtained, although some microcracks do develop in the matrix during cyclic loading.

The macroscopic behaviour of unidirectional composites closely follows from the microscopic observations. Awerbuck and Hahn [11] report that unidirectional graphite-epoxy specimens, cyclically loaded parallel to the fibers, failed abruptly, without early warning, and in a mode typical of static failures at maximum cyclic stresses within the scatter band of tensile strength data. At cyclic stresses slightly less than this level, fatigue damage was in the form of longitudinal matrix cracks between fibers near the edge of the specimens; however, most of these specimens survived 10^5 and 10^6 cycles with no measurable reduction in strength.

The fatigue strength of unidirectional composites suffers when the loading direction is not parallel to the fiber direction. At large deviations from the loading directions, the fibers become less effective in carrying load and the fatigue behaviour is much more sensitive to local inherent defects such as resin-rich regions and fabrication irregularities. Fatigue tests performed by Stinchcomb et al. [12] on 90-deg graphite-epoxy specimens produced fatigue and residual strength test failures which were parallel to the fibers with no visible evidence of fatigue damage on the fracture surface of the specimen.

Because the properties of a composite lamina are highly anisotropic, most structural applications require that several laminae be stacked together to form a laminate with fibers in individual plies having a specific orientation. Some strengthening may be realized if the angle between the load direction and fiber direction is small. In general, reducing the degree of anisotropy improves the

transverse strength and stiffness of the laminate while reducing the overall strength. It could also be shown that, although a simple cross-ply 0/90 deg stacking sequence laminate is in a state of biaxial in-plane stress in interior regions, near the free edges, the presence of interlaminar shear and normal stresses creates a three-dimensional state of stress. When the external loading is cyclic, the cyclic multiaxial stresses cause a variety of damage modes which interact to form a complex state of damage. Variations of the 0/90 deg stacking or other stacking sequences, such as quasi-isotropic (combinations of 0,+45,-45,90-deg plies), produce different stress states and therefore different damage states.

Tension-tension fatigue in cross-ply and quasi-isotropic laminates begins with cracks in the 90-deg plies. In many engineering situations, these cracks may initiate on the first loading cycle and increase in density and extend in a fashion dependent on the loading history, stacking sequence, and material system as observed by Tanimoto and Amijima [13] and Stalnaker and Stinchcomb [14]. These authors report that the density of transverse cracks increases with stress or cycles until a stable density for a particular laminate configuration is reached. It also appears that achieving a stable or saturation density of cracks in the 90-deg plies corresponds to the proportional limit in the static stress-strain curve. Grimes [15] has found the proportional limit stress to be the endurance limit for cross-ply graphite-epoxy laminates.

2.4.3 Delamination

Additional fatigue damage develops by delamination between plies and crack growth into adjacent plies. Under cyclic tensile loads, laminates with tensile interlaminar normal stresses at the free edges, such as those with basic $[0/90]_n$ and $[0/\pm 45/90]_n$ stacking sequences, develop delaminations which interact with the transverse cracks in the 90-deg plies. The delamination then progressively grow along the length and

through the width of the specimen.

Senecky and Stalnaker [16] have noted that delaminations are an important fatigue failure mode; however, they may not significantly influence residual strength or the site of residual strength test failures [8]. The tendency for a composite material to delaminate is strongly dependent on the stacking sequence and mode of loading. For example, the two basic laminates mentioned previously would develop compressive interlaminar normal stresses upon compression loading and would not be expected to delaminate.

Gustafson et al. [17] investigated the cyclic delamination crack growth of a unidirectional composite. They showed that the growth could be expressed as a power law relationship and showed little dependence on the stress ratio ($0.1 < R < 0.5$). Their results were applied to both mode I and mixed mode situations.

2.4.4 Effect of the Frequency of Cyclic Loading

Senecky and Stalnaker [16] have also studied the effect of frequency on the fatigue behaviour of unnotched composites. Using two zero-to-tension-to-zero trapezoidal waveforms differing only in the length of time at load, they have found that the longer hold time reduced the fatigue life.

Reifsnider et al. [18] mentioned that the effect of frequency of cyclic loads (or strains) was found to significantly influence the fatigue response of boron/epoxy and boron/aluminum plate specimens with a center hole. They found that low frequency fatigue loading produced more concentrated local, hole-related damage with corresponding greater stiffness reduction. In contrast, high-frequency loading produced more dispersed damage with more axial micro-structure-related damage and less stiffness reduction.

Tsai et al. [19] examined the frequency effect on the fatigue of graphite/epoxy

composites through stress controlled fatigue tests at different frequencies and different stress levels. They showed that fatigue damage is governed by the strain level and that frequency effects enter only in stress controlled situations and only through the frequency dependence of the Young's Modulus. They measured the dynamic modulus and the creep strain and found that changes in both correlate with damage.

Ellyin and Kujawski [20, 21] tested $[\pm 45]_s$ fiberglass-epoxy laminates under unidirectional cyclic loading. They concluded that the fatigue life of these laminates is affected by the frequency of loading and they explained that effect in terms of cyclic creep.

2.4.5 Stiffness Analysis

While fatigue strength and fatigue life are important properties of composite materials, stiffness is also an important property, and in some engineering designs (such as those in which stability is important), it may be a critical design factor. Broutman and Sahu [22] have presented data showing the correlation between the amount of fatigue damage, modulus change, and strength reduction. Salkind [23] suggested that the change in stiffness could be used as a definition of fatigue failure in composite materials. O'Brien and Reifsnider [24] have used experimental debonding and fiber breakage data along with a reduced stiffness analysis to predict stiffness changes in boron-epoxy laminates. The amount of matrix damage correlates well with stiffness change and fiber breakage correlates well with strength reduction.

2.4.6 Compression Fatigue

The response of composite materials when loaded in modes other than tension-tension fatigue have been studied less extensively, although currently there is some interest in tension-compression and compression-compression fatigue behaviour. It

appears that cyclic compression loading is more detrimental than cyclic tension at the same stress level. Dharan [10] noted that the graphite-polyester specimens cycled in one-way-four-point bending always failed on the compression side. Damage was observed to initiate at a zone of fiber buckling and develop by local delamination, crack propagation into the specimen, and large scale delamination.

A major damage mode in compression fatigue is delamination followed by out-of-plane buckling. Although delaminations can develop in tension-tension loading of quasi-isotropic laminates, as noted previously, they are more critical when the cyclic loading contains compression excursions as pointed out by Ryder and Walker [25]. They discussed the effect of compressive loading on the properties of a quasi-isotropic graphite/epoxy composite. For tension-tension tests, they defined failure as breakage of the coupon, while for tension-compression tests, failure was defined as coupon breakage or instability to sustain load due to severe delamination. Their primary observation was that significant visible delamination often did not occur in tension-tension testing prior to failure, but when such delamination did occur, the remaining cycles to failure could be small or large. However, specimens tested in tension-compression loading usually failed soon after delaminations formed. They suggested that delamination might be used as a definition of failure in tension-compression fatigue. They also noted that coupons tested in tension-compression fatigue failed similarly to those tested in tension-tension, but large out-of-plane buckling of the outer plies also occurred reducing life after the onset of delamination. They also mentioned that all coupons tested in tension-compression fatigue failed during the compression portion of the load cycle.

Rosenfeld and Huang [26] looked into the significance of compressive loading in fatigue of graphite/epoxy laminates. They concluded that compressive loads in fatigue produced a significant reduction in fatigue life when compared with the results for tension-tension loading. They described the mechanism of failure as progressive local fatigue failure of the matrix near a stress riser, thus causing fiber

split, progressive delamination, and fiber buckling, which then precipitates laminate failure. They also found that the delamination process was delayed if angle plies rather than 0-deg plies were used as outer plies.

Rotem and Nelson [27] compared the fatigue behaviour of graphite/epoxy laminates under tension-compression loading with their behaviour under tension-tension and compression-compression loading. They demonstrated that by presenting the experimental data for a given fatigue life in the form of a fatigue failure envelope, it is possible to reveal the fatigue behaviour for all types of loading and to distinguish between tensile and compressive failure modes.

2.4.7 Effect of Biaxial Loading

A major problem encountered in characterizing the properties of composite materials is the difficulty in testing these materials especially under combined stress conditions. Owen and Griffiths [28] state that the problem is even more significant when fatigue tests are being conducted. Difficulty in obtaining experimental results covering a particular region of the fatigue failure envelope and specimens failing outside the gauge area (mainly in the grip section) are examples of the problems encountered. Such difficulties probably account for the sparsity of published experimental results for these materials.

There are two basic specimen types that are suitable for fatigue testing under biaxial loading conditions. The cruciform specimen subjected to biaxial in-plane loading and the thin walled cylindrical specimens subjected to combined loading.

Fawaz [29] tested cruciform-type specimens under static and cyclic biaxial loading. He used the experimental results to obtain the parameters required in his biaxial static and fatigue failure criterion for fiber-reinforced laminae [30].

Krempel et al. [31, 32] tested thin-walled graphite/epoxy tubes under uniaxial and biaxial (axial-torsion) cyclic loading. Their tests showed much steeper fatigue

curves under biaxial loading compared to the uniaxial case.

Most of the experimental data on biaxial loading using thin walled cylindrical tubes have been obtained by subjecting the specimens to cyclic axial and torsional loading for which the in-plane principal strains vary in a narrow range. To cover all possible strain ratios, thin-walled tubes subjected to cyclic axial loading as well as cyclic differential pressure are more appropriate [33].

2.4.8 Effects of Environmental Conditions

The effects of environmental parameters, such as moisture and temperature, on fatigue mechanisms is another area which is also starting to receive needed attention. Hofer et al. [34] have examined the effect of moisture on fatigue and residual properties of an S-glass/graphite-epoxy hybrid composite and found no basic alteration in response due to moisture. From tests at cryogenic temperatures, Kasen et al. [35] have found fatigue response of boron-epoxy to be similar to that at room temperature, and Tobler and Read [36] report the fatigue life of glass-epoxy at $4^{\circ}K$ to be an order of magnitude greater than that at room temperature.

Sumsion and Williams [37] performed torsional and bending fatigue tests on both uniaxial (0-deg) and crossplied (± 45 -deg) graphite-epoxy materials at temperatures of $24^{\circ}C$ and $74^{\circ}C$ in an environment of air and water. The results of the torsion testing showed that the number of cycles to cause an initial decrease in stiffness as well as the rate of stiffness loss was a function of temperature and environment: the most significant losses were noted at the higher temperature in water.

Mahulikar et al. [38] carried out mixed-mode tensile and fatigue crack propagation tests on a boron reinforced titanium composite for the as-received, vacuum heat-treated, and air heat-treated conditions. The vacuum heat treatment had minimal effect on the tensile properties of the composite but improved the fatigue crack propagation properties. The air heat treatment degraded the fibers

and the interface, resulting in a loss of longitudinal strength but improvement of fatigue crack propagation properties. Humid environment accelerated the fatigue crack growth considerably compared to the vacuum and inert gas environments. Failure stress intensity (K_F) appeared to have a lower value in a humid environment.

Tennyson et al. [39] tested unidirectional AS4/3501-6 graphite-epoxy laminates (0-deg and 90-deg) under fatigue for both an ambient and a hot-wet environment. Their specimens were tested under tension fatigue and compression fatigue loading. For the 0-deg specimens under tension fatigue, the hot-wet S-N curve leveled off at a slightly higher stress than the ambient case. They concluded that it might be due to the normal variation present in all fatigue testing and therefore found that there was little or no effect of the hot-wet environment on the 0-deg tension fatigue properties. For the 90-deg tension fatigue tests, they found that the reduction in ambient fatigue strength due to hot-wet environment was proportional to the reduction in static strength. The results for the 0-deg specimens tested under compression fatigue showed that the hot-wet S-N curve decays rapidly before levelling out at a relatively low number of cycles (approximately 1000 cycles). This was unlike the behaviour of the ambient 0-deg compression fatigue behaviour which exhibits a more gradual decrease in stress with the number of cycles to failure. The 90-deg compression fatigue tests under ambient and hot-wet conditions showed some differences. The ambient fatigue tests had more scatter and the fitted S-N curve decreased more gradually but produced a large difference between the average and minimum curves.

2.5 Phenomenological Approach

Two different disciplines may be adopted to determine the physical properties of composites; they are, the mechanistic approach and the phenomenological approach.

The mechanistic approach relates the physical properties of the composite to the properties of the constituent materials through established methods of

analysis (e.g., continuum mechanics). This approach is particularly adaptable to the computation of composite properties which characterize the averaged global material responses, such as deformation and conductivity. A particular useful result from the mechanistic approach is the prediction of composite compliances from micromechanics analyses [40]. However, for composite properties which are governed by local material responses such as strength and interfacial phenomena, the mechanistic approach is less fruitful.

The phenomenological approach treats the heterogeneous composite as a continuum, and a mathematical model is used to correlate the occurrence of the material responses without necessarily explaining the mechanisms which lead to these material responses. If attention is paid to mathematical requirements of the model, the phenomenological approach is suitable for engineering characterization of the material properties governed by either the averaged global or the local material responses. Treatment of unidirectional composites as homogeneous anisotropic plates [41] exemplifies characterization in a global sense.

In order to establish a failure criterion from the mechanistic approach, the local irregularity of fiber-matrix geometry must be characterized, detailed analysis methodology beyond the realm of classical continuum mechanics must be established, and the physical mechanism of failure of the individual isotropic phases must be known. Since these basic ingredients, particularly the last, have yet to be firmly established, the mechanistic approach to composite failure appears to be intractable at present.

A phenomenological failure criterion may be considered as a mathematical model relating the external excitation to the material response. Failure is interpreted here as the occurrence of any definable discontinuity in the material response. The external excitation can be mechanical, thermal, chemical, or others. Thus, if the material parameters in the mathematical model are measured in a manner consistent with the discontinuity to be characterized, the failure criterion can be used in an

isolated context, to characterize yield or rupture.

Various theories [42], using this approach, have dealt with damage as a whole without studying the different damage modes. The tensor polynomial method [43, 44], the strain energy density ratio method [45], and the normal Tsai-Hill method [46] are examples of these theories.

Chapter 3

A Fatigue Failure Criterion for Unidirectional Fiber Reinforced Composite Laminae

3.1 Introduction

The problem of damage and crack initiation in a fiber reinforced component subjected to cyclic loading is of importance in design and inspection, especially in the aerospace industry.

The first crack initiated in a laminate can be simulated by the failure of a unidirectional lamina. This lamina will have the same fiber orientation angle as the weakest lamina in the laminate. It seems therefore necessary to establish a fatigue failure criterion for unidirectional laminae.

Some of the earlier attempts to investigate the fatigue of the fiber reinforced composite laminae will be briefly outlined. Hashin and Rotem [48] - [50] have shown that the use of fatigue functions based on simple static quadratic failure relations can, in certain instances, yield reasonable correlation with test data. They used

a criterion expressed in terms of three S-N curves obtained from fatigue testing of off-axis unidirectional specimens under uniaxial oscillatory load. The form of this criterion has suggested using two distinct experimentally observed failure modes: fiber failure mode and matrix failure mode.

Toth [51, 52] studied the fatigue behaviour of unidirectional (off-axis) and cross-ply composites. He discussed the failure mechanism in terms of buildups of stress concentration in the matrix to stress levels capable of fracturing proximate filaments.

Awerbuch and Hahn [53] have also performed some off-axis fatigue tests on composite laminae in an effort to characterize the matrix/interface - controlled failure. They used a homologous stress ratio to analyze their S-N data, and then attempted to fit their data using a power law but concluded that a more detailed investigation was necessary.

Tennyson [54] and Tennyson et al. [39] concluded that there was a reasonable cause to believe that their tensor polynomial criterion for the static failure can be modified to incorporate "fatigue functions" which will permit preliminary estimates of the fatigue life for a given lamina or laminate under axial load condition. Later, Tennyson et al. [55] developed a numerical procedure to estimate the fatigue life of laminates subject to constant amplitude and spectrum loading. A discussion of other static failure criteria such as the maximum stress and the maximum strain criteria, Hill-type criteria and tensor polynomial criteria are presented in a review paper by Labossière and Neale [42].

The response of unidirectional composite laminae loaded in modes other than tension-tension fatigue has not been systematically investigated, although, some results have been reported for cross-ply composite laminates.

Rosenfeld and Huang [26] performed a number of tests for $R = 0, -\infty$ and -1 loading to determine the significance of the compressive loading. These test results indicated a significant life reduction for both $R = -\infty$ and $R = -1$ compared to

the tension-tension loading, with the life reduction for $R = -1$ being greatest.

Rotem and Nelson [27] studied the tension-compression fatigue behaviour of graphite/epoxy laminates. They showed that tension-compression fatigue was more important than tension-tension or compression-compression fatigue in that it combined the behaviour of both. They also mentioned that the failure was dependent on the specific lay-up of the laminate as well as the difference between the tensile static strength and the absolute value of the compressive static strength.

Meanwhile, Ellyin et al. [56] and Ellyin [57] reported that, for metals, the fatigue process can usually be divided into two phases, viz. initiation of cracks and their subsequent propagation until failure occurs. They also stated that it would be extremely useful if one could find a unifying damage parameter which can describe these two processes. They thus introduced and successfully used strain energy criterion for fatigue failure of metals. The predicted results were in good agreement with the test data.

In the following it will be demonstrated that the strain energy approach is also an appropriate failure criterion for the fiber reinforced materials (FRM) under cyclic loading.

3.2 Stress-Strain Relation for Composite Laminae

For a plane stress condition, the elastic stress-strain relation for a unidirectional orthotropic lamina shown in Fig. 3.1, may be presented in the form [1]:

$$\begin{Bmatrix} \epsilon_x \\ \epsilon_y \\ \gamma_{xy} \end{Bmatrix} = \begin{bmatrix} \bar{S}_{11} & \bar{S}_{12} & \bar{S}_{16} \\ \bar{S}_{12} & \bar{S}_{22} & \bar{S}_{26} \\ \bar{S}_{16} & \bar{S}_{26} & \bar{S}_{66} \end{bmatrix} \begin{Bmatrix} \sigma_x \\ \sigma_y \\ \tau_{xy} \end{Bmatrix} \quad (3.1)$$

where:

\bar{S} are the transformed compliances ($\bar{S}_{ij} = \bar{S}_{ji}$):

$$\bar{S}_{11} = S_{11}m^4 + (2S_{12} + S_{66})m^2n^2 + S_{22}n^4,$$

$$\begin{aligned}
\bar{S}_{12} &= S_{12}(m^4 + n^4) + (S_{11} + S_{22} - S_{66})m^2n^2, \\
\bar{S}_{22} &= S_{11}n^4 + (2S_{12} + S_{66})m^2n^2 + S_{22}m^4, \\
\bar{S}_{16} &= (2S_{11} - 2S_{12} - S_{66})m^3n - (2S_{22} - 2S_{12} - S_{66})mn^3, \\
\bar{S}_{26} &= (2S_{11} - 2S_{12} - S_{66})mn^3 - (2S_{22} - 2S_{12} - S_{66})m^3n, \\
\bar{S}_{66} &= 2(2S_{11} + 2S_{22} - 4S_{12} - S_{66})m^2n^2 + S_{66}(m^4 + n^4),
\end{aligned}$$

and

$$\begin{aligned}
S_{11} &= 1/E_1, \\
S_{22} &= 1/E_2, \\
S_{66} &= 1/E_6, \\
S_{12} &= -\nu_{12}/E_1 = -\nu_{21}/E_2, \\
S_{16} &= 0, \\
S_{26} &= 0,
\end{aligned}$$

m, n are the cosine and the sine of the angle θ of Fig. 3.1 respectively

E_1, E_2 are the moduli of elasticity in the principal directions of the lamina

E_6 is the shear modulus of elasticity

ν_{12}, ν_{21} are the major and minor Poisson ratios respectively with respect to the principal directions of the lamina

Note that for a general anisotropic lamina,

$$\begin{aligned}
S_{16} &= \eta_{12,1}/E_1 = \eta_{1,12}/E_6 \\
S_{26} &= \eta_{12,2}/E_2 = \eta_{2,12}/E_6
\end{aligned}$$

where:

$\eta_{1,12}, \eta_{2,12}$ are the coefficients of mutual influence of the first kind [41]

$\eta_{12,1}, \eta_{12,2}$ are the coefficients of mutual influence of the second kind [41]

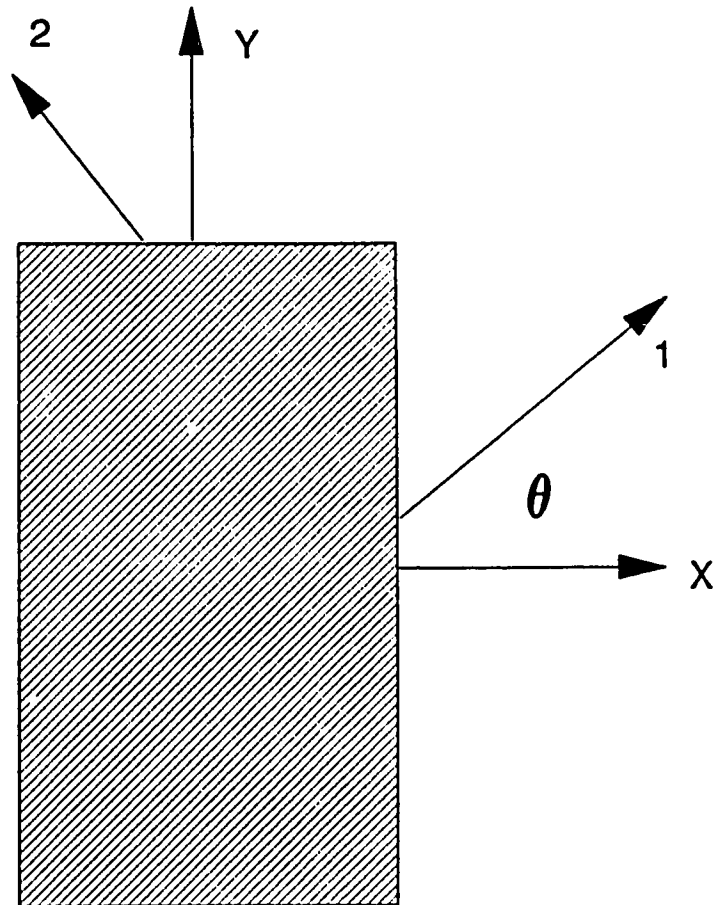


Figure 3.1: Positive Rotation of Principal Material Axes from Arbitrary xy Axes

3.3 Critical Strain Energy Criterion

Numerous proposals have been made to correlate fatigue test data. The multiplicity of the proposed criteria is an indication of the complexity of the problem and the lack of agreement on a unified approach.

Most of the proposed criteria are either stress or strain based. These criteria do not account for the interaction between stress and strain in a material deformation process. Furthermore, some of these criteria are not invariant with respect to the changes in the coordinate system.

Therefore, Ellyin [58] concluded that a better formulation was to use the strain energy as a fatigue failure criterion. He also explained that, in the low- and high- cycle fatigue failures, the total fatigue life can be divided into two parts: the nucleation of “starting” cracks, and their subsequent propagation until failure occurs.

For smooth specimens, the first process is primarily controlled by the amplitude of cyclic strain and/or stress of the bulk material. In the case of notched members, the crack nucleation process at the notch root is controlled by the nominal stress and/or strain and the notch geometry.

In the second phase, the crack propagation process is generally dominated by the local stress/strain field ahead of the crack tip. In the single parameter description of this process, the controlling parameters become the range of stress (strain) intensity factor, ΔK or the range of the path-independent J-integral, ΔJ .

In another study [59], Ellyin also showed that the cyclic strain energy ΔW , can describe both the critical damage (demarcation between initiation and propagation phases) and fatigue life. He proposed a fatigue failure criterion relating the total (elastic + plastic) cyclic strain energy ΔW^t to the number of cycles to failure N_f ; this criterion can be expressed as: $\Delta W^t = g(N_f)$. He also suggested a power law

type relation of the form:

$$\Delta W^t = \kappa N_f^\alpha + C \quad (3.2)$$

where:

κ , α , C were shown to be materials constants. In particular, κ is a function of the triaxiality constraint.

We wish now to investigate whether the strain energy could also be used as a damage function for composite materials. A major portion of the useful life of a composite structure/component involves subcritical damage accumulation which is finally manifested in various combinations of matrix cracking, fiber-matrix debonding, delamination and fiber breakage failure modes. A precise characterization of a composite material would therefore require a knowledge of the way the energy dissipates throughout the inhomogeneous structure as damage is being accumulated. The strain energy is a parameter which can be related to this damage process. This approach will be followed in this chapter.

For elastic plane stress problems, the strain energy can be expressed in terms of the stresses and strains as:

$$W = (\sigma_x \epsilon_x + \sigma_y \epsilon_y + \tau_{xy} \gamma_{xy}) / 2 \quad (3.3)$$

Substituting from (3.1) in (3.3) we can get an expression of the strain energy for composite laminae in terms of stresses only, i.e.

$$W = [\sigma_x (\bar{S}_{11} \sigma_x + \bar{S}_{12} \sigma_y + \bar{S}_{16} \gamma_{xy}) + \sigma_y (\bar{S}_{12} \sigma_x + \bar{S}_{22} \sigma_y + \bar{S}_{26} \gamma_{xy}) + \tau_{xy} (\bar{S}_{16} \sigma_x + \bar{S}_{26} \sigma_y + \bar{S}_{66} \gamma_{xy})] / 2 \quad (3.4)$$

Rearranging (3.4), we get:

$$W = [\bar{S}_{11} \sigma_x^2 + 2\bar{S}_{12} \sigma_x \sigma_y + \bar{S}_{22} \sigma_y^2 + 2\bar{S}_{16} \sigma_x \tau_{xy} + 2\bar{S}_{26} \sigma_y \tau_{xy} + \bar{S}_{66} \tau_{xy}^2] / 2 \quad (3.5)$$

Assuming that the stress-strain relation for a lamina is essentially elastic, for the case where both the maximum and minimum stresses are positive, the cyclic strain energy is equivalent to the area under the stress-strain curve associated with the tensile stress (Fig. 3.2):

$$\begin{aligned} \Delta W^+ = & \frac{1}{2} \bar{S}_{11} \Delta \sigma_x^2 \left[\frac{(1 + R_x)}{(1 - R_x)} \right] + \frac{1}{2} \bar{S}_{22} \Delta \sigma_y^2 \left[\frac{(1 + R_y)}{(1 - R_y)} \right] + \\ & \frac{1}{2} \bar{S}_{66} \Delta \tau_{xy}^2 \left[\frac{(1 + R_s)}{(1 - R_s)} \right] + \bar{S}_{12} \Delta \sigma_x \Delta \sigma_y \left[\frac{(1 - R_x R_y)}{(1 - R_x)(1 - R_y)} \right] + \\ & \bar{S}_{16} \Delta \sigma_x \Delta \tau_{xy} \left[\frac{(1 - R_x R_s)}{(1 - R_x)(1 - R_s)} \right] + \bar{S}_{26} \Delta \sigma_y \Delta \tau_{xy} \left[\frac{(1 - R_y R_s)}{(1 - R_y)(1 - R_s)} \right] \end{aligned} \quad (3.6)$$

where:

Δ before a symbol indicates its range,

R_i are the stress ratios = $\sigma_{min}/\sigma_{max}$ ($i = x, y, s$)

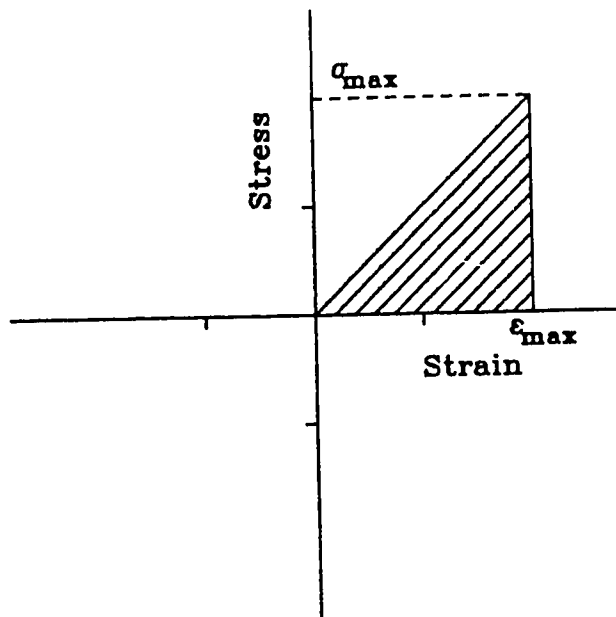
For the uniaxial case:

$$\Delta W^+ = \frac{1}{2} \bar{S}_{11} \Delta \sigma_x^2 \left[\frac{(1 + R_x)}{(1 - R_x)} \right] \quad (3.7)$$

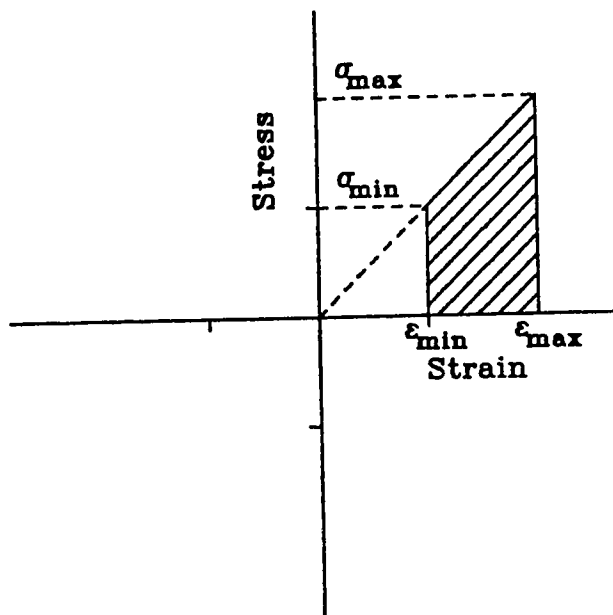
Thus, the LHS of (3.2) can be calculated once the applied stress range is specified. The constants on the RHS of (3.2) have to be determined from test data. For the general case, the expression of ΔW in terms of R would have to be determined through experiments (see section 3.6).

3.4 Comparison with Experimental Data ($R \approx 0$)

Tests performed by Hashin and Rotem [48] for different values of the fibers orientation angle, were used to validate the power law type relation (3.2) for the case of fiber reinforced laminae. The material used in [48] was E-glass fibers in an epoxy matrix with 0.6 volume fraction of fibers ($E_x = 54739.8 MPa$, $E_y =$



(a)



(b)

Figure 3.2: Definition of Cyclic Strain Energy for Positive Stress Ratios

(a) $R = 0$

(b) $R = 0.5$

17756.1MPa, $E_s = 6013.5MPa$ and $\nu = 0.285$). The stress ratio used was 0.1 under uniaxial condition. For this value of the stress ratio, eq. (3.7) reduces to:

$$\Delta W^+ = \bar{S}_{11} \left[\frac{\Delta \sigma_x^2}{1.636} \right] \quad (3.8)$$

Using eq. (3.2) and setting the constant $C = 0$, we get

$$\Delta W^+ = \kappa (2N_f)^\alpha \quad (3.9)$$

where α and κ in this case will depend on the fiber orientation and $2N_f$ represents the number of reversals to failure (1 cycle = 2 reversals).

The correlation with the experimental data seems to indicate that eq. (3.9) is an appropriate fatigue criterion to be used for the composites (Fig. 3.3). In this figure, the experimental data in the form of $\Delta \sigma$ vs $2N_f$ were replotted in ΔW^+ vs $2N_f$ coordinates, where ΔW^+ was calculated from (3.7). The lines represent the best fit regression curves for each fiber orientation angle, θ . Having established a correlation between the cyclic strain energy, ΔW^+ , and the number of reversals to failure, $2N_f$, the next step is to get a general expression for α and κ as a function of the fibers orientation angle.

The following expressions appear to correlate with the experimental observations:

$$\begin{aligned} \alpha &= \alpha_o + a\theta, \\ \log \kappa &= \log \kappa_o + b\theta^\beta, \end{aligned} \quad (3.10)$$

where:

a, b, β are material properties,

α_o, κ_o are the values of α and κ respectively at $\theta = 0$,

θ is the fibers orientation angle in degrees.

From the test data in [48], the constants of eq. (3.10) are found to be (see Figs. 3.4, 3.5):

$$\begin{aligned}\alpha &= -0.1494 + 0.0008 \theta, \\ \log \kappa &= 2.2240 - 0.9208 \theta^{0.2812},\end{aligned}\tag{3.11}$$

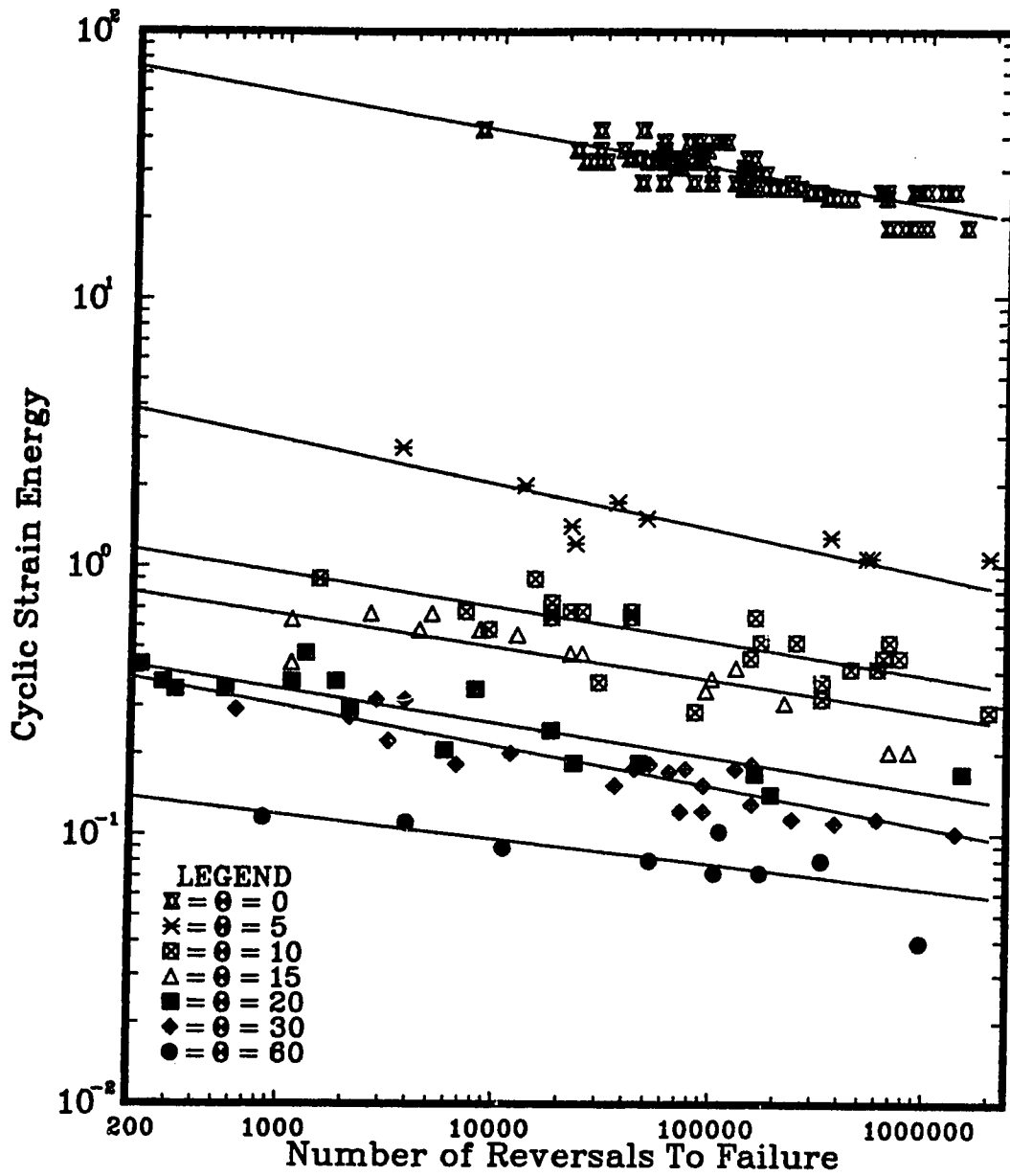


Figure 3.3: Correlation of the Strain Energy ΔW with the Experimental Data for Glass/Epoxy, Experimental Data from [48]

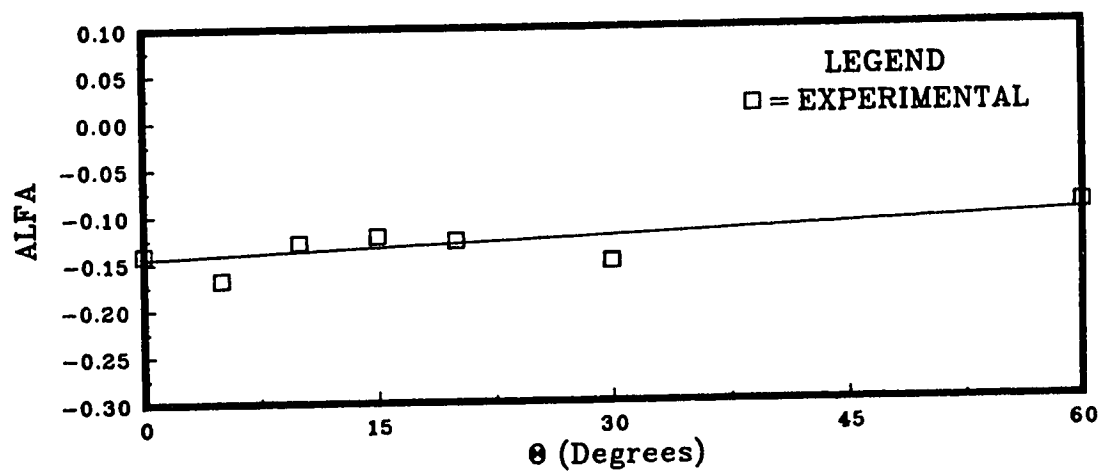


Figure 3.4: Variation of α with the Fibers Orientation Angle θ for the Glass/Epoxy Composite

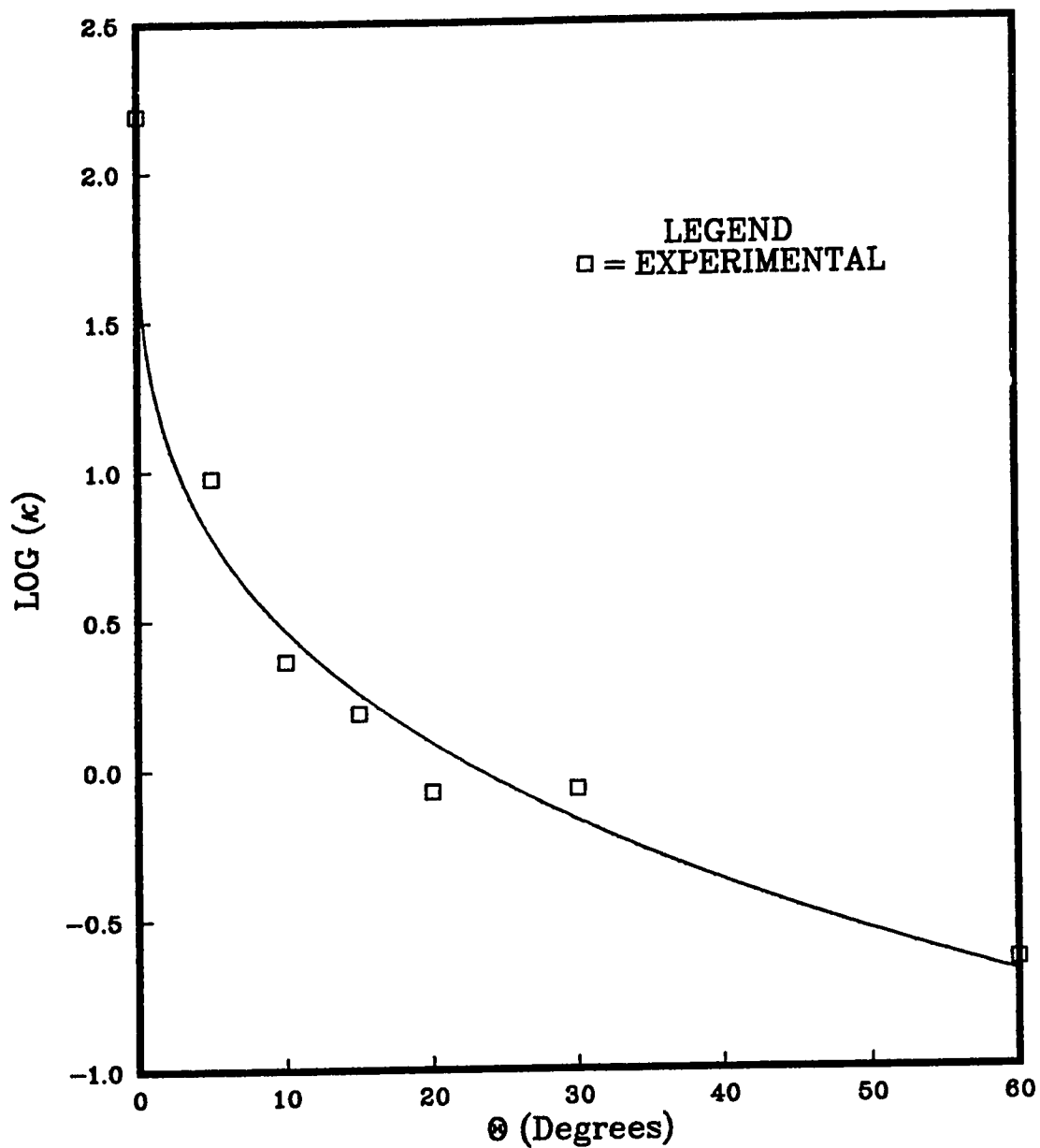


Figure 3.5: Variation of κ with the Fibers Orientation Angle θ for the Glass/Epoxy Composite

Using the values of α and κ given by (3.11) in eq. (3.9), the calculated results could be compared to the experimental data. Such a comparison is shown in Fig. 3.6, where the solid lines are now the predicted values from eqs.(3.9) and (3.10).

A second set of fatigue tests on unidirectional composites was taken from Toth [51, 52]. The material used was a 25 % volume boron filaments in a matrix of 6061 aluminum ($E_x = 139700MPa$, $E_y = 81360MPa$, $E_s = 68950MPa$ and $\nu = 0.3$). A stress ratio of 0.1 was used. The correlation seemed to indicate that eq.(3.9) is also appropriate in this case (Fig. 3.7).

The procedure described earlier was then repeated to obtain the constants of eq. (3.10) for the data given in [51, 52] which yielded (Figs. 3.8, 3.9):

$$\begin{aligned}\alpha &= -0.0436 + 0.00047\theta, \\ \log\kappa &= -0.6937 - 0.2766\theta^{0.38134},\end{aligned}\tag{3.12}$$

Using these relations in eq. (3.9), the calculated values are compared with the experiment data as shown in Fig. 3.10. It is seen that the experimental data of the fatigue life of this metal matrix composite, is well represented by eqs.(3.9) and (3.10).

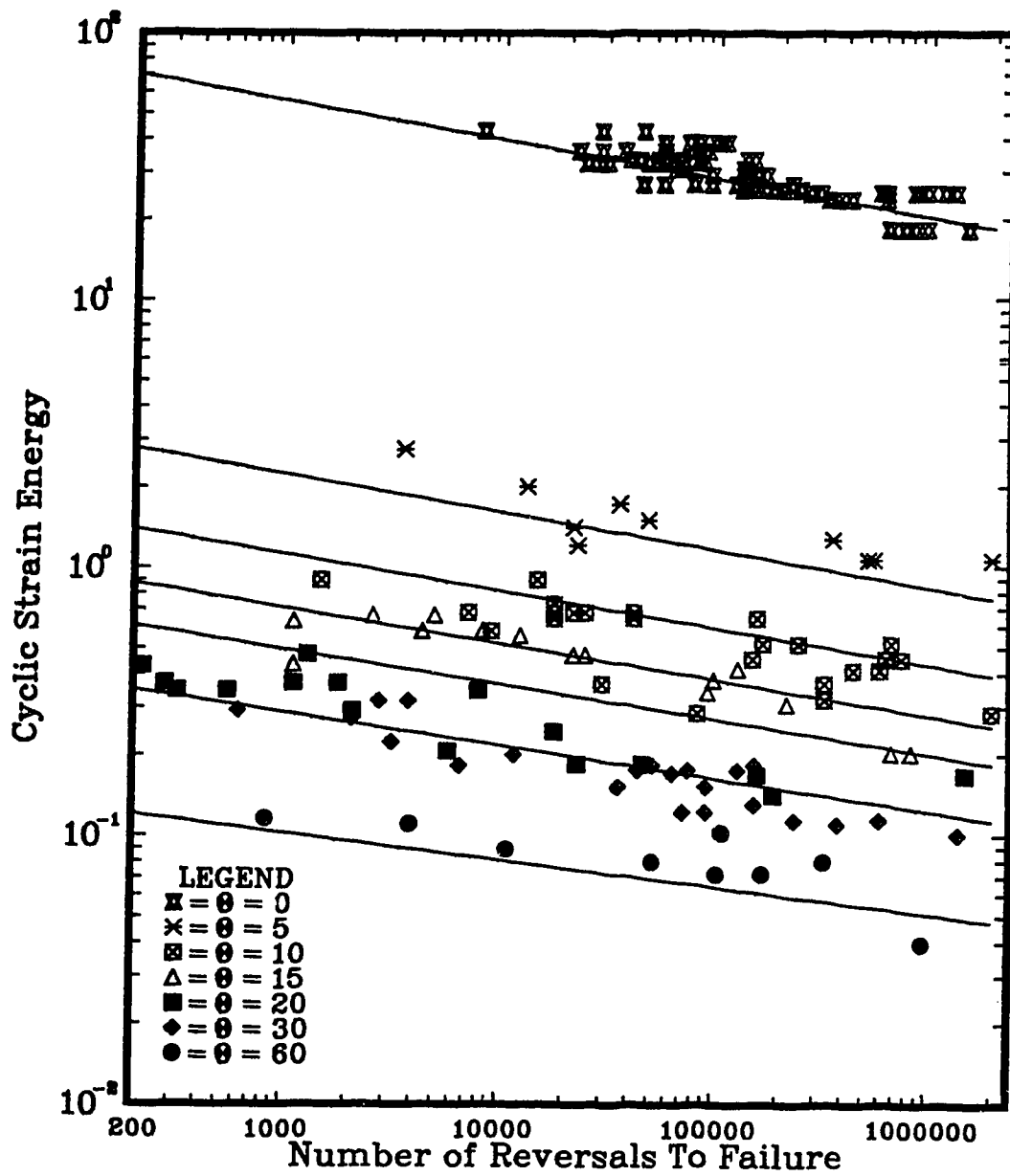


Figure 3.6: Comparison of Predicted Values with Experimental Results for Glass/Epoxy, Experimental Data from [48]

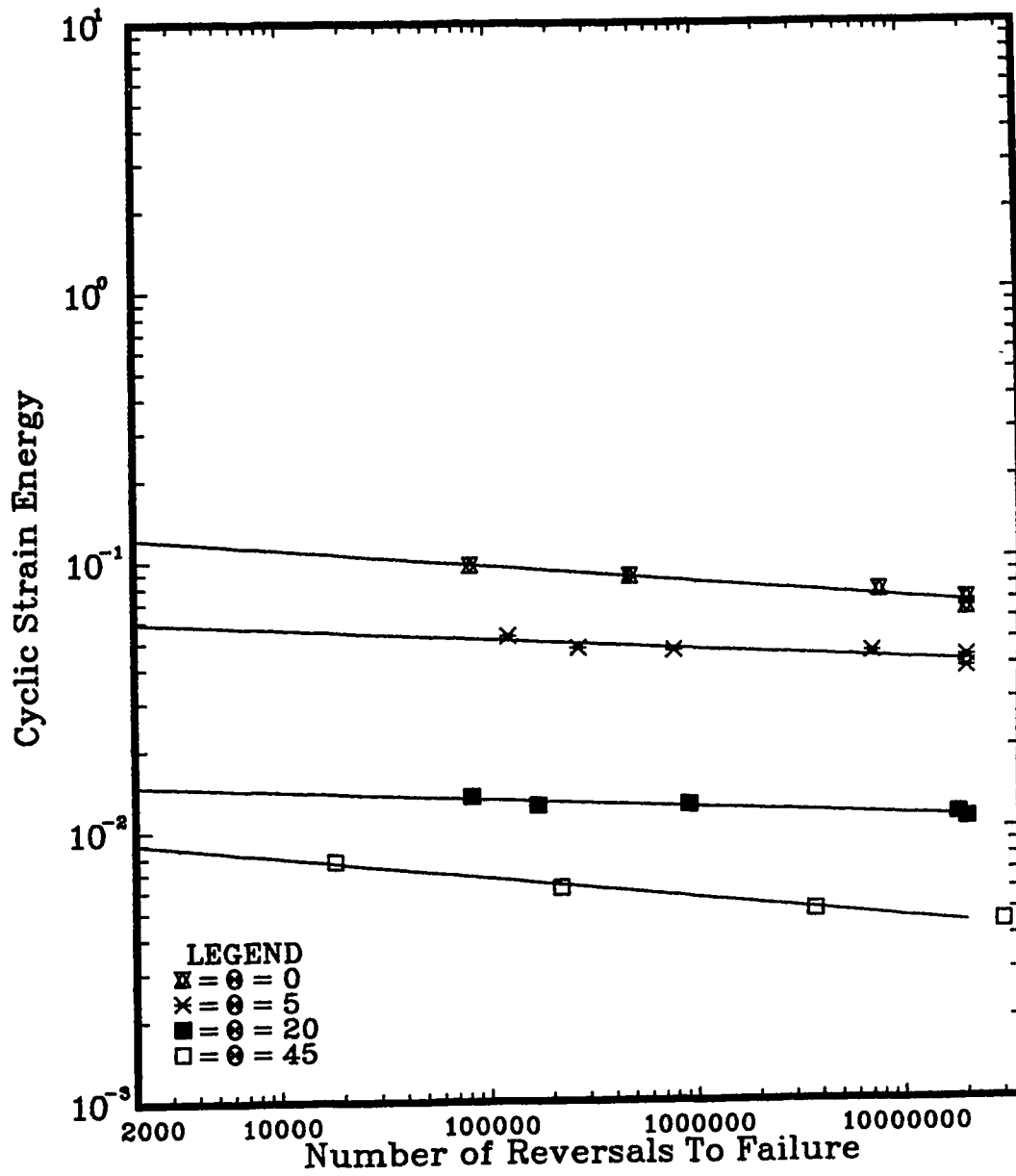


Figure 3.7: Correlation of the Strain Energy ΔW with the Experimental Data for Aluminum, Experimental Data from [51]

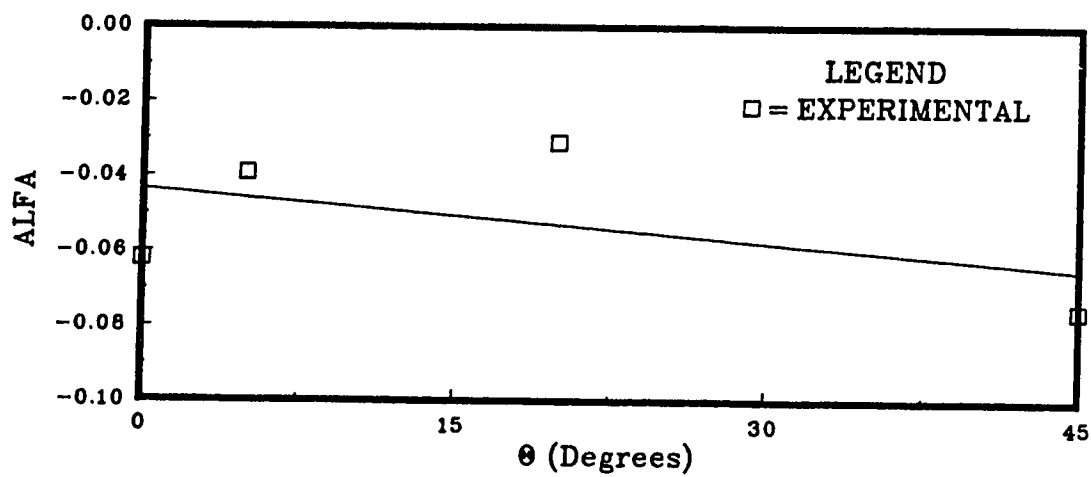


Figure 3.8: Variation of α with the Fibers Orientation Angle θ for the Boron/Aluminum Composite

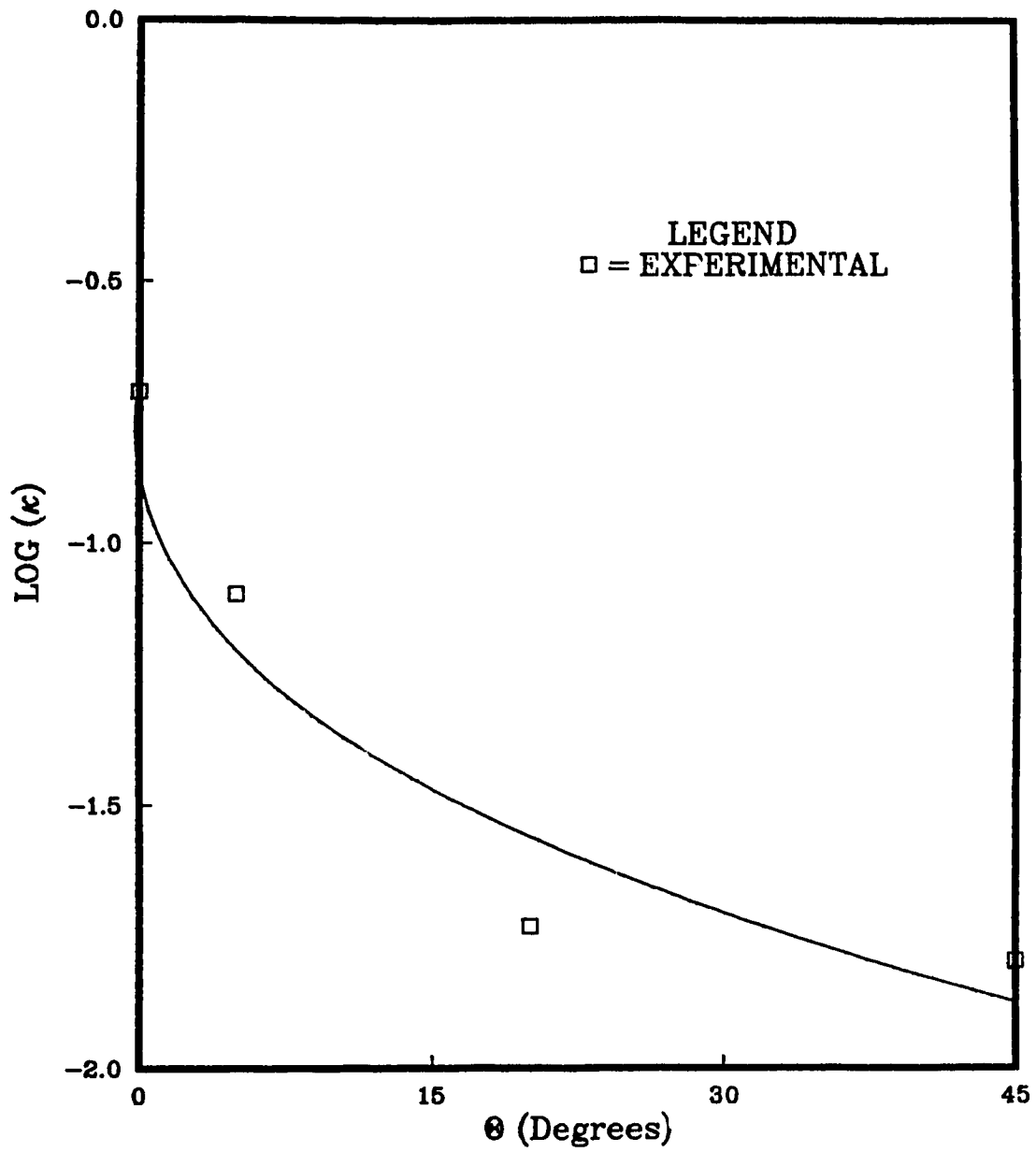


Figure 3.9: Variation of κ with the Fibers Orientation Angle θ for the Boron/Aluminum Composite

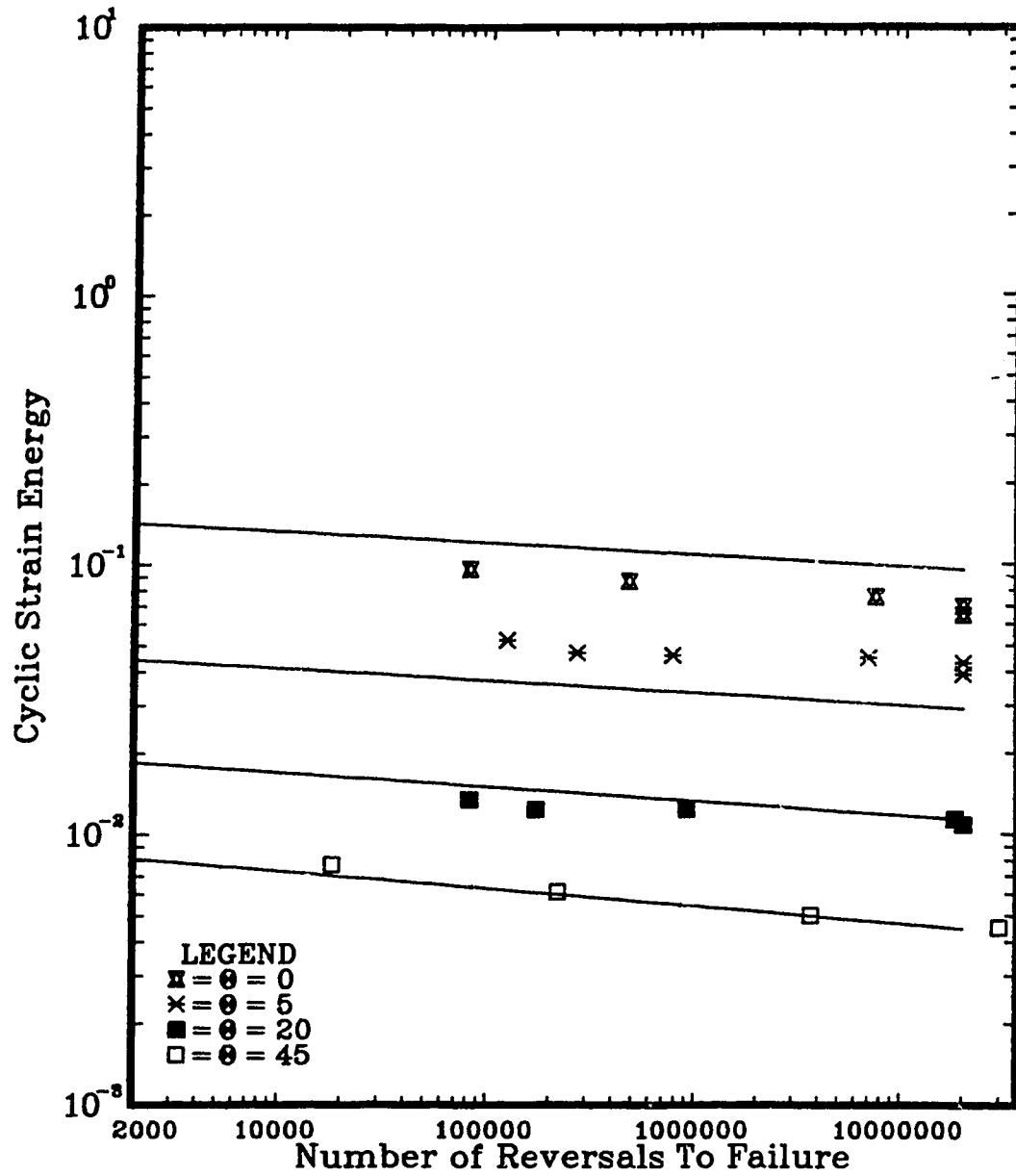


Figure 3.10: Comparison of Predicted Values with Experimental Results for Boron/Aluminum, Experimental Data from [51]

A third set of fatigue tests for different angles of orientation was performed by Awerbuch and Hahn [53]. This time, the material used was AS/3501-5A graphite-epoxy with a nominal fiber content of 70% by volume ($E_x = 135000MPa$, $E_y = 9600MPa$, $E_z = 5240MPa$ and $\nu = 0.3$). A stress ratio of 0.1 was used. Again the correlation with this set of data seems to indicate that eq. (3.9) is an appropriate criterion for fatigue life prediction (Fig. 3.11).

The same procedure was repeated and the constants of eq. (3.10) calculated for the test data in [53] were found to be (Figs. 3.12, 3.13):

$$\begin{aligned}\alpha &= -0.0746 - 0.00045\theta, \\ \log\kappa &= 1.7063 - 0.5946\theta^{0.2557},\end{aligned}\tag{3.13}$$

Using these values in eq. (3.9), the calculated results are compared with the experimental data as shown in Fig. 3.14.

Using eq. (3.10), the three sets of data under consideration led to average correlation coefficients of 0.2529 for the first equation (α) and an average of 0.9756 for the second equation ($\log\kappa$).

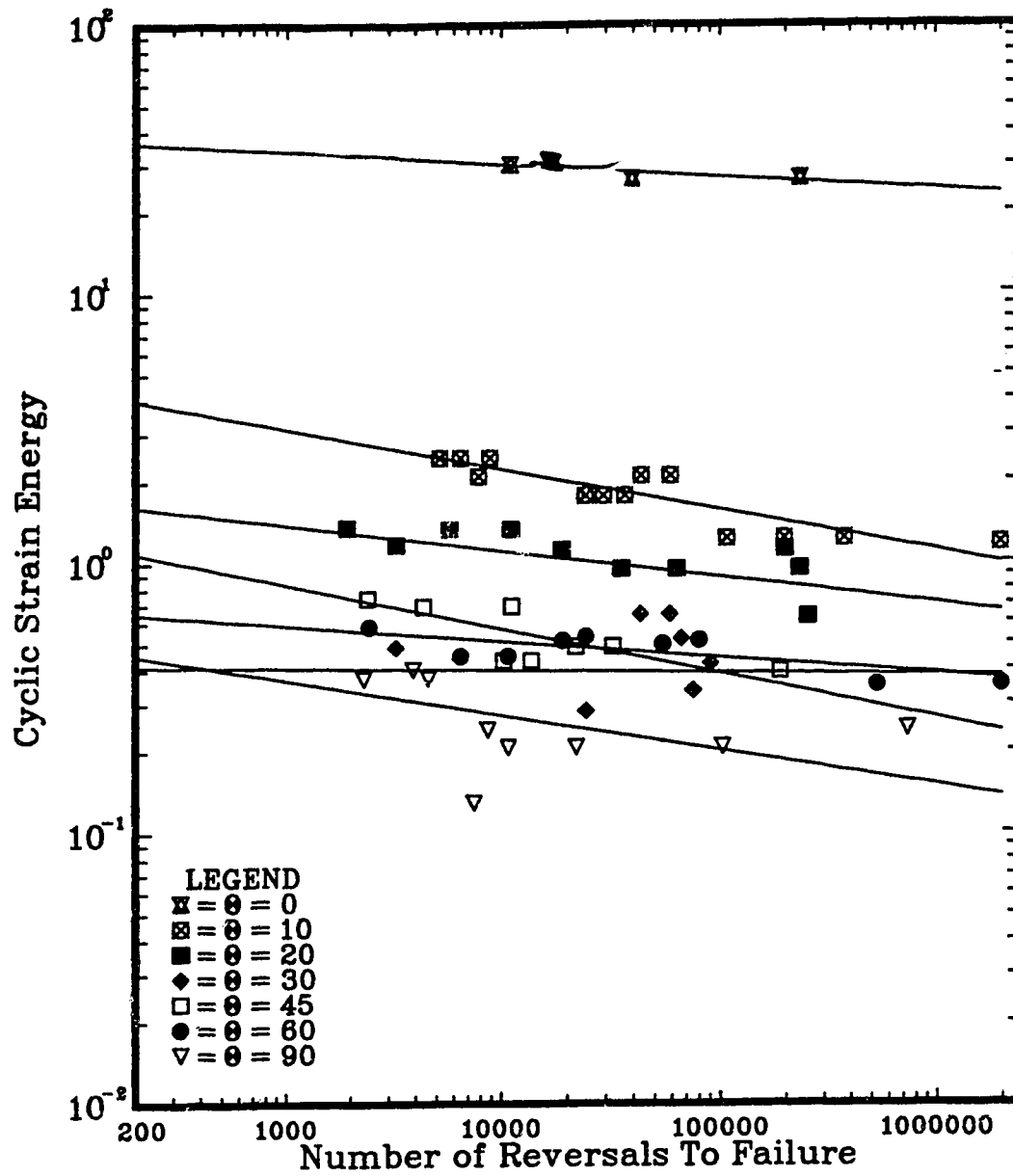


Figure 3.11: Correlation of the Strain Energy ΔW with the Experimental Data for Graphite/Epoxy, Experimental Data from [53]

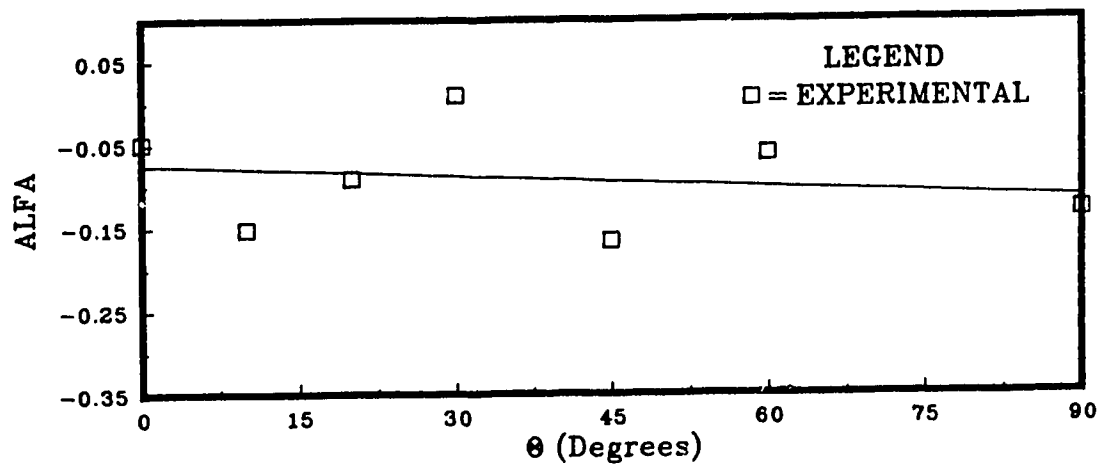


Figure 3.12: Variation of α with the Fibers Orientation Angle θ for the Graphite/Epoxy Composite

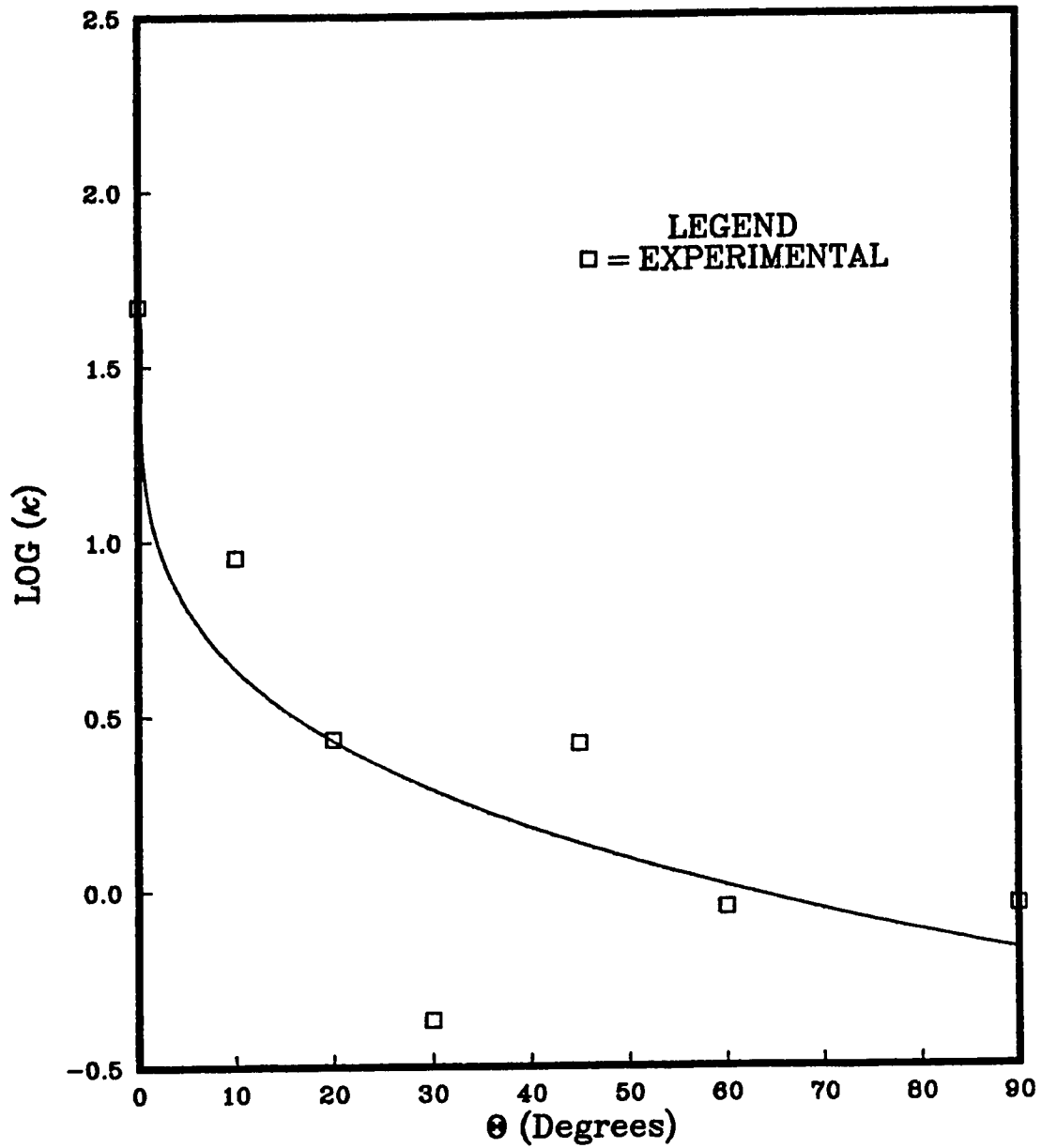


Figure 3.13: Variation of κ with the Fibers Orientation Angle θ for the Graphite/Epoxy Composite

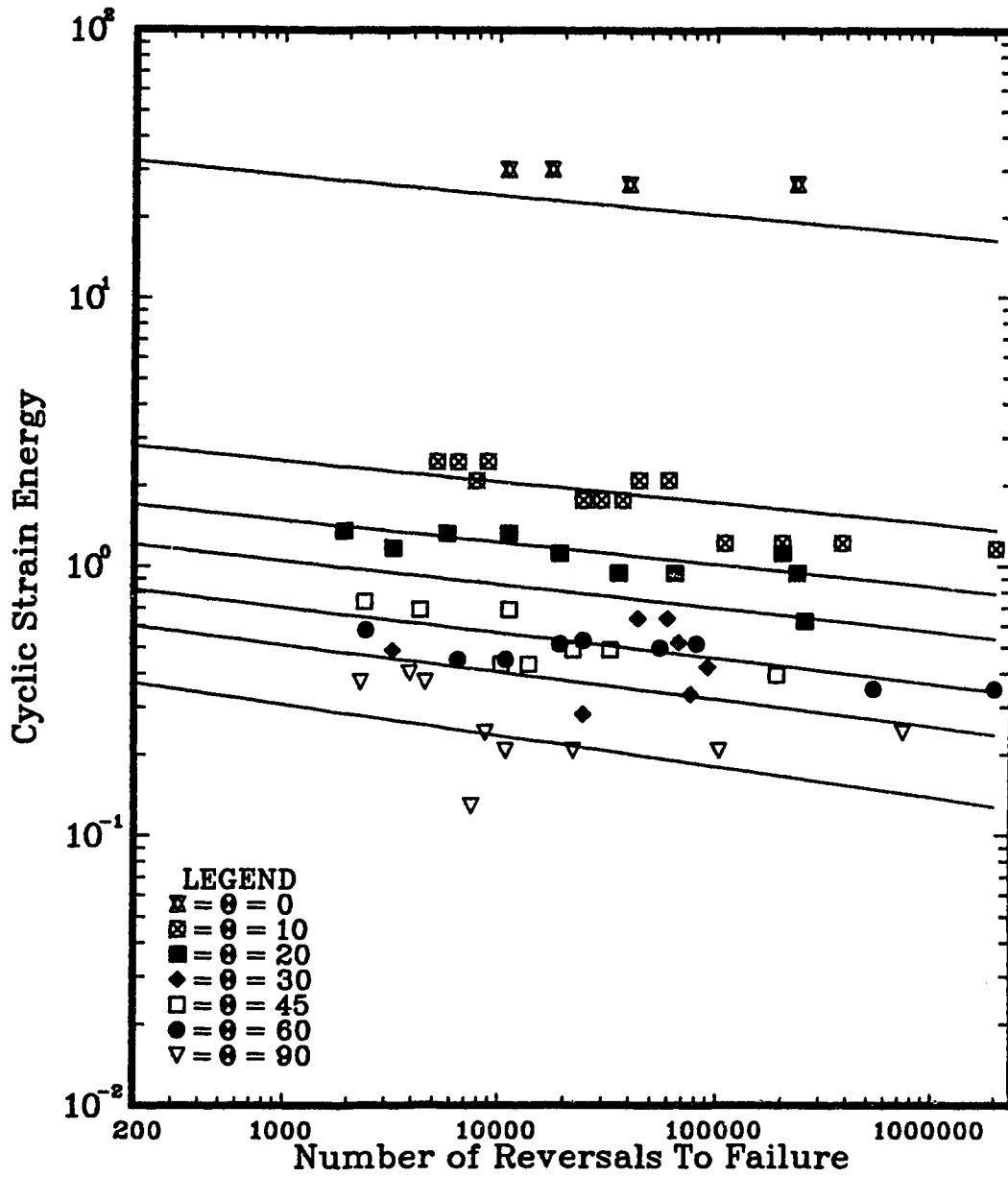


Figure 3.14: Comparison of Predicted Values with Experimental Results for Graphite/Epoxy, Experimental Data from [53]

3.5 Normalization of the Results

A comparison of fitted eqs. (3.11) to (3.13) indicates that the term $a\theta$ in the first of eqns. (3.10) is small compared to α_o , and we may neglect the second term. In doing so, then all predicted life curves for various fiber orientations will have a constant slope $\alpha = \alpha_o$. We may now collapse all these parallel lines by an appropriate normalization, i.e.

$$\Psi^+ = \frac{\Delta W^+}{\kappa} = (2N_f)^\alpha \quad (3.14)$$

where $\kappa = \kappa(\theta)$ is given by the second of eqs.(3.10).

A comparison between the normalized cyclic strain energy, $\Delta W^+/\kappa$, versus number of reversals to failure, $2N_f$, (3.14) and experimental data for the three materials, is shown in Figs. 3.15- 3.17. It is observed that within a reasonable scatter band, the fatigue life of composite laminae could be predicted by (3.14).

3.6 Effect of the Stress Ratio, R

Although tension-compression fatigue is extremely important in many composite structures, most fatigue studies have been performed either in tension-tension or in compression-compression (most probably because of the difficulties in conducting a tension-compression fatigue test).

It is to be noted that, in this chapter, all the previous relations were obtained for a stress ratio of about zero (tension loading). For a more general loading condition, the cyclic strain energy may be related to the number of reversals to failure and the stress ratio through a general form:

$$\Delta W = G(2N_f, R_i, \theta) \quad (3.15)$$

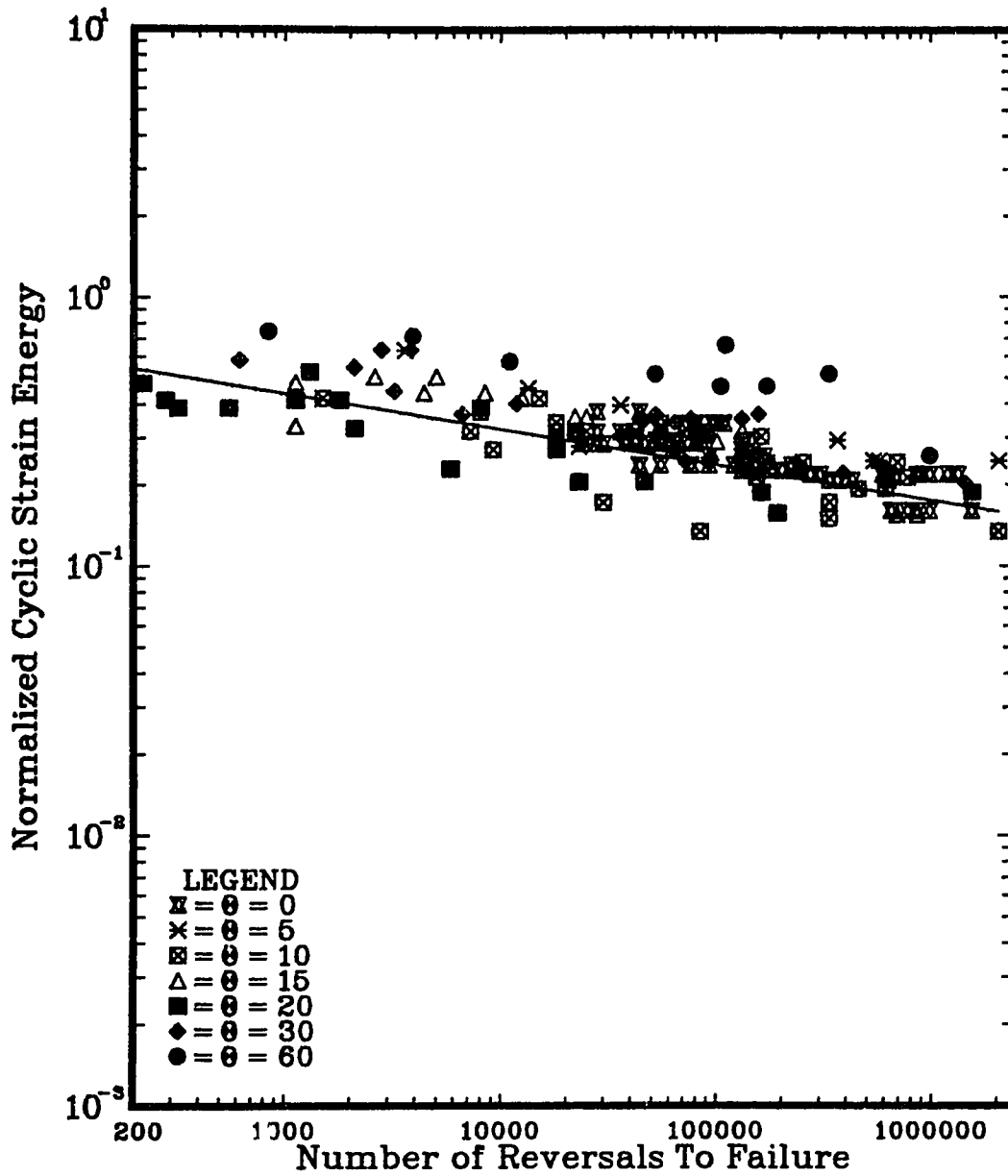


Figure 3.15: Normalized Strain Energy Curve for the Glass/Epoxy Composite, Experimental Data from [48]

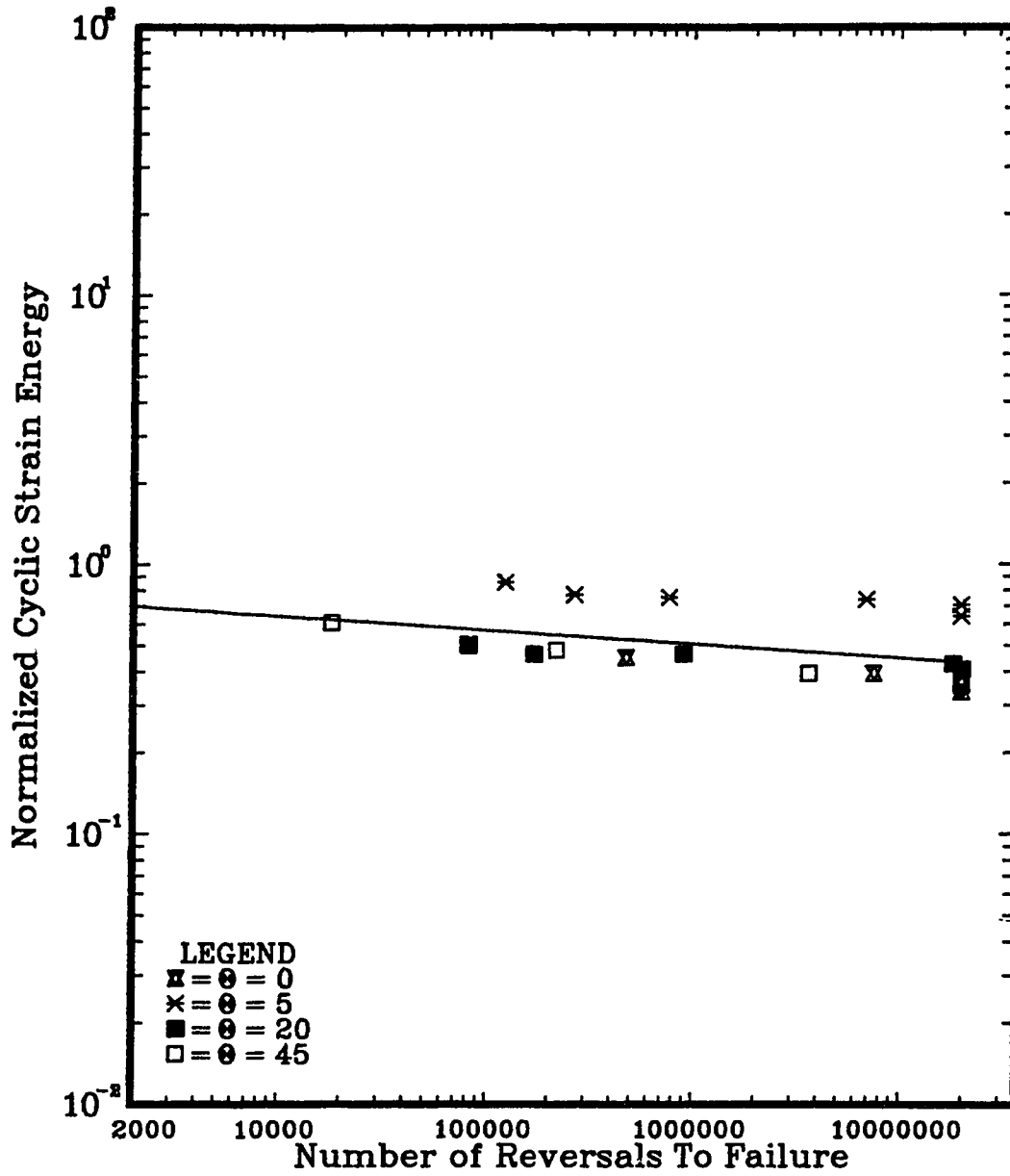


Figure 3.16: Normalized Strain Energy Curve for the Boron/Aluminum Composite, Experimental Data from [51]

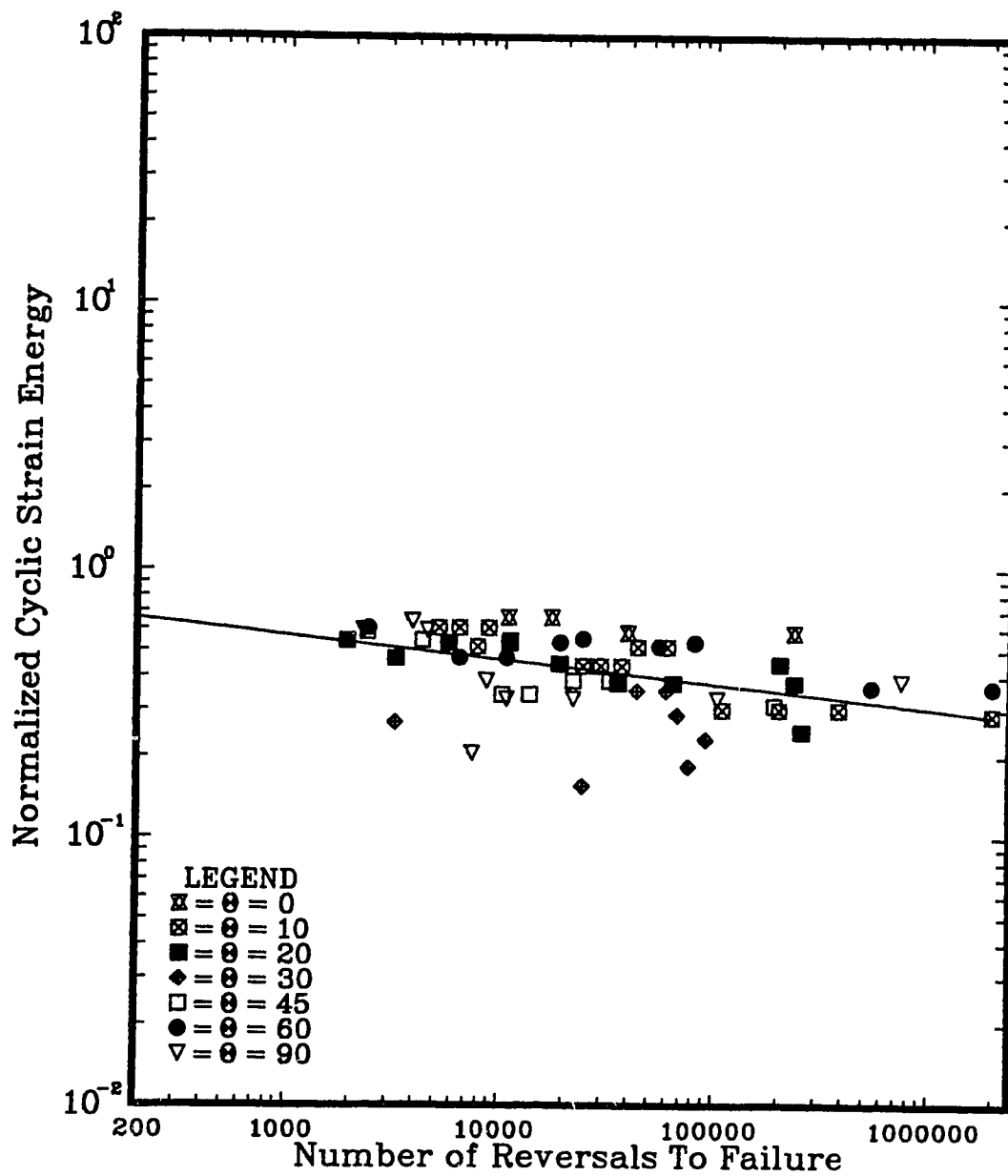


Figure 3.17: Normalized Strain Energy Curve for the Graphite/Epoxy Composite, Experimental Data from [53]

The functional form of this relation would have to be determined using a series of fatigue tests employing different values of the stress ratio.

3.6.1 Experimental Results

Unidirectional fiber reinforced specimens were cyclically tested at room temperature under load controlled conditions. Fiber orientations of 0° , 19° , 45° , 71° and 90° were used to prepare the specimens. The material used was the *Scotchply Reinforced Plastic type 1003* which is a non-woven fiberglass reinforced epoxy resin materials. A full description of the material properties, specimens' fabrication, testing procedure and experimental results are given in Appendix A.

The specimens with different orientations were tested under different stress ratios ($R = 0.5, 0$ and -1). For each case, the experimental results of the maximum cyclic stress vs. number of reversals to failure are tabulated and plotted in Appendix B.

Most of the tests were conducted using a loading frequency of 3.3 Hz (200 CPM). The effect of loading frequency was investigated on specimens with 45° fiber orientation angle. These specimens were tested under frequencies of 3.3 Hz (200 CPM) as well as 0.426 Hz (25 CPM). The frequency effect observed was minimal (see appendix A).

For the off-axis tests, failure was defined as the separation of the coupon, while for 0° specimens it was defined as a 10% drop in the load carrying capacity of the specimen. These definitions were used rather than, say, the change in stiffness because no modulus reduction was observed during the life regardless of the off-axis angle or the stress level (see Appendix A).

3.6.2 Negative Stress Ratios

Figure 3.18 shows that the value of κ , for positive values of the stress ratio ($R = 0$ and $R = 0.5$), is about the same as the maximum monotonic strain energy under tensile load, W_f^+ , for the same fiber orientation angle, θ . The solid curves in this figure are the best fit curves using the second of eq. (3.10). Equation (3.14) can therefore be written as:

$$\Psi^+ = \frac{\Delta W^+}{W_f^+} = 2N_f^\alpha \quad (3.16)$$

where Ψ^+ is the non-dimensional form of the strain energy under positive stress ratios, ΔW_f^+ , shown in eq.(3.7). The normalized strain energy (Ψ^+) for $R = 0$ and $R = 0.5$ is plotted vs the number of reversals to failure in Fig. 3.19.

For positive stress ratios, the damaging strain energy is represented by the shaded areas of Fig. 3.2. For the negative stress ratios, if it is assumed that only the energy associated with the tensile loading causes damage, then the damaging energy would be represented by the shaded area of Fig. 3.20. A plot of the energy values, associated with the positive stress, obtained from the experiments with $R = -1$ together with the best fit obtained from the positive stress ratio case, is shown in Fig. 3.21. It is noted that all the experimental data lie under the best fit of positive ratio tests. This suggests that the compressive part of the load also contributes to the damage. By a direct analogy, the corresponding form under positive or negative stress ratio can be written as:

$$\Psi = \Psi^+ + \Psi^- = \frac{\Delta W^+}{W_f^+} + \frac{\Delta W^-}{W_f^-} \quad (3.17)$$

where:

ΔW^- is the area under the stress-strain curve associated with the compressive stress (Fig. 3.22).

W_f^- is the monotonic value of the strain energy under compressive load.

and ΔW^+ and W_f^+ have been defined earlier.

The normalized strain energy can be related to the number of reversals to failure by:

$$\Psi = (2N_f)^\alpha \quad (3.18)$$

which is a generalized form of (3.14). The fatigue failure criterion (3.18) with the normalized energy on the LHS, given by (3.17), takes into account the effect of the stress ratio (positive or negative). The normalized strain energy parameter Ψ is plotted vs. the number of reversals to failure in Fig. 3.23. This plot includes test results obtained from different fiber orientation angles as well as positive and negative values of the stress ratio. It is observed that, within a reasonable scatter band, the fatigue lives of composite laminae could be predicted by (3.18).

A relationship for the (non-normalized) strain energy for any value of the stress ratio, R , can be obtained by multiplying both sides of (3.17) by the monotonic value of the strain energy under tensile load:

$$\Delta W = \Psi W_f^+ = \Delta W^+ + \frac{W_f^+}{W_f^-} \Delta W^- \quad (3.19)$$

The above equation implies that, in general, the tensile and compressive parts of the stress do not contribute equally to the damage. The ratio W_f^+/W_f^- depends on the orientation angle of the fibers. For certain fiber orientation angles, the damage caused by compressive loads might be higher than or equal to the damage caused by the tensile loads while in other cases the damage caused by compressive loads is so low that it could be neglected. Substituting from (3.19) into (3.18), we get

$$\Delta W^+ + \frac{W_f^+}{W_f^-} \Delta W^- = W_f^+ (2N_f)^\alpha \quad (3.20)$$

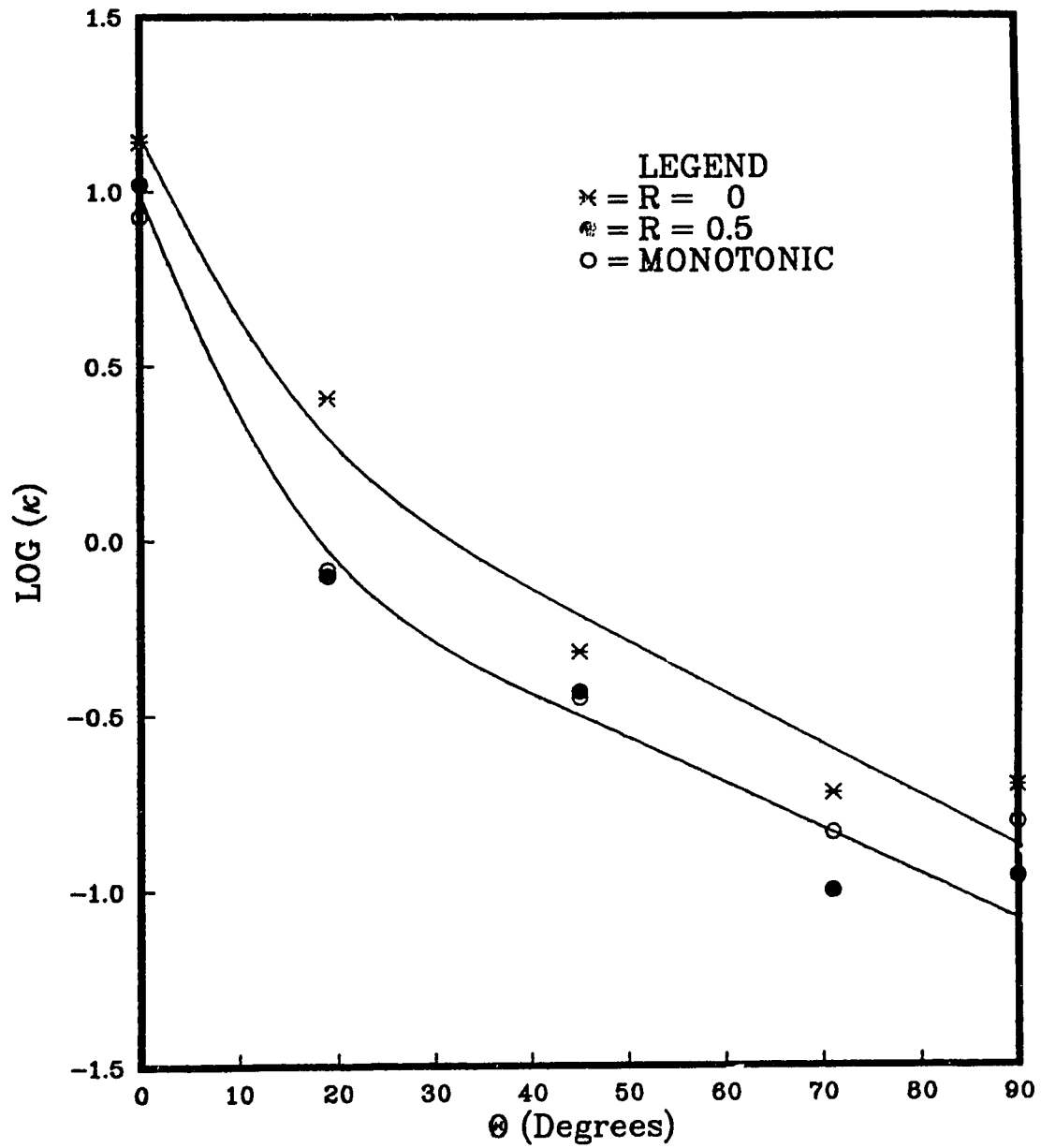


Figure 3.18: Variation of κ with the Fiber Orientation Angle, θ , for Positive Stress Ratios

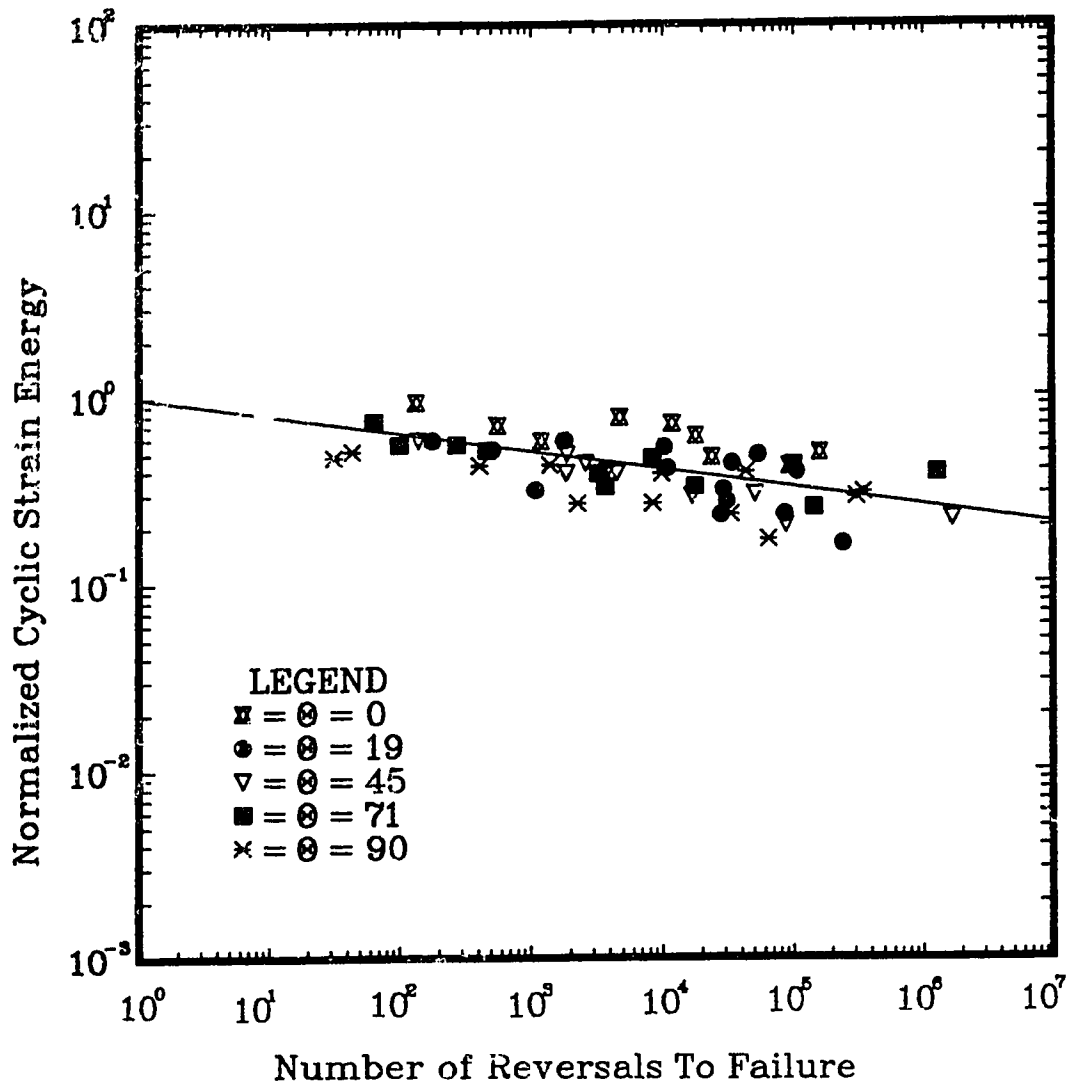


Figure 3.19: Normalized Cyclic Strain Energy vs. Number of Reversals to Failure for Various Fiber Orientation Angles and Positive Values of Stress Ratio

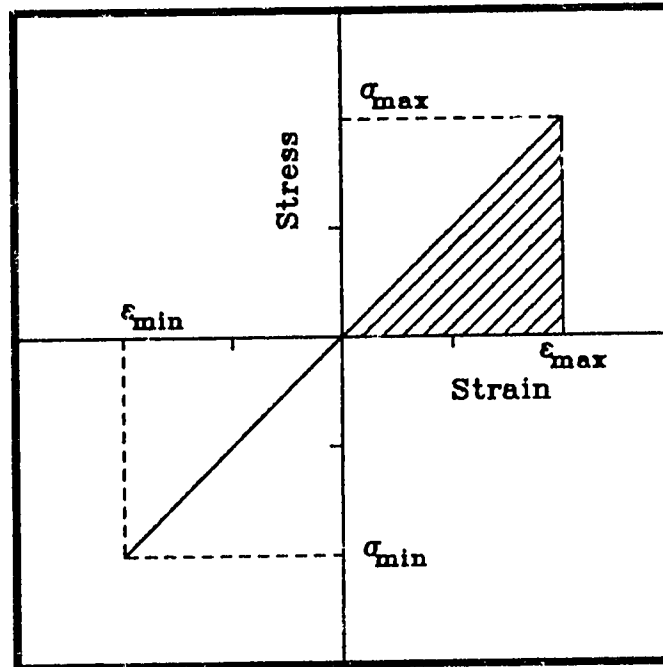


Figure 3.20: Definition of Cyclic Strain Energy for Negative Stress Ratios with Damage Associated with Tensile Stress Only

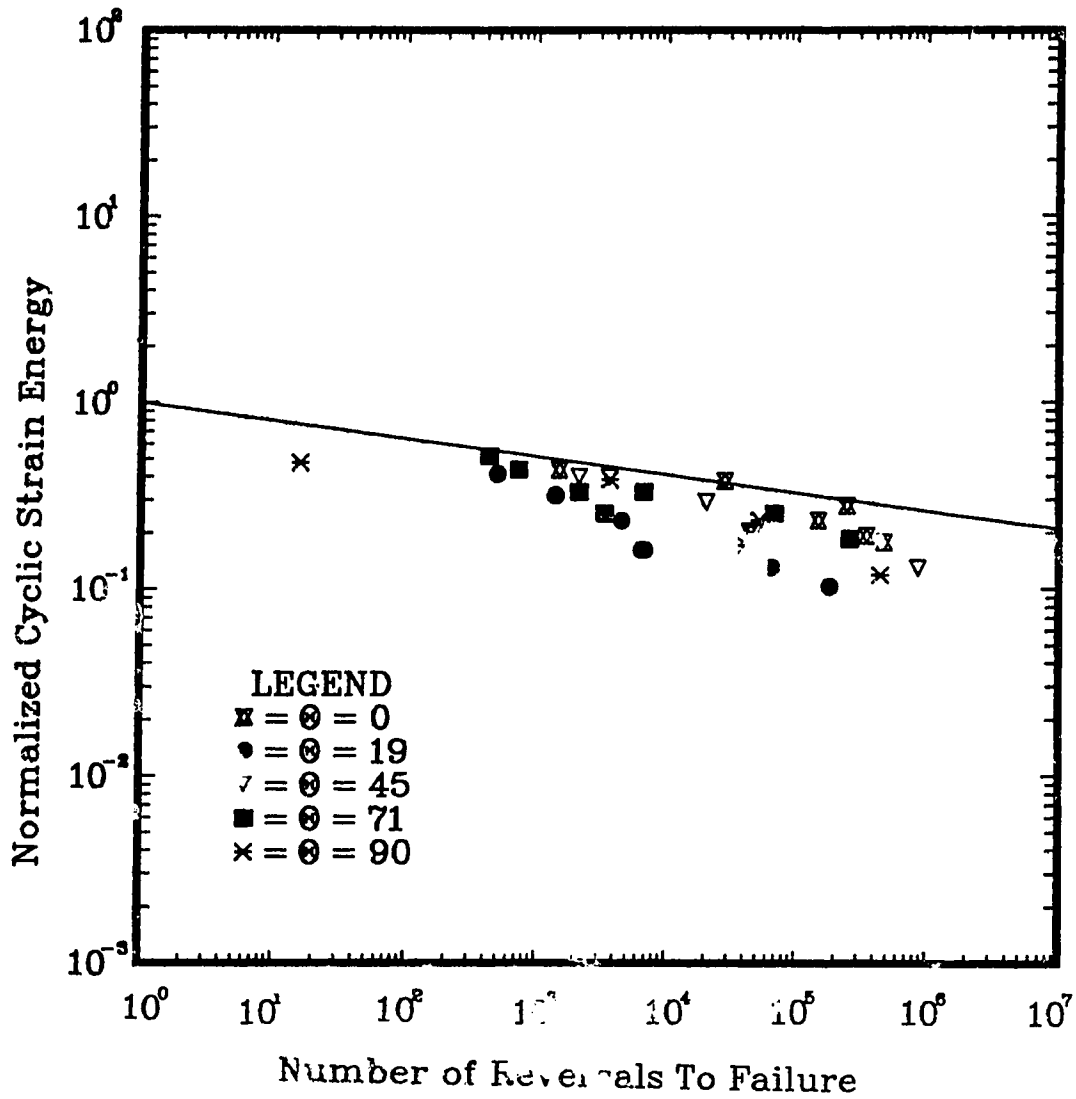


Figure 3.21: Normalized Cyclic Strain Energy vs. Number of Reversals to Failure for Various Fiber Orientation Angles and Stress Ratio of -1 (Only Tensile Loading Causes Damage)

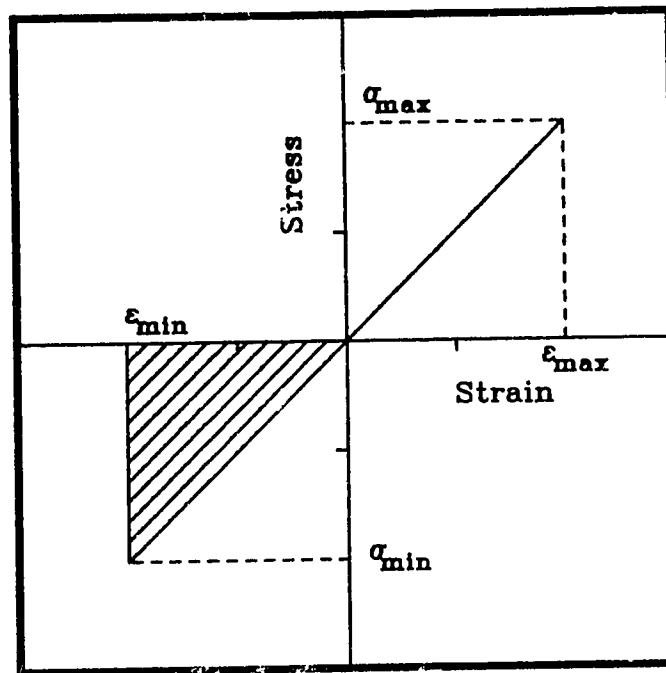


Figure 3.22: Definition of Cyclic Strain Energy for Negative Stress Ratios with Damage Associated with Compressive Stress Only

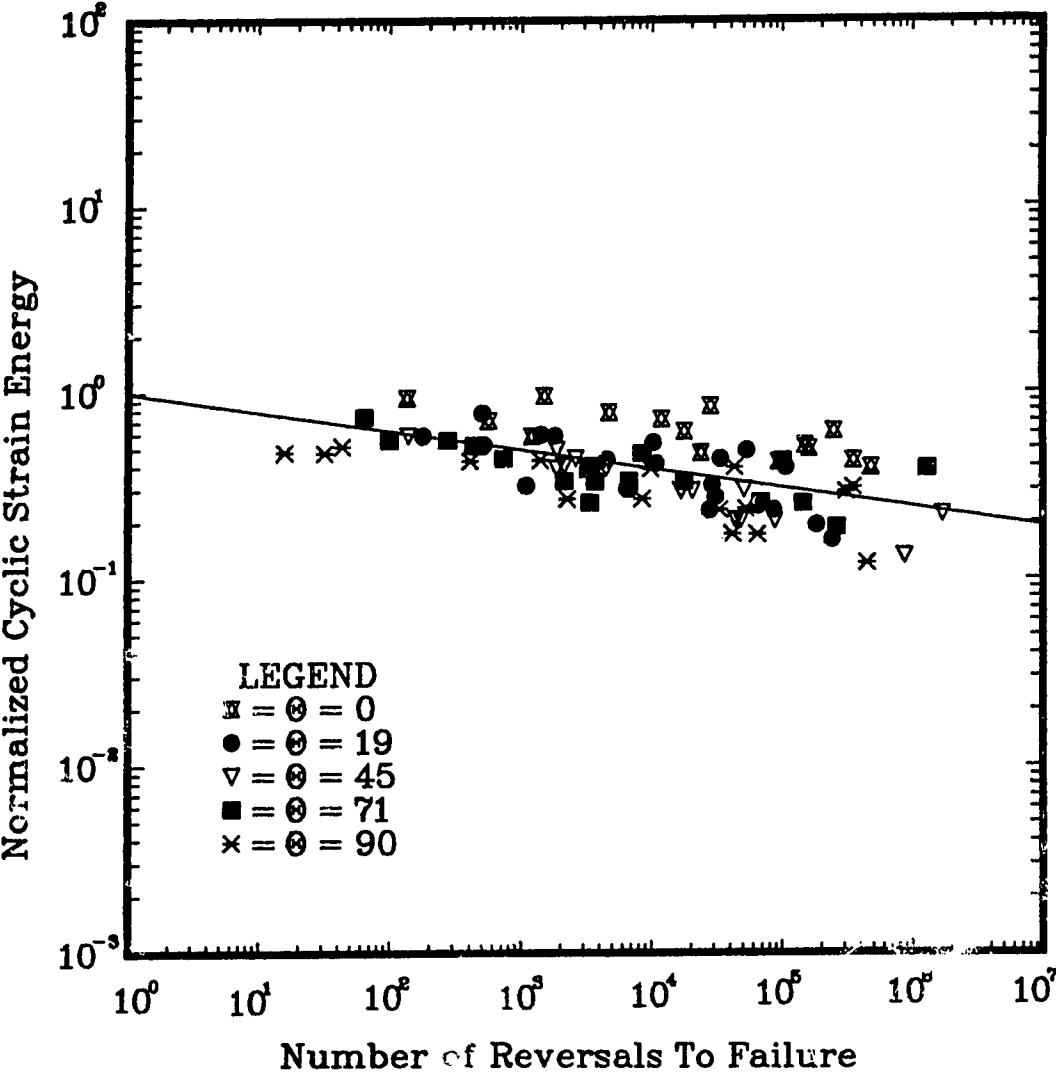


Figure 3.23: Normalized Cyclic Strain Energy vs. Number of Reversals to Failure for Various Fiber Orientation Angles and Different Stress Ratio (Positive and Negative)

To calculate the LHS of (3.20), the values of W_f^+ and W_f^- can be obtained for the required orientation from the monotonic stress-strain diagrams under uniaxial tension and compression, respectively. The value of ΔW^+ is obtained from (3.7) while the value of ΔW^- can be obtained using the compressive value of the compliance in the same equation. The RHS of (3.20) shows that, to predict the fatigue curve at any value of the stress ratio, we only need the curve for a positive (or zero) stress ratio. At least, two cyclic tests will be necessary to determine the relationship between α and the fiber orientation angle, θ , (3.10). For positive stress ratios, $\Delta W^- = 0$ which transforms (3.20) to the particular case given by (3.9).

It could be therefore concluded that, within a reasonable scatter band, the fatigue life of composite laminae for different fibers orientation angles and under various values of the stress ratio, can be predicted by (3.18) or (3.20).

3.7 Concluding Remarks

The strain energy may be used as a fatigue failure criterion for FRM. Since this parameter does not rely on the different failure modes obtained in composites, it gives equally good results independent of the failure mechanism. The relation between the strain energy and the number of reversals to failure was found to be of a power law type which applies to different material types. However, in contrast to metals, the constants are now functions of the fibers orientation angle. To include the effect of the stress ratio in this formulation, a normalized form of the strain energy (Ψ) is used (see Fig. 3.23). This parameter correlated fairly well with the experimental data for five different fibers orientation angles under three different values of the stress ratio.

For positive stress ratios, a simpler version of this relation (eq. 3.14) are shown to correlate well with the experimental data for three different composite materials: glass/epoxy, boron/aluminum and graphite/epoxy (see Figs. 3.15 - 3.17).

Chapter 4

Predicting Crack Growth Direction in Unidirectional Fiber Reinforced Composite Laminae

4.1 Introduction

A laminated component containing a cracked lamina is considered. To predict the component failure, it is necessary to determine the direction of crack growth in that lamina.

This chapter is concerned with predicting the direction of crack growth in unidirectional laminae. The material under investigation will be assumed to be elastic, homogeneous and anisotropic.

Three of the theories that have been used for predicting the direction of the crack extension in the homogeneous, anisotropic materials are: the tensor polynomial criterion [43], the minimum strain energy criterion [60] and the normal stress ratio criterion [61]. There are certain problems with each of the above mentioned criteria as will be shown later on.

A new criterion based on a critical value of the strain energy will be presented, and shown to accurately predict the direction of crack growth for the test cases considered.

4.2 Anisotropic Elasticity Analysis of Crack Tip Stress Fields

The stress analysis of an elliptical hole in an anisotropic plate can be directly related to a crack by reducing the minor axis dimension to zero. This problem has been extensively investigated since the late 1930's. A summary of these investigations can be found in [41].

Lekhnitskii's formulation of this problem, which is analogous to that of Muskhelishvili's counter-part in isotropic elasticity, is adapted in the following discussion.

For a plate made of a linear elastic anisotropic material where the plane under consideration is a plane of elastic symmetry, generalized Hooke's law can be expressed as:

$$\begin{Bmatrix} \epsilon_1 \\ \epsilon_2 \\ \gamma_{12} \end{Bmatrix} = \begin{bmatrix} A_{11} & A_{12} & A_{16} \\ A_{12} & A_{22} & A_{26} \\ A_{16} & A_{26} & A_{66} \end{bmatrix} \begin{Bmatrix} \sigma_1 \\ \sigma_2 \\ \tau_{12} \end{Bmatrix} \quad (4.1)$$

where A_{ij} are components of compliance tensor for plane stress (or plane strain).

For such a plate, shown in Fig. 4.1 the equations of stress equilibrium and strain compatibility can be represented in terms of Airy's stress function, Φ , in the familiar form:

$$\begin{aligned} A_{22} \left(\frac{\partial^4 \Phi}{\partial x^4} \right) - 2A_{26} \left(\frac{\partial^4 \Phi}{\partial x^3 \partial y} \right) + (2A_{12} + A_{66}) \left(\frac{\partial^4 \Phi}{\partial x^2 \partial y^2} \right) \\ - 2A_{16} \left(\frac{\partial^4 \Phi}{\partial x \partial y^3} \right) + A_{11} \left(\frac{\partial^4 \Phi}{\partial y^4} \right) = 0 \end{aligned} \quad (4.2)$$

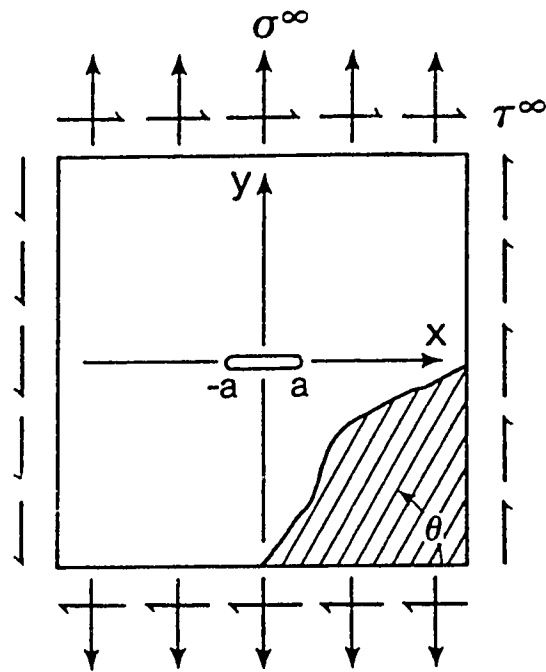


Figure 4.1: Infinite Center Cracked Plate with Far Field Stresses

The solution of equation (4.2) for an anisotropic plate containing a crack can be obtained in terms of two holomorphic functions, $U_1(Z_1)$ and $U_2(Z_2)$, of the two complex variables in the following form:

$$\Phi = 2 \Re[F_1(Z_1) + F_2(Z_2)] \quad (4.3)$$

where

$$\begin{aligned} U_1(Z_1) &= \frac{dF_1(Z_1)}{dZ_1} \\ U_2(Z_2) &= \frac{dF_2(Z_2)}{dZ_2} \end{aligned}$$

and the complex variables are defined as:

$$Z_1 = x + S_1 y \quad Z_2 = x + S_2 y \quad (4.4)$$

In (4.4) S_1 and S_2 are the roots of the characteristic equation of (4.2). These roots can be written in the form:

$$S_1 = \alpha_1 + i\beta_1 \quad S_2 = \alpha_2 + i\beta_2 \quad (4.5)$$

From these, the stress and displacement components in an anisotropic plate expressed in terms of the complex potentials $U_1(Z_1)$ and $U_2(Z_2)$ are:

$$\begin{aligned} \sigma_x &= 2\Re [S_1^2 U_1'(Z_1) + S_2^2 U_2'(Z_2)] \\ \sigma_y &= 2\Re [U_1'(Z_1) + U_2'(Z_2)] \\ \tau_{xy} &= -2\Re [S_1 U_1'(Z_1) + S_2 U_2'(Z_2)] \end{aligned} \quad (4.6)$$

and

$$\begin{aligned} u &= 2\Re [p_1 U_1(Z_1) + p_2 U_2(Z_2)] \\ v &= 2\Re [q_1 U_1(Z_1) + q_2 U_2(Z_2)] \end{aligned} \quad (4.7)$$

where

$$\begin{aligned}
 p_1 &= A_{11}S_1^2 + A_{12} - A_{16}S_1 \\
 p_2 &= A_{11}S_2^2 + A_{12} - A_{16}S_2 \\
 q_1 &= \frac{A_{12}S_1^2 + A_{22} - A_{26}S_1}{S_1} \\
 q_2 &= \frac{A_{12}S_2^2 + A_{22} - A_{26}S_2}{S_2}
 \end{aligned}$$

Using conformal mapping reduces the problem to that of obtaining the solution to the first fundamental problem for the circle. Then the holomorphic functions $U_1(\zeta_1)$ and $U_2(\zeta_2)$ which satisfy a given set of boundary conditions can be determined either by expanding them in Fourier Series or, by means of Schwartz Formula, expressed in terms of Cauchy Integrals. Assuming $\Phi = e^{x+Sv}$, the characteristic equation of 4.2 takes the form:

$$A_{11}S^4 - 2A_{16}S^3 + (2A_{12} + A_{66})S^2 - 2A_{26}S + A_{22} = 0 \quad (4.8)$$

The roots of the characteristic equation, S_1 and S_2 , are complex, and are functions of the material properties and the orientation of the crack relative to the principal material direction. Considering the case where $S_1 \neq S_2$, evaluation of the complex potential function near the crack tip yields expressions for the stress and displacement distributions of the form:

$$\begin{aligned}
 \sigma_x &= \frac{\sigma^\infty \sqrt{a}}{\sqrt{2r}} \Re \left\{ \frac{S_1 S_2}{S_1 - S_2} \left[\frac{S_2}{\psi_2^{\frac{1}{2}}} - \frac{S_1}{\psi_1^{\frac{1}{2}}} \right] \right\} + \frac{\tau^\infty \sqrt{a}}{\sqrt{2r}} \Re \left\{ \frac{1}{S_1 - S_2} \left[\frac{S_2^2}{\psi_2^{\frac{1}{2}}} - \frac{S_1^2}{\psi_1^{\frac{1}{2}}} \right] \right\} \\
 &\quad - \sigma^\infty + \sigma_x^\infty \\
 \sigma_y &= \frac{\sigma^\infty \sqrt{a}}{\sqrt{2r}} \Re \left\{ \frac{1}{S_1 - S_2} \left[\frac{S_1}{\psi_2^{\frac{1}{2}}} - \frac{S_2}{\psi_1^{\frac{1}{2}}} \right] \right\} + \frac{\tau^\infty \sqrt{a}}{\sqrt{2r}} \Re \left\{ \frac{1}{S_1 - S_2} \left[\frac{1}{\psi_2^{\frac{1}{2}}} - \frac{1}{\psi_1^{\frac{1}{2}}} \right] \right\} \\
 \tau_{xy} &= \frac{\sigma^\infty \sqrt{a}}{\sqrt{2r}} \Re \left\{ \frac{S_1 S_2}{S_1 - S_2} \left[\frac{1}{\psi_1^{\frac{1}{2}}} - \frac{1}{\psi_2^{\frac{1}{2}}} \right] \right\} + \frac{\tau^\infty \sqrt{a}}{\sqrt{2r}} \Re \left\{ \frac{1}{S_1 - S_2} \left[\frac{S_1}{\psi_1^{\frac{1}{2}}} - \frac{S_2}{\psi_2^{\frac{1}{2}}} \right] \right\}
 \end{aligned} \quad (4.9)$$

and

$$\begin{aligned}
 u &= \sigma^\infty \sqrt{2ar} \Re \left\{ \frac{1}{S_1 - S_2} \left[S_1 p_2 \psi_2^{\frac{1}{2}} - S_2 p_1 \psi_1^{\frac{1}{2}} \right] \right\} + \\
 &\quad \tau^\infty \sqrt{2ar} \Re \left\{ \frac{1}{S_1 - S_2} \left[p_2 \psi_2^{\frac{1}{2}} - p_1 \psi_1^{\frac{1}{2}} \right] \right\} \\
 v &= \sigma^\infty \sqrt{2ar} \Re \left\{ \frac{1}{S_1 - S_2} \left[S_1 q_2 \psi_2^{\frac{1}{2}} - S_2 q_1 \psi_1^{\frac{1}{2}} \right] \right\} + \\
 &\quad \tau^\infty \sqrt{2ar} \Re \left\{ \frac{1}{S_1 - S_2} \left[q_2 \psi_2^{\frac{1}{2}} - q_1 \psi_1^{\frac{1}{2}} \right] \right\}
 \end{aligned} \tag{4.10}$$

where σ^∞ and τ^∞ refer to the far field applied stresses, and

$$\begin{aligned}
 \psi_1 &= \cos \phi + S_1 \sin \phi \\
 \psi_2 &= \cos \phi + S_2 \sin \phi
 \end{aligned}$$

Compared to the isotropic case:

$$\begin{aligned}
 \sigma_x &= \frac{\sigma^\infty \sqrt{a}}{\sqrt{2r}} \cos \frac{\phi}{2} \left(1 - \sin \frac{\phi}{2} \sin \frac{3\phi}{2} \right) - \\
 &\quad \frac{\tau^\infty \sqrt{a}}{\sqrt{2r}} \sin \frac{\phi}{2} \left(2 + \cos \frac{\phi}{2} \cos \frac{3\phi}{2} \right) \\
 \sigma_y &= \frac{\sigma^\infty \sqrt{a}}{\sqrt{2r}} \cos \frac{\phi}{2} \left(1 + \sin \frac{\phi}{2} \sin \frac{3\phi}{2} \right) + \\
 &\quad \frac{\tau^\infty \sqrt{a}}{\sqrt{2r}} \sin \frac{\phi}{2} \cos \frac{\phi}{2} \cos \frac{3\phi}{2} \\
 \tau_{xy} &= \frac{\sigma^\infty \sqrt{a}}{\sqrt{2r}} \cos \frac{\phi}{2} \sin \frac{\phi}{2} \cos \frac{3\phi}{2} + \\
 &\quad \frac{\tau^\infty \sqrt{a}}{\sqrt{2r}} \cos \frac{\phi}{2} \left(1 - \sin \frac{\phi}{2} \sin \frac{3\phi}{2} \right)
 \end{aligned} \tag{4.11}$$

and

$$\begin{aligned}
u &= \frac{\sigma^\infty \sqrt{2ar}}{E} \cos \frac{\phi}{2} \left((1 - \nu) + (1 + \nu) \sin^2 \frac{\phi}{2} \right) + \\
&\quad \frac{\tau^\infty \sqrt{2ar}}{E} \sin \frac{\phi}{2} \left(2 + (1 + \nu) \cos^2 \frac{\phi}{2} \right) \\
v &= \frac{\sigma^\infty \sqrt{2ar}}{E} \sin \frac{\phi}{2} \left(2 - (1 + \nu) \cos^2 \frac{\phi}{2} \right) + \\
&\quad \frac{\tau^\infty \sqrt{2ar}}{E} \cos \frac{\phi}{2} \left((\nu - 1) + (1 + \nu) \sin^2 \frac{\phi}{2} \right)
\end{aligned} \tag{4.12}$$

As in the isotropic case, the crack tip stresses exhibit a singularity of $1/\sqrt{r}$. However, the magnitude of the stresses is not simply a function of the stress intensity factors ($K_I = \sigma^\infty \sqrt{\pi a}$ and $K_{II} = \tau^\infty \sqrt{\pi a}$). The quantities S_1 and S_2 also affect the magnitude of the stresses. This is an important difference between anisotropic and isotropic fracture. In anisotropic fracture, the magnitude of the crack tip stresses is a function of not only the applied load, specimen geometry and crack length, but also the material properties and the orientation of the crack relative to the principal material direction.

The problem under consideration (Fig. 4.2) has no restrictions as to the orientation of the crack defined by the angle α , or the principal material directions defined by the angle θ . Complete biaxial loading is allowed. The only constraint is that the crack is assumed to have a finite width. The problem defined in Fig. 4.2, can be solved by transforming the far field stresses to a crack tip coordinate system [62] as shown in Fig. 4.3, and observing that the far field stress parallel to the crack does not contribute to the singularity (this fact is discussed in [65]). The elasticity solution can then be applied to solve this general problem.

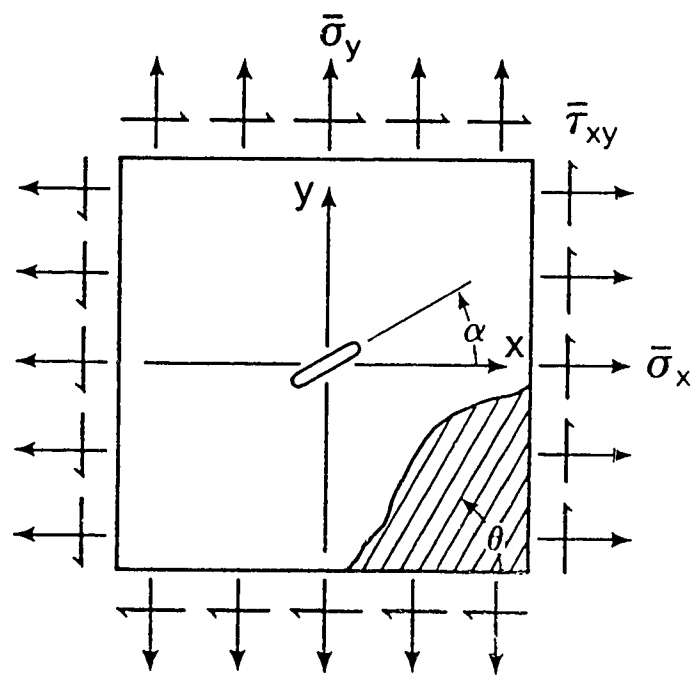


Figure 4.2: Infinite Center Cracked Plate Under Biaxial Loading

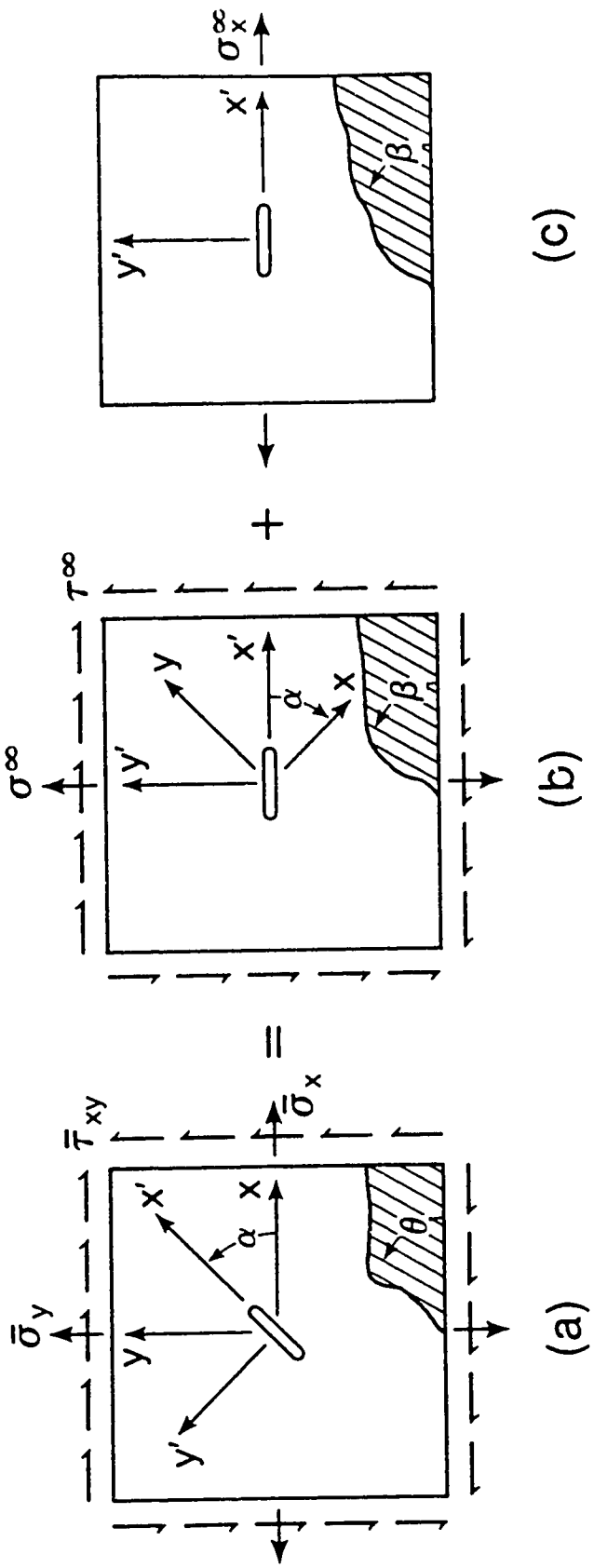


Figure 4.3: Transformation and Superposition of Far Field Stresses

(a) Total Stresses

(b) Singular Stresses

(c) Non-Singular Stresses

4.3 Criteria for Predicting Direction of Crack Growth

4.3.1 Tensor Polynomial Criterion

Tsai and Wu [43], Tennyson et al. [44], and others have presented a tensor polynomial as an anisotropic failure criterion. This criterion is based on the existence of a failure surface in the stress-space in the form of:

$$f(\sigma_i) = F_i\sigma_i + F_{ij}\sigma_i\sigma_j + F_{ijk}\sigma_i\sigma_j\sigma_k + \dots = 1 \quad (i, j, k = 1, 2, \dots, 6) \quad (4.13)$$

where

F_i, F_{ij}, F_{ijk} are strength tensors of second, fourth and sixth order respectively, and

σ_i is the contracted form of the stress tensor.

See the review by Labossière and Neale [42] for a discussion of various tensor polynomial criteria. The application of the tensor polynomial to fracture problems utilizes the assumption that the direction of crack extension corresponds to the radial direction of maximum $f(\sigma_i)$. The stress components, σ_i , must be evaluated at a finite distance, r_o , from the crack tip.

4.3.2 Minimum Strain Energy Criterion (MSE)

The minimum strain energy criterion is based on variations in the energy stored along the boundary of a core region surrounding a crack. This criterion was first proposed by Sih [66] for isotropic fracture and later modified for the application to anisotropic problems [60]. Sih defined the strain energy factor, S , by the expression:

$$W = \left(\frac{dU}{dV} \right) = \frac{S}{r} \quad (4.14)$$

where

(dU/dV) is the strain energy function, and

r is the radial distance from the crack tip.

For plane stress problems, the strain energy function can be expressed in terms of the stresses and strains near the crack tip as:

$$W = (\sigma_x \epsilon_x + \sigma_y \epsilon_y + \tau_{xy} \gamma_{xy})/2 \quad (4.15)$$

As a result, the strain energy factor can be defined explicitly as:

$$S = r (\sigma_x \epsilon_x + \sigma_y \epsilon_y + \tau_{xy} \gamma_{xy})/2 \quad (4.16)$$

The factor S was interpreted as the area under the (dU/dV) versus r curve [67].

The basic postulates of the minimum strain energy criterion are:

a) failure by fracture is assumed to initiate at sites corresponding to the maximum value of the local minima of the strain energy function, i.e.

$$\left[\left(\frac{dU}{dV} \right)_{min} \right]^{max} \text{ at } \phi = \phi_c \quad (4.17)$$

b) crack extension occurs when $(dU/dV)_{min}$ reaches its respective critical value:

$$\left[\left(\frac{dU}{dV} \right)_{min} \right]^{max} = \left(\frac{dU}{dV} \right)_c \quad (4.18)$$

c) postulates (a) & (b) are sufficient for determining where and when unstable crack propagation occurs in a two-dimensional problem in which all the elements at the same distance r_c from the straight crack front are assumed to fail simultaneously. In the three-dimensional case, the crack front is generally curved and the distance r_c may vary from one point on the crack border to the next. The location of the initial fracture points is described by a locus of elements with coordinates determined in accordance with the following conditions:

$$\left(\frac{dU}{dV} \right)_c = \frac{S_1}{r_1} = \frac{S_2}{r_2} = \dots = \frac{S_j}{r_j} = \dots = \frac{S_c}{r_c} \quad (4.19)$$

such that for unstable fracture:

$$r_1 < r_2 < \dots < r_j < \dots < r_c$$

and

$$S_1 < S_2 < \dots < S_j < \dots < S_c$$

4.3.3 Normal Stress Ratio Criterion (NSR)

Buczek and Herakovich [61] have proposed the normal stress ratio as a crack growth criterion. Using the isotropic results, where the cracks generally grow in the direction of the maximum normal stress, their model assumes that the direction of crack growth is controlled by the ratio of normal stress to tensile strength on a given plane. The normal stress ratio is defined as:

$$R(r_o, \phi) = \frac{\sigma_{\phi\phi}}{T_{\phi\phi}} \quad (4.20)$$

where

$\sigma_{\phi\phi}$ normal stress acting on the radial plane defined by ϕ at a distance r_o from the crack tip (Fig. 4.4), and

$T_{\phi\phi}$ tensile strength on the plane ϕ .

Buczek and Herakovich postulated that the crack will grow along the plane for which this ratio is maximum. Since the strength $T_{\phi\phi}$ on an arbitrary plane is very difficult to measure, they defined it as:

$$T_{\phi\phi} = X_T \sin^2 \gamma + Y_T \cos^2 \gamma \quad (4.21)$$

where

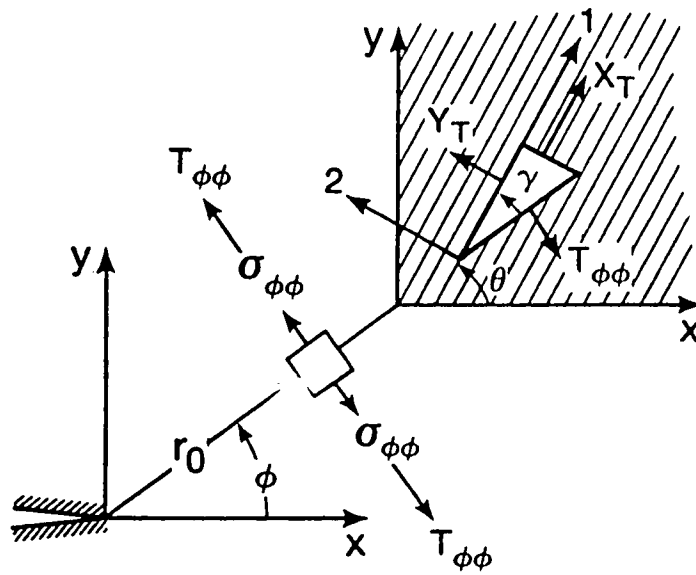


Figure 4.4: Normal Stress Ratio Parameters

X_T the longitudinal tensile strength of the material

Y_T the transverse tensile strength of the material

γ the angle from the plane of interest to the fiber direction (Fig. 4.4).

The definition of $T_{\phi\phi}$ satisfies the following necessary conditions:

- a) for isotropic materials, $T_{\phi\phi}$ does not depend on ϕ .
- b) for crack growth parallel to the fibers in a composite material, $T_{\phi\phi}$ is equal to the transverse tensile strength, Y_T .
- c) for crack growth perpendicular to the fibers of a composite material, $T_{\phi\phi}$ is equal to the longitudinal strength, X_T .

4.3.4 Critical Strain Energy Method - Present Criterion (CSE)

The critical strain energy method is based on the assumption that crack initiation takes place when the value of the strain energy defined by 4.15 reaches a critical value, i.e.

$$W = (\sigma_x \epsilon_x + \sigma_y \epsilon_y + \tau_{xy} \gamma_{xy})/2 = W_{crit} \quad (4.22)$$

The value of W will depend on the material properties and the fibers direction. The direction of crack growth will correspond to the radial direction having the maximum value of the strain energy. Thus the direction of crack extension $\phi = \phi_c$, is obtained from :

$$\frac{\partial W}{\partial \phi} = 0 \quad \text{and} \quad \frac{\partial^2 W}{\partial \phi^2} < 0 \quad (4.23)$$

It should be stated that although both Sih's method and the present criterion use strain energy as a criterion for crack growth direction, each method utilize a unique interpretation, c.f. 4.17 - 4.19 and 4.23. The physical basis of the proposed criterion is as follows: When a material element is loaded by an external agency, part of the

supplied energy is dissipated into heat and the remaining part is stored in the material. Damage is caused by the irrecoverable part of the stored energy [63], i.e.

$$dW_{\text{damage}} = dW_{\text{supplied}} - (dQ + dW_{\text{recoverable}}) \quad (4.24)$$

Each material has certain capacity to absorb damage, and failure results as a result of damage accumulation. Because of the difficulty in measuring the heat loss, dQ , it is generally assumed that damage is proportional to the supplied energy, i.e.

$$dW_{\text{damage}} \propto dW_{\text{supplied}} \quad (4.25)$$

In front of the crack, the strain energy varies with the distance r and angle ϕ . Its variation at the crack tip, $r \ll a$, can be calculated from 4.22. Crack propagation will ensue when the strain energy reaches the material critical value (absorption capacity), W_{crit} . The location at which this critical value is first reached is obviously the one where the strain energy is maximum, i.e. condition 4.23.

4.4 Analysis of Off-Axis Unidirectional Tensile Coupons

Numerical results (from [62, 68] and from the present criterion) are presented for graphite-epoxy tensile coupons containing central cracks. Lamina properties of the material considered, as well as specimen dimensions, are given in [62, 68].

In comparing the predictions of aforementioned criteria for the crack growth direction, the tensor polynomial criterion will be excluded. This is mainly due to the dramatic dependence of the results of this method on the distance from the crack tip, r_0 . Herakovich et al. [62] have shown that a small change in the value of r_0 can affect the predicted crack growth direction by as much as 40° .

The independence of ϕ_c from r_0 allows the prediction of the crack extension direction in unidirectional composites without prior knowledge of a proper r_0 .

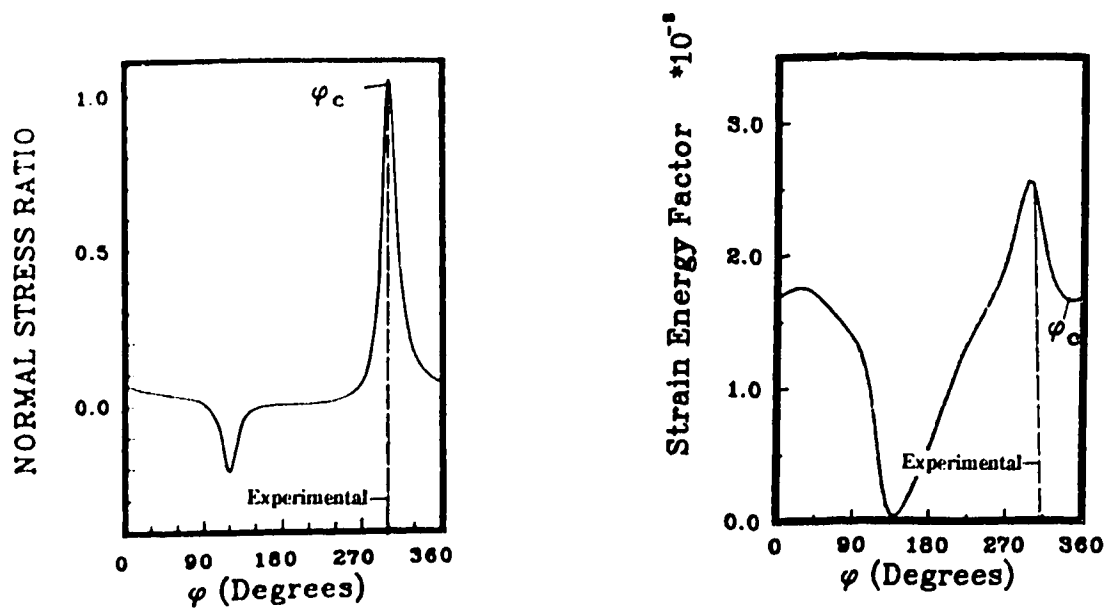
Table 4.1: Comparison Between Different Criteria and Experimental Results for Off-Axis Unidirectional Coupons

Test Data	N S R	M S E	C S E	Experimental Results
Case(1): T300/5208 $\theta = 120^\circ$ $\alpha = 0^\circ$ $2a = 5.08mm$ $r_o = 0.05mm$ $\sigma_y = 6.9MPa$	301°	350°	296°	300°
Case(2): AS4/3501-6 $\theta = 105^\circ$ $\alpha = 0^\circ$ $2a = 5.08mm$ $r_o = 0.05mm$ $\sigma_y = 6.9MPa$	286°	60°	284°	285°
Case(3): AS4/3501-6 $\theta = 120^\circ$ $\alpha = 15^\circ$ $2a = 5.08mm$ $r_o = 0.05mm$ $\sigma_y = 6.9MPa$	271°	320°	270°	270°
Case(4): AS4/3501-6 $\theta = 90^\circ$ $\alpha = 0^\circ$ $2a = 0.255mm$ $r_o = 1.064mm$ $\sigma_y = 6.9MPa$	88°	15°	87°	90°

value. The remaining three methods are compared with the experimental results of different off-axis tests in Table 4.1.

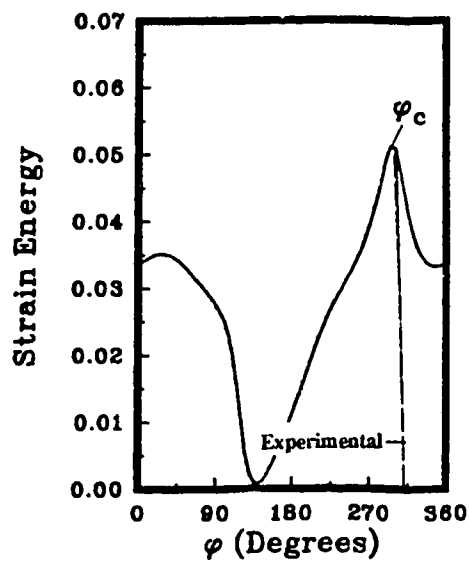
It is noted that the present model (critical strain energy) predictions are very consistent with the experimental results. This is in contrast to the minimum strain energy criterion of Sih which was shown in [62] as well as in Table 4.1, to be inconsistent in predicting the direction of crack growth.

The variation of the three crack growth criteria as a function of ϕ , for the various tests are shown in Fig. 4.5 through Fig. 4.7.



(a)

(b)



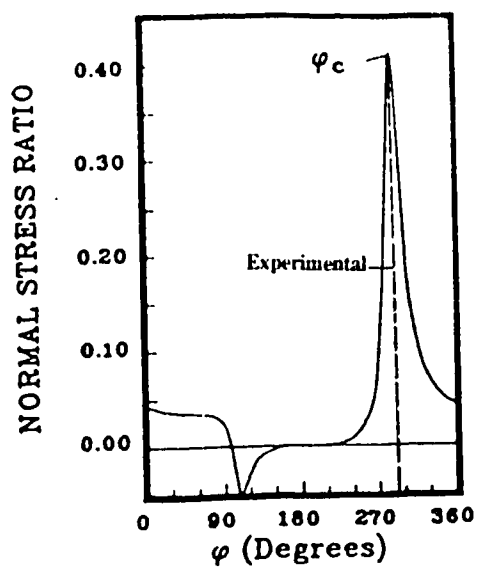
(c)

Figure 4.5: Variation of Crack Growth Criteria as a Function of ϕ for 30° Off-Axis Graphite/Epoxy Coupons.(case 1)

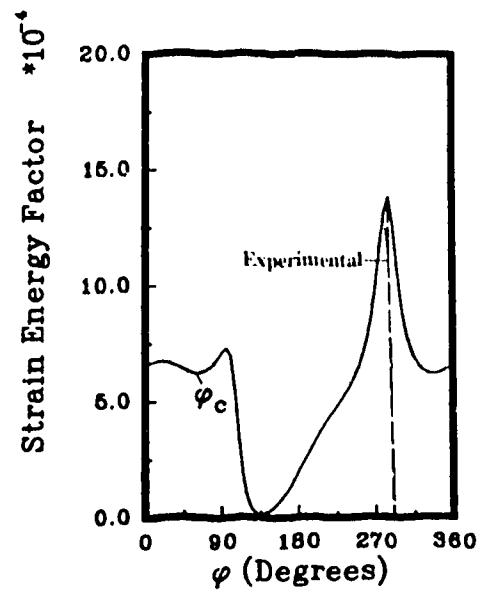
(a) Normal Stress Ratio

(b) Minimum Strain Energy

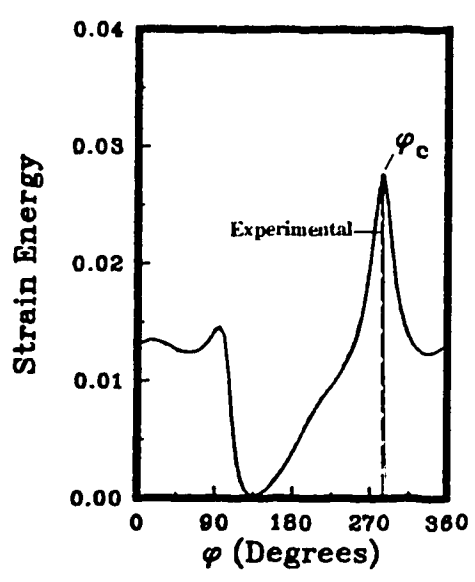
(c) Critical Strain Energy (present model)



(a)

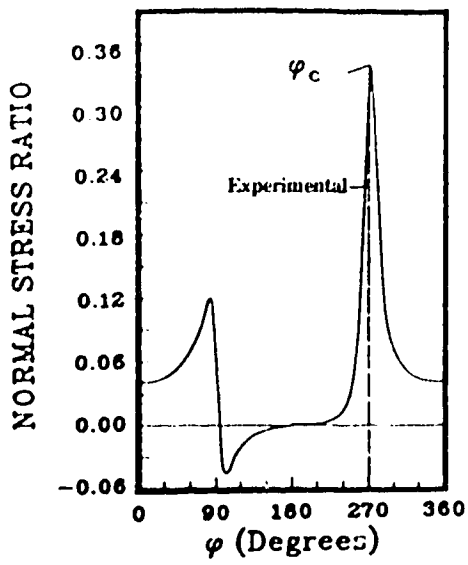


(b)

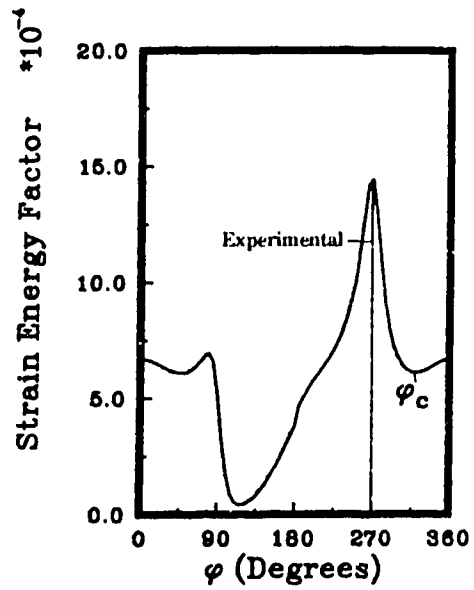


(c)

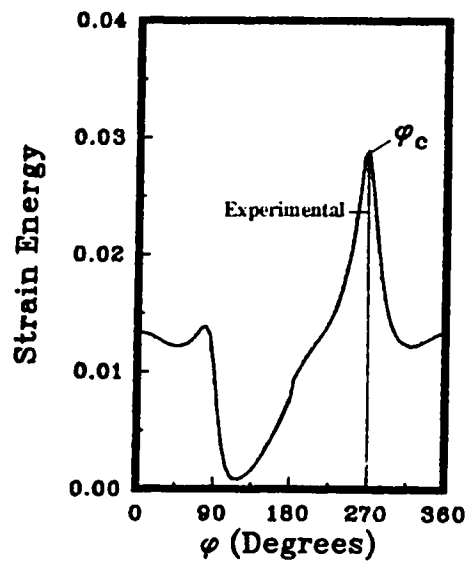
Figure 4.6: Variation of Crack Growth Criteria as a Function of ϕ for 15° Off-Axis Graphite/Epoxy Coupons.(case 2)
(a) Normal Stress Ratio
(b) Minimum Strain Energy
(c) Critical Strain Energy (present model)



(a)



(b)



(c)

Figure 4.7: Variation of Crack Growth Criteria as a Function of ϕ for 15° Off-Axis Graphite/Epoxy Coupons.(case 3)
 (a) Normal Stress Ratio
 (b) Minimum Strain Energy
 (c) Critical Strain Energy (present model)

In another work, Zhang et al. [64] presented a strain energy ratio criterion for composite materials. They compared that criterion with some of the well-known criteria (NSR, MSE, Tsai-Hill) for two types of materials: graphite fiber reinforced epoxy AS4/3501-6 and glass fiber reinforced polyester (GRP). Tables 4.2 and 4.3 show a comparison between the present method (CSE) and the aforementioned criteria. Once more the present method seems to compare very well with other presented methods except for one case (GRP with $\beta = 30^\circ$). The discrepancy observed for that case can be related to the properties of the GRP used. Although the ratio between the moduli of elasticity in both principal directions (E_1/E_2) is about 3.0, the ratio between the material strengths in the same directions (S_{y_1}/S_{y_2}) is 65.7 (For the AS4/3501-6 material, these ratios were 11.1 and 28.2 respectively). This might suggest that the material properties reported for this case could be inaccurate.

Table 4.2: Comparison Between Different Criteria for Off-Axis AS4/3501-6 Unidirectional Coupons

Orientation	N S R	M S E	S E R	C S E
$\beta = 5^\circ$	6.75°	40.5°	8.7°	5°
$\beta = 45^\circ$	43.5°	87°	38.5°	50°
$\beta = 105^\circ$	100.5°	59°	112°	104°

Table 4.3: Comparison Between Different Criteria for Off-Axis GRP Unidirectional Coupons

Orientation	N S R	Tsai-Hill	S E R	C S E
$\beta = 30^\circ$	30°	26°	27°	301°
$\beta = 45^\circ$	45°	39°	39°	52°
$\beta = 60^\circ$	60°	52°	52°	64°

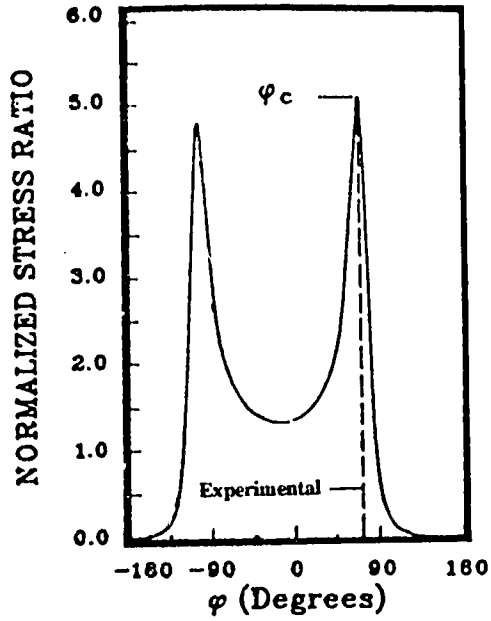
4.5 Unidirectional Laminae Subjected to Mixed-Mode Loading

In an attempt to verify the consistency of the proposed critical strain energy criterion, and to study crack growth of fibrous composites under more general loading conditions, unidirectional laminae were analyzed for various mixed-mode loading. The predicted values of ϕ_c , together with the experimental results [68, 69] are presented in Table 4.4.

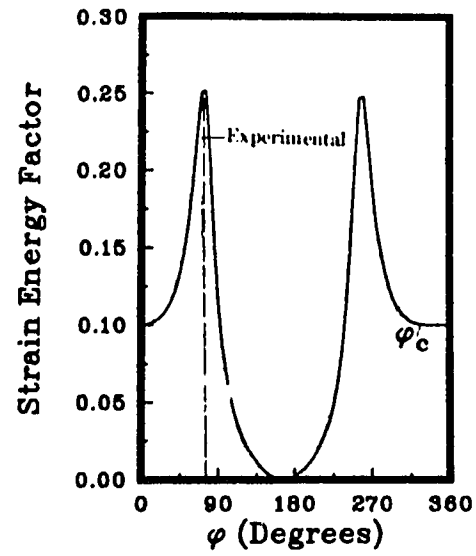
From the comparison, it is clear that the present model yields good predictions of the crack growth direction for all of the five cases studied. The variation of the crack growth criteria as a function of ϕ , for some of the cases presented in Table 4.4, are shown in Fig. 4.8 through Fig. 4.11.

Table 4.4: Comparison Between Different Criteria and Experimental Results for Unidirectional Laminae Subjected to Mixed-Mode Loading

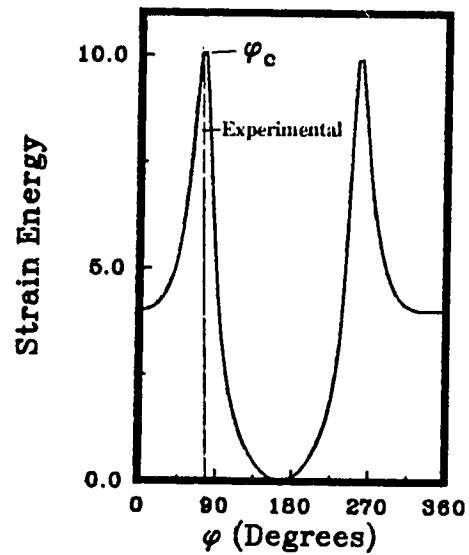
Test Data	N S R	M S E	C S E	Experimental Results
Case(5): AS4/3501-6 $\theta = 75^\circ$ $\alpha = 0^\circ$ $2a = 5.08mm$ $r_o = 0.05mm$ $\sigma_y = 110MPa$ $\tau_{xy} = 24.3MPa$	72°	335°	73°	75°
Case(6): AS4/3501-6 $\theta = 75^\circ$ $\alpha = -15^\circ$ $2a = 5.08mm$ $r_o = 0.05mm$ $\sigma_y = 110MPa$ $\tau_{xy} = 24.3MPa$	88°	20°	88°	90°
Case(7): AS4/3501-6 $\theta = 75^\circ$ $\alpha = 0^\circ$ $2a = 5.08mm$ $r_o = 0.05mm$ $\sigma_y = 76MPa$ $\tau_{xy} = 8MPa$	73°	315°	75°	75°
Case(8): AS4/3501-6 $\theta = 75^\circ$ $\alpha = -15^\circ$ $2a = 5.08mm$ $r_o = 0.05mm$ $\sigma_y = 76MPa$ $\tau_{xy} = 8MPa$	88°	330°	90°	90°
Case(9): AS4/3501-6 $\theta = 75^\circ$ $\alpha = -15^\circ$ $2a = 5.08mm$ $r_o = 0.05mm$ $\sigma_y = 65MPa$ $\tau_{xy} = 2.6MPa$	88°	320°	90°	90°



(a)



(b)



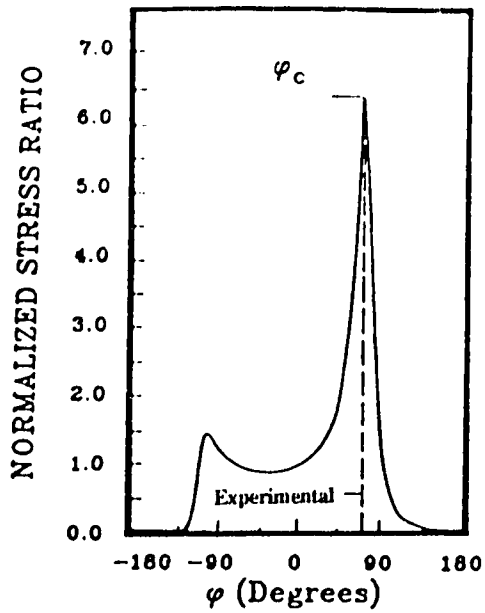
(c)

Figure 4.8: Variation of Crack Growth Criteria as a Function of ϕ for 15° Off-Axis Graphite/Epoxy Coupons.(case 5)

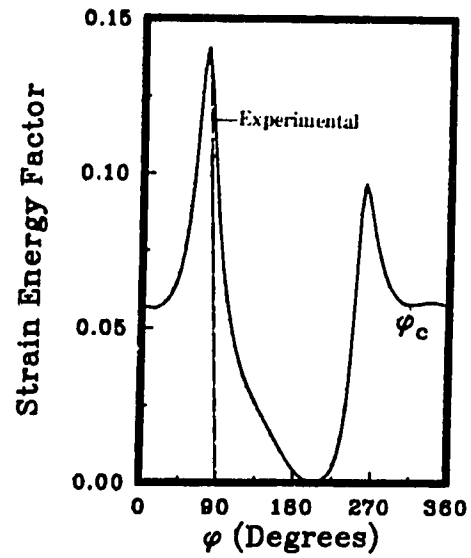
(a) Normal Stress Ratio

(b) Minimum Strain Energy

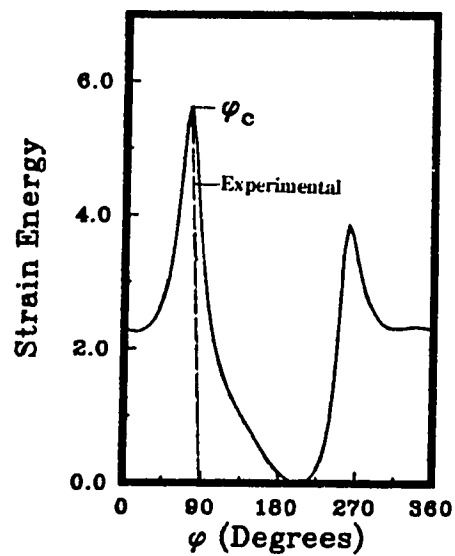
(c) Critical Strain Energy (present model)



(a)



(b)



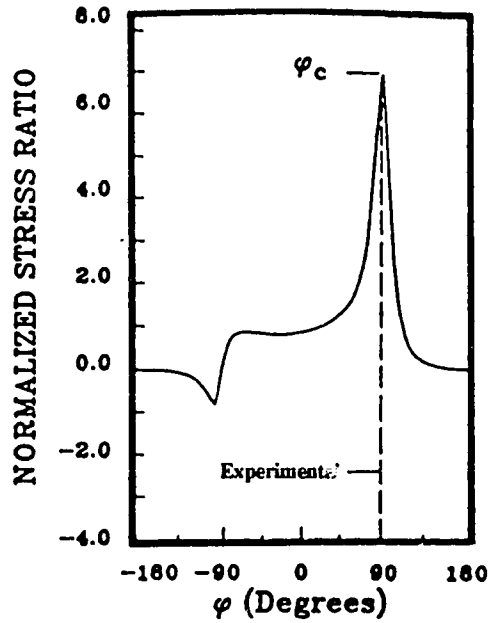
(c)

Figure 4.9: Variation of Crack Growth Criteria as a Function of ϕ for 15° Off-Axis Graphite/Epoxy Coupons.(case 7)

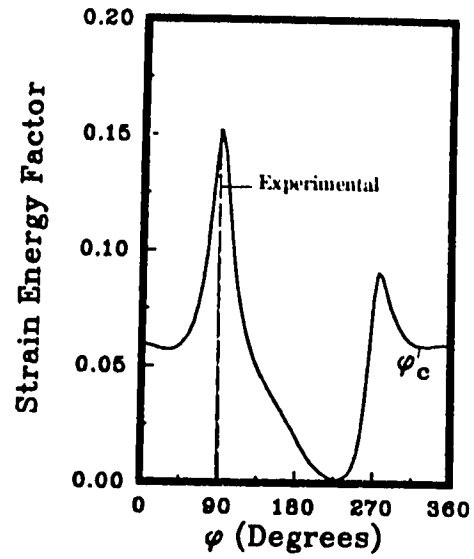
(a) Normal Stress Ratio

(b) Minimum Strain Energy

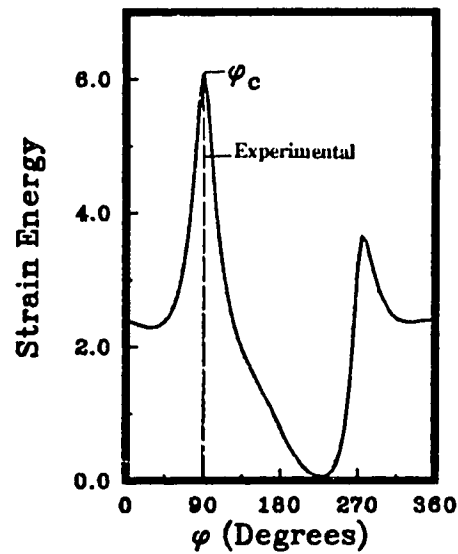
(c) Critical Strain Energy (present model)



(a)



(b)



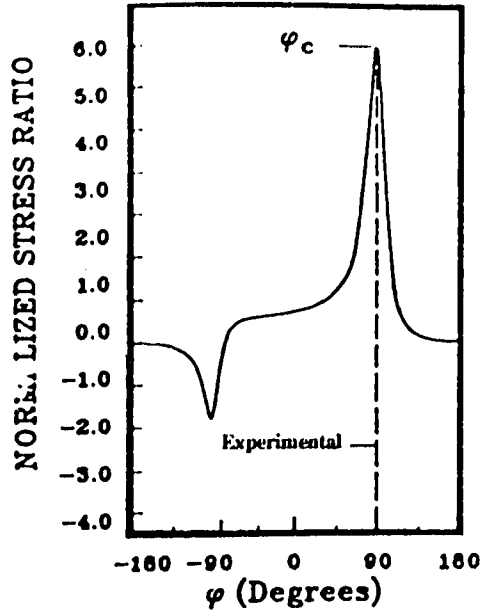
(c)

Figure 4.10: Variation of Crack Growth Criteria as a Function of ϕ for 15° Off-Axis Graphite/Epoxy Coupons.(case 8)

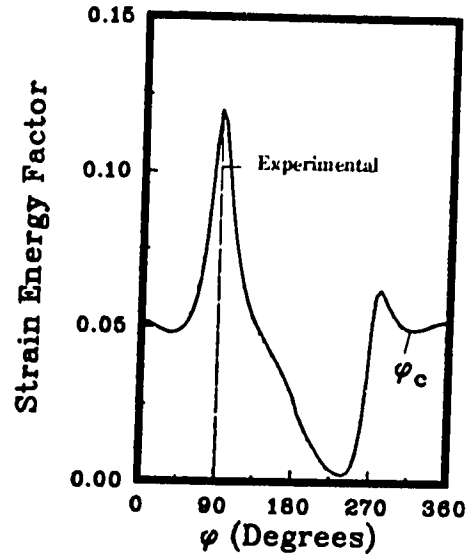
(a) Normal Stress Ratio

(b) Minimum Strain Energy

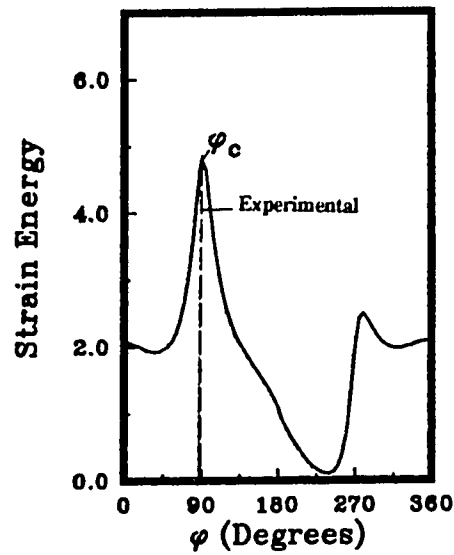
(c) Critical Strain Energy (present model)



(a)



(b)



(c)

Figure 4.11: Variation of Crack Growth Criteria as a Function of ϕ for 15° Off-Axis Graphite/Epoxy Coupons.(case 9)

(a) Normal Stress Ratio

(b) Minimum Strain Energy

(c) Critical Strain Energy (present model)

4.6 Limitations of the Normal Stress Ratio Criterion

Although the normal stress ratio criterion gives results comparable to those obtained when using the critical strain energy method, it has some limitations.

The case illustrated in Fig. 4.12 is that of an infinite unidirectional graphite-epoxy plate with a center-crack along the fibers direction and subjected to pure shear loading in the coordinate system of the crack. For the positive shear case illustrated, the direction of crack extension measured with respect to the crack predicted by the normal stress ratio theory is -12° if the theory is applied within the sharp crack analysis of Lekhnitskii.

For this loading case, it appears that the normal stress ratio theory is incapable of correctly predicting the direction of crack extension obtained from the experiments.

Beuth and Herakovich [70] mentioned that this result was valid for any notched anisotropic material regardless of its elastic and/or strength properties. They thus concluded that the apparent discrepancy between the theory's prediction and the experimental behaviour for this case was not due to potential inaccuracies, but instead due to a fundamental error in either the theory itself or in its method of application within the sharp crack analysis.

When using the critical strain energy criterion to predict the crack growth direction of that same problem, the value obtained was similar to the experimental value for that case (0°).

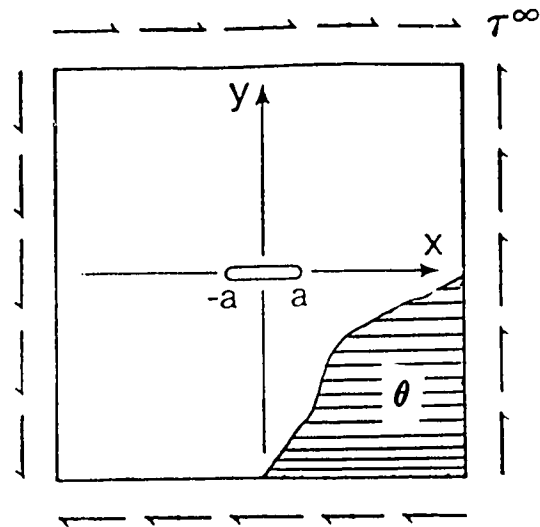


Figure 4.12: Infinite Center Plate Under Pure Shear Far-Field Stress

4.7 Concluding Remarks

A criterion based on the critical strain energy has been presented to predict the crack growth direction in a lamina.

The comparison of the experimental results with the different criteria for the crack growth direction indicates that the proposed critical strain energy method can be used to analyze the problem of a through-the-thickness central crack in a unidirectional composite.

The present approach leads to more consistent results than the minimum strain energy of Sih [60]. The advantage of the energy approach is in its universality by being a frame indifferent quantity. It is more general than the normal stress ratio criterion since it can be used even if inelastic behaviour are considered. In the elastic case, both methods give very comparable results.

Chapter 5

Theory of Symmetric Anisotropic Laminated Elastic Plates

5.1 Introduction

As mentioned in chapters 3 and 4, using the strain energy density criterion for a lamina was a first step towards using this criterion for a laminate. But to calculate the strain energy density of a laminate, the values of all stress components (including interlaminar stresses) must be determined.

The Classical Laminate Theory (CLT) described by, for example, Jones [1] is the most commonly used approach to the stress analysis of laminated elastic plates. This theory replaces the laminated plate by an equivalent plate of the same overall geometry with elastic constants which are appropriate weighted averages of the elastic constants of the individual laminae.

Although this theory gives satisfactory results for the mid-surface deflection of a plate, the average in-plane displacement and stress components, it gives no information about either the through-the-thickness distribution of stresses and displacements or the values of the interlaminar shear stresses. A more refined theory

of laminates is required to provide that missing information.

A second approach for obtaining this required information is through numerical techniques. Three dimensional numerical solutions have been obtained using either finite elements [71] or finite difference [72] methods. These methods provide accurate results but require a large number of computations which might be beyond the capacity of the available computer.

To get an analytical three dimensional solution, the so-called *higher-order theories* have been used [73] - [76]. In these theories, the displacement components are approximated through the plate thickness by polynomials in z , the coordinate normal to the plate.

Bonser [77] showed that this approach sometimes gave unsatisfactory results. Some of those theories fail to satisfy shear continuity conditions at the interlaminar interfaces while others do not satisfy the zero shear condition on the lateral surfaces.

Spencer et al. [78] presented an elasticity theory for isotropic elastic plates. In their work, a two dimensional CLT based on the equivalent plate was used to generate a three dimensional solution in each lamina of the laminate. The two dimensional solution could be obtained using any analytical or numerical method for solving plane elastic problems. The final solution was found to satisfy all traction and displacement continuity conditions at the interfaces as well as the zero traction condition on the lateral surfaces.

Two approximations were involved: The edge boundary conditions were specified only on an average rather than point-by-point, and the value of σ_{zz} , the stress in the direction normal to the laminate was assumed to be zero throughout the laminate. The expansion of this method to the anisotropic case was introduced without too many details in [79].

In this chapter, a generalization of the approach presented in [78] will be attempted in detail for the case of anisotropic laminates. The distribution of σ_{zz}

throughout the laminate will also be considered rather than assuming that this component of the stress is non-existent.

5.2 Stress-Strain Relation for an Orthotropic Lamina in the Principal Directions of a Laminate

Let us consider an anisotropic linear elastic layer; using cartesian coordinates X, Y, Z such that $Z = 0$ coincides with the mid-plane of that layer. U, V and W denote the displacement components in the X, Y and Z directions respectively.

The stress-strain relation for such a layer could be expressed as:

$$\begin{Bmatrix} \sigma_{xx} \\ \sigma_{yy} \\ \sigma_{zz} \\ \sigma_{yz} \\ \sigma_{xz} \\ \sigma_{xy} \end{Bmatrix} = \begin{bmatrix} C_{11} & C_{12} & C_{13} & 0 & 0 & C_{16} \\ C_{12} & C_{22} & C_{23} & 0 & 0 & C_{26} \\ C_{13} & C_{23} & C_{33} & 0 & 0 & C_{36} \\ 0 & 0 & 0 & C_{44} & C_{45} & 0 \\ 0 & 0 & 0 & C_{45} & C_{55} & 0 \\ C_{16} & C_{26} & C_{36} & 0 & 0 & C_{66} \end{bmatrix} \begin{Bmatrix} U_{,X} \\ V_{,Y} \\ W_{,Z} \\ (V_{,Z} + W_{,Y}) \\ (U_{,Z} + W_{,X}) \\ (U_{,Y} + V_{,X}) \end{Bmatrix} \quad (5.1)$$

where a comma denotes partial differentiation with respect to the suffix variables.

Using a method similar to the classical approximate solution of the three dimensional problem attributed to Kirchhoff and used by Reissner [80], we assume $\sigma_{zz} = 0$ in the constitutive relations (5.1). This will lead to:

$$C_{13}U_{,X} + C_{23}V_{,Y} + C_{33}W_{,Z} + C_{36}(U_{,Y} + V_{,X}) = 0 \quad (5.2)$$

or,

$$W_{,Z} = -(1/C_{33}) [C_{13}U_{,X} + C_{23}V_{,Y} + C_{36}(U_{,Y} + V_{,X})] \quad (5.3)$$

Relation 5.3 implies that the strain in the Z -direction is related to the plane components of the strain (Reissner neglected the effect of $\sigma_{xz}, \sigma_{yz}, \sigma_{zz}$ in the constitutive relations).

Substituting from 5.3 into the first, second and sixth equations of 5.1, we get:

$$\begin{aligned}
 \sigma_{xx} &= \left(C_{11} - \frac{C_{13}^2}{C_{33}} \right) U_{,X} + \left(C_{12} - \frac{C_{23}C_{13}}{C_{33}} \right) V_{,Y} + \left(C_{16} - \frac{C_{13}C_{36}}{C_{33}} \right) (U_{,Y} + V_{,X}) \\
 \sigma_{yy} &= \left(C_{12} - \frac{C_{13}C_{23}}{C_{33}} \right) U_{,X} + \left(C_{22} - \frac{C_{23}^2}{C_{33}} \right) V_{,Y} + \left(C_{26} - \frac{C_{23}C_{36}}{C_{33}} \right) (U_{,Y} + V_{,X}) \\
 \sigma_{xy} &= \left(C_{16} - \frac{C_{13}C_{36}}{C_{33}} \right) U_{,X} + \left(C_{26} - \frac{C_{23}C_{36}}{C_{33}} \right) V_{,Y} + \left(C_{66} - \frac{C_{36}^2}{C_{33}} \right) (U_{,Y} + V_{,X})
 \end{aligned} \tag{5.4}$$

Define

$$Q_{ij} = C_{ij} - \frac{C_{i3}C_{j3}}{C_{33}} \quad (i, j = 1, 2, 6)$$

The stress-strain relations will now have the form:

$$\begin{pmatrix} \sigma_{xx} \\ \sigma_{yy} \\ \sigma_{zz} \\ \sigma_{yz} \\ \sigma_{zx} \\ \sigma_{xy} \end{pmatrix} = \begin{bmatrix} Q_{11} & Q_{12} & 0 & 0 & 0 & Q_{16} \\ Q_{12} & Q_{22} & 0 & 0 & 0 & Q_{26} \\ 0 & 0 & 0 & 0 & 0 & 0 \\ 0 & 0 & 0 & C_{44} & C_{45} & 0 \\ 0 & 0 & 0 & C_{45} & C_{55} & 0 \\ Q_{16} & Q_{26} & 0 & 0 & 0 & Q_{66} \end{bmatrix} \begin{pmatrix} U_{,X} \\ V_{,Y} \\ W_{,Z} \\ (V_{,Z} + W_{,Y}) \\ (U_{,Z} + W_{,X}) \\ (U_{,Y} + V_{,X}) \end{pmatrix} \tag{5.5}$$

Although it was assumed that $\sigma_{zz} \approx 0$, its gradient, $\sigma_{zz,Z}$, need not be zero, the three dimensional equilibrium can then be written as:

$$\begin{aligned}
 \sigma_{xx,X} + \sigma_{xy,Y} + \sigma_{xz,Z} &= 0 \\
 \sigma_{xy,X} + \sigma_{yy,Y} + \sigma_{yz,Z} &= 0 \\
 \sigma_{xz,X} + \sigma_{yz,Y} + \sigma_{zz,Z} &= 0
 \end{aligned} \tag{5.6}$$

The above implies that while σ_{zz} may be small, its gradient need not be small.

5.3 Analysis of Stress and Deformation in a Homogeneous Layer

A distinction should be made between a homogeneous layer and a plate, which can be an assemblage of a number of layers of different materials. Consider a layer with uniform thickness $2h$, and define the following non-dimensional variables:

$$x = X/a \quad y = Y/a \quad z = Z/h$$

$$u = U/a \quad v = V/a \quad w = W/a$$

where a is a typical in-plane linear dimension.

Note that the plane $Z = 0$ (or $z = 0$) coincides with the mid-plane of the layer while $z = \pm 1$ coincide with the upper and lower surfaces of the layer respectively.

Define a non-dimensional parameter ϵ as:

$$\epsilon = h/a$$

which leads to:

$$z = Z/a\epsilon$$

writing 5.5 in terms of the non-dimensional variables, the stress-strain relation takes the form:

$$\begin{pmatrix} \sigma_{xx} \\ \sigma_{yy} \\ \sigma_{zz} \\ \sigma_{yz} \\ \sigma_{xz} \\ \sigma_{xy} \end{pmatrix} = \begin{bmatrix} Q_{11} & Q_{12} & 0 & 0 & 0 & Q_{16} \\ Q_{12} & Q_{22} & 0 & 0 & 0 & Q_{26} \\ 0 & 0 & 0 & 0 & 0 & 0 \\ 0 & 0 & 0 & C_{44} & C_{45} & 0 \\ 0 & 0 & 0 & C_{45} & C_{55} & 0 \\ Q_{16} & Q_{26} & 0 & 0 & 0 & Q_{66} \end{bmatrix} \begin{pmatrix} u_{,x} \\ v_{,y} \\ w_{,z} \\ (\epsilon^{-1}v_{,z} + w_{,y}) \\ (\epsilon^{-1}u_{,z} + w_{,x}) \\ (u_{,y} + v_{,x}) \end{pmatrix} \quad (5.7)$$

The equations of equilibrium become:

$$\begin{aligned}
 \sigma_{xx,x} + \sigma_{xy,y} + \epsilon^{-1}\sigma_{xz,x} &= 0 \\
 \sigma_{xy,x} + \sigma_{yy,y} + \epsilon^{-1}\sigma_{yz,x} &= 0 \\
 \sigma_{xz,x} + \sigma_{yz,y} + \epsilon^{-1}\sigma_{zz,x} &= 0
 \end{aligned} \tag{5.8}$$

and from eq. 5.3, we get:

$$\epsilon^{-1}w_{,z} = -(1/C_{33}) [C_{13}u_{,x} + C_{23}v_{,y} + C_{36}(u_{,y} + v_{,x})] \tag{5.9}$$

Substituting eq. 5.7 into the first two of eqs. 5.8, we obtain

$$\begin{aligned}
 \epsilon^2 [Q_{11}u_{,xx} + Q_{12}v_{,xy} + Q_{16}(2u_{,xy} + v_{,xx}) + Q_{26}v_{,yy} + Q_{66}(u_{,yy} + v_{,xy})] + \\
 \epsilon [C_{45}w_{,yz} + C_{55}w_{,xz}] + [C_{45}v_{,zz} + C_{55}u_{,zz}] &= 0 \\
 \\
 \epsilon^2 [Q_{16}u_{,xx} + Q_{12}u_{,xy} + Q_{26}(u_{,yy} + 2v_{,xy}) + Q_{22}v_{,yy} + Q_{66}(u_{,xy} + v_{,xx})] + \\
 \epsilon [C_{44}w_{,yz} + C_{45}w_{,xz}] + [C_{44}v_{,zz} + C_{45}u_{,zz}] &= 0
 \end{aligned} \tag{5.10}$$

in addition eq. 5.9 can be expressed as:

$$[C_{33}w_{,z}] + \epsilon [C_{13}u_{,x} + C_{23}v_{,y} + C_{36}(u_{,y} + v_{,x})] = 0 \tag{5.11}$$

Assuming that in a layer, the displacement components can be expressed by a power series in ϵ as:

$$\begin{Bmatrix} u(x, y, z, \epsilon) \\ v(x, y, z, \epsilon) \\ w(x, y, z, \epsilon) \end{Bmatrix} = \sum_{n=0}^{\infty} \epsilon^n \begin{Bmatrix} u_n(x, y, z) \\ v_n(x, y, z) \\ w_n(x, y, z) \end{Bmatrix} \tag{5.12}$$

which is the same form used in [78] for the isotropic case. At this point there is no indication as to the validity of this form for the anisotropic case. A converging

series would require decreasing values of u_n , v_n and w_n as n increases. This series would then have to be demonstrated as the true solution of the problem.

A solution is obtained by substituting from eq. 5.12 into 5.10 and 5.11, and for different values of n , equating the coefficients of ϵ^n . The terms independent of ϵ give:

$$\begin{aligned} C_{45}v_{o,zz} + C_{55}u_{o,zz} &= 0 \\ C_{44}v_{o,zz} + C_{45}u_{o,zz} &= 0 \\ C_{33}w_{o,z} &= 0 \end{aligned} \quad (5.13)$$

The solution of these equations (without restricting the values of C_{ij}) indicates that u_o and v_o are linear functions of z while w_o is a function of only x and y . i.e.

$$\begin{aligned} u_o &= F_1(x, y) z + u_o(x, y) \\ v_o &= F_2(x, y) z + v_o(x, y) \\ w_o &= w_o(x, y) \end{aligned}$$

The functions $F_1(x, y)$ and $F_2(x, y)$ will be given a value of zero. The reason for this will be discussed below. The general form for u_o , v_o and w_o can therefore be written as:

$$u_o = u_o(x, y), \quad v_o = v_o(x, y), \quad w_o = w_o(x, y)$$

Equating the terms of order 1 in the expansion gives:

$$\begin{aligned} C_{45}v_{1,zz} + C_{55}u_{1,zz} + C_{45}w_{o,yz} + C_{55}w_{o,xz} &= 0 \\ C_{44}v_{1,zz} + C_{45}u_{1,zz} + C_{44}w_{o,yz} + C_{45}w_{o,xz} &= 0 \\ C_{33}w_{1,z} + C_{13}u_{o,x} + C_{23}v_{o,y} + C_{36}(u_{o,y} + v_{o,x}) &= 0 \end{aligned} \quad (5.14)$$

Using the third of eqs. 5.14, it can be shown that:

$$w_{1,z} = -\frac{1}{C_{33}} [C_{13}u_{o,x} + C_{23}v_{o,y} + C_{36}(u_{o,y} + v_{o,x})] \quad (5.15)$$

Integrating,

$$w_1 = -\frac{1}{C_{33}} [C_{13}u_{o,x} + C_{23}v_{o,y} + C_{36}(u_{o,y} + v_{o,x})] z + S_1(x, y) \quad (5.16)$$

where $S_1(x, y)$ is as yet an undetermined function of x and y . This equation can be simplified as:

$$w_1 = [A]z + S_1(x, y) \quad (5.17)$$

where

$$[A] = -(1/C_{33}) [C_{13}u_{o,x} + C_{23}v_{o,y} + C_{36}(u_{o,y} + v_{o,x})]$$

Now integrating the first two equations of 5.14,

$$\begin{aligned} C_{45}v_{1,z} + C_{55}u_{1,z} &= -[C_{45}w_{o,y} + C_{55}w_{o,x}] + F_3(x, y) \\ C_{44}v_{1,z} + C_{45}u_{1,z} &= -[C_{44}w_{o,y} + C_{45}w_{o,x}] + F_4(x, y) \end{aligned} \quad (5.18)$$

which leads to:

$$u_{1,z} = -w_{o,x} - \frac{C_{44}}{C_{45}^2 - C_{44}C_{55}} F_3(x, y) + \frac{C_{45}}{C_{45}^2 - C_{44}C_{55}} F_4(x, y) \quad (5.19)$$

or, without loss of generality could be written as:

$$u_{1,z} = -w_{o,x} + G(x, y) \quad (5.20)$$

Integrating with respect to z ,

$$u_1 = [-w_{o,x} + G(x, y)] z + B_1(x, y) \quad (5.21)$$

Similarly,

$$v_1 = [-w_{o,y} + H(x, y)] z + B_2(x, y) \quad (5.22)$$

where B_1 and B_2 are yet undetermined functions of x and y .

The functions $G(x, y)$ and $H(x, y)$ will be assigned a value of zero and again the reason will be discussed below. The general form of u_1 and v_1 will then take the form:

$$\begin{aligned} u_1 &= -w_{o,x} z + B_1(x, y) \\ v_1 &= -w_{o,y} z + B_2(x, y) \end{aligned} \quad (5.23)$$

Now from eq. 5.12 for $n \geq 2$, equating the terms of order n gives:

$$\begin{aligned} C_{45}v_{n,zz} + C_{55}u_{n,zz} + C_{45}w_{n-1,yz} + C_{55}w_{n-1,xz} + \\ Q_{11}u_{n-2,xx} + Q_{12}v_{n-2,xy} + Q_{16}(2u_{n-2,xy} + v_{n-2,xx}) + \\ Q_{26}v_{n-2,yy} + Q_{66}(u_{n-2,yy} + v_{n-2,xy}) = 0 \end{aligned}$$

$$\begin{aligned} C_{44}v_{n,zz} + C_{45}u_{n,zz} + C_{44}w_{n-1,yz} + C_{45}w_{n-1,xz} + \\ Q_{16}u_{n-2,xx} + Q_{12}u_{n-2,xy} + Q_{26}(2v_{n-2,xy} + u_{n-2,yy}) + \\ Q_{22}v_{n-2,yy} + Q_{66}(u_{n-2,xy} + v_{n-2,xx}) = 0 \end{aligned}$$

$$C_{33}w_{n,z} + C_{13}u_{n-1,x} + C_{23}v_{n-1,y} + C_{36}(u_{n-1,y} + v_{n-1,x}) = 0 \quad (5.24)$$

From the third of eq. 5.24 with $n = 2$,

$$C_{33}w_{2,x} + C_{13}u_{1,x} + C_{23}v_{1,y} + C_{36}(u_{1,y} + v_{1,x}) = 0 \quad (5.25)$$

Differentiating eqs. 5.23 with respect to x and y ,

$$\begin{aligned} u_{1,x} &= -w_{o,xx} z + B_{1,x} \\ u_{1,y} &= -w_{o,xy} z + B_{1,y} \\ v_{1,x} &= -w_{o,xy} z + B_{2,x} \\ v_{1,y} &= -w_{o,yy} z + B_{2,y} \end{aligned} \quad (5.26)$$

Substituting from eqs. 5.26 into 5.25,

$$\begin{aligned} C_{33}w_{2,z} &= [C_{13}w_{o,xx} + C_{23}w_{o,yy} + 2C_{36}w_{o,xy}]z \\ &- [C_{13}B_{1,x} + C_{23}B_{2,y} + C_{36}(B_{1,y} + B_{2,x})] \end{aligned} \quad (5.27)$$

Integration of the previous equation leads to the expression for w_2 :

$$\begin{aligned} w_2 &= \frac{1}{C_{33}} [C_{13}w_{o,xx} + C_{23}w_{o,yy} + 2C_{36}w_{o,xy}] \frac{z^2}{2} \\ &- \frac{1}{C_{33}} [C_{13}B_{1,x} + C_{23}B_{2,y} + C_{36}(B_{1,y} + B_{2,x})]z + B_3(x, y) \end{aligned} \quad (5.28)$$

where B_3 is a yet unknown function of x and y . This equation can be simplified as:

$$w_2 = [\mathbf{B}] \frac{z^2}{2} + [\mathbf{C}]z + B_3 \quad (5.29)$$

Now using the first two of eqs. 5.24 with $n = 2$, the values of u_2 and v_2 can be obtained.

$$\begin{aligned} C_{45}v_{2,zz} + C_{55}u_{2,zz} &= -[C_{45}w_{1,yz} + C_{55}w_{1,xz} + Q_{11}u_{o,xx} + Q_{12}v_{o,xy} \\ &+ Q_{16}(2u_{o,xy} + v_{o,xx}) + Q_{26}v_{o,yy} + Q_{66}(u_{o,yy} + v_{o,xy})] \\ C_{44}v_{2,zz} + C_{45}u_{2,zz} &= -[C_{44}w_{1,yz} + C_{45}w_{1,xz} + Q_{16}u_{o,xx} + Q_{12}u_{o,xy}] \\ &+ Q_{26}(2v_{o,xy} + u_{o,yy}) + Q_{22}v_{o,yy} + Q_{66}(u_{o,xy} + v_{o,xx}) \end{aligned} \quad (5.30)$$

which leads to:

$$\begin{aligned} u_{2,zz} &= -w_{1,xz} - \frac{1}{C_{44}C_{55} - C_{45}^2} [(C_{44}Q_{11} - C_{45}Q_{16})u_{o,xx} \\ &+ (C_{44}Q_{66} - C_{45}Q_{26})u_{o,yy} + (2C_{44}Q_{16} - C_{45}Q_{12} - C_{45}Q_{66})u_{o,xy} \\ &+ (C_{44}Q_{16} - C_{45}Q_{66})v_{o,xx} + (C_{44}Q_{26} - C_{45}Q_{22})v_{o,yy} \\ &+ (C_{44}Q_{12} + C_{44}Q_{66} - 2C_{45}Q_{26})v_{o,xy}] \end{aligned} \quad (5.31)$$

also differentiating eq. 5.15 with respect to x , we get:

$$w_{1,xx} = -\frac{1}{C_{33}} [C_{13}u_{o,xx} + C_{23}v_{o,xy} + C_{36}(u_{o,xy} + v_{o,xx})] \quad (5.32)$$

Substituting from eq. 5.32 into 5.31 then integrating, we obtain the expression for u_2 ,

$$\begin{aligned} u_2 = & \frac{-1}{C_{44}C_{55} - C_{45}^2} \left\{ \left[-\left(\frac{C_{13}}{C_{33}}\right) (C_{44}C_{55} - C_{45}^2) + (Q_{11}C_{44} - C_{45}Q_{16}) \right] u_{o,xx} \right. \\ & + [C_{44}Q_{66} - C_{45}Q_{26}] u_{o,yy} + [C_{44}Q_{26} - C_{45}Q_{22}] v_{o,yy} \\ & + \left[-\left(\frac{C_{36}}{C_{33}}\right) (C_{44}C_{55} - C_{45}^2) + (2C_{44}Q_{16} - C_{45}Q_{12} - C_{45}Q_{66}) \right] u_{o,xy} \\ & + \left[-\left(\frac{C_{36}}{C_{33}}\right) (C_{44}C_{55} - C_{45}^2) + (C_{44}Q_{16} - C_{45}Q_{66}) \right] v_{o,xx} \\ & + \left. \left[-\left(\frac{C_{23}}{C_{33}}\right) (C_{44}C_{55} - C_{45}^2) + (C_{44}Q_{12} + C_{44}Q_{66} - 2C_{45}Q_{26}) \right] v_{o,xy} \right\} \frac{z^2}{2} \\ & + S_2z + S_4 \end{aligned} \quad (5.33)$$

Similarly,

$$\begin{aligned} v_2 = & \frac{1}{C_{44}C_{55} - C_{45}^2} \left\{ \left[\left(\frac{C_{36}}{C_{33}}\right) (C_{44}C_{55} - C_{45}^2) + (C_{45}Q_{66} - C_{55}Q_{26}) \right] u_{o,yy} \right. \\ & + [C_{45}Q_{11} - C_{55}Q_{16}] u_{o,xx} + [C_{45}Q_{16} - C_{55}Q_{66}] v_{o,xx} \\ & + \left[\left(\frac{C_{13}}{C_{33}}\right) (C_{44}C_{55} - C_{45}^2) + (2C_{45}Q_{16} - C_{55}Q_{66} - C_{55}Q_{12}) \right] u_{o,xy} \\ & + \left[\left(\frac{C_{23}}{C_{33}}\right) (C_{44}C_{55} - C_{45}^2) + (Q_{26}C_{45} - C_{55}Q_{22}) \right] v_{o,yy} \\ & + \left. \left[\left(\frac{C_{36}}{C_{33}}\right) (C_{44}C_{55} - C_{45}^2) + (C_{45}Q_{12} + C_{45}Q_{66} - 2C_{55}Q_{26}) \right] v_{o,xy} \right\} \frac{z^2}{2} \\ & + S_3z + S_5 \end{aligned} \quad (5.34)$$

where S_2, S_3, S_4 and S_5 are yet unknown functions of x and y . Equations 5.33 and 5.34 can simply be written as:

$$\begin{aligned} u_2 &= [\mathbf{D}] \frac{z^2}{2} + S_2z + S_4 \\ v_2 &= [\mathbf{E}] \frac{z^2}{2} + S_3z + S_5 \end{aligned} \quad (5.35)$$

From the third of eq. 5.24 with $n = 3$,

$$C_{33}w_{3,z} + C_{13}u_{2,x} + C_{23}v_{2,y} + C_{36}(u_{2,y} + v_{2,x}) = 0 \quad (5.36)$$

Differentiating eqs. 5.35 with respect to x and y ,

$$\begin{aligned} u_{2,x} &= [\mathbf{D},x] \frac{z^2}{2} + S_{2,x} z + S_{4,x} \\ u_{2,y} &= [\mathbf{D},y] \frac{z^2}{2} + S_{2,y} z + S_{4,y} \\ v_{2,x} &= [\mathbf{E},x] \frac{z^2}{2} + S_{3,x} z + S_{5,x} \\ v_{2,y} &= [\mathbf{E},y] \frac{z^2}{2} + S_{3,y} z + S_{5,y} \end{aligned} \quad (5.37)$$

Substituting from eq. 5.37 into eq. 5.36, we get:

$$\begin{aligned} C_{33}w_{3,z} &= - \left\{ C_{13} \left([\mathbf{D},x] \frac{z^2}{2} + S_{2,x} z + S_{4,x} \right) \right. \\ &+ C_{23} \left([\mathbf{E},y] \frac{z^2}{2} + S_{3,y} z + S_{5,y} \right) \\ &\left. + C_{36} \left([\mathbf{D},y + \mathbf{E},x] \frac{z^2}{2} + [S_{2,y} + S_{3,x}] z + [S_{4,y} + S_{5,x}] \right) \right\} \end{aligned} \quad (5.38)$$

Integrating the previous equation, we obtain a relation for w_3 :

$$\begin{aligned} w_3 &= \frac{-1}{C_{33}} \left\{ (C_{13} [\mathbf{D},x] + C_{23} [\mathbf{E},y] + C_{36} [\mathbf{D},y + \mathbf{E},x]) \frac{z^3}{6} \right. \\ &+ (C_{13} S_{2,x} + C_{23} S_{3,y} + C_{36} (S_{2,y} + S_{3,x})) \frac{z^2}{2} \\ &+ (C_{13} S_{4,x} + C_{23} S_{5,y} + C_{36} (S_{4,y} + S_{5,x})) z \\ &\left. + S_6(x, y) \right\} \end{aligned} \quad (5.39)$$

where S_6 is a yet undetermined function of x and y . This equation can be simply written as:

$$w_3 = [\mathbf{F}] \frac{z^3}{6} + [\mathbf{G}] \frac{z^2}{2} + [\mathbf{H}] z + S_6 \quad (5.40)$$

From the first two of eq. 5.24 with $n = 3$,

$$\begin{aligned}
u_{3,zz} &= -w_{2,zz} - \frac{1}{C_{44}C_{55} - C_{45}^2} [(C_{44}Q_{11} - C_{45}Q_{16})u_{1,xx} \\
&+ (C_{44}Q_{66} - C_{45}Q_{26})u_{1,yy} + (2C_{44}Q_{16} - C_{45}Q_{12} - C_{45}Q_{66})u_{1,xy} \\
&+ (C_{44}Q_{16} - C_{45}Q_{66})v_{1,xx} + (C_{44}Q_{26} - C_{45}Q_{22})v_{1,yy} \\
&+ (C_{44}Q_{12} + C_{44}Q_{66} - 2C_{45}Q_{26})v_{1,xy}] \quad (5.41)
\end{aligned}$$

where:

$$w_{2,zz} = \frac{1}{C_{33}} [C_{13}w_{o,xxx} + C_{23}w_{o,xyy} + 2C_{36}w_{o,xyy}]z + [C_{,x}] \quad (5.42)$$

and the equations for the second derivative of u_1 and v_1 can be obtained by differentiating eqs. 5.26 with respect to x and y . Integrating eq. 5.41, we get:

$$\begin{aligned}
u_3 &= - \left\{ \left[\frac{C_{13}}{C_{33}} - \frac{C_{44}Q_{11} - C_{45}Q_{16}}{C_{44}C_{55} - C_{45}^2} \right] w_{o,xxx} + \left[\frac{C_{44}Q_{26} - C_{45}Q_{22}}{C_{44}C_{55} - C_{45}^2} \right] w_{o,yyy} \right. \\
&+ \left[\frac{2C_{36}}{C_{33}} - \frac{3C_{44}Q_{16} - C_{45}Q_{12} - 2C_{45}Q_{66}}{C_{44}C_{55} - C_{45}^2} \right] w_{o,xyy} \\
&+ \left. \left[\frac{C_{23}}{C_{33}} - \frac{2C_{44}Q_{66} + C_{44}Q_{12} - 3C_{45}Q_{26}}{C_{44}C_{55} - C_{45}^2} \right] w_{o,xyy} \right\} \frac{z^3}{6} \\
&- \left\{ [C_{,x}] + \left[\frac{C_{44}Q_{11} - C_{45}Q_{16}}{C_{44}C_{55} - C_{45}^2} \right] B_{1,xx} + \left[\frac{C_{44}Q_{66} - C_{45}Q_{26}}{C_{44}C_{55} - C_{45}^2} \right] B_{1,yy} \right. \\
&+ \left[\frac{2C_{44}Q_{16} - C_{45}Q_{12} - C_{45}Q_{66}}{C_{44}C_{55} - C_{45}^2} \right] B_{1,xy} + \left[\frac{C_{44}Q_{16} - C_{45}Q_{66}}{C_{44}C_{55} - C_{45}^2} \right] B_{2,xx} \\
&+ \left. \left[\frac{C_{44}Q_{26} - C_{45}Q_{22}}{C_{44}C_{55} - C_{45}^2} \right] B_{2,yy} + \left[\frac{C_{44}Q_{12} + C_{44}Q_{66} - 2C_{45}Q_{26}}{C_{44}C_{55} - C_{45}^2} \right] B_{2,xy} \right\} \frac{z^2}{2} \\
&+ B_4z + B_6 \quad (5.43)
\end{aligned}$$

Similarly,

$$\begin{aligned}
v_3 &= - \left\{ \left[\frac{C_{45}Q_{11} - C_{55}Q_{16}}{C_{44}C_{55} - C_{45}^2} \right] w_{o,xxx} + \left[\frac{C_{23}}{C_{33}} + \frac{C_{45}Q_{26} - C_{55}Q_{22}}{C_{44}C_{55} - C_{45}^2} \right] w_{o,yyy} \right. \\
&+ \left[\frac{C_{13}}{C_{33}} + \frac{3C_{45}Q_{16} - C_{55}Q_{12} - 2C_{55}Q_{66}}{C_{44}C_{55} - C_{45}^2} \right] w_{o,xyy} \\
&+ \left. \left[\frac{2C_{36}}{C_{33}} + \frac{2C_{45}Q_{66} - 3C_{55}Q_{26} + C_{45}Q_{12}}{C_{44}C_{55} - C_{45}^2} \right] w_{o,xyy} \right\} \frac{z^3}{6}
\end{aligned}$$

$$\begin{aligned}
& + \left\{ -[C,y] + \left[\frac{C_{45}Q_{11} - C_{55}Q_{16}}{C_{44}C_{55} - C_{45}^2} \right] B_{1,xx} + \left[\frac{C_{45}Q_{66} - C_{55}Q_{26}}{C_{44}C_{55} - C_{45}^2} \right] B_{1,yy} \right. \\
& + \left[\frac{2C_{45}Q_{16} - C_{55}Q_{12} - C_{55}Q_{66}}{C_{44}C_{55} - C_{45}^2} \right] B_{1,xy} + \left[\frac{C_{45}Q_{16} - C_{55}Q_{66}}{C_{44}C_{55} - C_{45}^2} \right] B_{2,xx} \\
& + \left[\frac{C_{45}Q_{26} - C_{55}Q_{22}}{C_{44}C_{55} - C_{45}^2} \right] B_{2,yy} + \left[\frac{C_{45}Q_{66} + C_{45}Q_{12} - 2C_{55}Q_{26}}{C_{44}C_{55} - C_{45}^2} \right] B_{2,xy} \left. \right\} \frac{z^2}{2} \\
& + B_5z + B_7 \tag{5.44}
\end{aligned}$$

These last two equations can be simply written as:

$$\begin{aligned}
u_3 &= [I] \frac{z^3}{6} + [J] \frac{z^2}{2} + B_4z + B_6 \\
v_3 &= [K] \frac{z^3}{6} + [L] \frac{z^2}{2} + B_5z + B_7 \tag{5.45}
\end{aligned}$$

where B_4, B_5, B_6 and B_7 are yet undetermined functions of x and y .

From the third of eq. 5.24 with $n = 4$,

$$C_{33}w_{4,z} + C_{13}u_{3,x} + C_{23}v_{3,y} + C_{36}(u_{3,y} + v_{3,x}) = 0 \tag{5.46}$$

Differentiating eqs. 5.45 with respect to x and y ,

$$\begin{aligned}
u_{3,x} &= [I,x] \frac{z^3}{6} + [J,x] \frac{z^2}{2} + B_{4,x}z + B_{6,x} \\
u_{3,y} &= [I,y] \frac{z^3}{6} + [J,y] \frac{z^2}{2} + B_{4,y}z + B_{6,y} \\
v_{3,x} &= [K,x] \frac{z^3}{6} + [L,x] \frac{z^2}{2} + B_{5,x}z + B_{7,x} \\
v_{3,y} &= [K,y] \frac{z^3}{6} + [L,y] \frac{z^2}{2} + B_{5,y}z + B_{7,y} \tag{5.47}
\end{aligned}$$

Substituting from eq. 5.47 into eq. 5.46, we get:

$$\begin{aligned}
C_{33}w_{4,z} &= - \left\{ C_{13} \left([I,x] \frac{z^3}{6} + [J,x] \frac{z^2}{2} + B_{4,x}z + B_{6,x} \right) \right. \\
& + C_{23} \left([K,y] \frac{z^3}{6} + [L,y] \frac{z^2}{2} + B_{5,y}z + B_{7,y} \right) \\
& + C_{36} \left([I,y + K,x] \frac{z^3}{6} + [J,y + L,x] \frac{z^2}{2} \right. \\
& \left. \left. + [B_{4,y} + B_{5,x}]z + [B_{6,y} + B_{7,x}] \right) \right\} \tag{5.48}
\end{aligned}$$

Integrating the previous equation, we obtain a relation for w_4 :

$$\begin{aligned}
w_4 = & -\frac{1}{C_{33}} \left\{ (C_{13} [I, x] + C_{23} [K, y] + C_{36} [I, y + K, x]) \frac{z^4}{24} \right. \\
& + (C_{13} [J, x] + C_{23} [L, y] + C_{36} [J, y + L, x]) \frac{z^3}{6} \\
& + (C_{13} B_{4,x} + C_{23} B_{5,y} + C_{36} (B_{4,y} + B_{5,x})) \frac{z^2}{2} \\
& + (C_{13} B_{6,x} + C_{23} B_{7,y} + C_{36} (B_{6,y} + B_{7,x})) z \\
& \left. + B_8(x, y) \right\} \tag{5.49}
\end{aligned}$$

where B_8 is a yet undetermined function of x and y . This equation can be simply written as:

$$w_4 = [M] \frac{z^4}{24} + [N] \frac{z^3}{6} + [O] \frac{z^2}{2} + [P] z + B_8 \tag{5.50}$$

From the first two of eq. 5.24 with $n = 4$,

$$\begin{aligned}
u_{4,zz} = & -w_{3,zz} - \frac{1}{C_{44}C_{55} - C_{45}^2} [(C_{44}Q_{11} - C_{45}Q_{16}) u_{2,xx} \\
& + (C_{44}Q_{66} - C_{45}Q_{26}) u_{2,yy} + (2C_{44}Q_{16} - C_{45}Q_{12} - C_{45}Q_{66}) u_{2,xy} \\
& + (C_{44}Q_{16} - C_{45}Q_{66}) v_{2,xx} + (C_{44}Q_{26} - C_{45}Q_{22}) v_{2,yy} \\
& + (C_{44}Q_{12} + C_{44}Q_{66} - 2C_{45}Q_{26}) v_{2,xy}] \tag{5.51}
\end{aligned}$$

where:

$$w_{3,zz} = [F, x] \frac{z^2}{2} + [G, x] z + [H, x] \tag{5.52}$$

and the equations for the second derivative of u_2 and v_2 can be obtained by differentiating eqs. 5.37 with respect to x and y . Integrating eq. 5.51, we get:

$$\begin{aligned}
u_4 = & - \left\{ [F, x] + \left(\frac{C_{44}Q_{11} - C_{45}Q_{16}}{C_{44}C_{55} - C_{45}^2} \right) [D, xx] \right. \\
& + \left(\frac{C_{44}Q_{66} - C_{45}Q_{26}}{C_{44}C_{55} - C_{45}^2} \right) [D, yy] + \left(\frac{2C_{44}Q_{16} - C_{45}Q_{12} - C_{45}Q_{66}}{C_{44}C_{55} - C_{45}^2} \right) [D, xy] \\
& \left. + \left(\frac{C_{44}Q_{16} - C_{45}Q_{66}}{C_{44}C_{55} - C_{45}^2} \right) [E, xx] + \left(\frac{C_{44}Q_{26} - C_{45}Q_{22}}{C_{44}C_{55} - C_{45}^2} \right) [E, yy] \right\}
\end{aligned}$$

$$\begin{aligned}
& + \left(\frac{C_{44}Q_{12} + C_{44}Q_{66} - 2C_{45}Q_{26}}{C_{44}C_{55} - C_{45}^2} \right) [\mathbf{E}, \mathbf{xy}] \left. \right\} \frac{z^4}{24} \\
& - \left\{ [\mathbf{G}, \mathbf{x}] + \left(\frac{C_{44}Q_{11} - C_{45}Q_{16}}{C_{44}C_{55} - C_{45}^2} \right) [S_{2,xx}] \right. \\
& + \left(\frac{C_{44}Q_{66} - C_{45}Q_{26}}{C_{44}C_{55} - C_{45}^2} \right) [S_{2,yy}] + \left(\frac{2C_{44}Q_{16} - C_{45}Q_{12} - C_{45}Q_{66}}{C_{44}C_{55} - C_{45}^2} \right) [S_{2,xy}] \\
& + \left(\frac{C_{44}Q_{16} - C_{45}Q_{66}}{C_{44}C_{55} - C_{45}^2} \right) [S_{3,xx}] + \left(\frac{C_{44}Q_{26} - C_{45}Q_{22}}{C_{44}C_{55} - C_{45}^2} \right) [S_{3,yy}] \\
& + \left. \left(\frac{C_{44}Q_{12} + C_{44}Q_{66} - 2C_{45}Q_{26}}{C_{44}C_{55} - C_{45}^2} \right) [S_{3,xy}] \right\} \frac{z^3}{6} \\
& - \left\{ [\mathbf{H}, \mathbf{x}] + \left(\frac{C_{44}Q_{11} - C_{45}Q_{16}}{C_{44}C_{55} - C_{45}^2} \right) [S_{4,xx}] \right. \\
& + \left(\frac{C_{44}Q_{66} - C_{45}Q_{26}}{C_{44}C_{55} - C_{45}^2} \right) [S_{4,yy}] + \left(\frac{2C_{44}Q_{16} - C_{45}Q_{12} - C_{45}Q_{66}}{C_{44}C_{55} - C_{45}^2} \right) [S_{4,xy}] \\
& + \left(\frac{C_{44}Q_{16} - C_{45}Q_{66}}{C_{44}C_{55} - C_{45}^2} \right) [S_{5,xx}] + \left(\frac{C_{44}Q_{26} - C_{45}Q_{22}}{C_{44}C_{55} - C_{45}^2} \right) [S_{5,yy}] \\
& + \left. \left(\frac{C_{44}Q_{12} + C_{44}Q_{66} - 2C_{45}Q_{26}}{C_{44}C_{55} - C_{45}^2} \right) [S_{5,xy}] \right\} \frac{z^2}{2} \\
& + S_7z + S_9 \tag{5.53}
\end{aligned}$$

Similarly,

$$\begin{aligned}
v_4 = & \left\{ -[\mathbf{F}, \mathbf{y}] + \left(\frac{C_{45}Q_{11} - C_{55}Q_{16}}{C_{44}C_{55} - C_{45}^2} \right) [\mathbf{D}, \mathbf{xx}] \right. \\
& + \left(\frac{C_{45}Q_{66} - C_{55}Q_{26}}{C_{44}C_{55} - C_{45}^2} \right) [\mathbf{D}, \mathbf{yy}] + \left(\frac{2C_{45}Q_{16} - C_{55}Q_{12} - C_{55}Q_{66}}{C_{44}C_{55} - C_{45}^2} \right) [\mathbf{D}, \mathbf{xy}] \\
& + \left(\frac{C_{45}Q_{16} - C_{55}Q_{66}}{C_{44}C_{55} - C_{45}^2} \right) [\mathbf{E}, \mathbf{xx}] + \left(\frac{C_{45}Q_{26} - C_{55}Q_{22}}{C_{44}C_{55} - C_{45}^2} \right) [\mathbf{E}, \mathbf{yy}] \\
& + \left. \left(\frac{C_{45}Q_{12} + C_{45}Q_{66} - 2C_{55}Q_{26}}{C_{44}C_{55} - C_{45}^2} \right) [\mathbf{E}, \mathbf{xy}] \right\} \frac{z^4}{24} \\
& + \left\{ -[\mathbf{G}, \mathbf{y}] + \left(\frac{C_{45}Q_{11} - C_{55}Q_{16}}{C_{44}C_{55} - C_{45}^2} \right) [S_{2,xx}] \right. \\
& + \left(\frac{C_{45}Q_{66} - C_{55}Q_{26}}{C_{44}C_{55} - C_{45}^2} \right) [S_{2,yy}] + \left(\frac{2C_{45}Q_{16} - C_{55}Q_{12} - C_{55}Q_{66}}{C_{44}C_{55} - C_{45}^2} \right) [S_{2,xy}] \\
& + \left(\frac{C_{45}Q_{16} - C_{55}Q_{66}}{C_{44}C_{55} - C_{45}^2} \right) [S_{3,xx}] + \left(\frac{C_{45}Q_{26} - C_{55}Q_{22}}{C_{44}C_{55} - C_{45}^2} \right) [S_{3,yy}] \\
& + \left. \left(\frac{C_{45}Q_{12} + C_{45}Q_{66} - 2C_{55}Q_{26}}{C_{44}C_{55} - C_{45}^2} \right) [S_{3,xy}] \right\} \frac{z^3}{6}
\end{aligned}$$

$$\begin{aligned}
& + \left\{ -[\mathbf{H},y] + \left(\frac{C_{45}Q_{11} - C_{55}Q_{16}}{C_{44}C_{55} - C_{45}^2} \right) [S_{4,xx}] \right. \\
& + \left(\frac{C_{45}Q_{66} - C_{55}Q_{26}}{C_{44}C_{55} - C_{45}^2} \right) [S_{4,yy}] + \left(\frac{2C_{45}Q_{16} - C_{55}Q_{12} - C_{55}Q_{66}}{C_{44}C_{55} - C_{45}^2} \right) [S_{4,xy}] \\
& + \left(\frac{C_{45}Q_{16} - C_{55}Q_{66}}{C_{44}C_{55} - C_{45}^2} \right) [S_{5,xx}] + \left(\frac{C_{45}Q_{26} - C_{55}Q_{22}}{C_{44}C_{55} - C_{45}^2} \right) [S_{5,yy}] \\
& + \left. \left(\frac{C_{45}Q_{12} + C_{45}Q_{66} - 2C_{55}Q_{26}}{C_{44}C_{55} - C_{45}^2} \right) [S_{5,xy}] \right\} \frac{z^2}{2} \\
& + S_8 z + S_{10} \tag{5.54}
\end{aligned}$$

where S_7, S_8, S_9 and S_{10} are yet undetermined functions of x and y . The last two equations can be simplified as:

$$\begin{aligned}
u_4 &= [\mathbf{Q}] \frac{z^4}{24} + [\mathbf{R}] \frac{z^3}{6} + [\mathbf{S}] \frac{z^2}{2} + S_7 z + S_9 \\
v_4 &= [\mathbf{T}] \frac{z^4}{24} + [\mathbf{U}] \frac{z^3}{6} + [\mathbf{V}] \frac{z^2}{2} + S_8 z + S_{10} \tag{5.55}
\end{aligned}$$

Collecting the terms of the series, the complete solution (up to $n = 4$) is:

$$\begin{bmatrix} u \\ v \\ w \end{bmatrix} = \begin{bmatrix} u_o(x, y) \\ v_o(x, y) \\ w_o(x, y) \end{bmatrix} + \epsilon \begin{bmatrix} u_1 \\ v_1 \\ w_1 \end{bmatrix} + \epsilon^2 \begin{bmatrix} u_2 \\ v_2 \\ w_2 \end{bmatrix} + \epsilon^3 \begin{bmatrix} u_3 \\ v_3 \\ w_3 \end{bmatrix} + \epsilon^4 \begin{bmatrix} u_4 \\ v_4 \\ w_4 \end{bmatrix} + \dots \tag{5.56}$$

For a symmetric laminate, the solution shown in eq. 5.56 can be decomposed into the sum of two independent solutions, which could be termed as stretching and bending solutions. In the stretching solution, $w_o = 0$, while in the bending solution $u_o = 0$ and $v_o = 0$. In anticipation of this decomposition, the arbitrary yet undetermined functions have been denoted so that S relate to stretching while B relate to bending. We can then deal with each solution separately.

5.4 Stretching Solution for a Lamina

The stretching solution for a lamina can be obtained from eq. 5.56. The displacements u and v will have the form:

$$\begin{bmatrix} u \\ v \end{bmatrix} = \begin{bmatrix} u_o(x, y) \\ v_o(x, y) \end{bmatrix} + \epsilon^2 \begin{bmatrix} u_2 \\ v_2 \end{bmatrix} + \epsilon^4 \begin{bmatrix} u_4 \\ v_4 \end{bmatrix} + \dots \quad (5.57)$$

while the expression for w will be:

$$w = \epsilon w_1 + \epsilon^3 w_3 + \dots \quad (5.58)$$

The corresponding expressions for the stresses can be calculated using eq. 5.7.

5.5 Bending Solution for a Lamina

The bending solution for a lamina is obtained from eq. 5.56. The displacements u and v will have the form:

$$\begin{bmatrix} u \\ v \end{bmatrix} = \epsilon \begin{bmatrix} u_1 \\ v_1 \end{bmatrix} + \epsilon^3 \begin{bmatrix} u_3 \\ v_3 \end{bmatrix} + \dots \quad (5.59)$$

while the expression for w will be:

$$w = w_o(x, y) + \epsilon^2 w_2 + \epsilon^4 w_4 + \dots \quad (5.60)$$

The corresponding expressions for the stresses can also be calculated using eq. 5.7.

5.6 Laminate Geometry

Let's now consider a laminated plate comprised of $2N - 1$ laminae, each of which is of an anisotropic linear elastic material. In general, these laminae would have different fiber orientations and thus different elastic constants. For convenience, we confine our attention to laminates symmetric about the mid-plane $Z = 0$, so that

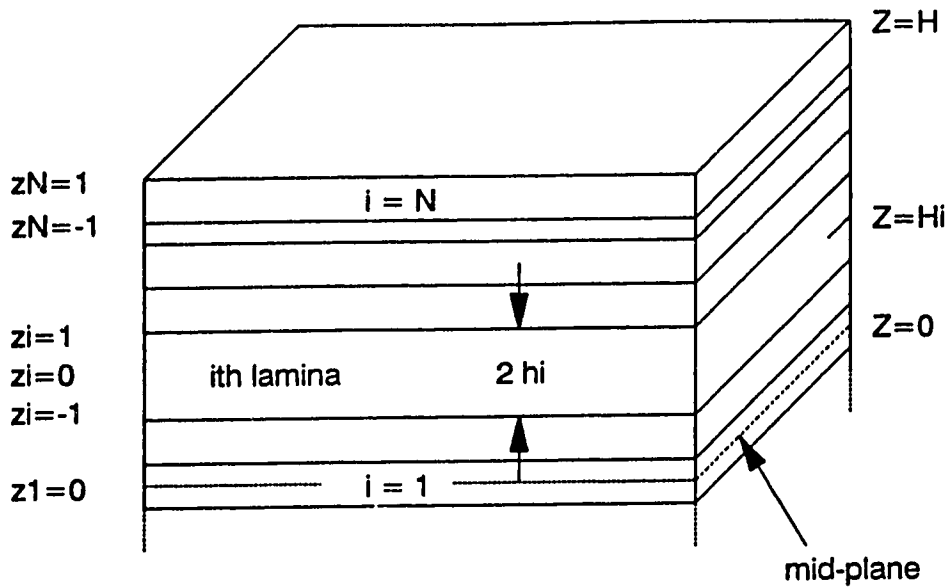


Figure 5.1: Laminate Geometry and Notation

the i th lamina above the mid-plane would have the same thickness and properties to the i th lamina below the mid-plane. Since we are dealing with a symmetric laminated plate, we will only be considering half of that plate.

Any quantity related to the i th lamina will be identified by the index i . The layers are numbered as shown in Fig. 5.1; the layer $i = 1$ contains the mid-plane of the laminated plate and the layer $i = N$ is the layer adjacent to the upper surface. The overall thickness of the laminate is denoted by $2H$, such that:

$$H = h_1 + 2 \sum_{i=2}^N h_i \quad (5.61)$$

We also denote by H_i the distance from the mid-plane of the plate to the mid-plane of lamina i , so that:

$$\begin{aligned} H_1 &= 0 \\ H_2 &= h_1 + h_2 \end{aligned}$$

$$\begin{aligned}
H_i &= h_1 + 2 \sum_{r=2}^{N-1} h_r + h_i \quad (i = 3, 4, \dots, N) \\
H_N &= H - h_N
\end{aligned} \tag{5.62}$$

We also use scaled variables x, y, z, u, v and w similar to those introduced in section 5.3 as follows:

$$\begin{aligned}
x &= X/a & y &= Y/a & z &= Z/H \\
u &= U/a & v &= V/a & w &= W/a
\end{aligned}$$

where now H is the overall laminate half-thickness, and $Z = 0$ coincides with the mid-plane of the laminated plate. In addition, a scaled local coordinate z_i in the z - direction in each lamina, is introduced:

$$\begin{aligned}
z_i &= Z_i/h_i \\
Z_i &= Z - H_i \quad (i = 1, 2, 3, \dots, N)
\end{aligned} \tag{5.63}$$

Thus $z_i = 0$ is the mid-plane of the lamina i , and $z_i = \pm 1$ are the upper and lower surfaces of layer i respectively. In addition a parameter ϵ similar to the one used in section 5.3 is introduced,

$$\epsilon = H/a$$

and

$$\epsilon_i = h_i/a \quad (i = 1, 2, \dots, N) \tag{5.64}$$

From eq 5.61 it then follows that:

$$\epsilon = \epsilon_1 + 2 \sum_{i=2}^N \epsilon_i \tag{5.65}$$

5.7 Solution of the Two-Dimensional Classical Thin Plate Theory - The Equivalent Plate

5.7.1 The Equivalent Plate

In the *Classical Laminate theory* (CLT), the laminated plate is replaced by a homogeneous plate which can be termed **the equivalent plate**. This equivalent plate has the same overall geometry as the laminate (for example it has a thickness of $2H$). For stretching deformations, the elastic constants of the equivalent plate are such that for homogeneous deformations under specified edge tractions, the mean in-plane displacements of the laminate and the equivalent plate coincide. For bending deformations, the constants are chosen such that in pure bending under given edge moment, the mid-plane deflection of the laminate and the equivalent plate are the same. These material properties are as follows:

$$(\hat{Q}_{ij}, \tilde{Q}_{ij}) = \int_{-h/2}^{h/2} Q_{ij}^{(k)}(1, z^2) dz \quad (5.66)$$

where:

\hat{Q}_{ij} are called the extensional stiffnesses

\tilde{Q}_{ij} are called the bending stiffnesses

5.7.2 The Stretching Case

The equations of equilibrium governing the average in-plane displacements (\hat{u}, \hat{v}) for the stretching case are as follows:

$$\begin{aligned} \hat{Q}_{11}\hat{u}_{,xx} + 2\hat{Q}_{16}\hat{u}_{,xy} + \hat{Q}_{66}\hat{u}_{,yy} + \hat{Q}_{16}\hat{v}_{,xx} + (\hat{Q}_{12} + \hat{Q}_{66})\hat{v}_{,xy} + \hat{Q}_{26}\hat{v}_{,yy} &= 0 \\ \hat{Q}_{16}\hat{u}_{,xx} + (\hat{Q}_{12} + \hat{Q}_{66})\hat{u}_{,xy} + \hat{Q}_{26}\hat{u}_{,yy} + \hat{Q}_{66}\hat{v}_{,xx} + 2\hat{Q}_{26}\hat{v}_{,xy} + \hat{Q}_{22}\hat{v}_{,yy} &= 0 \end{aligned} \quad (5.67)$$

The stress resultants for the equivalent plate are:

$$\begin{aligned}
 \hat{N}_{xx} &= \hat{Q}_{11}\hat{u}_{,x} + \hat{Q}_{12}\hat{v}_{,y} + \hat{Q}_{16}(\hat{u}_{,y} + \hat{v}_{,x}) \\
 \hat{N}_{xy} &= \hat{Q}_{12}\hat{u}_{,x} + \hat{Q}_{22}\hat{v}_{,y} + \hat{Q}_{26}(\hat{u}_{,y} + \hat{v}_{,x}) \\
 \hat{N}_{yx} &= \hat{Q}_{16}\hat{u}_{,x} + \hat{Q}_{26}\hat{v}_{,y} + \hat{Q}_{66}(\hat{u}_{,y} + \hat{v}_{,x})
 \end{aligned}
 \tag{5.68}$$

5.7.3 The Bending Case

The deflection \tilde{w} , associated with bending, for the equivalent plate is governed by the relation:

$$\tilde{Q}_{11}\tilde{w}_{,xxxx} + 4\tilde{Q}_{16}\tilde{w}_{,xxxxy} + 2(\tilde{Q}_{12} + 2\tilde{Q}_{66})\tilde{w}_{,xxyy} + 4\tilde{Q}_{26}\tilde{w}_{,xyyy} + \tilde{Q}_{22}\tilde{w}_{,yyyy} = 0 \tag{5.69}$$

The resultant moments for the equivalent plate are defined as:

$$\begin{aligned}
 \tilde{M}_{xx} &= \tilde{Q}_{11}\tilde{w}_{,xx} + \tilde{Q}_{12}\tilde{w}_{,yy} + 2\tilde{Q}_{16}\tilde{w}_{,xy} \\
 \tilde{M}_{xy} &= \tilde{Q}_{12}\tilde{w}_{,xx} + \tilde{Q}_{22}\tilde{w}_{,yy} + 2\tilde{Q}_{26}\tilde{w}_{,xy} \\
 \tilde{M}_{yx} &= \tilde{Q}_{16}\tilde{w}_{,xx} + \tilde{Q}_{26}\tilde{w}_{,yy} + 2\tilde{Q}_{66}\tilde{w}_{,xy}
 \end{aligned}
 \tag{5.70}$$

5.8 Three Dimensional Theory for Laminates - Stretching Deformations

In the theory presented next, the three dimensional field equations and interface conditions are exactly satisfied (up to $n = 4$). The only limitation, as mentioned before, is that in this theory the edge boundary conditions are satisfied only in an average fashion, rather than point by point.

Considering the stretching deformations of the laminate, we seek a solution in which, in each lamina, the displacements are of the form of eq. 5.57 and eq. 5.58

with ϵ replaced by ϵ_i , the material constants \hat{Q}_{jk} by $\hat{Q}_{jk}^{(i)}$ and z by z_i . Also the functions S_1, S_2, \dots should be replaced by $S_1^{(i)}, S_2^{(i)}, \dots$ for the lamina i since these functions, in the general case, can have different values in each lamina.

The functions $u_o(x, y)$ and $v_o(x, y)$ are required to satisfy the two dimensional solution. Because the CLT appears to give satisfactory results for the average values of u and v , we can choose these displacements to be those of the equivalent plate under the given boundary conditions. Thus, in the layer i , the displacements u and v will be assumed to have the form:

$$\begin{bmatrix} u^{(i)} \\ v^{(i)} \end{bmatrix} = \begin{bmatrix} \hat{u} \\ \hat{v} \end{bmatrix} + \epsilon_i^2 \begin{bmatrix} u_2^{(i)} \\ v_2^{(i)} \end{bmatrix} + \epsilon_i^4 \begin{bmatrix} u_4^{(i)} \\ v_4^{(i)} \end{bmatrix} + \dots \quad (5.71)$$

while the expression for w will be:

$$w^{(i)} = \epsilon_i w_1^{(i)} + \epsilon_i^3 w_3^{(i)} + \dots \quad (5.72)$$

The corresponding expressions for the stresses can be calculated using eq. 5.7. The remaining task now is to determined the unknown functions $S_k^{(i)}(x, y)$. To accomplish that, the following conditions have to be satisfied:

- Symmetry conditions at $z_1 = 0$:

$$w^{(1)} = 0 \quad \sigma_{xz}^{(1)} = 0 \quad \sigma_{yz}^{(1)} = 0 \quad \text{at } z = 0$$

- Continuity of displacement and traction at each interface between layer $(i-1)$ at $z_{i-1} = 1$ and layer (i) at $z_i = -1$ ($i=2,3,\dots,N$):

$$u^{(i-1)} = u^{(i)}, \quad v^{(i-1)} = v^{(i)}, \quad w^{(i-1)} = w^{(i)}$$

$$\sigma_{xz}^{(i-1)} = \sigma_{xz}^{(i)}, \quad \sigma_{yz}^{(i-1)} = \sigma_{yz}^{(i)}, \quad \sigma_{zz}^{(i-1)} = \sigma_{zz}^{(i)}$$

- The traction condition on the upper surface ($z_N = 1$) should vanish:

$$\sigma_{xz}^{(N)} = 0, \quad \sigma_{yz}^{(N)} = 0, \quad \sigma_{zz}^{(N)} = 0$$

5.8.1 Two-Dimensional Solution

In solving eq. 5.13, the functions $F_1(x, y)$ and $F_2(x, y)$ were assumed to be zero. The reason for that will be shown here.

For this first step assume that:

$$\begin{aligned} u^{(i)} &= F_1^{(i)}(x, y)z_i + \hat{u}^{(i)}(x, y) \\ v^{(i)} &= F_2^{(i)}(x, y)z_i + \hat{v}^{(i)}(x, y) \\ w^{(i)} &= \hat{w}^{(i)}(x, y) \end{aligned} \quad (5.73)$$

1. Due to symmetry, $w^{(1)} = 0$ at $z = 0$, i.e.

$$\hat{w}^{(1)}(x, y) = 0 \quad (5.74)$$

2. Continuity of w at each interface, i.e.

$$\hat{w}^{(i-1)} = \hat{w}^{(i)}$$

using eq. 5.74, we get:

$$\hat{w}^{(i)}(x, y) = 0 \quad (5.75)$$

3. Due to symmetry, both σ_{xz} and $\sigma_{yz} = 0$ at $z = 0$

$$\begin{aligned} C_{45}^{(1)} [v_{,z}^{(1)} + w_{,y}^{(1)}] + C_{55}^{(1)} [u_{,z}^{(1)} + w_{,x}^{(1)}] &= 0 \\ C_{44}^{(1)} [v_{,z}^{(1)} + w_{,y}^{(1)}] + C_{45}^{(1)} [u_{,z}^{(1)} + w_{,x}^{(1)}] &= 0 \end{aligned} \quad (5.76)$$

from eq. 5.73, taking into consideration eq. 5.74, we get:

$$C_{45}^{(1)} F_2^{(1)} + C_{55}^{(1)} F_1^{(1)} = 0 \quad (5.77)$$

$$C_{44}^{(1)} F_2^{(1)} + C_{45}^{(1)} F_1^{(1)} = 0 \quad (5.78)$$

For no restrictions on the values of the coefficients $C_{44}^{(1)}$, $C_{45}^{(1)}$ and $C_{55}^{(1)}$,

$$F_1^{(1)} = F_2^{(1)} = 0 \quad (5.79)$$

4. Continuity of σ_{xz} and σ_{yz} at each interface, making use of eq. 5.75, these equations reduce to:

$$\begin{aligned} C_{45}^{(i-1)} F_2^{(i-1)} + C_{55}^{(i-1)} F_1^{(i-1)} &= C_{45}^{(i)} F_2^{(i)} + C_{55}^{(i)} F_1^{(i)} \\ C_{44}^{(i-1)} F_2^{(i-1)} + C_{45}^{(i-1)} F_1^{(i-1)} &= C_{44}^{(i)} F_2^{(i)} + C_{45}^{(i)} F_1^{(i)} \end{aligned} \quad (5.80)$$

making use of eq. 5.79, the last relation implies that:

$$F_1^{(i)} = F_2^{(i)} = 0 \quad (5.81)$$

5.8.2 First Approximation

For this first approximation, assume that:

$$\begin{aligned} u^{(i)} &= \hat{u}(x, y) \\ v^{(i)} &= \hat{v}(x, y) \\ w^{(i)} &= \epsilon_i w_1^{(i)} = \frac{h_i}{a} \left\{ [\mathbf{A}]^{(i)} z_i + S_1^{(i)}(x, y) \right\} \end{aligned} \quad (5.82)$$

1. Due to symmetry, $w^{(1)} = 0$ at $z = 0$, i.e.

$$\frac{h_1}{a} \left\{ [\mathbf{A}]^{(1)}(0) + S_1^{(1)} \right\} = 0$$

which leads to:

$$S_1^{(1)} = 0 \quad (5.83)$$

2. Continuity of w at each interface, i.e.

$$\begin{aligned} \frac{h_{i-1}}{a} w_1^{(i-1)} &= \frac{h_i}{a} w_1^{(i)} \\ \frac{h_{i-1}}{a} \left\{ [\mathbf{A}]^{(i-1)} z_{i-1} + S_1^{(i-1)} \right\} &= \frac{h_i}{a} \left\{ [\mathbf{A}]^{(i)} z_i + S_1^{(i)} \right\} \\ \frac{h_{i-1}}{a} \left\{ [\mathbf{A}]^{(i-1)}(1) + S_1^{(i-1)} \right\} &= \frac{h_i}{a} \left\{ [\mathbf{A}]^{(i)}(-1) + S_1^{(i)} \right\} \end{aligned} \quad (5.84)$$

leading to a recurrence formula of the form:

$$S_1^{(i)} = \frac{h_{i-1}}{h_i} \left\{ [\mathbf{A}]^{(i-1)} + S_1^{(i-1)} \right\} + [\mathbf{A}]^{(i)} \quad (i = 2, 3, \dots, N) \quad (5.85)$$

5.8.3 Second Approximation

For this second approximation, assume that:

$$\begin{aligned} u^{(i)} &= \hat{u}(x, y) + \epsilon_i^2 \left\{ [\mathbf{D}]^{(i)} \frac{z_i^2}{2} + S_2^{(i)} z_i + S_4^{(i)} \right\} \\ v^{(i)} &= \hat{v}(x, y) + \epsilon_i^2 \left\{ [\mathbf{E}]^{(i)} \frac{z_i^2}{2} + S_3^{(i)} z_i + S_5^{(i)} \right\} \\ w^{(i)} &= \epsilon_i \left\{ [\mathbf{A}]^{(i)} z_i + S_1^{(i)} \right\} \end{aligned} \quad (5.86)$$

Since the expression for $w^{(i)}$ has not changed, the conditions presented in the first approximation are still valid.

1. Due to symmetry, both σ_{xz} and $\sigma_{yz} = 0$ at $z = 0$

$$\begin{aligned} C_{45}^{(1)} \left\{ \frac{h_1}{a} [v_{2,z}^{(1)} + w_{1,y}^{(1)}] \right\} + C_{55}^{(1)} \left\{ \frac{h_1}{a} [u_{2,z}^{(1)} + w_{1,x}^{(1)}] \right\} &= 0 \\ C_{44}^{(1)} \left\{ \frac{h_1}{a} [v_{2,z}^{(1)} + w_{1,y}^{(1)}] \right\} + C_{45}^{(1)} \left\{ \frac{h_1}{a} [u_{2,z}^{(1)} + w_{1,x}^{(1)}] \right\} &= 0 \end{aligned} \quad (5.87)$$

which would lead to:

$$\begin{aligned} C_{45}^{(1)} \left\{ [\mathbf{E}]^{(1)}(0) + S_3^{(1)} + [\mathbf{A}_{,y}]^{(1)}(0) + S_{1,y}^{(1)} \right\} + \\ C_{55}^{(1)} \left\{ [\mathbf{D}]^{(1)}(0) + S_2^{(1)} + [\mathbf{A}_{,x}]^{(1)}(0) + S_{1,x}^{(1)} \right\} &= 0 \\ C_{44}^{(1)} \left\{ [\mathbf{E}]^{(1)}(0) + S_3^{(1)} + [\mathbf{A}_{,y}]^{(1)}(0) + S_{1,y}^{(1)} \right\} + \\ C_{45}^{(1)} \left\{ [\mathbf{D}]^{(1)}(0) + S_2^{(1)} + [\mathbf{A}_{,x}]^{(1)}(0) + S_{1,x}^{(1)} \right\} &= 0 \end{aligned} \quad (5.88)$$

For no restrictions on the values of the coefficients $C_{44}^{(i)}$, $C_{45}^{(i)}$ and $C_{55}^{(i)}$,

$$S_2^{(1)} = S_3^{(1)} = 0 \quad (5.89)$$

2. Continuity of σ_{xz} and σ_{yz} at each interface.

$$\begin{aligned}
C_{45}^{(i-1)} \left\{ \frac{h_{i-1}}{a} [v_{2,z}^{(i-1)} + w_{1,y}^{(i-1)}] \right\} + C_{55}^{(i-1)} \left\{ \frac{h_{i-1}}{a} [u_{2,z}^{(i-1)} + w_{1,x}^{(i-1)}] \right\} &= \\
C_{45}^{(i)} \left\{ \frac{h_i}{a} [v_{2,z}^{(i)} + w_{1,y}^{(i)}] \right\} + C_{55}^{(i)} \left\{ \frac{h_i}{a} [u_{2,z}^{(i)} + w_{1,x}^{(i)}] \right\} & \\
C_{44}^{(i-1)} \left\{ \frac{h_{i-1}}{a} [v_{2,z}^{(i-1)} + w_{1,y}^{(i-1)}] \right\} + C_{45}^{(i-1)} \left\{ \frac{h_{i-1}}{a} [u_{2,z}^{(i-1)} + w_{1,x}^{(i-1)}] \right\} &= \\
C_{44}^{(i)} \left\{ \frac{h_i}{a} [v_{2,z}^{(i)} + w_{1,y}^{(i)}] \right\} + C_{45}^{(i)} \left\{ \frac{h_i}{a} [u_{2,z}^{(i)} + w_{1,x}^{(i)}] \right\} & \quad (5.90)
\end{aligned}$$

For the continuity of σ_{xz} , we get:

$$\begin{aligned}
\left(\frac{h_{i-1}}{a} \right) C_{45}^{(i-1)} \left\{ [\mathbf{E}]^{(i-1)}(1) + S_3^{(i-1)} + [\mathbf{A},y]^{(i-1)}(1) + S_{1,y}^{(i-1)} \right\} + \\
\left(\frac{h_{i-1}}{a} \right) C_{55}^{(i-1)} \left\{ [\mathbf{D}]^{(i-1)}(1) + S_2^{(i-1)} + [\mathbf{A},x]^{(i-1)}(1) + S_{1,x}^{(i-1)} \right\} &= \\
\left(\frac{h_i}{a} \right) C_{45}^{(i)} \left\{ [\mathbf{E}]^{(i)}(-1) + S_3^{(i)} + [\mathbf{A},y]^{(i)}(-1) + S_{1,y}^{(i)} \right\} + \\
\left(\frac{h_i}{a} \right) C_{55}^{(i)} \left\{ [\mathbf{D}]^{(i)}(-1) + S_2^{(i)} + [\mathbf{A},x]^{(i)}(-1) + S_{1,x}^{(i)} \right\} & \quad (5.91)
\end{aligned}$$

The equation for the continuity of σ_{xz} reduces to:

$$\begin{aligned}
\left(\frac{h_{i-1}}{h_i} \right) \left\{ C_{45}^{(i-1)} \left([\mathbf{E}]^{(i-1)} + S_3^{(i-1)} + [\mathbf{A},y]^{(i-1)} + S_{1,y}^{(i-1)} \right) + \right. \\
C_{55}^{(i-1)} \left([\mathbf{D}]^{(i-1)} + S_2^{(i-1)} + [\mathbf{A},x]^{(i-1)} + S_{1,x}^{(i-1)} \right) \left. \right\} + \\
\left\{ C_{45}^{(i)} \left([\mathbf{E}]^{(i)} + [\mathbf{A},y]^{(i)} - S_{1,y}^{(i)} \right) + \right. \\
C_{55}^{(i)} \left([\mathbf{D}]^{(i)} + [\mathbf{A},x]^{(i)} - S_{1,x}^{(i)} \right) \left. \right\} = \\
C_{45}^{(i)} S_3^{(i)} + C_{55}^{(i)} S_2^{(i)} & \quad (5.92)
\end{aligned}$$

Similarly, for the continuity of σ_{yz} ,

$$\begin{aligned}
\left(\frac{h_{i-1}}{h_i} \right) \left\{ C_{44}^{(i-1)} \left([\mathbf{E}]^{(i-1)} + S_3^{(i-1)} + [\mathbf{A},y]^{(i-1)} + S_{1,y}^{(i-1)} \right) + \right. \\
C_{45}^{(i-1)} \left([\mathbf{D}]^{(i-1)} + S_2^{(i-1)} + [\mathbf{A},x]^{(i-1)} + S_{1,x}^{(i-1)} \right) \left. \right\} +
\end{aligned}$$

$$\begin{aligned} & \left\{ C_{44}^{(i)} \left([\mathbf{E}]^{(i)} + [\mathbf{A}, \mathbf{y}]^{(i)} - S_{1,y}^{(i)} \right) + \right. \\ & \left. C_{45}^{(i)} \left([\mathbf{D}]^{(i)} + [\mathbf{A}, \mathbf{x}]^{(i)} - S_{1,x}^{(i)} \right) \right\} = \\ & C_{44}^{(i)} S_3^{(i)} + C_{45}^{(i)} S_2^{(i)} \end{aligned} \quad (5.93)$$

Solving the last two equations for $i = 2 \rightarrow N$ the expressions for $S_2^{(i)}$ and $S_3^{(i)}$ are obtained.

3. Continuity of u and v at each interface, i.e.

$$\begin{aligned} \hat{u} + \left(\frac{h_{i-1}}{a} \right)^2 u_2^{(i-1)} &= \hat{u} + \left(\frac{h_i}{a} \right)^2 u_2^{(i)} \\ \left(\frac{h_{i-1}}{a} \right)^2 \left\{ [\mathbf{D}]^{(i-1)} \frac{z_{i-1}^2}{2} + S_2^{(i-1)} z_{i-1} + S_4^{(i-1)} \right\} \\ &= \left(\frac{h_i}{a} \right)^2 \left\{ [\mathbf{D}]^{(i)} \frac{z_i^2}{2} + S_2^{(i)} z_i + S_4^{(i)} \right\} \end{aligned} \quad (5.94)$$

which leads to:

$$S_4^{(i)} = \left(\frac{h_{i-1}}{h_i} \right)^2 \left\{ \frac{1}{2} [\mathbf{D}]^{(i-1)} + S_2^{(i-1)} + S_4^{(i-1)} \right\} - \frac{1}{2} [\mathbf{D}]^{(i)} + S_2^{(i)} \quad (5.95)$$

Similarly for the continuity of the displacement v ,

$$S_5^{(i)} = \left(\frac{h_{i-1}}{h_i} \right)^2 \left\{ \frac{1}{2} [\mathbf{E}]^{(i-1)} + S_3^{(i-1)} + S_5^{(i-1)} \right\} - \frac{1}{2} [\mathbf{E}]^{(i)} + S_3^{(i)} \quad (5.96)$$

To obtain the values of $S_4^{(i)}$ and $S_5^{(i)}$, an extra condition is required for each of the two displacements. A possible choice could be to require that the mean in-plane displacement components $\bar{u}(x, y)$ and $\bar{v}(x, y)$ to coincide with the mean displacement components $\hat{u}(x, y)$ and $\hat{v}(x, y)$ of the equivalent plate. This would seem to be the natural condition to use when the mean in-plane displacements are prescribed at the edge of the plate.

Another condition could be that the stress resultants (N_{xx}, N_{yy}, N_{xy}) coincide with the corresponding stress resultants $(\hat{N}_{xx}, \hat{N}_{yy}, \hat{N}_{xy})$ of the equivalent

plate. This would be the natural condition to use if traction boundary conditions at the edge of the plate are prescribed.

From one of the previous two conditions together with eq. 5.95 and eq. 5.96, the values of $S_4^{(i)}$ and $S_5^{(i)}$ for $i = 1 \rightarrow N$ are determined.

5.8.4 Third Approximation

For this third approximation, assume that:

$$\begin{aligned}
 u^{(i)} &= \hat{u}(x, y) + \epsilon_i^2 \left\{ [\mathbf{D}]^{(i)} \frac{z_i^2}{2} + S_2^{(i)} z_i + S_4^{(i)} \right\} \\
 v^{(i)} &= \hat{v}(x, y) + \epsilon_i^2 \left\{ [\mathbf{E}]^{(i)} \frac{z_i^2}{2} + S_3^{(i)} z_i + S_5^{(i)} \right\} \\
 w^{(i)} &= \epsilon_i \left\{ [\mathbf{A}]^{(i)} z_i + S_1^{(i)} \right\} \\
 &\quad + \epsilon_i^3 \left\{ [\mathbf{F}]^{(i)} \frac{z_i^3}{6} + [\mathbf{G}]^{(i)} \frac{z_i^2}{2} + [\mathbf{H}]^{(i)} z_i + S_6^{(i)} \right\}
 \end{aligned} \tag{5.97}$$

1. Due to symmetry, $w^{(1)} = 0$ at $z = 0$, i.e.

$$\frac{h_1}{a} \left\{ [\mathbf{A}]^{(1)}(0) + S_1^{(1)} \right\} + \left(\frac{h_1}{a} \right)^3 \left\{ [\mathbf{F}]^{(1)}(0) + [\mathbf{G}]^{(1)}(0) + [\mathbf{H}]^{(1)}(0) + S_6^{(1)} \right\} = 0$$

which leads to:

$$S_6^{(1)} = 0 \tag{5.98}$$

2. Continuity of w at each interface (taking into account the first approximation), i.e.

$$\left(\frac{h_{i-1}}{a} \right)^3 w_3^{(i-1)} = \left(\frac{h_i}{a} \right)^3 w_3^{(i)} \tag{5.99}$$

that leads to:

$$\begin{aligned}
 \left(\frac{h_{i-1}}{a} \right)^3 \left\{ \frac{1}{6} [\mathbf{F}]^{(i-1)} + \frac{1}{2} [\mathbf{G}]^{(i-1)} + [\mathbf{H}]^{(i-1)} + S_6^{(i-1)} \right\} = \\
 \left(\frac{h_i}{a} \right)^3 \left\{ \frac{-1}{6} [\mathbf{F}]^{(i)} + \frac{1}{2} [\mathbf{G}]^{(i)} - [\mathbf{H}]^{(i)} + S_6^{(i)} \right\}
 \end{aligned} \tag{5.100}$$

leading to a recurrence formula of the form:

$$\begin{aligned}
S_6^{(i)} &= \left(\frac{h_{i-1}}{h_i}\right)^3 \left\{ \frac{1}{6}[\mathbf{F}]^{(i-1)} + \frac{1}{2}[\mathbf{G}]^{(i-1)} + [\mathbf{H}]^{(i-1)}(1) + S_8^{(i-1)} \right\} \\
&+ \frac{1}{6}[\mathbf{F}]^{(i)} - \frac{1}{2}[\mathbf{G}]^{(i)} + [\mathbf{H}]^{(i)} \quad (i = 2, 3, \dots, N) \quad (5.101)
\end{aligned}$$

5.8.5 Fourth Approximation

For this fourth approximation, assume that:

$$\begin{aligned}
u^{(i)} &= \hat{u}(x, y) + \epsilon_i^2 \left\{ [\mathbf{D}]^{(i)} \frac{z_i^2}{2} + S_2^{(i)} z_i + S_4^{(i)} \right\} \\
&+ \epsilon_i^4 \left\{ [\mathbf{Q}]^{(i)} \frac{z_i^4}{24} + [\mathbf{R}]^{(i)} \frac{z_i^3}{6} + [\mathbf{S}]^{(i)} \frac{z_i^2}{2} + S_7^{(i)} z_i + S_9^{(i)} \right\} \\
v^{(i)} &= \hat{v}(x, y) + \epsilon_i^2 \left\{ [\mathbf{E}]^{(i)} \frac{z_i^2}{2} + S_3^{(i)} z_i + S_5^{(i)} \right\} \\
&+ \epsilon_i^4 \left\{ [\mathbf{T}]^{(i)} \frac{z_i^4}{24} + [\mathbf{U}]^{(i)} \frac{z_i^3}{6} + [\mathbf{V}]^{(i)} \frac{z_i^2}{2} + S_8^{(i)} z_i + S_{10}^{(i)} \right\} \\
w^{(i)} &= \epsilon_i \left\{ [\mathbf{A}]^{(i)} z_i + S_1^{(i)} \right\} \\
&+ \epsilon_i^3 \left\{ [\mathbf{F}]^{(i)} \frac{z_i^3}{6} + [\mathbf{G}]^{(i)} \frac{z_i^2}{2} + [\mathbf{H}]^{(i)} z_i + S_6^{(i)} \right\} \quad (5.102)
\end{aligned}$$

Since the expression for $w^{(i)}$ has not changed, the conditions presented in the third approximation are still valid.

1. Due to symmetry, both σ_{xz} and $\sigma_{yz} = 0$ at $z = 0$

$$\begin{aligned}
&C_{45}^{(1)} \left\{ \left(\frac{h_1}{a}\right) [v_{2,z}^{(1)} + w_{1,y}^{(1)}] + \left(\frac{h_1}{a}\right)^3 [v_{4,z}^{(1)} + w_{3,y}^{(1)}] \right\} + \\
&C_{55}^{(1)} \left\{ \left(\frac{h_1}{a}\right) [u_{2,z}^{(1)} + w_{1,x}^{(1)}] + \left(\frac{h_1}{a}\right)^3 [u_{4,z}^{(1)} + w_{3,x}^{(1)}] \right\} = 0 \\
&C_{44}^{(1)} \left\{ \left(\frac{h_1}{a}\right) [v_{2,z}^{(1)} + w_{1,y}^{(1)}] + \left(\frac{h_1}{a}\right)^3 [v_{4,z}^{(1)} + w_{3,y}^{(1)}] \right\} + \\
&C_{45}^{(1)} \left\{ \left(\frac{h_1}{a}\right) [u_{2,z}^{(1)} + w_{1,x}^{(1)}] + \left(\frac{h_1}{a}\right)^3 [u_{4,z}^{(1)} + w_{3,x}^{(1)}] \right\} = 0 \quad (5.103)
\end{aligned}$$

Taking the results of the second approximation into consideration, and substituting for $u_4^{(i)}, v_4^{(i)}$ and $w_3^{(i)}$ from eq. 5.102, at $z = 0$ these equations reduce to:

$$\begin{aligned} C_{45}^{(1)} S_8^{(1)} + C_{55}^{(1)} S_7^{(1)} &= 0 \\ C_{44}^{(1)} S_8^{(1)} + C_{45}^{(1)} S_7^{(1)} &= 0 \end{aligned} \quad (5.104)$$

For no restrictions of the values of the coefficients $C_{44}^{(i)}, C_{45}^{(i)}$ and $C_{55}^{(i)}$,

$$S_7^{(1)} = S_8^{(1)} = 0 \quad (5.105)$$

2. Continuity of σ_{xz} and σ_{yz} at each interface. For the case of, σ_{xz} ,

$$\begin{aligned} C_{45}^{(i-1)} \left\{ \left(\frac{h_{i-1}}{a} \right) [v_{2,z}^{(i-1)} + w_{1,y}^{(i-1)}] + \left(\frac{h_{i-1}}{a} \right)^3 [v_{4,z}^{(i-1)} + w_{3,y}^{(i-1)}] \right\} + \\ C_{55}^{(i-1)} \left\{ \left(\frac{h_{i-1}}{a} \right) [u_{2,z}^{(i-1)} + w_{1,x}^{(i-1)}] + \left(\frac{h_{i-1}}{a} \right)^3 [u_{4,z}^{(i-1)} + w_{3,x}^{(i-1)}] \right\} = \\ C_{45}^{(i)} \left\{ \left(\frac{h_i}{a} \right) [v_{2,z}^{(i)} + w_{1,y}^{(i)}] + \left(\frac{h_i}{a} \right)^3 [v_{4,z}^{(i)} + w_{3,y}^{(i)}] \right\} + \\ C_{55}^{(i)} \left\{ \left(\frac{h_i}{a} \right) [u_{2,z}^{(i)} + w_{1,x}^{(i)}] + \left(\frac{h_i}{a} \right)^3 [u_{4,z}^{(i)} + w_{3,x}^{(i)}] \right\} \end{aligned} \quad (5.106)$$

Taking the results of the second approximation into consideration, and substituting for $u_4^{(i)}, v_4^{(i)}$ and $w_3^{(i)}$ from eq. 5.102, the equation for σ_{xz} reduces to:

$$\begin{aligned} \left(\frac{h_{i-1}}{h_i} \right)^3 \left\{ C_{45}^{(i-1)} \left(\frac{1}{6} [\mathbf{T}]^{(i-1)} + \frac{1}{2} [\mathbf{U}]^{(i-1)} + [\mathbf{V}]^{(i-1)} + S_8^{(i-1)} + \right. \right. \\ \left. \frac{1}{6} [\mathbf{F}, \mathbf{y}]^{(i-1)} + \frac{1}{2} [\mathbf{G}, \mathbf{y}]^{(i-1)} + [\mathbf{H}, \mathbf{y}]^{(i-1)} + S_{6,y}^{(i-1)} \right) + \\ \left. C_{55}^{(i-1)} \left(\frac{1}{6} [\mathbf{Q}]^{(i-1)} + \frac{1}{2} [\mathbf{R}]^{(i-1)} + [\mathbf{S}]^{(i-1)} + S_7^{(i-1)} + \right. \right. \end{aligned}$$

$$\begin{aligned}
& \left. \frac{1}{6}[\mathbf{F},\mathbf{x}]^{(i-1)} + \frac{1}{2}[\mathbf{G},\mathbf{x}]^{(i-1)} + [\mathbf{H},\mathbf{x}]^{(i-1)} + S_{6,x}^{(i-1)} \right\} - \\
& \quad \left\{ C_{45}^{(i)} \left(-\frac{1}{6}[\mathbf{T}]^{(i)} + \frac{1}{2}[\mathbf{U}]^{(i)} - [\mathbf{V}]^{(i)} - \right. \right. \\
& \quad \left. \frac{1}{6}[\mathbf{F},\mathbf{y}]^{(i)} + \frac{1}{2}[\mathbf{G},\mathbf{y}]^{(i)} - [\mathbf{H},\mathbf{y}]^{(i)} + S_{6,y}^{(i-1)} \right) + \\
& \quad \left. C_{55}^{(i)} \left(-\frac{1}{6}[\mathbf{Q}]^{(i)} + \frac{1}{2}[\mathbf{R}]^{(i)} - [\mathbf{S}]^{(i)} - \right. \right. \\
& \quad \left. \left. \frac{1}{6}[\mathbf{F},\mathbf{x}]^{(i)} + \frac{1}{2}[\mathbf{G},\mathbf{x}]^{(i)} - [\mathbf{H},\mathbf{x}]^{(i)} + S_{6,x}^{(i)} \right) \right\} = \\
& \qquad C_{45}^{(i)} S_8^{(i)} + C_{55}^{(i)} S_7^{(i)} \quad (5.107)
\end{aligned}$$

Similarly for the continuity of σ_{yz} ,

$$\begin{aligned}
& \left(\frac{h_{i-1}}{h_i} \right)^3 \left\{ C_{44}^{(i-1)} \left(\frac{1}{6}[\mathbf{T}]^{(i-1)} + \frac{1}{2}[\mathbf{U}]^{(i-1)} + [\mathbf{V}]^{(i-1)} + S_8^{(i-1)} + \right. \right. \\
& \quad \left. \frac{1}{6}[\mathbf{F},\mathbf{y}]^{(i-1)} + \frac{1}{2}[\mathbf{G},\mathbf{y}]^{(i-1)} + [\mathbf{H},\mathbf{y}]^{(i-1)} + S_{6,y}^{(i-1)} \right) + \\
& \quad C_{45}^{(i-1)} \left(\frac{1}{6}[\mathbf{Q}]^{(i-1)} + \frac{1}{2}[\mathbf{R}]^{(i-1)} + [\mathbf{S}]^{(i-1)} + S_7^{(i-1)} + \right. \\
& \quad \left. \frac{1}{6}[\mathbf{F},\mathbf{x}]^{(i-1)} + \frac{1}{2}[\mathbf{G},\mathbf{x}]^{(i-1)} + [\mathbf{H},\mathbf{x}]^{(i-1)} + S_{6,x}^{(i-1)} \right) \right\} - \\
& \quad \left\{ C_{44}^{(i)} \left(-\frac{1}{6}[\mathbf{T}]^{(i)} + \frac{1}{2}[\mathbf{U}]^{(i)} - [\mathbf{V}]^{(i)} - \right. \right. \\
& \quad \left. \frac{1}{6}[\mathbf{F},\mathbf{y}]^{(i)} + \frac{1}{2}[\mathbf{G},\mathbf{y}]^{(i)} - [\mathbf{H},\mathbf{y}]^{(i)} + S_{6,y}^{(i-1)} \right) + \\
& \quad C_{45}^{(i)} \left(-\frac{1}{6}[\mathbf{Q}]^{(i)} + \frac{1}{2}[\mathbf{R}]^{(i)} - [\mathbf{S}]^{(i)} - \right. \\
& \quad \left. \frac{1}{6}[\mathbf{F},\mathbf{x}]^{(i)} + \frac{1}{2}[\mathbf{G},\mathbf{x}]^{(i)} - [\mathbf{H},\mathbf{x}]^{(i)} + S_{6,x}^{(i)} \right) \right\} = \\
& \qquad C_{44}^{(i)} S_8^{(i)} + C_{45}^{(i)} S_7^{(i)} \quad (5.108)
\end{aligned}$$

Solving the last two equations for $i = 2 \rightarrow N$ the expressions for $S_7^{(i)}$ and $S_8^{(i)}$ are obtained.

3. Continuity of u and v at each interface. The continuity of u :

$$\hat{u} + \left(\frac{h_{i-1}}{a}\right)^2 u_2^{(i-1)} + \left(\frac{h_{i-1}}{a}\right)^4 u_4^{(i-1)} = \hat{u} + \left(\frac{h_i}{a}\right)^2 u_2^{(i)} + \left(\frac{h_i}{a}\right)^4 u_4^{(i)} \quad (5.109)$$

taking into consideration the second approximation :

$$\begin{aligned} \left(\frac{h_{i-1}}{a}\right)^4 \left\{ \frac{1}{24}[\mathbf{Q}]^{(i-1)} + \frac{1}{6}[\mathbf{R}]^{(i-1)} + \frac{1}{2}[\mathbf{S}]^{(i-1)} + S_7^{(i-1)} + S_9^{(i-1)} \right\} = \\ \left(\frac{h_i}{a}\right)^4 \left\{ \frac{1}{24}[\mathbf{Q}]^{(i)} - \frac{1}{6}[\mathbf{R}]^{(i)} + \frac{1}{2}[\mathbf{S}]^{(i)} - S_7^{(i)} + S_9^{(i)} \right\} \quad (5.110) \end{aligned}$$

from which we can get a recurrence formula for $S_9^{(i)}$ of the form:

$$\begin{aligned} S_9^{(i)} &= \left(\frac{h_{i-1}}{h_i}\right)^4 \left\{ \frac{1}{24}[\mathbf{Q}]^{(i-1)} + \frac{1}{6}[\mathbf{R}]^{(i-1)} + \frac{1}{2}[\mathbf{S}]^{(i-1)} + S_7^{(i-1)} + S_9^{(i-1)} \right\} \\ &- \left\{ \frac{1}{24}[\mathbf{Q}]^{(i)} - \frac{1}{6}[\mathbf{R}]^{(i)} + \frac{1}{2}[\mathbf{S}]^{(i)} - S_7^{(i)} \right\} \quad (5.111) \end{aligned}$$

Similarly, using the continuity condition for v , we get:

$$\begin{aligned} S_{10}^{(i)} &= \left(\frac{h_{i-1}}{h_i}\right)^4 \left\{ \frac{1}{24}[\mathbf{T}]^{(i-1)} + \frac{1}{6}[\mathbf{U}]^{(i-1)} + \frac{1}{2}[\mathbf{V}]^{(i-1)} + S_8^{(i-1)} + S_{10}^{(i-1)} \right\} \\ &- \left\{ \frac{1}{24}[\mathbf{T}]^{(i)} - \frac{1}{6}[\mathbf{U}]^{(i)} + \frac{1}{2}[\mathbf{V}]^{(i)} - S_8^{(i)} \right\} \quad (5.112) \end{aligned}$$

As was the case for the second approximation, to find $S_9^{(i)}$ and $S_{10}^{(i)}$, an extra condition is required for each of the two displacements. As before the choice could be to require that the mean in-plane displacement components $\bar{u}(x, y)$ and $\bar{v}(x, y)$ to coincide with the mean displacement components $\hat{u}(x, y)$ and $\hat{v}(x, y)$ of the equivalent plate. This would seem to be the natural condition to use when the mean in-plane displacements are prescribed at the edge of the plate. Another condition could be that the stress resultants (N_{xx}, N_{yy}, N_{xy}) coincide with the corresponding stress resultants ($\hat{N}_{xx}, \hat{N}_{yy}, \hat{N}_{xy}$) of the equivalent plate. This would be the natural condition to use if traction boundary conditions at the edge of the plate are prescribed.

From one of the previous two conditions together with eq. 5.111 and eq. 5.112, the values of $S_9^{(i)}$ and $S_{10}^{(i)}$ for $i = 1 \rightarrow N$ are determined.

5.8.6 Determination of σ_{zz}

In the work done by Spencer and co-workers [78] for isotropic materials, the value of σ_{zz} , the stress in the direction normal to the laminate was assumed to be zero throughout the laminate. But due to the importance of σ_{zz} in affecting delamination, this stress component cannot be neglected.

In this section, the third equilibrium equation of 5.8 will be used, together with the fact that the stress σ_{zz} vanishes on the lateral boundary of the laminate and the continuity of this stress through each interface, to account for this component in the analysis under consideration.

From the third of eqs. 5.8,

$$\sigma_{zz,z}^{(i)} = -\epsilon_i [\sigma_{xz,x}^{(i)} + \sigma_{yz,y}^{(i)}] \quad (5.113)$$

Integrating, we get:

$$\sigma_{zz}^{(i)} = - \int \left(\frac{h_i}{a} \right) [\sigma_{xz,x}^{(i)} + \sigma_{yz,y}^{(i)}] dz + S_{11}^{(i)}(x, y) \quad (5.114)$$

Substituting for the expressions of $u^{(i)}$, $v^{(i)}$ and $w^{(i)}$ from the fourth approximation in the expressions for σ_{xz} and σ_{yz} given in eq. 5.7, we obtain:

$$\begin{aligned} \sigma_{xz}^{(i)} &= C_{45}^{(i)} \{ \epsilon_i v_{2,z}^{(i)} + \epsilon_i^3 v_{4,z}^{(i)} + \epsilon_i w_{1,y}^{(i)} + \epsilon_i^3 w_{3,y}^{(i)} \} \\ &+ C_{55}^{(i)} \{ \epsilon_i u_{2,z}^{(i)} + \epsilon_i^3 u_{4,z}^{(i)} + \epsilon_i w_{1,x}^{(i)} + \epsilon_i^3 w_{3,x}^{(i)} \} \\ \sigma_{yz}^{(i)} &= C_{44}^{(i)} \{ \epsilon_i v_{2,z}^{(i)} + \epsilon_i^3 v_{4,z}^{(i)} + \epsilon_i w_{1,y}^{(i)} + \epsilon_i^3 w_{3,y}^{(i)} \} \\ &+ C_{45}^{(i)} \{ \epsilon_i u_{2,z}^{(i)} + \epsilon_i^3 u_{4,z}^{(i)} + \epsilon_i w_{1,x}^{(i)} + \epsilon_i^3 w_{3,x}^{(i)} \} \end{aligned} \quad (5.115)$$

Substituting for the values of $w_1^{(i)}$, $w_3^{(i)}$, $u_2^{(i)}$, $u_4^{(i)}$, $v_2^{(i)}$ and $v_4^{(i)}$, and differentiating,

then substituting in eq. 5.115, we get:

$$\begin{aligned}
\sigma_{zz}^{(i)} = & -\left(\frac{a}{H}\right)\left(\frac{h_i}{a}\right)^3 \left\{ C_{45}^{(i)} \left([E, x]^{(i)} \frac{z_i^2}{2} + S_{3,x}^{(i)} z_i + [A, xy]^{(i)} \frac{z_i^2}{2} + S_{1,xy}^{(i)} z_i \right) \right. \\
& + C_{55}^{(i)} \left([D, x]^{(i)} \frac{z_i^2}{2} + S_{2,x}^{(i)} z_i + [A, xx]^{(i)} \frac{z_i^2}{2} + S_{1,xx}^{(i)} z_i \right) \\
& + C_{44}^{(i)} \left([E, y]^{(i)} \frac{z_i^2}{2} + S_{3,y}^{(i)} z_i + [A, yy]^{(i)} \frac{z_i^2}{2} + S_{1,yy}^{(i)} z_i \right) \\
& \left. + C_{45}^{(i)} \left([D, y]^{(i)} \frac{z_i^2}{2} + S_{2,y}^{(i)} z_i + [A, xy]^{(i)} \frac{z_i^2}{2} + S_{1,xy}^{(i)} z_i \right) \right\} \\
& - \left(\frac{a}{H}\right)\left(\frac{h_i}{a}\right)^5 \left\{ C_{45}^{(i)} \left([T, x]^{(i)} \frac{z_i^4}{24} + [U, x]^{(i)} \frac{z_i^3}{6} + [V, x]^{(i)} \frac{z_i^2}{2} + S_{8,x}^{(i)} z_i \right) \right. \\
& + [F, xy]^{(i)} \frac{z_i^4}{24} + [G, xy]^{(i)} \frac{z_i^3}{6} + [H, xy]^{(i)} \frac{z_i^2}{2} + S_{6,xy}^{(i)} z_i \left. \right) \\
& + C_{55}^{(i)} \left([Q, x]^{(i)} \frac{z_i^4}{24} + [R, x]^{(i)} \frac{z_i^3}{6} + [S, x]^{(i)} \frac{z_i^2}{2} + S_{7,x}^{(i)} z_i \right. \\
& \left. + [F, xx]^{(i)} \frac{z_i^4}{24} + [G, xx]^{(i)} \frac{z_i^3}{6} + [H, xx]^{(i)} \frac{z_i^2}{2} + S_{6,xx}^{(i)} z_i \right) \\
& + C_{44}^{(i)} \left([T, y]^{(i)} \frac{z_i^4}{24} + [U, y]^{(i)} \frac{z_i^3}{6} + [V, y]^{(i)} \frac{z_i^2}{2} + S_{8,y}^{(i)} z_i \right. \\
& \left. + [F, yy]^{(i)} \frac{z_i^4}{24} + [G, yy]^{(i)} \frac{z_i^3}{6} + [H, yy]^{(i)} \frac{z_i^2}{2} + S_{6,yy}^{(i)} z_i \right) \\
& + C_{45}^{(i)} \left([Q, y]^{(i)} \frac{z_i^4}{24} + [R, y]^{(i)} \frac{z_i^3}{6} + [S, y]^{(i)} \frac{z_i^2}{2} + S_{7,y}^{(i)} z_i \right. \\
& \left. + [F, xy]^{(i)} \frac{z_i^4}{24} + [G, xy]^{(i)} \frac{z_i^3}{6} + [H, xy]^{(i)} \frac{z_i^2}{2} + S_{6,xy}^{(i)} z_i \right) \left. \right\} \\
& + S_{11}^{(i)}(x, y) \tag{5.116}
\end{aligned}$$

Now use the following condition, for no stress condition on the lateral boundary of the laminate:

$$\sigma_{zz}^{(N)} = 0$$

in eq. 5.116, to obtain the value of the function $S_{11}^{(N)}$. Knowing this function, the $\sigma_{zz}^{(i)}$ continuity condition at every interface will enable us to determine $S_{11}^{(i)}$ for $i = 1, 2, \dots, N-1$.

5.9 Three Dimensional Theory for Laminates - Bending Deformations

Considering the bending deformations of the laminate, we seek a solution in which, in each lamina, the displacements are of the form of eq. 5.59 and eq. 5.60 with ϵ replaced by ϵ_i , the material constants \tilde{Q}_{jk} by $\tilde{Q}_{jk}^{(i)}$ and z by z_i . Also the functions B_1, B_2, \dots etc should be replaced by $B_1^{(i)}, B_2^{(i)}, \dots$ for the lamina i since these functions, in the general case, can have different values in each lamina.

The function $w_o(x, y)$ is required to satisfy the two dimensional solution. Because the CLT appears to give satisfactory results for the average value of w , we can choose this displacement to be that of the equivalent plate under the given boundary conditions. Thus, in the layer i , the displacements u and v will be assumed to have the form:

$$\begin{bmatrix} u^{(i)} \\ v^{(i)} \end{bmatrix} = \epsilon_i \begin{bmatrix} u_1^{(i)} \\ v_1^{(i)} \end{bmatrix} + \epsilon_i^3 \begin{bmatrix} u_3^{(i)} \\ v_3^{(i)} \end{bmatrix} + \dots \quad (5.117)$$

while the expression for w will be:

$$w^{(i)} = w_o(x, y) + \epsilon_i^2 w_2^{(i)} + \epsilon_i^4 w_4^{(i)} + \dots \quad (5.118)$$

The corresponding expressions for the stresses can be calculated using eq. 5.7. The remaining task now is to determine the unknown functions $B_k^{(i)}(x, y)$. To accomplish that, the following conditions have to be satisfied:

- Symmetry conditions at $z_1 = 0$:

$$u^{(1)} = 0 \quad v^{(1)} = 0 \quad \sigma_{xx}^{(1)} = 0 \quad \sigma_{yy}^{(1)} = 0 \quad \sigma_{xy}^{(1)} = 0 \quad \text{at } z = 0$$

- Continuity of displacement and traction at each interface between layer $(i-1)$ at $z_{i-1} = 1$ and layer (i) at $z_i = -1$ ($i=2,3,\dots,N$):

$$u^{(i-1)} = u^{(i)}, \quad v^{(i-1)} = v^{(i)}, \quad w^{(i-1)} = w^{(i)}$$

$$\sigma_{xz}^{(i-1)} = \sigma_{xz}^{(i)}, \quad \sigma_{yz}^{(i-1)} = \sigma_{yz}^{(i)}, \quad \sigma_{zz}^{(i-1)} = \sigma_{zz}^{(i)}$$

- The traction condition on the upper surface ($z_N = 1$) should vanish:

$$\sigma_{xz}^{(N)} = 0, \quad \sigma_{yz}^{(N)} = 0, \quad \sigma_{zz}^{(N)} = 0$$

5.9.1 First Approximation

For this first approximation, assume that:

$$\begin{aligned} u^{(i)} &= \epsilon_i u_1^{(i)} = \frac{h_i}{a} \left\{ -\tilde{w}_{,x} z_i + B_1^{(i)}(x, y) \right\} \\ v^{(i)} &= \epsilon_i v_1^{(i)} = \frac{h_i}{a} \left\{ -\tilde{w}_{,y} z_i + B_1^{(i)}(x, y) \right\} \\ w^{(i)} &= \tilde{w}(x, y) \end{aligned} \quad (5.119)$$

1. Due to symmetry, $u^{(1)} = v^{(1)} = \sigma_{xz}^{(1)} = \sigma_{yz}^{(1)} = \sigma_{xy}^{(1)} = 0$ at $z = 0$. For the displacement u :

$$\left(\frac{h_1}{a} \right) \left\{ -\tilde{w}_{,x}(0) + B_1^{(1)} \right\} = 0$$

which leads to:

$$B_1^{(1)} = 0 \quad (5.120)$$

Similarly, the symmetry condition for v leads to:

$$B_2^{(1)} = 0 \quad (5.121)$$

Note that satisfying the symmetry condition for u and v , automatically satisfies that condition for σ_{xz} , σ_{yz} and σ_{xy}

2. Continuity of u at each interface, i.e.

$$\begin{aligned} \left(\frac{h_{i-1}}{a} \right) u_1^{(i-1)} &= \left(\frac{h_i}{a} \right) u_1^{(i)} \\ \left(\frac{h_{i-1}}{a} \right) \left\{ -\tilde{w}_{,x}(1) + B_1^{(i-1)} \right\} &= \left(\frac{h_i}{a} \right) \left\{ -\tilde{w}_{,x}(-1) + B_1^{(i)} \right\} \end{aligned} \quad (5.122)$$

leading to a recurrence formula of the form:

$$B_1^{(i)} = \left(\frac{h_{i-1}}{h_i} \right) \left\{ -\tilde{w}_{,x} + B_1^{(i-1)} \right\} - \tilde{w}_{,x} \quad (i = 2, 3, \dots, N) \quad (5.123)$$

Similarly, for the continuity of the displacement v ,

$$B_2^{(i)} = \left(\frac{h_{i-1}}{h_i} \right) \left\{ -\tilde{w}_{,y} + B_2^{(i-1)} \right\} - \tilde{w}_{,y} \quad (i = 2, 3, \dots, N) \quad (5.124)$$

3. The traction condition on the upper surface ($z_N = 1$) should vanish.

In eqs. 5.21 and 5.22, two functions $G(x, y)$ and $H(x, y)$ were assumed to be equal to zero. The reason for that will be shown here. The values of $\sigma_{xz}^{(N)} = \sigma_{yz}^{(N)} = 0$. Substituting from the values of $u^{(i)}, v^{(i)}$ and $w^{(i)}$ from the first approximation in the form of these two stress components from eq. 5.7, leads to:

$$\begin{aligned} \sigma_{xz}^{(N)} &= C_{45}^{(N)} (v_{1,z}^{(N)} + \tilde{w}_{,y}) + C_{55}^{(N)} (u_{1,z}^{(N)} + \tilde{w}_{,x}) \\ \sigma_{yz}^{(N)} &= C_{44}^{(N)} (v_{1,z}^{(N)} + \tilde{w}_{,y}) + C_{45}^{(N)} (u_{1,z}^{(N)} + \tilde{w}_{,x}) \end{aligned} \quad (5.125)$$

Substituting for the values of u_1 and v_1 from eqs. 5.21 and 5.22, we get:

$$\begin{aligned} \sigma_{xz}^{(N)} &= C_{45}^{(N)} (-\tilde{w}_{,y} + H^{(N)}(x, y) + \tilde{w}_{,y}) + C_{55}^{(N)} (-\tilde{w}_{,x} + G^{(N)}(x, y) + \tilde{w}_{,x}) \\ \sigma_{yz}^{(N)} &= C_{44}^{(N)} (-\tilde{w}_{,y} + H^{(N)}(x, y) + \tilde{w}_{,y}) + C_{45}^{(N)} (-\tilde{w}_{,x} + G^{(N)}(x, y) + \tilde{w}_{,x}) \end{aligned} \quad (5.126)$$

which finally leads to:

$$\begin{aligned} \sigma_{xz}^{(N)} &= C_{45}^{(N)} H^{(N)}(x, y) + C_{55}^{(N)} G^{(N)}(x, y) \\ \sigma_{yz}^{(N)} &= C_{44}^{(N)} H^{(N)}(x, y) + C_{45}^{(N)} G^{(N)}(x, y) \end{aligned} \quad (5.127)$$

But since $\sigma_{xz}^{(N)} = \sigma_{yz}^{(N)} = 0$, for general unrestricted values of $C_{44}^{(N)}, C_{45}^{(N)}$ and $C_{55}^{(N)}$,

$$H^{(N)}(x, y) = G^{(N)}(x, y) = 0 \quad (5.128)$$

Also, since the stress components in eqs. 5.126 are independent of z , the continuity of these stresses at every interface will show that:

$$H^{(i)}(x, y) = G^{(i)}(x, y) = 0 \quad (5.129)$$

5.9.2 Second Approximation

For this second approximation, assume that:

$$\begin{aligned} u^{(i)} &= \epsilon_i \left\{ -\tilde{w}_{,x} z_i + B_1^{(i)} \right\} \\ v^{(i)} &= \epsilon_i \left\{ -\tilde{w}_{,y} z_i + B_2^{(i)} \right\} \\ w^{(i)} &= \tilde{w}(x, y) + \epsilon_i^2 \left\{ [\mathbf{B}]^{(i)} \frac{z_i^2}{2} + [\mathbf{C}]^{(i)} z_i + B_3^{(i)} \right\} \end{aligned} \quad (5.130)$$

Since the expressions for $u^{(i)}$ and $v^{(i)}$ are the same as for the first approximation, the conditions satisfied in the first approximation are still valid.

1. Continuity of w at every interface results in:

$$\begin{aligned} \tilde{w}(x, y) + \epsilon_i^2 \left\{ [\mathbf{B}]^{(i)} \frac{z_i^2}{2} + [\mathbf{C}]^{(i)} z_i + B_3^{(i)} \right\} \\ = \tilde{w}(x, y) + \epsilon_{i-1}^2 \left\{ [\mathbf{B}]^{(i-1)} \frac{z_{i-1}^2}{2} + [\mathbf{C}]^{(i-1)} z_{i-1} + B_3^{(i-1)} \right\} \end{aligned} \quad (5.131)$$

which leads to the following recurrence formula for $B_3^{(i)}$:

$$B_3^{(i)} = \left(\frac{h_{i-1}}{h_i} \right)^2 \left\{ \frac{1}{2} [\mathbf{B}]^{(i-1)} + [\mathbf{C}]^{(i-1)} + B_3^{(i-1)} \right\} - \left\{ \frac{1}{2} [\mathbf{B}]^{(i)} - [\mathbf{C}]^{(i)} \right\} \quad (5.132)$$

Another condition is required for the full determination of the functions $B_3^{(i)}$. A possible choice is to require that the mid-surface deflection coincides with the deflection of the equivalent plate; i.e.

$$w^{(i)} \Big|_{z=0} = \tilde{w}$$

This would be the natural choice if edge boundary conditions are imposed on the deflection.

Alternatively, if the edge moments are specified as boundary conditions, we may specify that the resultant bending moments (M_{xx}, M_{yy}, M_{xy}) coincide with those of the equivalent plate $(\tilde{M}_{xx}, \tilde{M}_{yy}, \tilde{M}_{xy})$.

Using one of the above-mentioned conditions together with eq. 5.132 the values of all $B_3^{(i)}$ for $i = 1 \rightarrow N$ are determined.

5.9.3 Third Approximation

For this third approximation, assume that:

$$\begin{aligned} u^{(i)} &= \epsilon_i \left\{ -\tilde{w}_{,x} z_i + B_1^{(i)} \right\} + \epsilon_i^3 \left\{ [\mathbf{I}]^{(i)} \frac{z_i^3}{6} + [\mathbf{J}]^{(i)} \frac{z_i^2}{2} + B_4^{(i)} z_i + B_6^{(i)} \right\} \\ v^{(i)} &= \epsilon_i \left\{ -\tilde{w}_{,y} z_i + B_2^{(i)} \right\} + \epsilon_i^3 \left\{ [\mathbf{K}]^{(i)} \frac{z_i^3}{6} + [\mathbf{L}]^{(i)} \frac{z_i^2}{2} + B_5^{(i)} z_i + B_7^{(i)} \right\} \\ w^{(i)} &= \tilde{w}(x, y) + \epsilon_i^2 \left\{ [\mathbf{B}]^{(i)} \frac{z_i^2}{2} + [\mathbf{C}]^{(i)} z_i + B_3^{(i)} \right\} \end{aligned} \quad (5.133)$$

Since the expression for $w^{(i)}$ is the same as for the second approximation, the conditions satisfied in the second approximation are still valid.

1. Due to symmetry, $u^{(1)} = v^{(1)} = \sigma_{xx}^{(1)} = \sigma_{yy}^{(1)} = \sigma_{xy}^{(1)} = 0$ at $z = 0$. For the displacement u :

$$\frac{h_1}{a} \left\{ -\tilde{w}_{,x}(0) + B_1^{(1)} \right\} + \frac{h_1^3}{a} \left\{ [\mathbf{I}]^{(1)}(0) + [\mathbf{J}]^{(1)}(0) + B_4^{(1)}(0) + B_6^{(1)} \right\} = 0 \quad (5.134)$$

which leads to:

$$B_6^{(1)} = 0 \quad (5.135)$$

Similarly, the symmetry condition for v leads to:

$$B_7^{(1)} = 0 \quad (5.136)$$

Note that satisfying the symmetry condition for u and v , automatically satisfies that condition for σ_{xx}, σ_{yy} and σ_{xy}

2. The tractions on the upper surface ($z_N = 1$) should vanish:

$$\sigma_{xz}^{(N)} = 0, \quad \sigma_{yz}^{(N)} = 0$$

Expanding the above conditions, we get:

$$\begin{aligned} \sigma_{xz}^{(N)} &= C_{45}^{(N)} (v_{1,z}^{(N)} + \epsilon_N^2 v_{3,z}^{(N)} + \tilde{w}_{,y} + \epsilon_N^2 w_{2,y}^{(N)}) \\ &\quad + C_{55}^{(N)} (u_{1,z}^{(N)} + \epsilon_N^2 u_{3,z}^{(N)} + \tilde{w}_{,x} + \epsilon_N^2 w_{2,x}^{(N)}) \\ \sigma_{yz}^{(N)} &= C_{44}^{(N)} (v_{1,z}^{(N)} + \epsilon_N^2 v_{3,z}^{(N)} + \tilde{w}_{,y} + \epsilon_N^2 w_{2,y}^{(N)}) \\ &\quad + C_{45}^{(N)} (u_{1,z}^{(N)} + \epsilon_N^2 u_{3,z}^{(N)} + \tilde{w}_{,x} + \epsilon_N^2 w_{2,x}^{(N)}) \end{aligned} \quad (5.137)$$

Substituting for the values of u_1, u_3, v_1, v_3 and w_3 from eqs. 5.133 replacing z_N by 1 leads to:

$$\begin{aligned} \sigma_{xz}^{(N)} &= \epsilon_N^2 \left(C_{45}^{(N)} \left\{ \left(\frac{1}{2} \right) [\mathbf{K} + \mathbf{B}_{,y}]^{(N)} + [\mathbf{L} + \mathbf{C}_{,y}]^{(N)} + B_5^{(N)} + B_{3,y}^{(N)} \right\} \right. \\ &\quad \left. + C_{55}^{(N)} \left\{ \left(\frac{1}{2} \right) [\mathbf{I} + \mathbf{B}_{,x}]^{(N)} + [\mathbf{J} + \mathbf{C}_{,x}]^{(N)} + B_4^{(N)} + B_{3,z}^{(N)} \right\} \right) \\ \sigma_{yz}^{(N)} &= \epsilon_N^2 \left(C_{44}^{(N)} \left\{ \left(\frac{1}{2} \right) [\mathbf{K} + \mathbf{B}_{,y}]^{(N)} + [\mathbf{L} + \mathbf{C}_{,y}]^{(N)} + B_5^{(N)} + B_{3,y}^{(N)} \right\} \right. \\ &\quad \left. + C_{45}^{(N)} \left\{ \left(\frac{1}{2} \right) [\mathbf{I} + \mathbf{B}_{,x}]^{(N)} + [\mathbf{J} + \mathbf{C}_{,x}]^{(N)} + B_4^{(N)} + B_{3,z}^{(N)} \right\} \right) \end{aligned} \quad (5.138)$$

For both of these stresses to be zero and for no restrictions on the values of $C_{44}^{(N)}, C_{45}^{(N)}$ and $C_{55}^{(N)}$, equations for determining $B_4^{(N)}$ and $B_5^{(N)}$ are now

obtained:

$$\begin{aligned} B_4^{(N)} &= - \left\{ \left(\frac{1}{2} \right) [\mathbf{I} + \mathbf{B}_{,x}]^{(N)} + [\mathbf{J} + \mathbf{C}_{,x}]^{(N)} + B_{3,x}^{(N)} \right\} \\ B_5^{(N)} &= - \left\{ \left(\frac{1}{2} \right) [\mathbf{K} + \mathbf{B}_{,y}]^{(N)} + [\mathbf{L} + \mathbf{C}_{,y}]^{(N)} + B_{3,y}^{(N)} \right\} \end{aligned} \quad (5.139)$$

3. Continuity of tractions at each interface between layer $(i-1)$ at $z_{i-1} = 1$ and layer (i) at $z_i = -1$ ($i=2,3,\dots,N$):

$$\sigma_{xz}^{(i-1)} = \sigma_{xz}^{(i)}, \quad \sigma_{yz}^{(i-1)} = \sigma_{yz}^{(i)}$$

Expanding the above conditions, we get:

$$\begin{aligned} & \epsilon_i^2 \left(C_{45}^{(i)} \left\{ \left(\frac{1}{2} \right) [\mathbf{K} + \mathbf{B}_{,y}]^{(i)} - [\mathbf{L} + \mathbf{C}_{,y}]^{(i)} + B_5^{(i)} + B_{3,y}^{(i)} \right\} \right. \\ & + C_{55}^{(i)} \left\{ \left(\frac{1}{2} \right) [\mathbf{I} + \mathbf{B}_{,x}]^{(i)} - [\mathbf{J} + \mathbf{C}_{,x}]^{(i)} + B_4^{(i)} + B_{3,x}^{(i)} \right\} \left. \right) \\ & = \epsilon_{i-1}^2 \left(C_{45}^{(i-1)} \left\{ \left(\frac{1}{2} \right) [\mathbf{K} + \mathbf{B}_{,y}]^{(i-1)} + [\mathbf{L} + \mathbf{C}_{,y}]^{(i-1)} + B_5^{(i-1)} + B_{3,y}^{(i-1)} \right\} \right. \\ & + C_{55}^{(i-1)} \left\{ \left(\frac{1}{2} \right) [\mathbf{I} + \mathbf{B}_{,x}]^{(i-1)} + [\mathbf{J} + \mathbf{C}_{,x}]^{(i-1)} + B_4^{(i-1)} + B_{3,x}^{(i-1)} \right\} \left. \right) \\ & \epsilon_i^2 \left(C_{44}^{(i)} \left\{ \left(\frac{1}{2} \right) [\mathbf{K} + \mathbf{B}_{,y}]^{(i)} - [\mathbf{L} + \mathbf{C}_{,y}]^{(i)} + B_5^{(i)} + B_{3,y}^{(i)} \right\} \right. \\ & + C_{45}^{(i)} \left\{ \left(\frac{1}{2} \right) [\mathbf{I} + \mathbf{B}_{,x}]^{(i)} - [\mathbf{J} + \mathbf{C}_{,x}]^{(i)} + B_4^{(i)} + B_{3,x}^{(i)} \right\} \left. \right) \\ & = \epsilon_{i-1}^2 \left(C_{44}^{(i-1)} \left\{ \left(\frac{1}{2} \right) [\mathbf{K} + \mathbf{B}_{,y}]^{(i-1)} + [\mathbf{L} + \mathbf{C}_{,y}]^{(i-1)} + B_5^{(i-1)} + B_{3,y}^{(i-1)} \right\} \right. \\ & + C_{45}^{(i-1)} \left\{ \left(\frac{1}{2} \right) [\mathbf{I} + \mathbf{B}_{,x}]^{(i-1)} + [\mathbf{J} + \mathbf{C}_{,x}]^{(i-1)} + B_4^{(i-1)} + B_{3,x}^{(i-1)} \right\} \left. \right) \end{aligned} \quad (5.140)$$

The values of $B_4^{(i)}$ and $B_5^{(i)}$ are then determined from:

$$\begin{aligned} & C_{45}^{(i-1)} B_5^{(i-1)} + C_{55}^{(i-1)} B_4^{(i-1)} \\ & = \left(\frac{h_i}{h_{i-1}} \right)^2 \left(C_{45}^{(i)} \left\{ \frac{1}{2} [\mathbf{K} + \mathbf{B}_{,y}]^{(i)} - [\mathbf{L} + \mathbf{C}_{,y}]^{(i)} + B_5^{(i)} + B_{3,y}^{(i)} \right\} \right. \end{aligned}$$

$$\begin{aligned}
& + C_{55}^{(i)} \left\{ \left(\frac{1}{2} \right) [\mathbf{I} + \mathbf{B}_{,x}]^{(i)} - [\mathbf{J} + \mathbf{C}_{,x}]^{(i)} + B_4^{(i)} + B_{3,x}^{(i)} \right\} \\
& - \left(C_{45}^{(i-1)} \left\{ \frac{1}{2} [\mathbf{K} + \mathbf{B}_{,y}]^{(i-1)} + [\mathbf{L} + \mathbf{C}_{,y}]^{(i-1)} + B_{3,y}^{(i-1)} \right\} \right. \\
& \left. + C_{55}^{(i-1)} \left\{ \left(\frac{1}{2} \right) [\mathbf{I} + \mathbf{B}_{,x}]^{(i-1)} + [\mathbf{J} + \mathbf{C}_{,x}]^{(i-1)} + B_{3,x}^{(i-1)} \right\} \right) \\
& = \left(\frac{h_i}{h_{i-1}} \right)^2 \left(C_{44}^{(i)} \left\{ \frac{1}{2} [\mathbf{K} + \mathbf{B}_{,y}]^{(i)} - [\mathbf{L} + \mathbf{C}_{,y}]^{(i)} + B_5^{(i)} + B_{3,y}^{(i)} \right\} \right. \\
& + C_{45}^{(i)} \left\{ \left(\frac{1}{2} \right) [\mathbf{I} + \mathbf{B}_{,x}]^{(i)} - [\mathbf{J} + \mathbf{C}_{,x}]^{(i)} + B_4^{(i)} + B_{3,x}^{(i)} \right\} \left. \right) \\
& - \left(C_{44}^{(i-1)} \left\{ \frac{1}{2} [\mathbf{K} + \mathbf{B}_{,y}]^{(i-1)} + [\mathbf{L} + \mathbf{C}_{,y}]^{(i-1)} + B_{3,y}^{(i-1)} \right\} \right. \\
& \left. + C_{45}^{(i-1)} \left\{ \left(\frac{1}{2} \right) [\mathbf{I} + \mathbf{B}_{,x}]^{(i-1)} + [\mathbf{J} + \mathbf{C}_{,x}]^{(i-1)} + B_{3,x}^{(i-1)} \right\} \right)
\end{aligned} \tag{5.141}$$

The two previous equations together with the formula of eq. 5.139, allow us to determine $B_4^{(i)}$ and $B_5^{(i)}$ for $i = 1, 2, \dots, N$.

4. Continuity of u and v at every interface, i.e.

$$u^{(i)} = u^{(i-1)} \quad \text{and} \quad v^{(i)} = v^{(i-1)}$$

Using the results given by the first approximation, two recurrence formulae for $B_6^{(i)}$ and $B_7^{(i)}$ are obtained:

$$\begin{aligned}
B_6^{(i)} & = \left(\frac{h_{i-1}}{h_i} \right)^3 \left\{ \frac{1}{6} [\mathbf{I}]^{(i-1)} + \frac{1}{2} [\mathbf{J}]^{(i-1)} + B_4^{(i-1)} + B_6^{(i-1)} \right\} \\
& - \left\{ -\frac{1}{6} [\mathbf{I}]^{(i)} + \frac{1}{2} [\mathbf{J}]^{(i)} - B_4^{(i)} \right\} \\
B_7^{(i)} & = \left(\frac{h_{i-1}}{h_i} \right)^3 \left\{ \frac{1}{6} [\mathbf{K}]^{(i-1)} + \frac{1}{2} [\mathbf{L}]^{(i-1)} + B_5^{(i-1)} + B_7^{(i-1)} \right\} \\
& - \left\{ -\frac{1}{6} [\mathbf{K}]^{(i)} + \frac{1}{2} [\mathbf{L}]^{(i)} - B_5^{(i)} \right\}
\end{aligned} \tag{5.142}$$

Making use of eqs. 5.135 and 5.136, $B_8^{(i)}$ and $B_7^{(i)}$ are determined.

5.9.4 Determination of σ_{zz}

As was the case for the stretching problem, in this section, the third equilibrium equation of 5.8 will be used, together with the fact that the stress σ_{xz} vanishes on the lateral boundary of the laminate and the continuity of that stress through each interface, to account for that stress component in the analysis under consideration.

Integrating the third of eqs. 5.8,

$$\sigma_{zz}^{(i)} = - \int \left(\frac{h_i}{a} \right) [\sigma_{zz,x}^{(i)} + \sigma_{yz,y}^{(i)}] dz + B_8^{(i)}(x, y) \quad (5.143)$$

Substituting for the expressions of $u^{(i)}$, $v^{(i)}$ and $w^{(i)}$ from the fourth approximation in the expressions for σ_{xz} and σ_{yz} given in eq. 5.7, we obtain:

$$\begin{aligned} \sigma_{xz}^{(i)} &= C_{45}^{(i)} \{ v_{1,z}^{(i)} + \epsilon_i^2 v_{3,z}^{(i)} + \tilde{w}_{,y} + \epsilon_i^2 w_{2,y}^{(i)} \} \\ &+ C_{55}^{(i)} \{ u_{1,z}^{(i)} + \epsilon_i^2 u_{3,z}^{(i)} + \tilde{w}_{,x} + \epsilon_i^2 w_{2,x}^{(i)} \} \\ \sigma_{yz}^{(i)} &= C_{44}^{(i)} \{ v_{1,z}^{(i)} + \epsilon_i^2 v_{3,z}^{(i)} + \tilde{w}_{,y} + \epsilon_i^2 w_{2,y}^{(i)} \} \\ &+ C_{45}^{(i)} \{ u_{1,z}^{(i)} + \epsilon_i^2 u_{3,z}^{(i)} + \tilde{w}_{,x} + \epsilon_i^2 w_{2,x}^{(i)} \} \end{aligned} \quad (5.144)$$

Substituting for the values of $w_2^{(i)}$, $u_1^{(i)}$, $u_3^{(i)}$, $v_1^{(i)}$ and $v_3^{(i)}$, and differentiating, then substituting in eq. 5.143, we get:

$$\begin{aligned} \sigma_{zz}^{(i)} &= - \left(\frac{a}{H} \right) \left(\frac{h_i}{a} \right)^4 \left\{ C_{45}^{(i)} \left([\mathbf{K}_{,x} + \mathbf{B}_{,xy}]^{(i)} \frac{z_i^3}{6} + [\mathbf{B}_{,x} + \mathbf{C}_{,xy}]^{(i)} \frac{z_i^2}{2} + [B_{5,x}^{(i)} + B_{3,xy}^{(i)}] z_i \right) \right. \\ &+ C_{55}^{(i)} \left([\mathbf{I}_{,x} + \mathbf{B}_{,xx}]^{(i)} \frac{z_i^3}{6} + [\mathbf{J}_{,x} + \mathbf{C}_{,xx}]^{(i)} \frac{z_i^2}{2} + [B_{4,x}^{(i)} + B_{3,xx}^{(i)}] z_i \right) \\ &+ C_{44}^{(i)} \left([\mathbf{K}_{,y} + \mathbf{B}_{,yy}]^{(i)} \frac{z_i^3}{6} + [\mathbf{B}_{,y} + \mathbf{C}_{,yy}]^{(i)} \frac{z_i^2}{2} + [B_{5,y}^{(i)} + B_{3,yy}^{(i)}] z_i \right) \\ &+ C_{45}^{(i)} \left([\mathbf{I}_{,y} + \mathbf{B}_{,xy}]^{(i)} \frac{z_i^3}{6} + [\mathbf{J}_{,y} + \mathbf{C}_{,xy}]^{(i)} \frac{z_i^2}{2} + [B_{4,y}^{(i)} + B_{3,xy}^{(i)}] z_i \right) \left. \right\} \\ &+ B_8^{(i)}(x, y) \end{aligned} \quad (5.145)$$

Now use the following condition, for no stress condition on the lateral boundary of the laminate:

$$\sigma_{zz}^{(N)} = 0$$

in eq. 5.145, to obtain the value of the function $B_8^{(N)}$. Knowing this function, the $\sigma_{zz}^{(i)}$ continuity condition at every interface will enable us to determine $B_8^{(i)}$ for $i = 1, 2, \dots, N - 1$.

5.10 Limitation of the Present Method

The general series solution assumed for the isotropic case always converges. This is obviously due to the fact that the series terminates after three terms. Using the same form of solution for the anisotropic case, resulted in an infinite (non-converging) series; thus reducing our goal to obtain an approximate rather than an "exact" solution.

In order to handle the size of the equations, the series was only expanded up to the fourth order in ϵ . Since ϵ is a function of the laminate thickness and the coefficients of the series (u_i, v_i and w_i) are functions of the position (x, y and z) and the material properties Q_{ij} , the convergence of the solution would depend on these aforementioned factors. For example, away from a hole (or a free edge) or when using a very thin laminate, the higher terms of the infinite series will be negligible and the solution converges. This is not the case near the hole or for a laminate with a hole size to thickness ratio (R/t) of less than 10.

Mathematically, the convergence and divergence for the different cases can be explained by comparing the isotropic solution to the solution of the general anisotropic problem as follows:

The plane isotropic equilibrium equations can be written as

$$2(\eta + 1)u_{,xx} + (2\eta + 1)v_{,xy} + u_{,yy} = 0$$

$$v_{,xx} + (2\eta + 1)u_{,xy} + 2(\eta + 1)v_{,yy} = 0$$

where η is an average property of the laminate. Due to the special nature of the coefficients of these two equations, the displacements satisfying them will have the following properties:

$$u_{,xx} = -v_{,xy} = -u_{,yy}$$

and

$$v_{,xx} = -u_{,xy} = -v_{,yy}$$

For a specific lamina (i) in the laminate the terms:

$$[2(\eta^{(i)} + 1)u_{,xx} + (2\eta^{(i)} + 1)v_{,xy} + u_{,yy}]$$

and

$$[v_{,xx} + (2\eta^{(i)} + 1)u_{,xy} + 2(\eta^{(i)} + 1)v_{,yy}]$$

and their derivatives will always be equal to zero no matter what the value of $\eta^{(i)}$ is. These terms and their derivatives appear numerous times in the present formulation in terms like [D], [E], ... and their derivatives.

For the anisotropic case, the plane equations of equilibrium can be written as:

$$Q_{11}u_{,xx} + Q_{12}v_{,xy} + Q_{16}(2u_{,xy} + v_{,xx}) + Q_{26}v_{,yy} + Q_{66}(u_{,yy} + v_{,xy}) = 0$$

$$Q_{16}u_{,xx} + Q_{12}u_{,xy} + Q_{26}(u_{,yy} + 2v_{,xy}) + Q_{22}v_{,yy} + Q_{66}(u_{,xy} + v_{,xx}) = 0$$

where Q_{ij} are average properties of the laminate. Since there is no apparent relation between the various coefficients in these equations (they depend on the fiber orientation), then no special form of displacements can be obtained. Furthermore, for a specific lamina (i) in the laminate, the terms:

$$\left[Q_{11}^{(i)}u_{,xx} + Q_{12}^{(i)}v_{,xy} + Q_{16}^{(i)}(2u_{,xy} + v_{,xx}) + Q_{26}^{(i)}v_{,yy} + Q_{66}^{(i)}(u_{,yy} + v_{,xy}) \right]$$

and

$$\left[Q_{16}^{(i)}u_{,xx} + Q_{12}^{(i)}u_{,xy} + Q_{26}^{(i)}(u_{,yy} + 2v_{,xy}) + Q_{22}^{(i)}v_{,yy} + Q_{66}^{(i)}(u_{,xy} + v_{,xx}) \right]$$

and their derivatives will, in general, not be equal to zero. The accumulation of the error obtained by using these non-zero values create the erroneous results to be reported in the next chapter.

5.11 Concluding Remarks

An attempt is made to extend a theory for stretching and bending of laminated isotropic elastic plates to the anisotropic case. The laminae were in general of different anisotropic elastic materials. The form of the solution chosen (eq. 5.12) is the same as for the isotropic case [78]. At this point, there is serious doubt as the validity of this form for the anisotropic case.

The solution is generated using the two-dimensional CLT, and enough unknown functions are obtained to satisfy all traction and displacement continuity conditions at the interlaminar interfaces as well as the zero traction condition on the lateral surfaces. The only approximation involved in this approach is that edge boundary conditions can only be satisfied in an average manner rather than point by point.

Chapter 6

Applications

6.1 Introduction

As an illustration of the theory of laminated anisotropic plates presented in chapter 5, two cases will be considered. First, The reduction of the anisotropic case to the isotropic solution is observed. The anisotropic solution, if correct, would have to reduce to the isotropic solution shown in [78] when isotropic material properties are used.

Another case considered here is that of an anisotropic laminated plate containing a traction-free circular hole and subjected to uniaxial tension at infinity.

6.2 Reduction to the Isotropic Case

The theory of anisotropic laminates introduced in chapter 5, has to reduce to the isotropic case if the properties of the material considered are isotropic. Furthermore, these results should reduce to those obtained in [78].

The stress-strain relation (similar to eq. 5.1) for an isotropic material can be

written as:

$$\begin{Bmatrix} \sigma_{xx} \\ \sigma_{yy} \\ \sigma_{zz} \\ \sigma_{yz} \\ \sigma_{zx} \\ \sigma_{xy} \end{Bmatrix} = \begin{bmatrix} (\lambda + 2\mu) & \lambda & \lambda & 0 & 0 & 0 \\ \lambda & (\lambda + 2\mu) & \lambda & 0 & 0 & 0 \\ \lambda & \lambda & (\lambda + 2\mu) & 0 & 0 & 0 \\ 0 & 0 & 0 & \mu & 0 & 0 \\ 0 & 0 & 0 & 0 & \mu & 0 \\ 0 & 0 & 0 & 0 & 0 & \mu \end{bmatrix} \begin{Bmatrix} u_{,x} \\ v_{,y} \\ w_{,z} \\ (v_{,z} + w_{,y}) \\ (u_{,z} + w_{,x}) \\ (u_{,y} + v_{,x}) \end{Bmatrix} \quad (6.1)$$

where λ and μ are the Lamé constants and commas denote partial differentiation with respect to the suffix variables. As before, assuming that $\sigma_{zz} = 0$, we obtain:

$$\lambda u_{,x} + \lambda v_{,y} + (\lambda + 2\mu)w_{,z} = 0$$

which can be written as:

$$w_{,z} = -\left(\frac{\lambda}{\lambda + 2\mu}\right)(u_{,x} + v_{,y})$$

We obtain a stress-strain relation similar to eq. 5.5 for the isotropic material:

$$\begin{Bmatrix} \sigma_{xx} \\ \sigma_{yy} \\ \sigma_{zz} \\ \sigma_{yz} \\ \sigma_{zx} \\ \sigma_{xy} \end{Bmatrix} = \begin{bmatrix} (\lambda' + 2\mu) & \lambda' & 0 & 0 & 0 & 0 \\ \lambda' & (\lambda' + 2\mu) & 0 & 0 & 0 & 0 \\ 0 & 0 & 0 & 0 & 0 & 0 \\ 0 & 0 & 0 & \mu & 0 & 0 \\ 0 & 0 & 0 & 0 & \mu & 0 \\ 0 & 0 & 0 & 0 & 0 & \mu \end{bmatrix} \begin{Bmatrix} u_{,x} \\ v_{,y} \\ w_{,z} \\ (v_{,z} + w_{,y}) \\ (u_{,z} + w_{,x}) \\ (u_{,y} + v_{,x}) \end{Bmatrix} \quad (6.2)$$

where:

$$\lambda' = \frac{2\lambda\mu}{(\lambda + 2\mu)}$$

For the purpose of comparing with [13], let:

$$\bar{\eta} = \frac{\lambda}{\lambda + 2\mu} = \frac{\lambda'}{2\mu}$$

Substituting for the properties of eq. 6.1 in the expressions for $u^{(i)}$, $v^{(i)}$ and $w^{(i)}$ of the anisotropic case, and reducing the functions $S_i^{(k)}(x, y)$ and $B_i^{(k)}(x, y)$ to constants $S_i^{(k)}$ and $B_i^{(k)}$, the isotropic solution of [78] should be recovered.

It is worth noticing here that the present formulation uses two of the three equilibrium equations (as shown in eq. 5.10) and using eq. 5.11 as a third equation in the formulation. The third equilibrium equation is used later on to determine σ_{zz} .

In the isotropic work [78], σ_{zz} was assumed to be zero throughout the laminate. So four equations seemed to have been used to obtain the solution. But a second look at these four equations would reveal that only three equations are sufficient to obtain the solution. The fourth equation automatically satisfies the solution obtained; this fourth equation can therefore be termed redundant.

6.2.1 First Order Solution ($n = 1$)

The anisotropic form of the equation for $w_1^{(i)}$ is shown in 5.16 as:

$$w_1^{(i)} = -\frac{1}{C_{33}^{(i)}} \left[C_{13}^{(i)} u_{o,x} + C_{23}^{(i)} v_{o,y} + C_{36}^{(i)} (u_{o,y} + v_{o,x}) \right] z + S_1^{(i)}(x, y) \quad (6.3)$$

Substituting for the values of $C_{jk}^{(i)}$ from eq. 6.1, the equation reduces to:

$$w_1^{(i)} = -\frac{1}{(\lambda + 2\mu)} [\lambda u_{o,x} + \lambda v_{o,y} + 0(u_{o,y} + v_{o,x})] z + S_1^{(i)} \quad (6.4)$$

Rearranging,

$$w_1 = -\frac{\lambda}{(\lambda + 2\mu)} [u_{o,x} + v_{o,y}] z + S_1^{(i)} \quad (6.5)$$

Define:

$$\Delta_n = u_{n,x} + v_{n,y}$$

the previous equation can be written as:

$$w_1^{(i)} = - \left[z + S_1^{(i)} \right] \eta \Delta_o \quad (6.6)$$

which is similar to eq. 2.44 in [78]. The anisotropic form of the equations for $u_1^{(i)}$ and $v_1^{(i)}$ is shown in 5.23 as:

$$\begin{aligned} u_1^{(i)} &= -w_{o,x} z_i + B_1^{(i)}(x, y) \\ v_1^{(i)} &= -w_{o,y} z_i + B_2^{(i)}(x, y) \end{aligned} \quad (6.7)$$

Reducing the two functions $B_1^{(i)}$ and $B_2^{(i)}$ to one constant $B_1^{(i)}$, these two equations can be written as:

$$\begin{aligned} u_1^{(i)} &= - \left[z_i + B_1^{(i)} \right] w_{o,x} \\ v_1^{(i)} &= - \left[z_i + B_1^{(i)} \right] w_{o,y} \end{aligned} \quad (6.8)$$

which are similar to the equation of the isotropic case shown in eq. 2.44 in [78].

6.2.2 Second Order Solution ($n = 2$)

The anisotropic form of the equation for $w_2^{(i)}$ is shown in eq. 5.28 as:

$$\begin{aligned} w_2^{(i)} &= \frac{1}{C_{33}^{(i)}} \left[C_{13}^{(i)} w_{o,xx} + C_{23}^{(i)} w_{o,yy} + 2C_{36}^{(i)} w_{o,xy} \right] \frac{z_i^2}{2} \\ &\quad - \frac{1}{C_{33}^{(i)}} \left[C_{13}^{(i)} B_1^{(i)}{}_{,x} + C_{23}^{(i)} B_2^{(i)}{}_{,y} + C_{36}^{(i)} (B_1^{(i)}{}_{,y} + B_2^{(i)}{}_{,x}) \right] z_i + B_3^{(i)}(x, y) \end{aligned} \quad (6.9)$$

For the isotropic case, the previous equation reduces to:

$$\begin{aligned} w_2^{(i)} &= \frac{1}{(\lambda + 2\mu)} \left\{ [\lambda (w_{o,xx} + w_{o,yy})] \frac{z_i^2}{2} - [\lambda (B_1^{(i)}{}_{,x} + B_2^{(i)}{}_{,y})] z_i \right\} + B_3^{(i)} \\ w_2^{(i)} &= \eta (\nabla^2 w_o) \frac{z_i^2}{2} + C_1 \eta z_i + B_3^{(i)} \end{aligned} \quad (6.10)$$

This could be rearranged as:

$$w_2^{(i)} = \left(\frac{1}{2} z_i^2 + B_1^{(i)} z_i + B_2^{(i)} \right) \eta \nabla^2 w_o \quad (6.11)$$

which is the form shown in eq. 2.46 of [78]. The anisotropic form of the equations for $u_2^{(i)}$ and $v_2^{(i)}$ are shown in eqs. 5.33 and 5.34 as:

$$\begin{aligned}
u_2^{(i)} &= \left(\frac{-1}{C_{44}C_{55} - C_{45}^2} \right)^{(i)} \\
&\quad \left\{ \left[- \left(\frac{C_{13}}{C_{33}} \right) (C_{44}C_{55} - C_{45}^2) + (Q_{11}C_{44} - C_{45}Q_{16}) \right]^{(i)} u_{o,xx} \right. \\
&\quad + [C_{44}Q_{66} - C_{45}Q_{26}]^{(i)} u_{o,yy} + [C_{44}Q_{26} - C_{45}Q_{22}]^{(i)} v_{o,yy} \\
&\quad + \left[- \left(\frac{C_{36}}{C_{33}} \right) (C_{44}C_{55} - C_{45}^2) + (2C_{44}Q_{16} - C_{45}Q_{12} - C_{45}Q_{66}) \right]^{(i)} u_{o,xy} \\
&\quad + \left[- \left(\frac{C_{36}}{C_{33}} \right) (C_{44}C_{55} - C_{45}^2) + (C_{44}Q_{16} - C_{45}Q_{66}) \right]^{(i)} v_{o,xx} \\
&\quad + \left. \left[- \left(\frac{C_{23}}{C_{33}} \right) (C_{44}C_{55} - C_{45}^2) + (C_{44}Q_{12} + C_{44}Q_{66} - 2C_{45}Q_{26}) \right]^{(i)} v_{o,xy} \right\} \frac{z_i^2}{2} \\
&\quad + S_2^{(i)} z_i + S_4^{(i)} \\
v_2^{(i)} &= \left(\frac{1}{C_{44}C_{55} - C_{45}^2} \right)^{(i)} \\
&\quad \left\{ \left[\left(\frac{C_{36}}{C_{33}} \right) (C_{44}C_{55} - C_{45}^2) + (C_{45}Q_{66} - C_{55}Q_{26}) \right]^{(i)} u_{o,yy} \right. \\
&\quad + [C_{45}Q_{11} - C_{55}Q_{16}]^{(i)} u_{o,xx} + [C_{45}Q_{16} - C_{55}Q_{66}]^{(i)} v_{o,xx} \\
&\quad + \left[\left(\frac{C_{13}}{C_{33}} \right) (C_{44}C_{55} - C_{45}^2) + (2C_{45}Q_{16} - C_{55}Q_{66} - C_{55}Q_{12}) \right]^{(i)} u_{o,xy} \\
&\quad + \left[\left(\frac{C_{23}}{C_{33}} \right) (C_{44}C_{55} - C_{45}^2) + (Q_{26}C_{45} - C_{55}Q_{22}) \right]^{(i)} v_{o,yy} \\
&\quad + \left. \left[\left(\frac{C_{36}}{C_{33}} \right) (C_{44}C_{55} - C_{45}^2) + (C_{45}Q_{12} + C_{45}Q_{66} - 2C_{55}Q_{26}) \right]^{(i)} v_{o,xy} \right\} \frac{z_i^2}{2} \\
&\quad + S_3^{(i)} z_i + S_5^{(i)} \tag{6.12}
\end{aligned}$$

For the displacement u_2 substituting using the material properties of 6.1, we get:

$$\begin{aligned}
u_2^{(i)} &= - \left\{ u_{o,yy} + \frac{1}{\mu} \left[(\lambda + 2\mu) - \frac{\lambda^2}{\lambda + 2\mu} - \frac{\mu\lambda}{\lambda + 2\mu} \right] u_{o,xx} \right. \\
&\quad + \left. \frac{1}{\mu} \left[\lambda - \frac{\lambda^2}{\lambda + 2\mu} + \mu - \frac{\mu\lambda}{\lambda + 2\mu} \right] v_{o,xy} \right\} \frac{z_i^2}{2} + S_2^{(i)} z_i + S_4^{(i)} \tag{6.13}
\end{aligned}$$

which reduces to:

$$u_2^{(i)} = -[(\eta + 2) \Delta_{o,x} - \Omega_{o,y}] \frac{z_i^2}{2} + S_2^{(i)} z_i + S_4^{(i)} \quad (6.14)$$

where:

$$\Omega_{o,y} = v_{o,xy} - u_{o,yy}$$

and

$$\Delta_{o,x} = u_{o,xx} + v_{o,xy}$$

Equation 6.14 can finally be written as:

$$u_2^{(i)} = - \left(\frac{1}{2} z_i^2 + S_2^{(i)} z_i + S_3^{(i)} \right) [(\eta + 2) \Delta_{o,x} - \Omega_{o,y}] \quad (6.15)$$

Similarly, the equation for v_2 reduces to:

$$v_2^{(i)} = - \left(\frac{1}{2} z_i^2 + S_2^{(i)} z_i + S_3^{(i)} \right) [(\eta + 2) \Delta_{o,y} + \Omega_{o,x}] \quad (6.16)$$

which are the same equations as 2.46 shown in [78] for the isotropic case.

6.2.3 Third Order Solution ($n = 3$)

The anisotropic form of the equation for $w_3^{(i)}$ is shown in eq. 5.39 as:

$$\begin{aligned} w_3^{(i)} = & \frac{-1}{C_{33}^{(i)}} \left\{ \left(C_{13}^{(i)} [\mathbf{D}_{,x}^{(i)}] + C_{23}^{(i)} [\mathbf{E}_{,y}^{(i)}] + C_{36}^{(i)} [\mathbf{D}_{,y}^{(i)} + \mathbf{E}_{,x}^{(i)}] \right) \frac{z_i^3}{6} \right. \\ & + \left(C_{13}^{(i)} S_{2, ,x}^{(i)} + C_{23}^{(i)} S_{3, ,y}^{(i)} + C_{36}^{(i)} (S_{2, ,y}^{(i)} + S_{3, ,x}^{(i)}) \right) \frac{z_i^2}{2} \\ & + \left(C_{13}^{(i)} S_{4, ,x}^{(i)} + C_{23}^{(i)} S_{5, ,y}^{(i)} + C_{36}^{(i)} (S_{4, ,y}^{(i)} + S_{5, ,x}^{(i)}) \right) z_i \\ & \left. + S_6^{(i)}(x, y) \right\} \quad (6.17) \end{aligned}$$

For the isotropic case this equation reduces to:

$$\begin{aligned} w_3^{(i)} = & -\frac{1}{\lambda + 2\mu} \left\{ \left(\lambda [\mathbf{D}_{,x}^{(i)} + \mathbf{E}_{,y}^{(i)}] \right) \frac{z_i^3}{6} + \left(\lambda [S_{2, ,x}^{(i)} + S_{3, ,y}^{(i)}] \right) \frac{z_i^2}{2} \right. \\ & \left. + \left(\lambda [S_{4, ,x}^{(i)} + S_{5, ,y}^{(i)}] \right) z_i + S_6^{(i)} \right\} \quad (6.18) \end{aligned}$$

Using the isotropic form of $[\mathbf{D}]$ and $[\mathbf{E}]$,

$$\begin{aligned} [\mathbf{D},x] &= -[(\eta + 2) \Delta_{o,xx} - \Omega_{o,xy}] \\ [\mathbf{E},y] &= -[(\eta + 2) \Delta_{o,yy} + \Omega_{o,xy}] \end{aligned} \quad (6.19)$$

the form of w_3 reduces to:

$$\begin{aligned} w_3^{(i)} &= -\frac{\lambda}{\lambda + 2\mu} \left\{ (\lambda + 2) (\Delta_{o,xx} + \Omega_{o,yy}) \frac{z_i^3}{6} + (S_2^{(i)},x + S_3^{(i)},y) \frac{z_i^2}{2} \right. \\ &\quad \left. + (\lambda S_4^{(i)},x + S_5^{(i)},y) z_i + \frac{1}{\lambda} S_6^{(i)} \right\} \end{aligned} \quad (6.20)$$

where:

$$\Delta_{o,xx} + \Omega_{o,yy} = \nabla^2 \Delta_o = 0$$

and all the derivatives of $S_k^{(i)}$ reduce to zero (since they are now constants rather than functions of x and y). The final form will then be:

$$w_3^{(i)} = -\frac{1}{(\lambda + 2\mu)} S_6^{(i)} \quad (6.21)$$

Due to symmetry at $z = 0$,

$$w^{(1)} = 0 \quad \text{or} \quad S_6^{(1)} = 0$$

which, because $w \neq w(z)$ would lead to:

$$S_6^{(i)} = 0$$

eq. 6.20 now reduces to:

$$w_3^{(i)} = 0 \quad (6.22)$$

which has the same form as for the isotropic case. The anisotropic form of the equations for $u_3^{(i)}$ and $v_3^{(i)}$ are shown in eqs. 5.43 and 5.44. Reducing the equation for u_3 for the isotropic case we get:

$$\begin{aligned} u_3^{(i)} &= -\left\{ \left[\frac{\lambda}{(\lambda + 2\mu)} - \left(\frac{(\lambda + 2\mu)}{\lambda} - \frac{\lambda^2}{\mu(\lambda + 2\mu)} \right) \right] w_{o,xxx} \right. \\ &\quad \left. + \left[\frac{\lambda}{(\lambda + 2\mu)} - \frac{(\lambda + 2\mu)}{\lambda} + \frac{\lambda^2}{\mu(\lambda + 2\mu)} \right] w_{o,yyy} \right\} \frac{z_i^3}{6} + C_1^{(i)} \frac{z_i^2}{2} + C_2^{(i)} z_i + C_3^{(i)} \end{aligned} \quad (6.23)$$

Rearranging,

$$u_3^{(i)} = - \left[\eta - \frac{2\lambda + 2(\lambda + 2\mu)}{\lambda + 2\mu} \right] (w_{o,xxx} + w_{o,yyy}) \frac{z_i^3}{6} + C_1^{(i)} \frac{z_i^2}{2} + C_2^{(i)} z_i + C_3^{(i)} \quad (6.24)$$

which finally leads to:

$$u_3^{(i)} = (\eta + 2) \nabla^2 w_{o,x} \frac{z_i^3}{6} + C_1^{(i)} \frac{z_i^2}{2} + C_2^{(i)} z_i + C_3^{(i)} \quad (6.25)$$

Similarly for v_3 ,

$$v_3^{(i)} = (\eta + 2) \nabla^2 w_{o,y} \frac{z_i^3}{6} + C_1^{(i)} \frac{z_i^2}{2} + C_2^{(i)} z_i + C_3^{(i)} \quad (6.26)$$

The last two equations are similar to those given in [78] for the isotropic case.

6.2.4 Fourth Order Solution ($n = 4$)

The anisotropic form of the equation for $w_4^{(i)}$ is shown in eq. 5.50 as:

$$w_4^{(i)} = [\mathbf{M}^{(i)}] \frac{z_i^4}{24} + [\mathbf{N}^{(i)}] \frac{z_i^3}{6} + [\mathbf{O}^{(i)}] \frac{z_i^2}{2} + [\mathbf{P}^{(i)}] z_i + B_8^{(i)} \quad (6.27)$$

The term $[\mathbf{M}^{(i)}]$ contains terms that would eventually reduce to:

$$(w_{o,xxxx} + w_{o,yyyy} + 2w_{o,xyxy})$$

which are equal to zero for the isotropic case. The other terms of eq. 6.27 will also reduce to zero since they are differentials of constants. It should be noted that for any order higher than four the same arguments will hold true. i.e.

$$w_n^{(i)} = 0 \quad \text{for } n \geq 4 \quad (6.28)$$

The anisotropic form of the equations for $u_4^{(i)}$ and $v_4^{(i)}$ are shown in eqs 5.55 as:

$$\begin{aligned} u_4^{(i)} &= [\mathbf{Q}^{(i)}] \frac{z_i^4}{24} + [\mathbf{R}^{(i)}] \frac{z_i^3}{6} + [\mathbf{S}^{(i)}] \frac{z_i^2}{2} + S_7^{(i)} z_i + S_9^{(i)} \\ v_4^{(i)} &= [\mathbf{T}^{(i)}] \frac{z_i^4}{24} + [\mathbf{U}^{(i)}] \frac{z_i^3}{6} + [\mathbf{V}^{(i)}] \frac{z_i^2}{2} + S_8^{(i)} z_i + S_{10}^{(i)} \end{aligned} \quad (6.29)$$

The terms $[\mathbf{Q}^{(i)}]$ and $[\mathbf{T}^{(i)}]$ contain terms that contain fourth derivatives such as $u_{o,xxxx}$ or in other words terms which only contain expressions such as $(\nabla^2 \Delta_o)_{,r}$. These equations reduce to zero since, in the isotropic case, $(\nabla^2 \Delta_o) = 0$.

The other terms of eq. 6.29 will also reduce to zero since they are differentials of constants. It should be noted that for any order higher than four the same arguments will hold true. i.e.

$$u_n^{(i)} = v_n^{(i)} = 0 \quad \text{for } n \geq 4 \quad (6.30)$$

which are the same results obtained in [78]. As a result, the method presented in chapter 5 for anisotropic materials reduces to the case of isotropic materials when the isotropic material properties are used.

6.3 Stretching of an Anisotropic Plate Containing a Traction-Free Circular Hole

In this section, an anisotropic plate containing a traction-free circular hole and subjected to uniaxial tension at infinity is considered. The two-dimensional solution for this problem for a homogeneous plate is given in [81]. This solution will be chosen as the equivalent plate solution.

6.3.1 The Equivalent Plate Solution

It is assumed that an infinitely large anisotropic elastic plate contains an elliptical hole. The coordinates axes OX and OY are chosen in the directions of the axes of the ellipse and the semi-axes of the ellipse are denoted by a and b . Let the stress state at infinity be tensile and of amount P acting at an angle ζ to the OX axis as shown in Fig. 6.1. The expressions for the stress components close to the hole are:

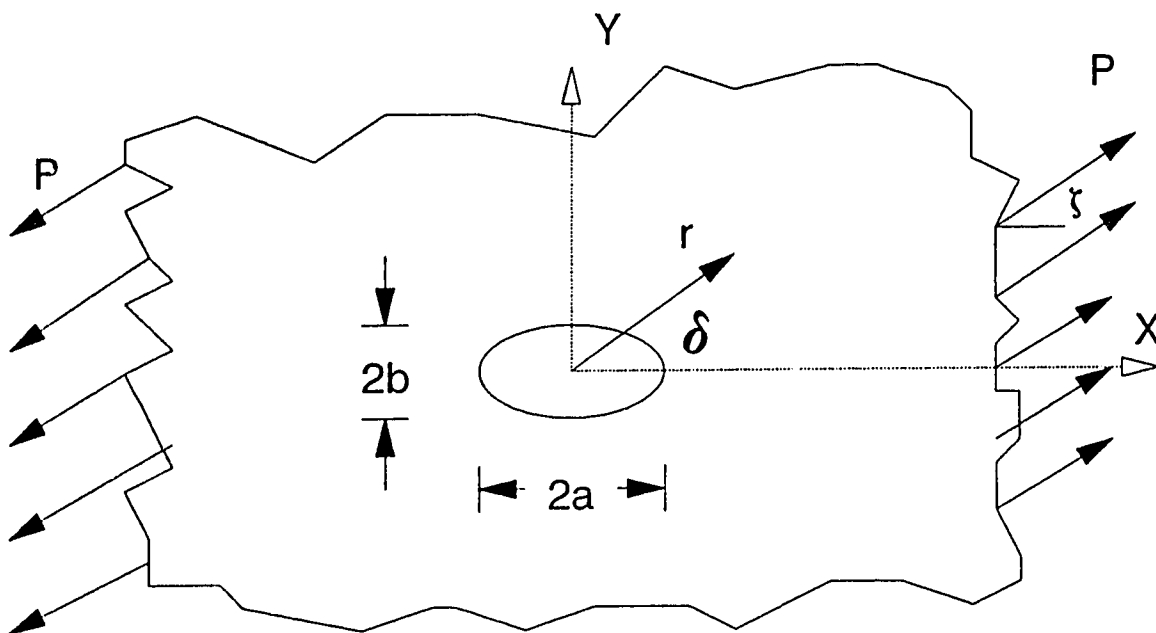


Figure 6.1: Plate with an Elliptical Hole Subjected to a Stress P at Infinity

$$\begin{aligned}
 \sigma_x &= P \cos^2 \zeta + 2\Re [S_1^2 \phi'_o(z_1) + S_2^2 \psi'_o(z_2)] \\
 \sigma_y &= P \sin^2 \zeta + 2\Re [\phi'_o(z_1) + \psi'_o(z_2)] \\
 \sigma_{xy} &= P \sin \zeta \cos \zeta - 2\Re [S_1 \phi'_o(z_1) + S_2 \psi'_o(z_2)]
 \end{aligned} \tag{6.31}$$

where:

$$S_1 = \alpha_1 + i\beta_1$$

$$S_2 = \alpha_2 + i\beta_2$$

are the roots of the equation:

$$A_{11}S^4 - 2A_{16}S^3 + (2A_{12} + A_{66})S^2 - 2A_{26}S + A_{22} = 0 \quad (6.32)$$

and

$$z_1 = x + S_1y$$

$$z_2 = x + S_2y$$

and the functions ϕ_o and ψ_o are:

$$\begin{aligned} \phi_o = & - \frac{iP(a - iS_1b)}{4(S_1 - S_2)} \left\{ \frac{b(S_2 \sin 2\zeta + 2 \cos^2 \zeta)}{z_1 + \sqrt{z_1^2 - (a^2 + S_1^2 b^2)}} \right. \\ & \left. + \frac{ia(2S_2 \sin^2 \zeta + \sin 2\zeta)}{z_1 + \sqrt{z_1^2 - (a^2 + S_1^2 b^2)}} \right\} \\ \psi_o = & \frac{iP(a - iS_2b)}{4(S_1 - S_2)} \left\{ \frac{b(S_1 \sin 2\zeta + 2 \cos^2 \zeta)}{z_2 + \sqrt{z_2^2 - (a^2 + S_2^2 b^2)}} \right. \\ & \left. + \frac{ia(2S_1 \sin^2 \zeta + \sin 2\zeta)}{z_2 + \sqrt{z_2^2 - (a^2 + S_2^2 b^2)}} \right\} \end{aligned} \quad (6.33)$$

The displacement components for the same problem are:

$$\begin{aligned} u &= 2\Re [p_1 \phi(z_1) + p_2 \psi(z_2)] - \gamma_o y + \alpha_o \\ v &= 2\Re [q_1 \phi(z_1) + q_2 \psi(z_2)] + \gamma_o x + \beta_o \end{aligned} \quad (6.34)$$

where:

$$p_1 = A_{11}S_1^2 + A_{12} - A_{16}S_1$$

$$p_2 = A_{11}S_2^2 + A_{12} - A_{16}S_2$$

$$q_1 = \frac{A_{12}S_1^2 + A_{22} - A_{26}S_1}{S_1}$$

$$q_2 = \frac{A_{12}S_2^2 + A_{22} - A_{26}S_2}{S_2}$$

The coefficients α_o , β_o and γ_o are arbitrary real constants where $(-\gamma_o y + \alpha_o)$ and $(\gamma_o x + \beta_o)$ are the expressions for the rigid body displacement of the entire body and can be disregarded when investigating elastic equilibrium. For stresses given at infinity, we can define:

$$\begin{aligned}\phi(z_1) &= B^* z_1 + \phi_o(z_1) \\ \psi(z_2) &= (B'^* + iC'^*)z_2 + \psi_o(z_2)\end{aligned}\quad (6.35)$$

where:

$$\begin{aligned}B^* &= P \left\{ \frac{\cos^2 \zeta + (\alpha_2^2 + \beta_2^2) \sin^2 \zeta + \alpha_2 \sin 2\zeta}{2[(\alpha_2 - \alpha_1)^2 + (\beta_2^2 - \beta_1^2)]} \right\} \\ B'^* &= P \left\{ \frac{[(\alpha_1^2 - \beta_1^2) - 2\alpha_1\alpha_2] \sin^2 \zeta + \cos^2 \zeta - \alpha_2 \sin 2\zeta}{2[(\alpha_2 - \alpha_1)^2 + (\beta_2^2 - \beta_1^2)]} \right\} \\ C'^* &= P \left\{ \frac{(\alpha_1 - \alpha_2) \cos^2 \zeta + [\alpha_2(\alpha_1^2 - \beta_1^2) - \alpha_1(\alpha_2^2 - \beta_2^2)] \sin^2 \zeta}{2\beta_2[(\alpha_2 - \alpha_1)^2 + (\beta_2^2 - \beta_1^2)]} \right. \\ &\quad \left. + \frac{[(\alpha_1^2 - \beta_1^2) - (\alpha_2^2 - \beta_2^2)] \sin \zeta \cos \zeta}{2\beta_2[(\alpha_2 - \alpha_1)^2 + (\beta_2^2 - \beta_1^2)]} \right\}\end{aligned}$$

These values of $u(x, y)$ and $v(x, y)$ will be considered as \hat{u} and \hat{v} (as explained in chapter 5) respectively.

6.3.2 Reduction to the Isotropic Case

For the isotropic case, the same general equations, developed in the previous section for the anisotropic case, can be used.

It should be noted however that a slight modification in the computer program is necessary. This deals with the fact that the anisotropic formulation is not equipped to deal with the case when $S_1 = S_2 = i$ (see eq. 6.33). The solution to that problem is presented in [82]. This solution involves replacing the original values of S_1 and S_2 by $S_1 = 1.000001 i$ and $S_2 = 0.999999 i$. The apparent indeterminacy in eq. 6.33 is thus avoided while introducing negligible errors in the stress results. It should

be noted however that values of $S_1 = 1.001 i$ and $S_2 = 0.999 i$ did not result in stresses comparable to those in [78].

6.3.3 Solution of the Isotropic Laminated Plate Problem

In [78], although no numerical values were given, an example was presented. This example considered a laminated plate containing a traction-free circular hole of radius R and subjected to uniaxial tensile stress P at infinity. The laminate of thickness t was chosen to comprised of three layers each of equal thickness $2h_1$, the inner layer having elastic constants λ'_1, μ_1 and the two outer layers having elastic constants λ'_2, μ_2 .

Denoting by τ_i the shear traction between layers $(i-1)$ and (i) , then τ_i has x and y components $\sigma_{xz}^{(i)}$ and $\sigma_{yz}^{(i)}$ evaluated at $z_i = -1$.

The magnitude of the shear traction at the interface between the two layer was calculated to be:

$$\tau_1 = \frac{4\epsilon_1\mu_1(\eta_1 - \hat{\eta})P}{R^3\hat{\mu}(2\hat{\eta} + 1)} \quad (6.36)$$

where:

$$(\hat{\lambda}', \hat{\mu}) = \frac{1}{2} \int_{-1}^1 \{\lambda'(z), \mu(z)\} dz,$$

$$\lambda' = \frac{2\lambda\mu}{\lambda + 2\mu} \quad \text{and} \quad \hat{\eta} = \frac{\hat{\lambda}'}{2\hat{\mu}}$$

Giving the following numerical values,

$$\begin{aligned} E_1 &= 69 \text{ GPa} \quad (10^7 \text{ psi}) \\ E_2 &= 107.6 \text{ GPa} \quad (1.56 \times 10^7 \text{ psi}) \end{aligned}$$

$$\begin{aligned}
 \nu_1 &= 0.33 \\
 \nu_2 &= 0.355 \\
 \epsilon_1 &= 0.02 \\
 P &= 1.0 \text{ MPa (145 psi)}
 \end{aligned}$$

the interlaminar shear traction resulting from eq. 6.36 is $0.1246 \times 10^{-2} \text{ MPa}$ (0.1809 psi). Numerically, using the anisotropic formulation with terms up to the second order in ϵ , the value of the same interlaminar shear traction was calculated to be $0.1242 \times 10^{-2} \text{ MPa}$ (0.1801 psi).

It should also be noticed that using terms up to the fourth order in ϵ is not supposed to make any difference in the calculated values of the stresses (as explained in §.2.4), which was found to be the case since the values of the stress obtained using higher orders in ϵ did not alter the results.

The value of the interlaminar normal stress component, σ_{zz} , was calculated for this case and its value of $0.105 \times 10^{-6} \text{ MPa}$ ($0.1523 \times 10^{-4} \text{ psi}$) confirmed the initial assumption of $\sigma_{zz} \approx 0$.

In [78] it was mentioned that the value of the interlaminar shear traction was independent of the angle δ . This was confirmed using the present formulation.

The value of the radial component of the stress, σ_{rr} , at the hole is supposed to be zero. But since the boundary conditions are not satisfied point by point, the values obtained is non-zero but very small when compared to the applied stress. It should however be noted here that if the ratio R/t decreases, a significant increase of this stress component at the hole results. For example, for $R/t = 8.33$, the maximum value of σ_{rr} at the hole is about 5% of the applied load. If a thicker laminate is used ($R/t = 0.833$), the maximum value of the same stress component at the hole increases to 42% of the applied load.

6.3.4 Solution of the Anisotropic Laminated Plate Problem

To determine the suitability of the present method (presented in chapter 5) for the case of anisotropic elastic plates, a problem similar to the one considered for the isotropic case was studied. The problem of an anisotropic laminated plate containing a traction-free circular hole and subjected to a uniaxial tensile stress P at infinity, will be attempted (Fig. 6.2). Two symmetric laminates made of the same material will be considered here: $[0/90]_s$ and $[\pm 45]_s$. These laminate configurations were not chosen for any specific reasons, but just to be used as examples.

Parametric Numerical Study

In this section, the two aforementioned laminates containing a traction-free circular hole of radius R and subjected to uniaxial tensile stress P at infinity will be considered. The effects of the layer thickness t and the anisotropy factor ($A.F.$) on the results will be addressed; The anisotropy factor can be defined as the ratio between the modulus of elasticity in the fiber direction (E_1) and the modulus of elasticity in the direction perpendicular to the direction of the fibers (E_2), i.e.

$$A.F. = \frac{E_1}{E_2}$$

Two materials will be used to demonstrate the anisotropy effect: *Material A* with an anisotropy factor of 3 and *Material B* with an anisotropy factor of 7. The mechanical properties of these materials can be for a Graphite/Epoxy or an E-Glass/Epoxy. Some of the properties used for the two materials are shown in Table 6.1. For each of these materials, the effect of the plate thickness will be addressed.

For each of the materials and laminates examined, cases of $R/t = 5, 10$ and 20 are considered. For an applied stress of $P = 1MPa$, the values of the different

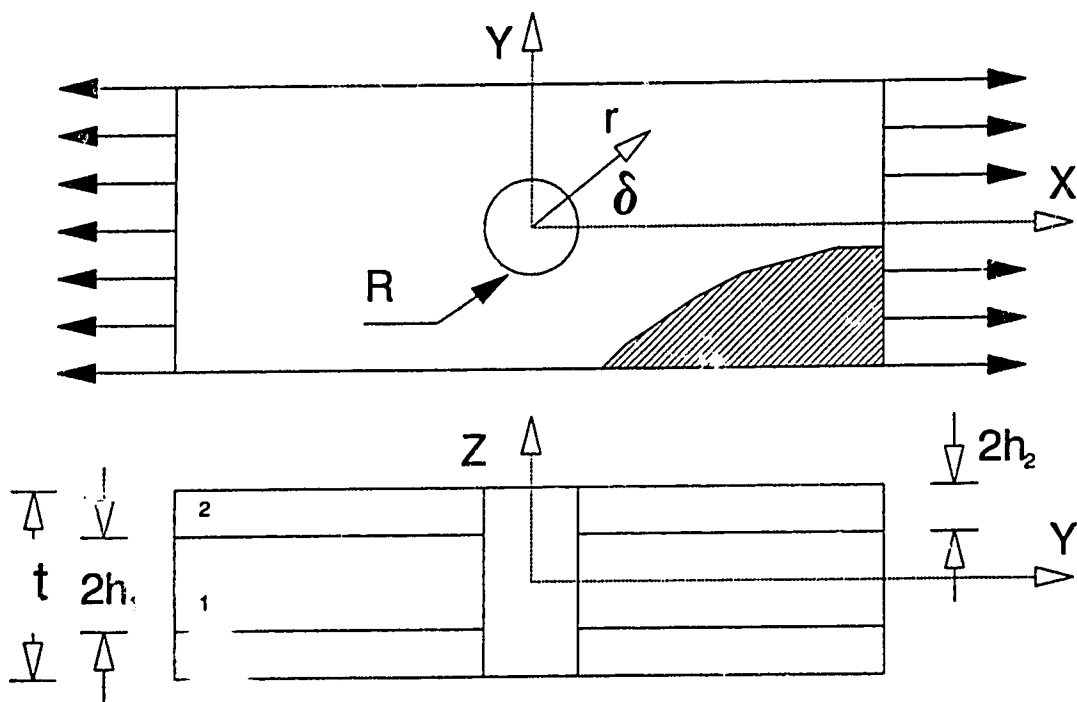


Figure 6.2: Anisotropic Elastic Symmetric Laminated Plate with a Circular Hole Subjected to a Stress P at Infinity

Table 6.1: Mechanical Properties of Different Materials Under Consideration

	Material	
	A	B
E_1 (GPa)	36	84
E_2, E_3 (GPa)	12	12
G_1, G_2, G_3 (GPa)	5.5	5.5
$\nu_{12}, \nu_{13}, \nu_{23}$	0.20	0.20
<i>A.F.</i>	3	7

stress components are evaluated around the hole at different values of the normalized radial distance (r/R) and position angles (δ).

For the $[0/90]_s$ laminate constructed using *Material A*, the variations of the normalized (with respect to the applied stress) plane stress components obtained at the centerline of the laminate versus the normalized radial distance are shown in Figs. 6.3-6.5. The normalized values of the same stress components obtained using the classical laminate theory are included as solid lines in the same figures. The distribution of the plane stress components for the same laminate built using *Material B* are shown in Figs. 6.6-6.8.

From Figs. 6.3-6.8, a few observations can be made. For the same material, as the laminate becomes thinner (R/t increases) and as we move further away from the hole (higher r/R), the values of the various plane stress components approach those of the CLT. Also, for the same laminate thickness (constant R/t), the maximum deviation from the CLT occurs at the hole for a position angle, δ , of 90° . This trend is very clear for the radial stress component, σ_{rr} , distribution in Figs. 6.3 and 6.6.

It can also be shown that this deviation increases with the increase of the anisotropy factor. For example, at the hole, $\sigma_{rr} = 1.5P$ for *Material A* but increases to $115P$ if *Material B* is used. Close to the hole, for thicker laminates ($R/t = 5$) made of *Material B*, the circumferential stress component, $\sigma_{\theta\theta}$, also deviates from the CLT with the largest deviation observed at $\delta = 90^\circ$ (Fig. 6.7). The value of the plane shear component, $\sigma_{r\theta}$, does not show any discrepancy to that obtained using the CLT.

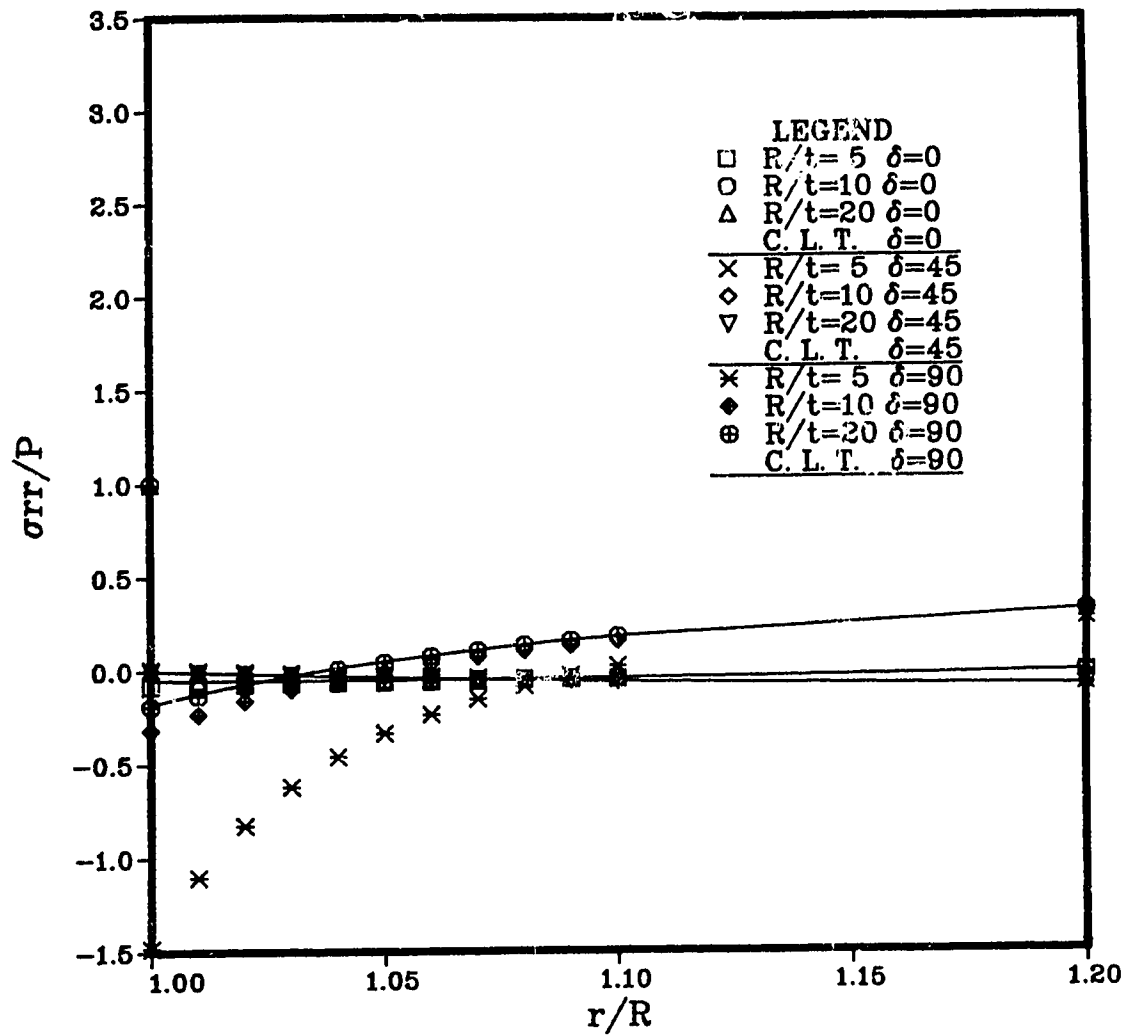


Figure 6.3: Radial Distribution of σ_{rr} at the Mid-Plane of the [0/90], Laminate Arcund the Hole (Material A)

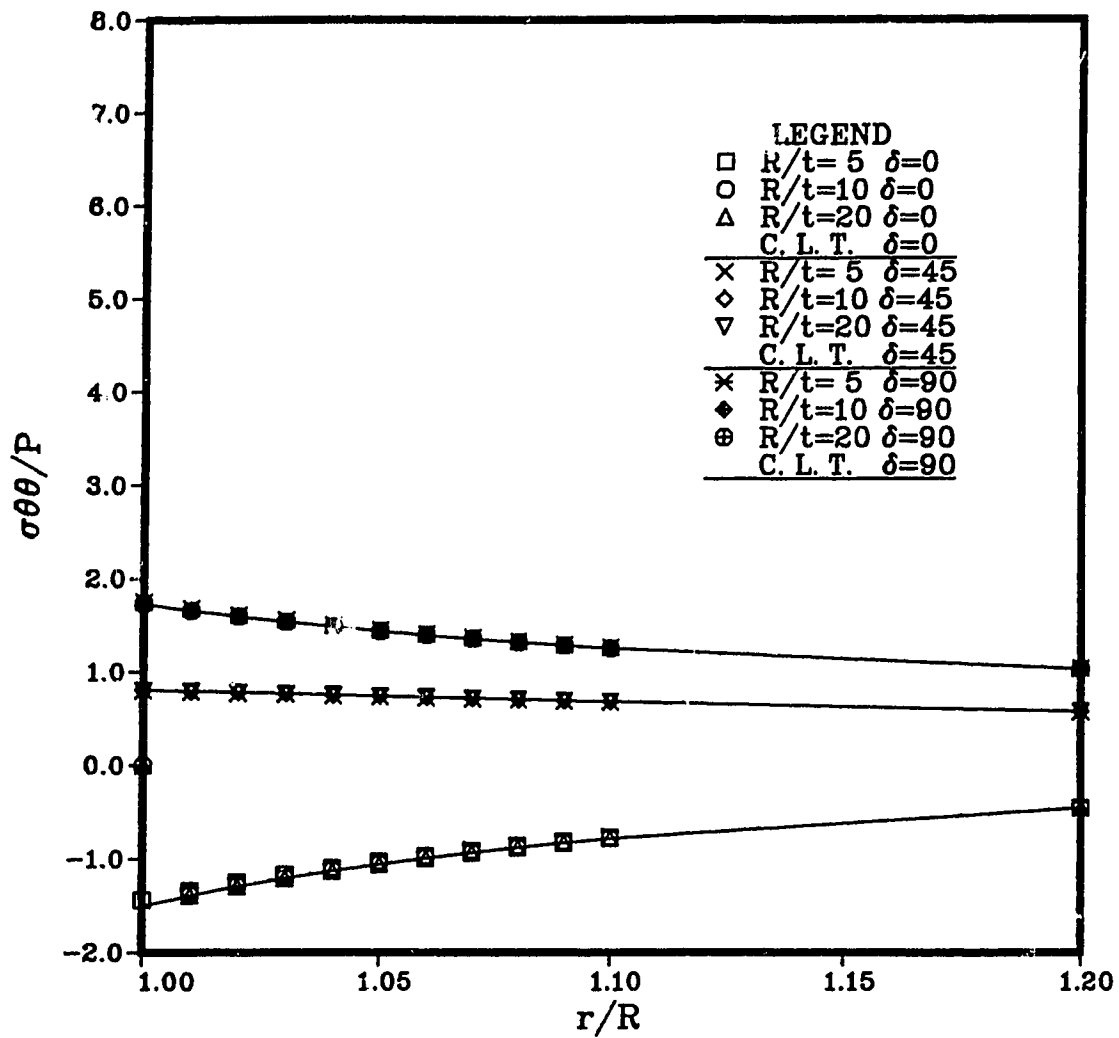


Figure 6.4: Radial Distribution of $\sigma_{\theta\theta}$ at the Mid-Plane of the $[0/90]_s$ Laminate Around the Hole (Material A)

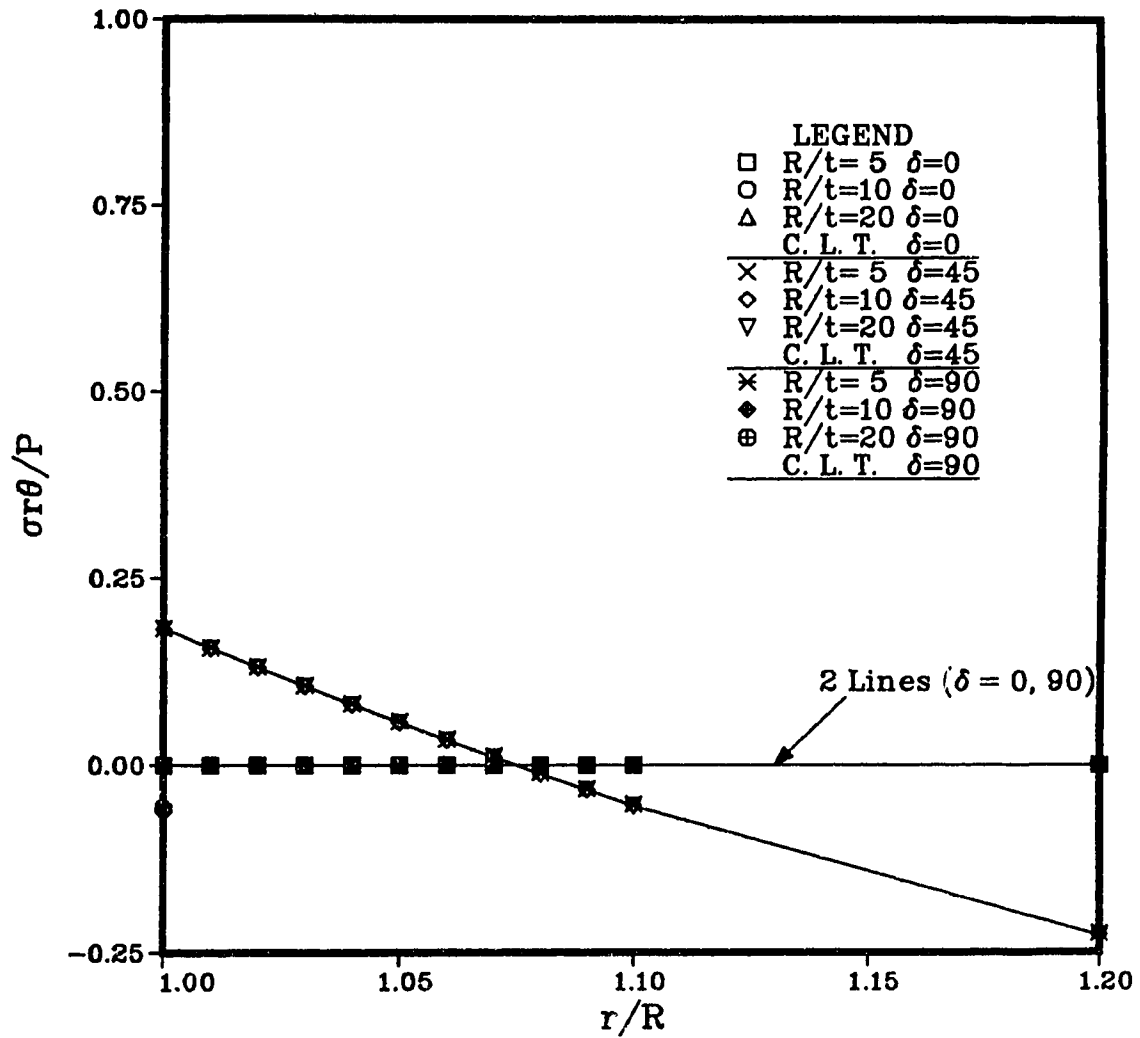


Figure 6.5: Radial Distribution of $\sigma_{r\theta}$ at the Mid-Plane of the $[0/90]_s$ Laminate Around the Hole (Material A)

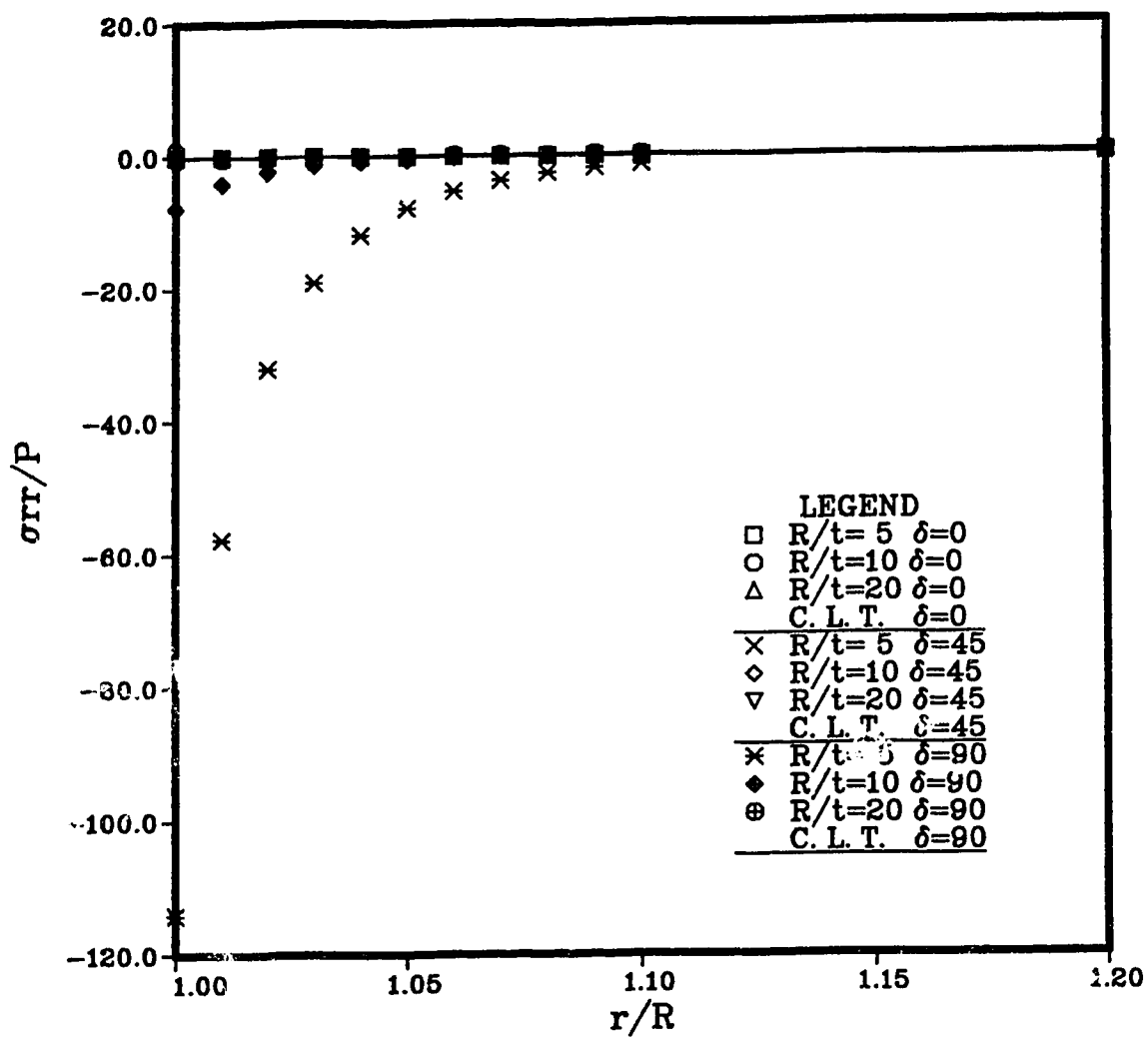


Figure 6.6: Radial Distribution of σ_{rr} at the Mid-Plane of the [0/90], Laminate Around the Hole (Material B)

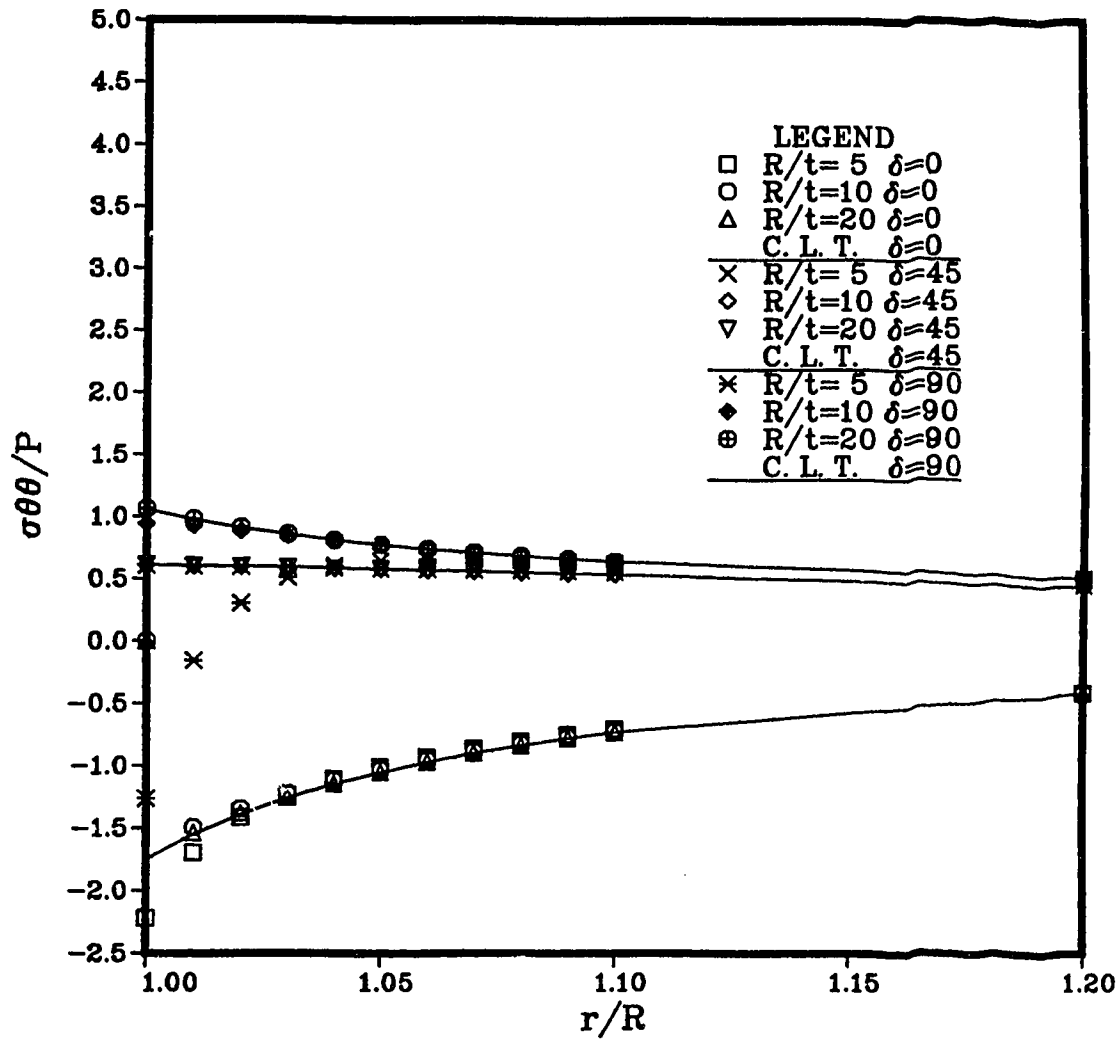


Figure 6.7: Radial Distribution of $\sigma_{\theta\theta}$ at the Mid-Plane of the [0/90], Laminate Around the Hole (Material B)

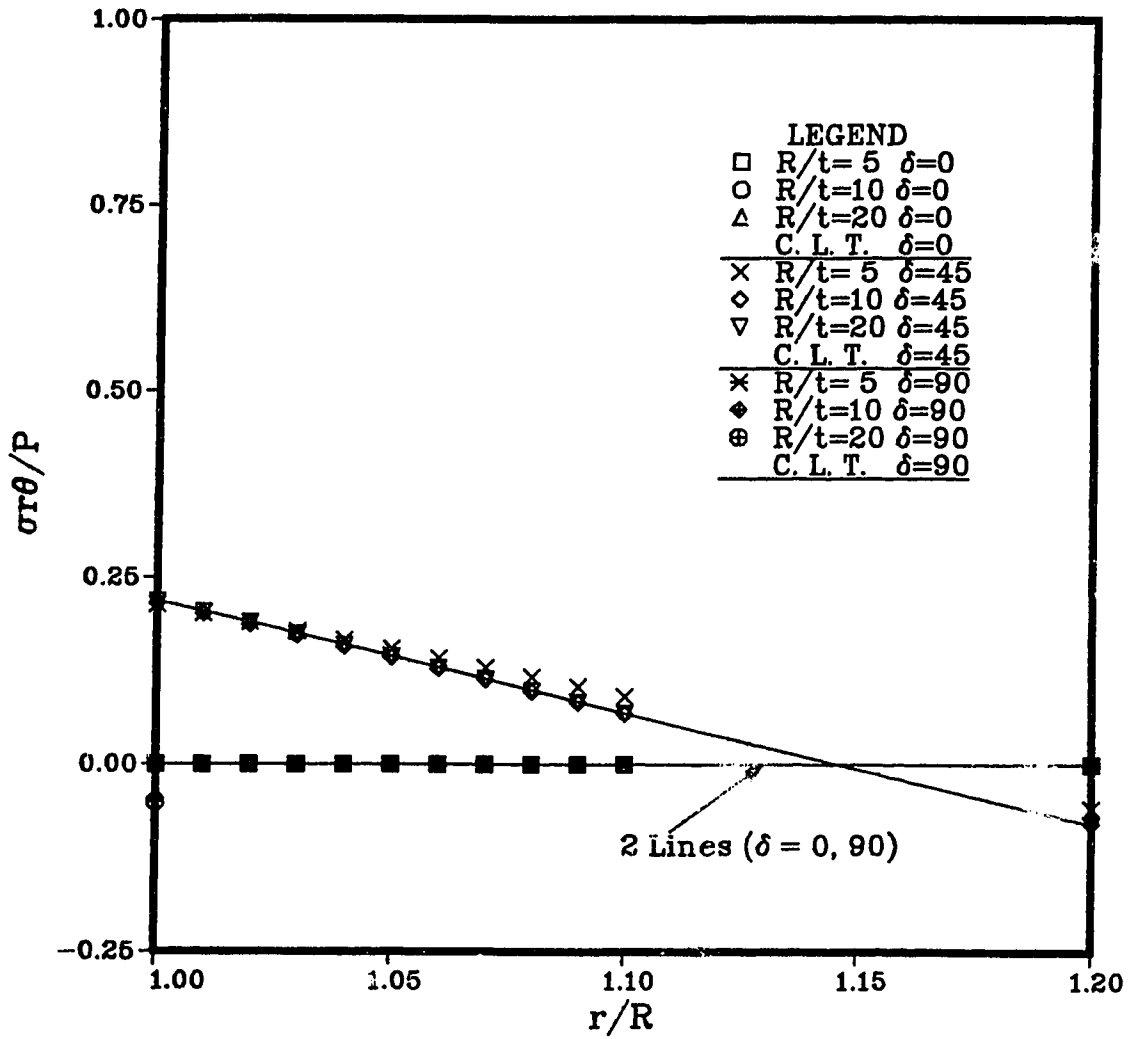


Figure 6.8: Radial Distribution of $\sigma_{r\theta}$ at the Mid-Plane of the $[0/90]_s$ Laminate Around the Hole (Material B)

For the $[\pm 45]_s$ laminate, the distribution for the plane stress components is shown in Figs. 6.9-6.11 and Figs. 6.12-6.14 for *Material A* and *Material B* respectively.

Similar trends are observed in this case with the maximum variation from the CLT observed at $\delta = 45^\circ$. The radial stress component, σ_{rr} , shows the largest deviation from the CLT. This deviation increases with the increase of the laminate thickness and the anisotropy factor. For *Material B*, at the hole, the plane shear stress component, $\sigma_{r\theta}$, also shows a departure from the CLT.

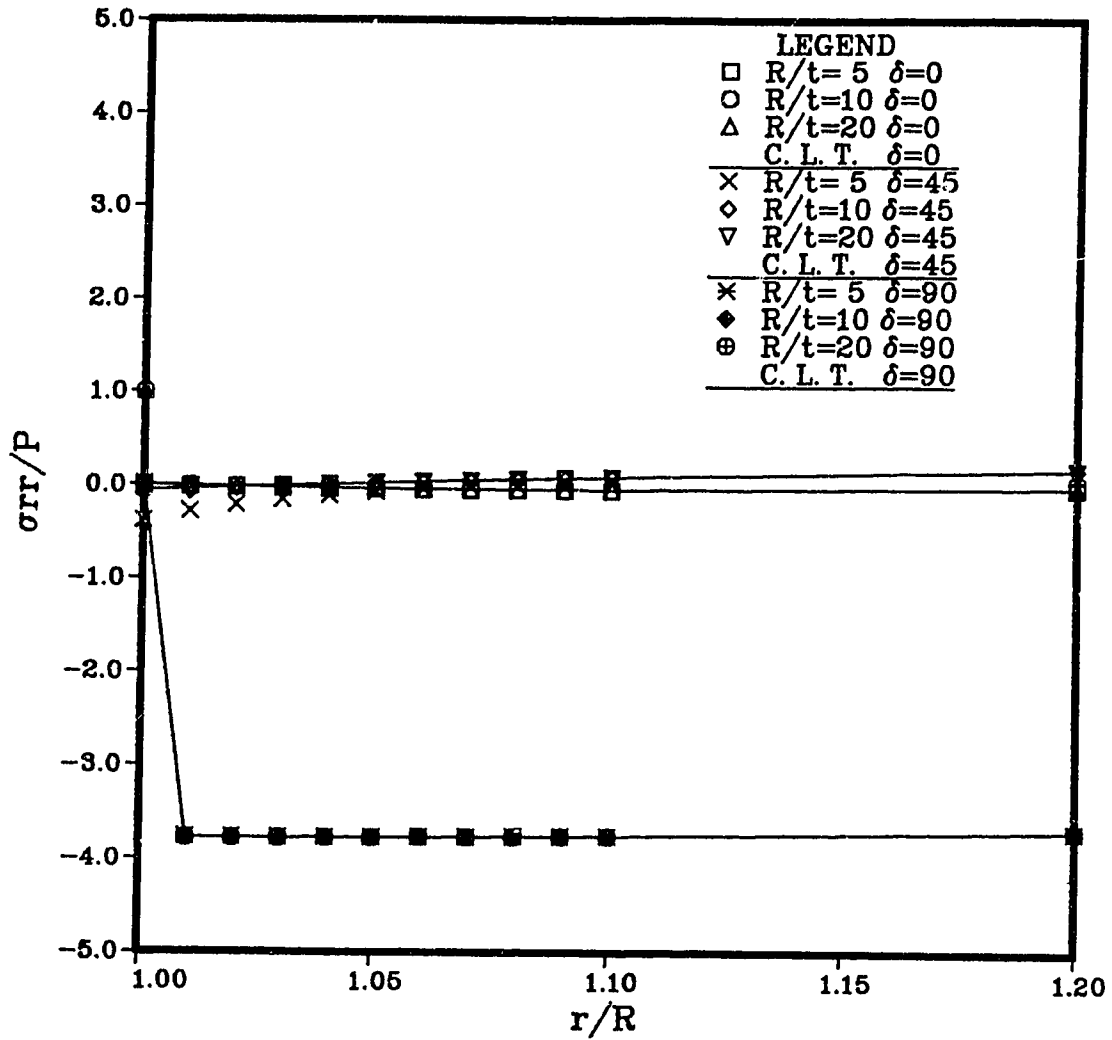


Figure 6.9: Radial Distribution of σ_{rr} at the Mid-Plane of the $[\pm 45]_s$ Laminate Around the Hole (Material A)

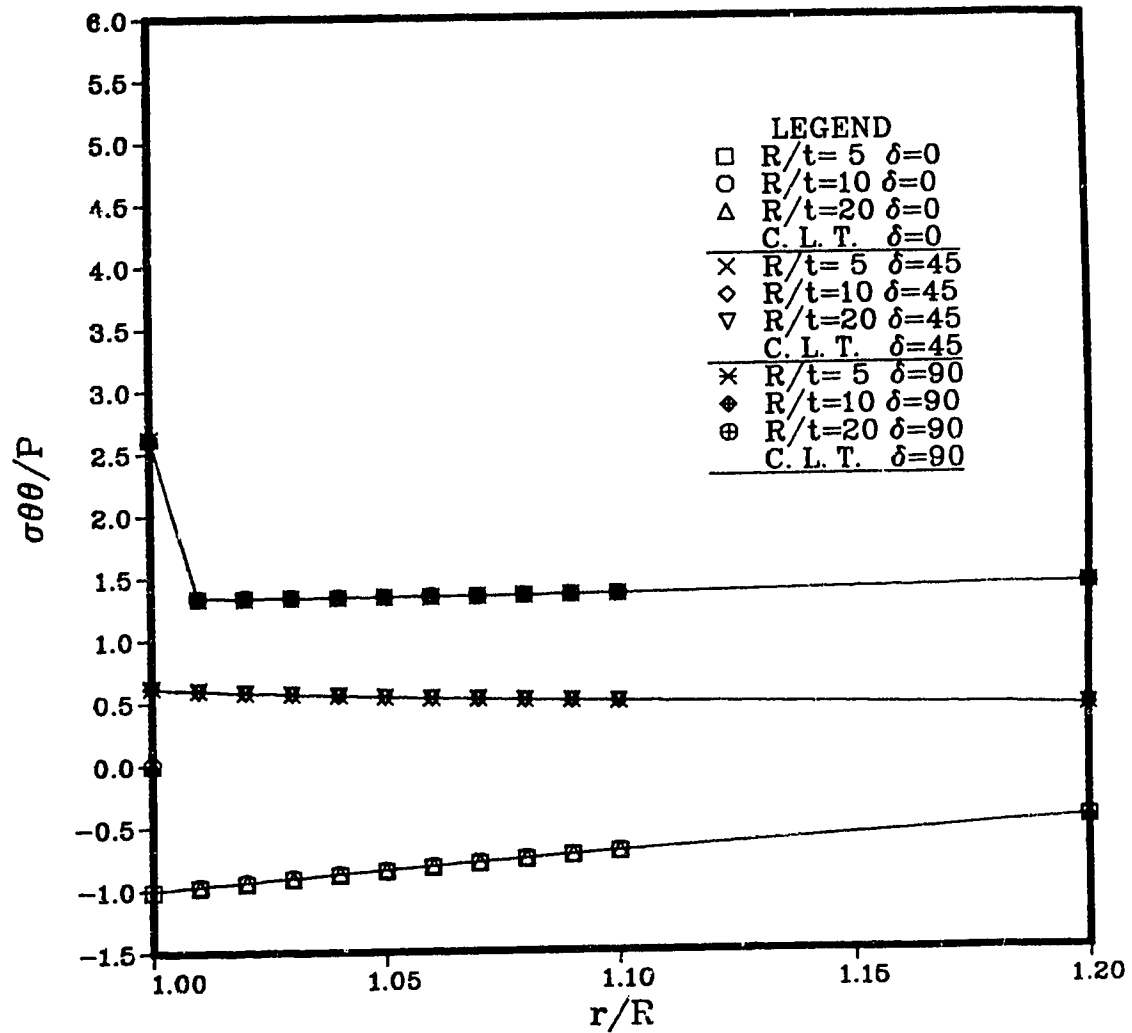


Figure 6.10: Radial Distribution of $\sigma_{\theta\theta}$ at the Mid-Plane of the $[\pm 45]$, Laminate Around the Hole (Material A)

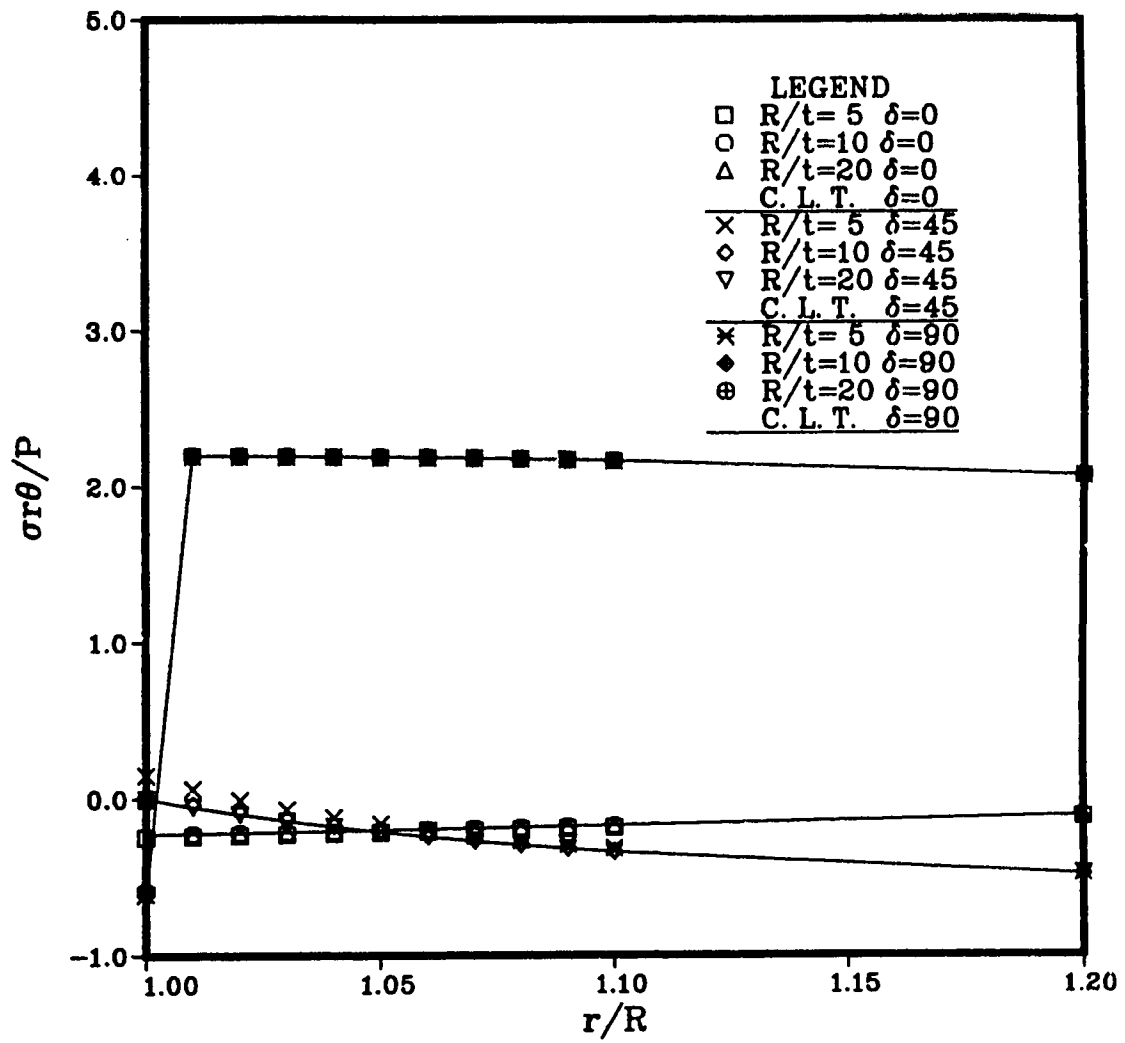


Figure 6.11: Radial Distribution of $\sigma_{r\theta}$ at the Mid-Plane of the $[\pm 45]_s$ Laminate Around the Hole (Material A)

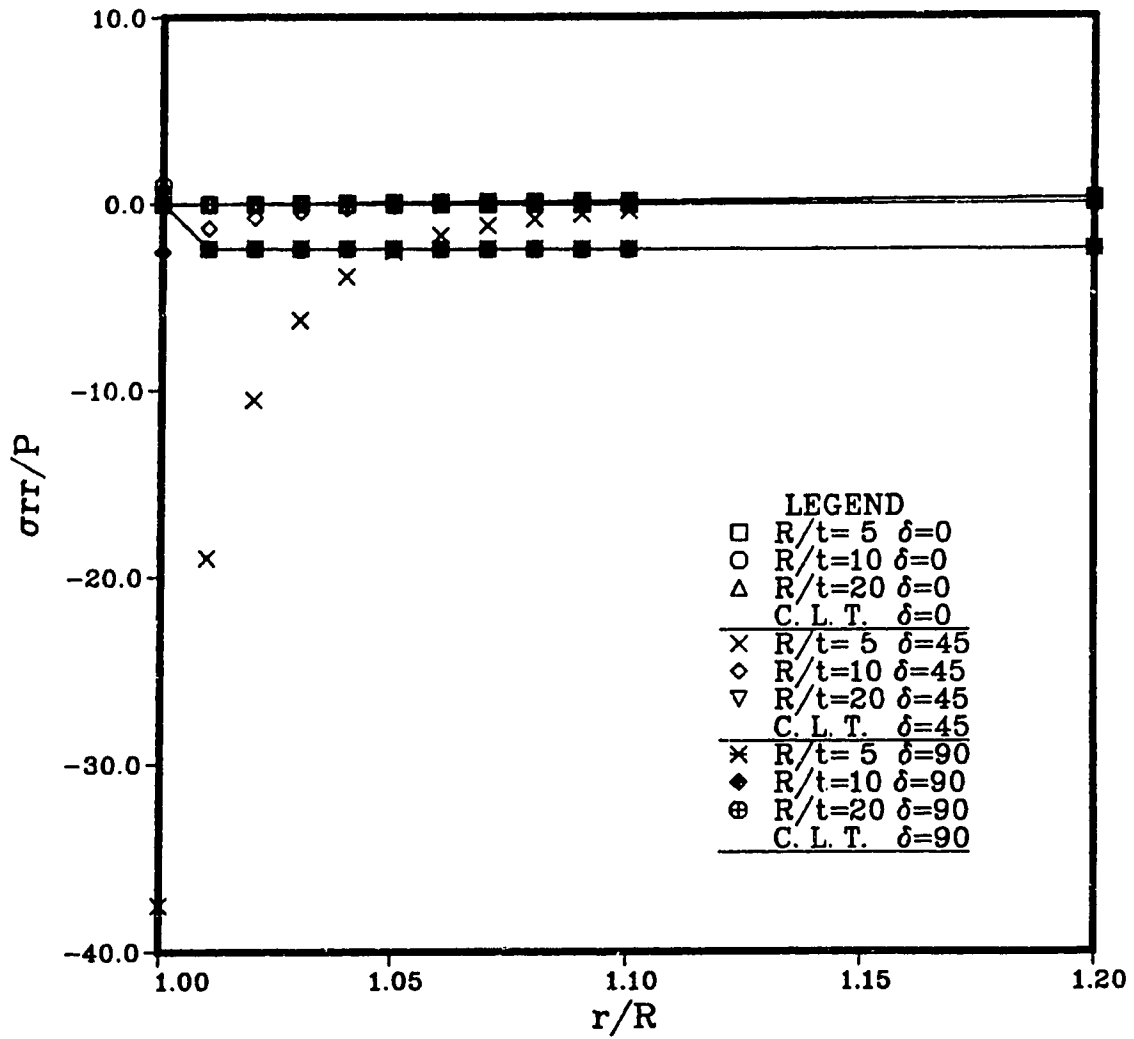


Figure 6.12: Radial Distribution of σ_{rr} at the Mid-Plane of the $[\pm 45]$, Laminate Around the Hole (Material B)

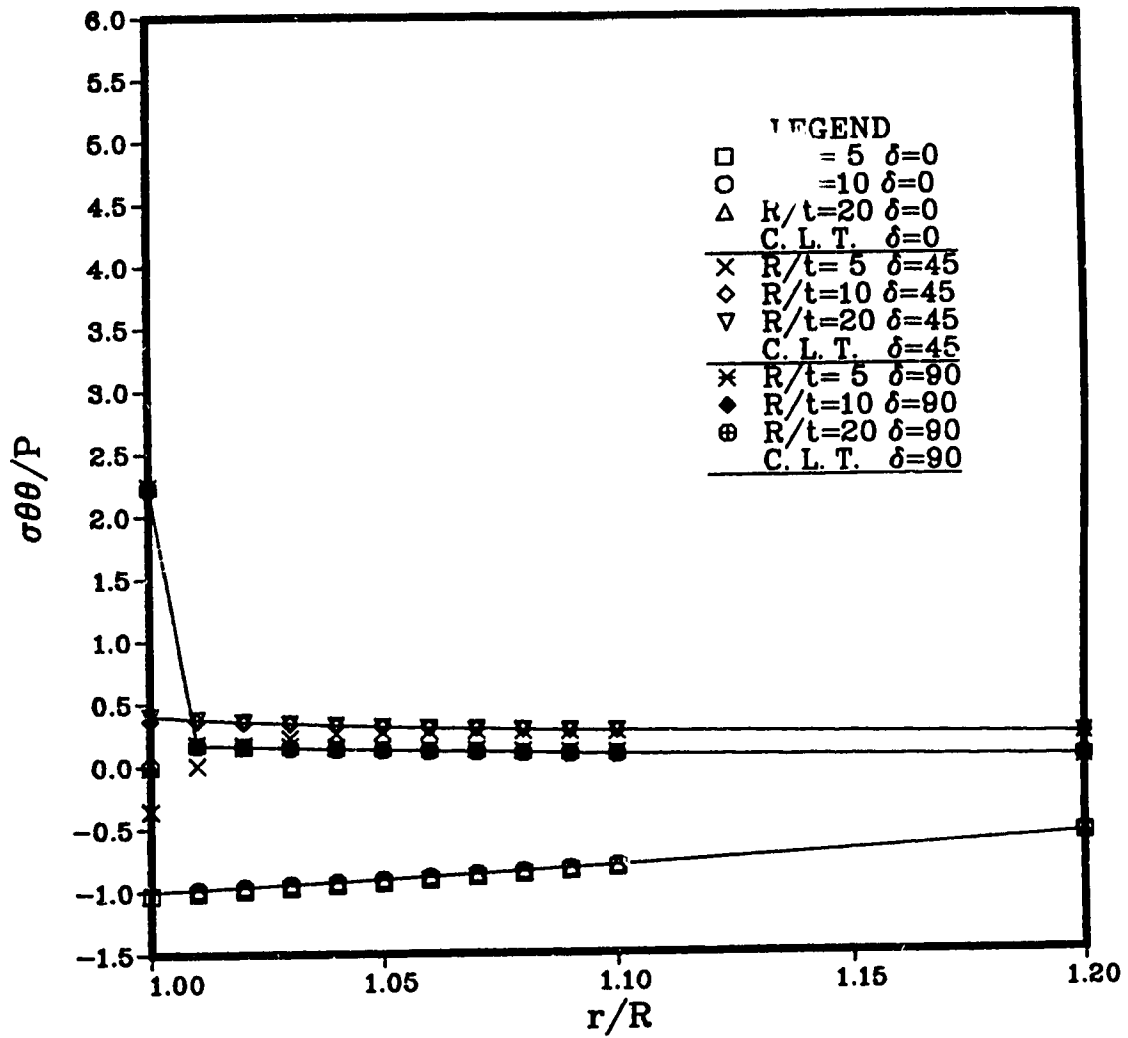


Figure 6.13: Radial Distribution of $\sigma_{\theta\theta}$ at the Mid-Plane of the $[\pm 45]_s$ Laminate Around the Hole (Material B)

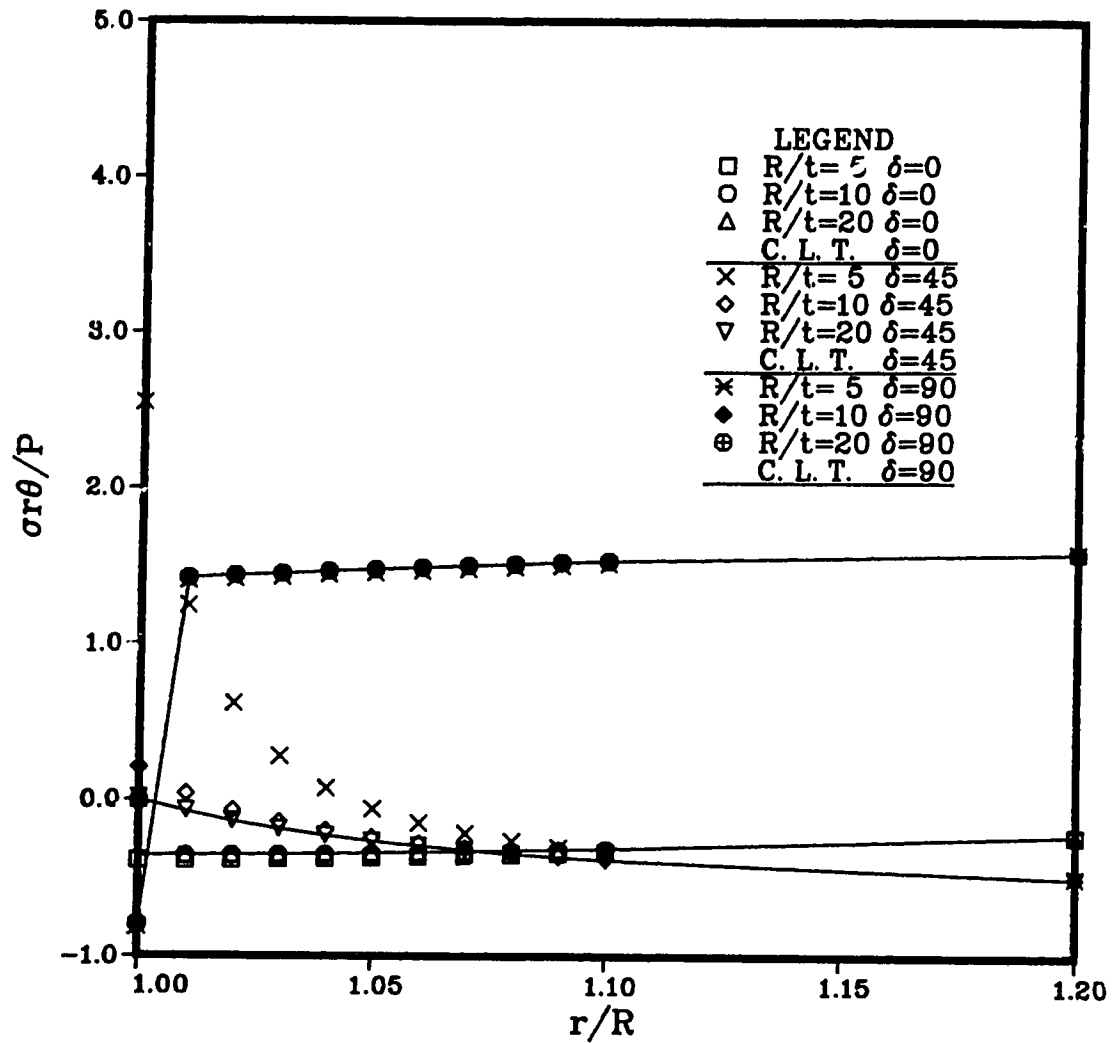


Figure 6.14: Radial Distribution of $\sigma_{r\theta}$ at the Mid-Plane of the $[\pm 45]_s$ Laminate Around the Hole (Material B)

Although these results are only for the few cases considered here (two anisotropy factors and two laminate geometries), it seems that this method will give acceptable results (for the plane stress components) for the case of a very thin laminate made with a highly anisotropic material or a thicker laminate built with a material with smaller anisotropy.

Interlaminar Stresses

For each material and laminate geometry, the variation of the normalized values (with respect to the applied stress) of the interlaminar stress components are presented next. The normal interlaminar stress (σ_{zz}) is calculated at the centerline of the laminate while the interlaminar shear stresses (σ_{rz} and $\sigma_{\theta z}$) are calculated at the interlaminar interface between the first and second layer (since they are equal to zero at the centerline of a symmetric laminate).

For the case of the $[0/90]_s$ laminate built using *Material A*, the interlaminar shear distributions for different values of the normalized radial distance (r/R) and of the position angle (δ) are shown in Figs. 6.15-6.17. The stress distributions for the same laminate geometry constructed using *Material B*, are shown in Figs. 6.18-6.20.

Similar to the plane stress components, the values of the interlaminar stress components depend on the laminate thickness (R/t), the anisotropy factor ($A.F.$), the position angle (δ) and the radial distance from the hole (r/R). For the same material, the maximum of the stress components σ_{rz} and σ_{zz} at the hole was observed at $\delta = 90^\circ$. The values of these two components were observed to increase with the increase of the anisotropy factor (for example, for *Material A*, the maximum value of σ_{zz} at the hole is about $0.12P$, this value increases to $5.8P$ for *Material B*). For both materials, the stress components σ_{rz} and σ_{zz} decreased rapidly as we move away from the hole. The stress component $\sigma_{\theta z}$ existed only at $\delta = 45^\circ$ and did not reduce to zero away from the hole.

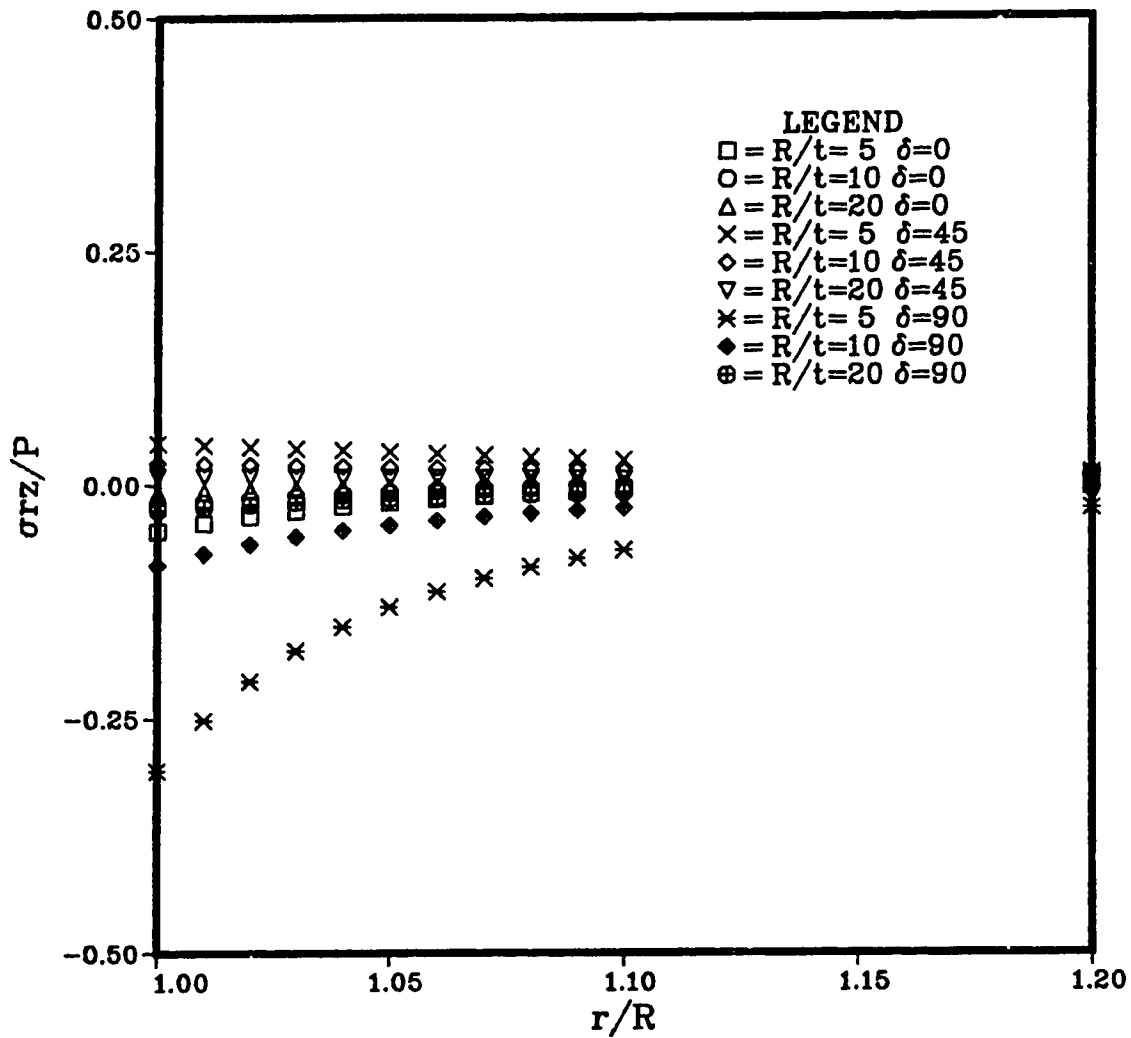


Figure 6.15: Radial Distribution of σ_{rz} at the Interlaminar Interface of the [0/90], Laminate Around the Hole (Material A)

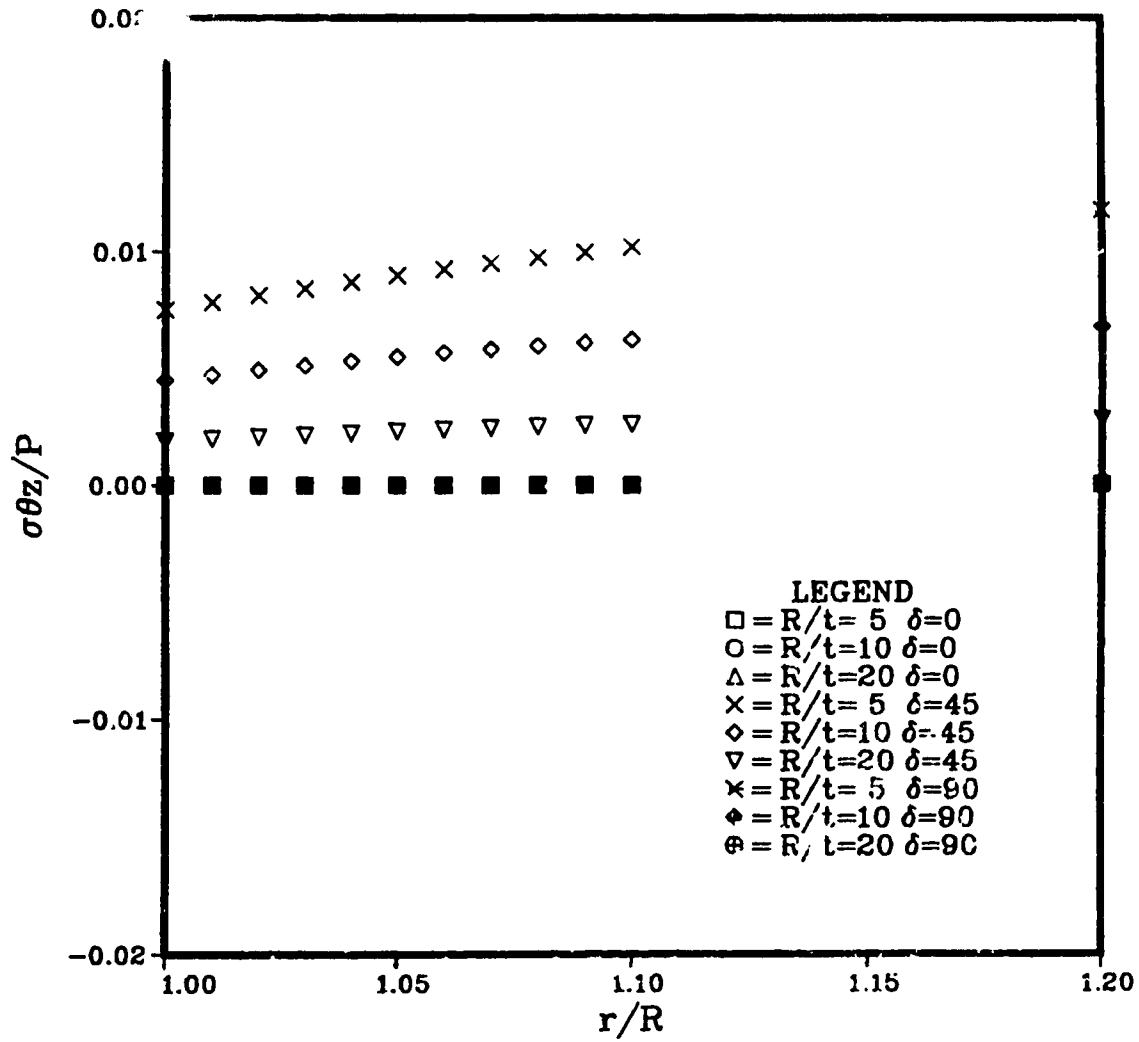


Figure 6.16: Radial Distribution of $\sigma_{\theta z}$ at the Interlaminar Interface of the [0/90], Laminate Around the Hole (Material A)

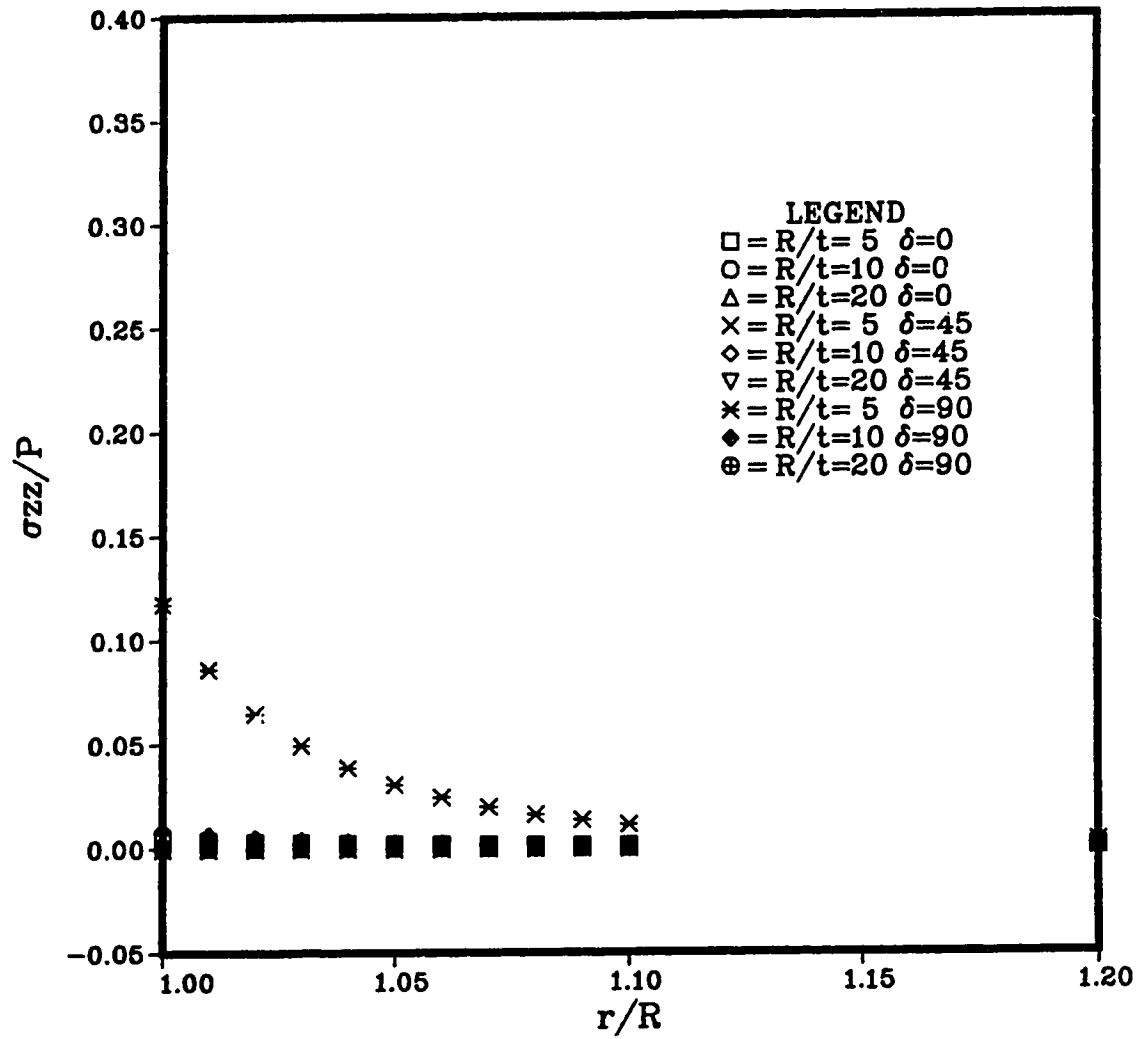


Figure 6.17: Radial Distribution of σ_{zz} at the Mid-Plane of the $[0/90]_s$ Laminate Around the Hole (Material A)

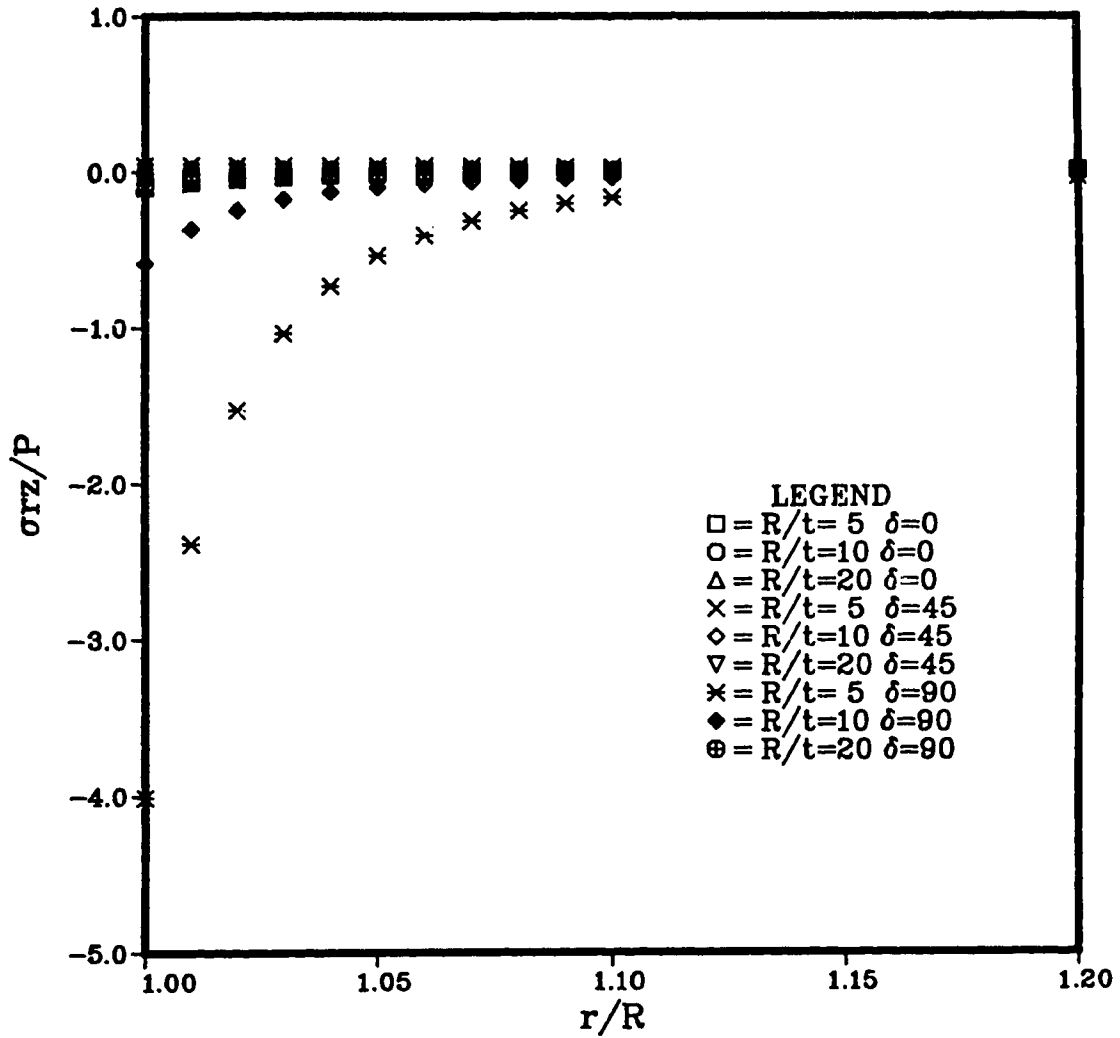


Figure 6.18: Radial Distribution of σ_{rz} at the Interlaminar Interface of the $[0/90]_s$ Laminate Around the Hole (Material B)

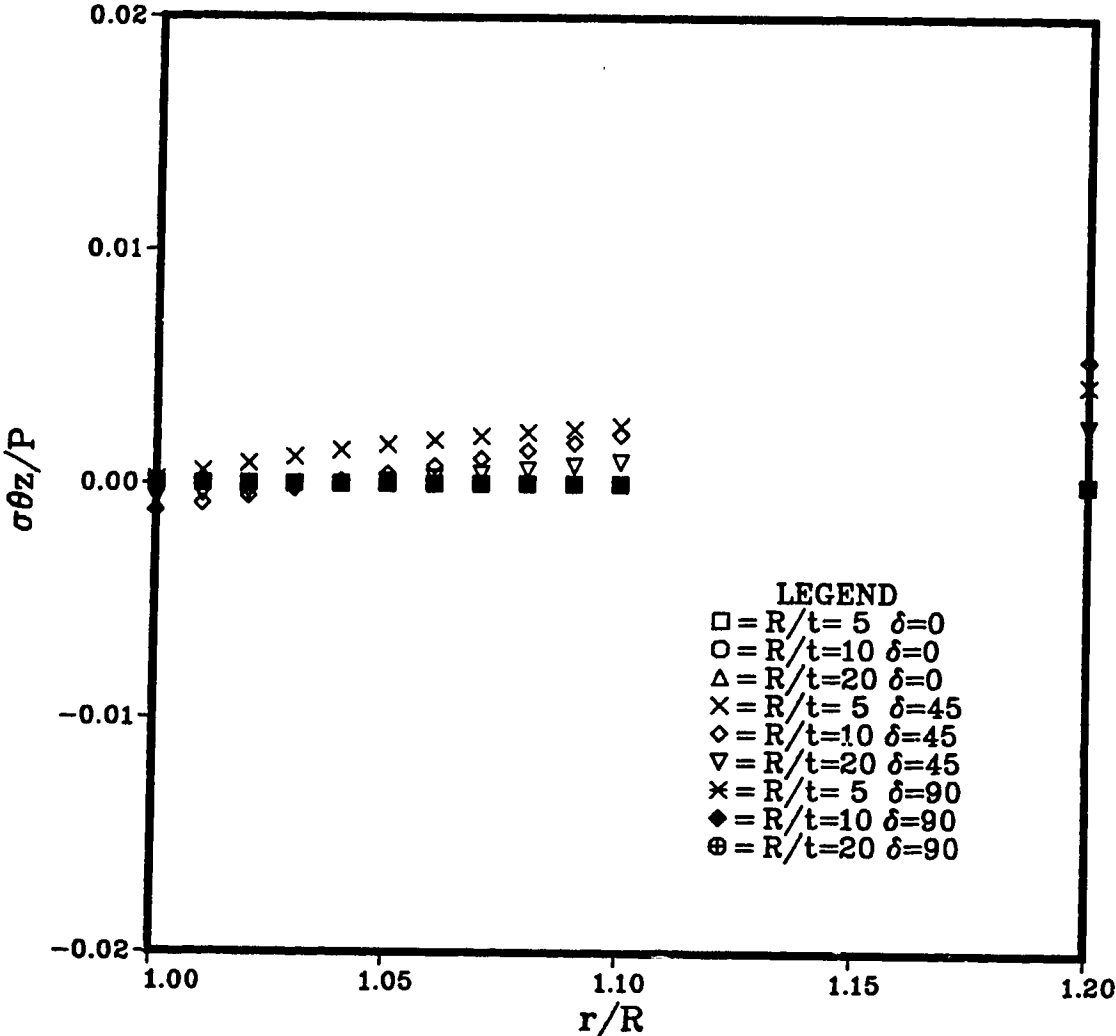


Figure 6.19: Radial Distribution of $\sigma_{\theta z}$ at the Interlaminar Interface of the $[0/90]_s$ Laminate Around the Hole (Material B)

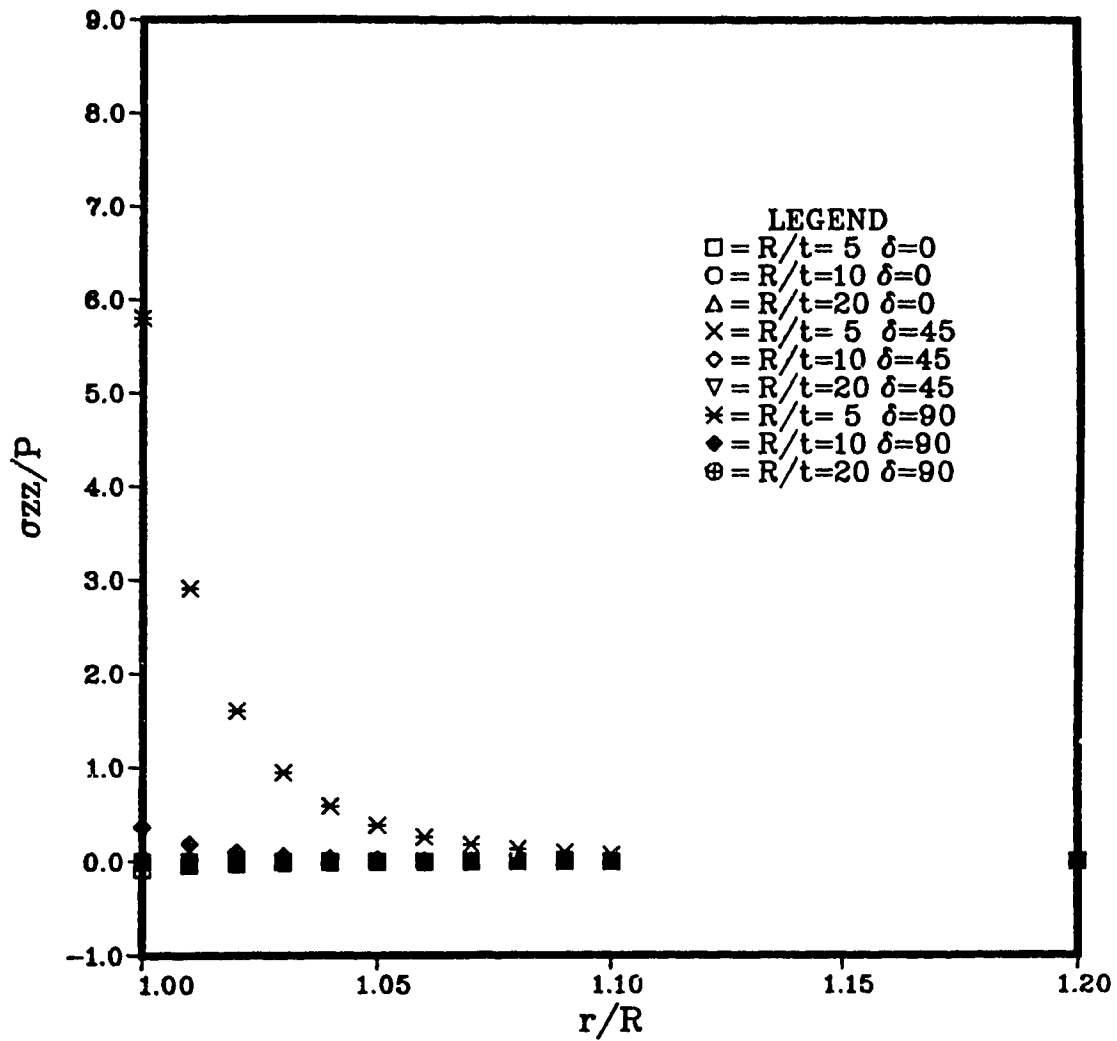


Figure 6.20: Radial Distribution of σ_{zz} at the Mid-Plane of the [0/90]_s Laminate Around the Hole (Material B)

For the $[\pm 45]_s$ laminate, the interlaminar stress distributions using *Material A* and *Material B* are shown in Figs. 6.21-6.23 and Figs. 6.24-6.26 respectively.

For the same material, the maximum of the stress components σ_{rz} and σ_{zz} was observed at $\delta = 45^\circ$. The values of all components were higher with an increase of the anisotropy factor. For example, for *Material A*, the maximum value of σ_{zz} at the hole was about $0.03P$, this value increased to $1.19P$ for *Material B*. As was the case for the $[0/90]_s$ laminate, the stress component $\sigma_{\theta z}$ had a non-zero value for the case of $\delta = 45^\circ$ only.

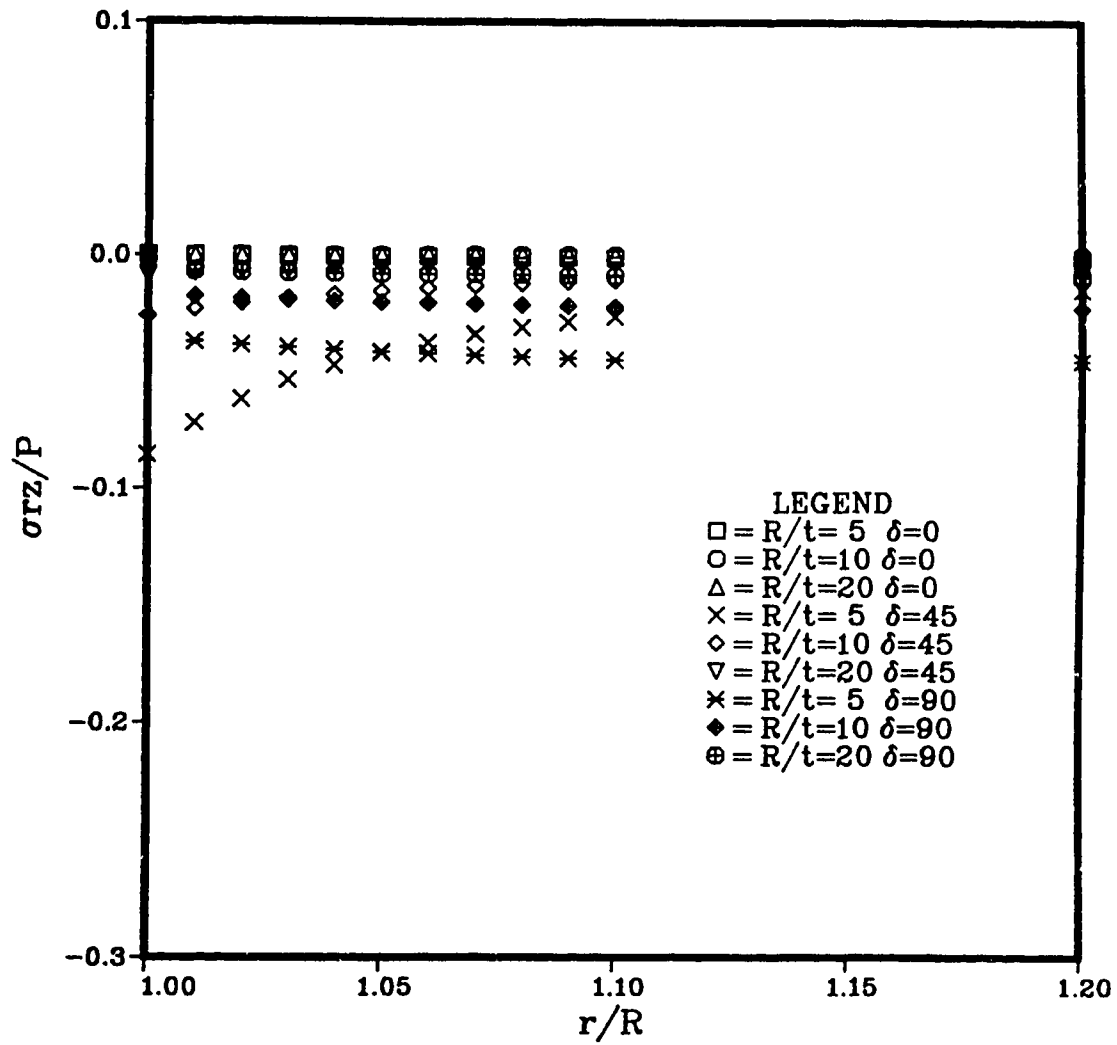


Figure 6.21: Radial Distribution of σ_{rz} at the Interlaminar Interface of the $[\pm 45]$, Laminate Around the Hole (Material A)

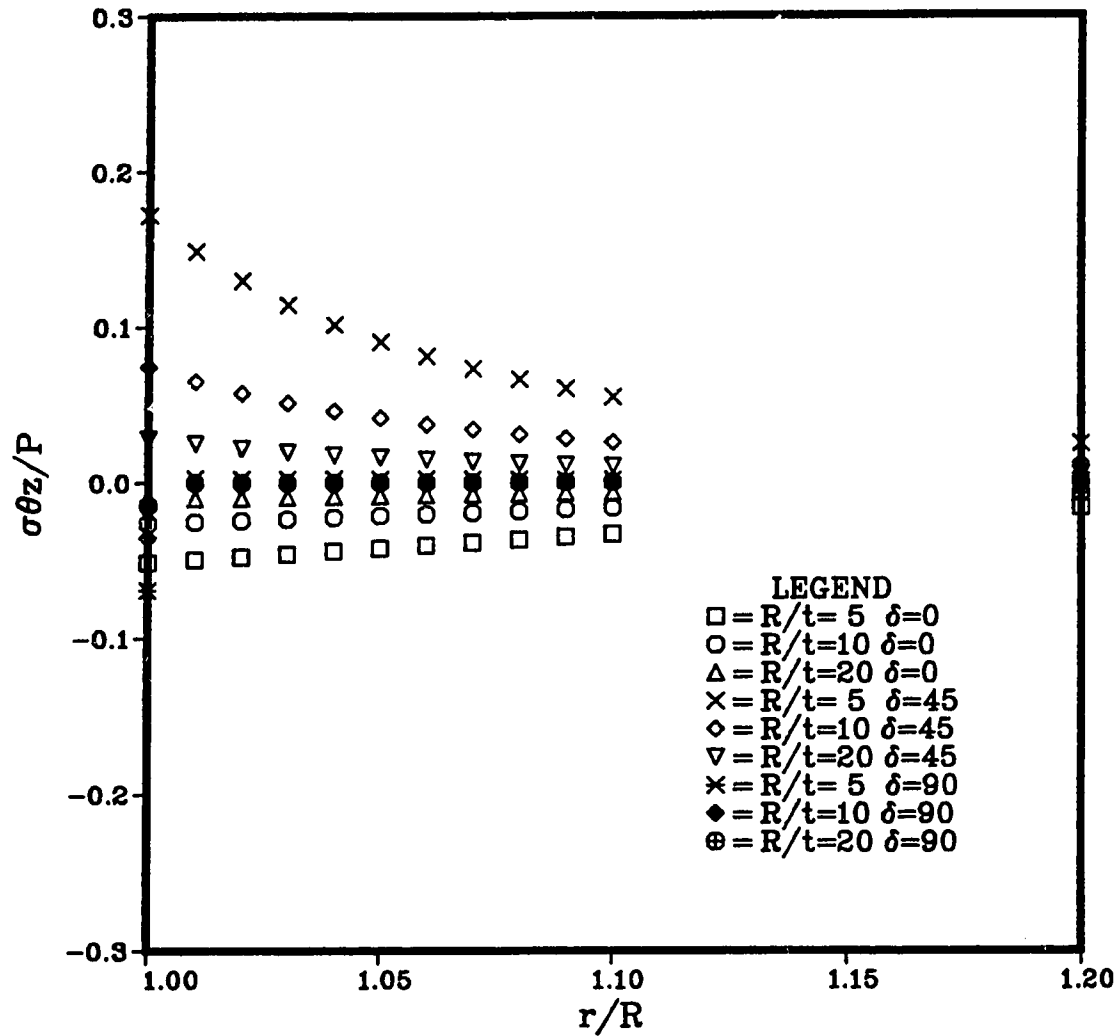


Figure 6.22: Radial Distribution of $\sigma_{\theta z}$ at the Interlaminar Interface of the $[\pm 45]_s$ Laminate Around the Hole (Material A)

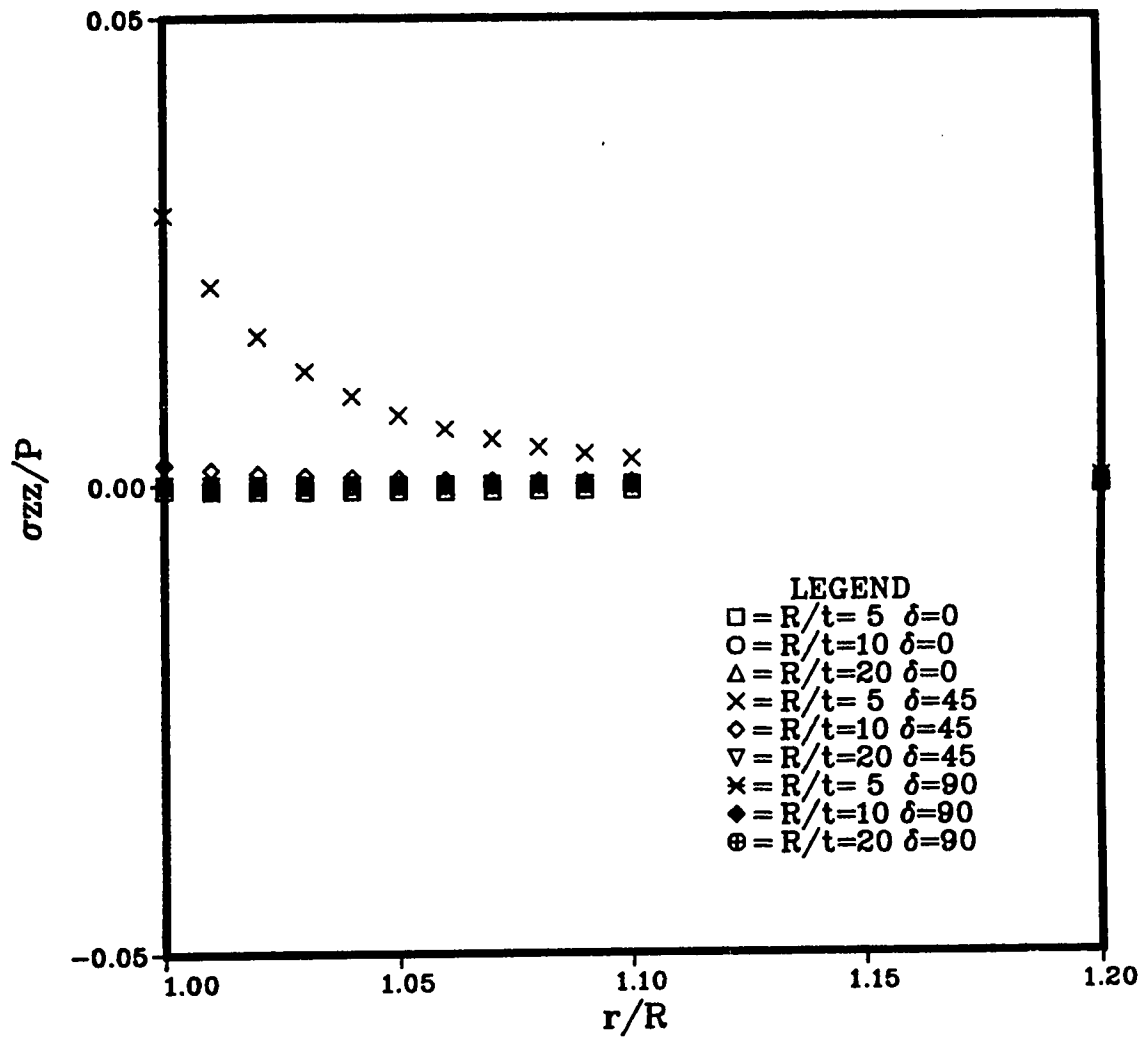


Figure 6.23: Radial Distribution of σ_{zz} at the Mid-Plane of the $[\pm 45]_n$ Laminate Around the Hole (Material A)

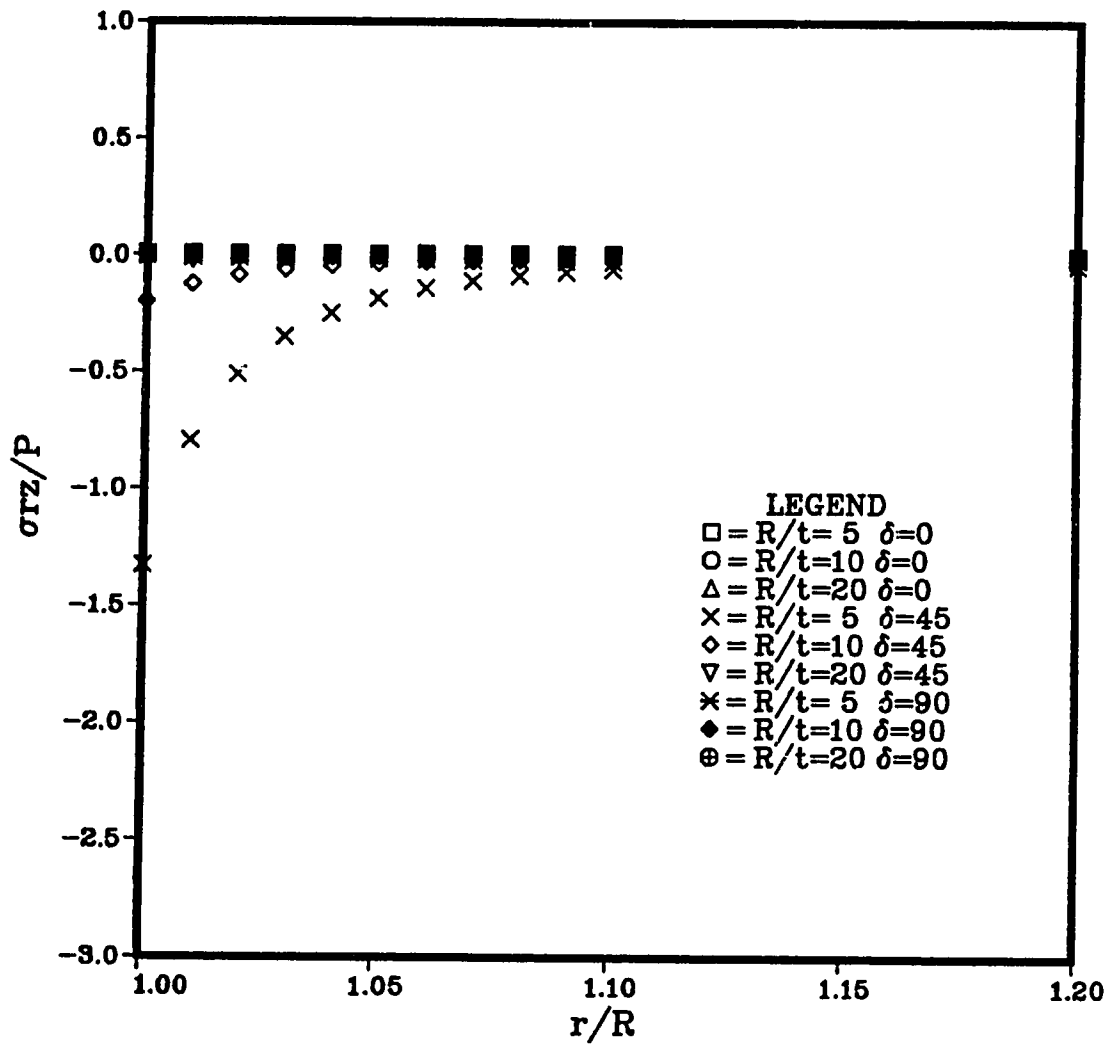


Figure 6.24: Radial Distribution of σ_{rz} at the Interlaminar Interface of the $[\pm 45]_s$ Laminate Around the Hole (Material B)

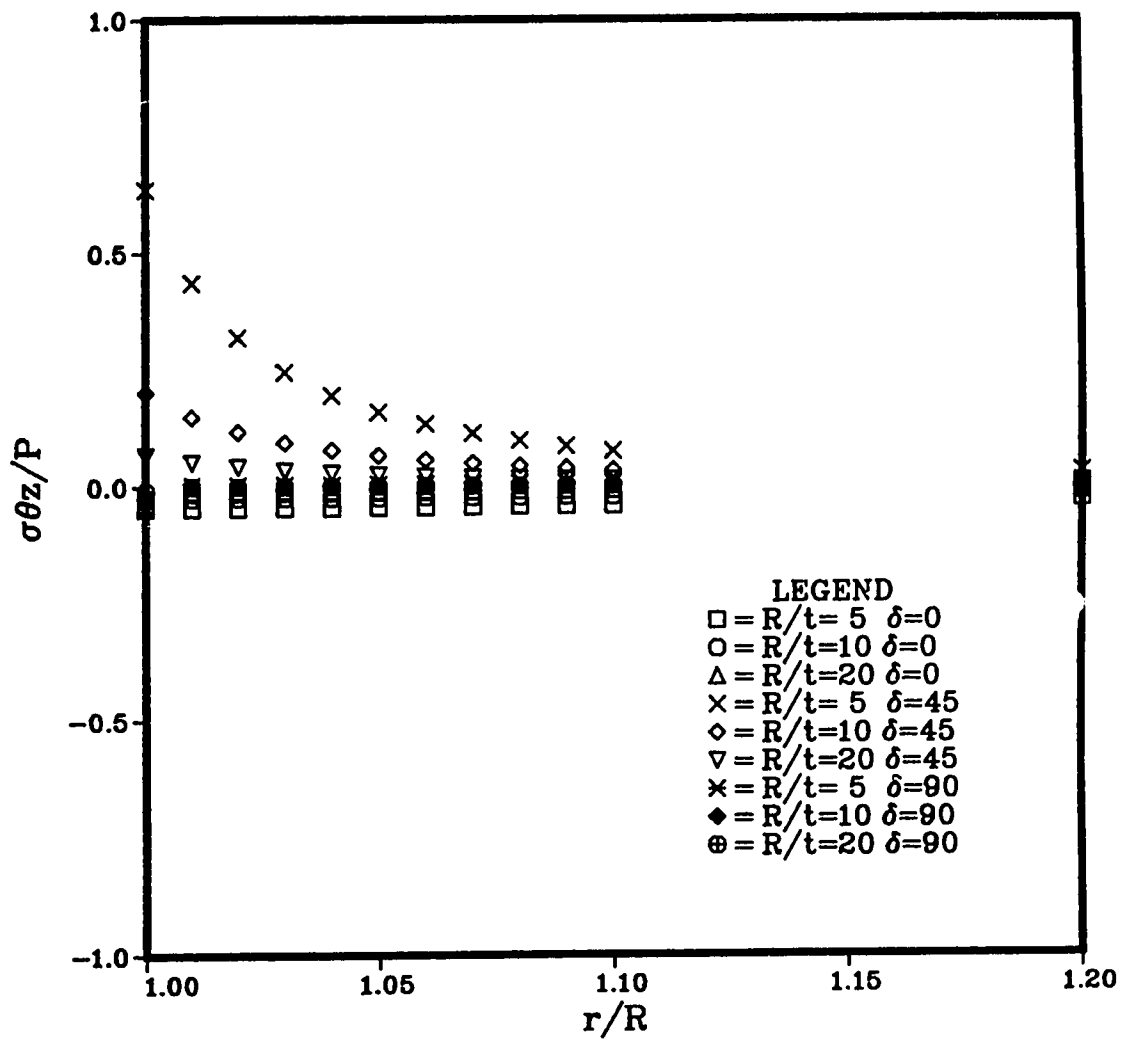


Figure 6.25: Radial Distribution of $\sigma_{\theta z}$ at the Interlaminar Interface of the $[\pm 45]_s$ Laminate Around the Hole (Material B)

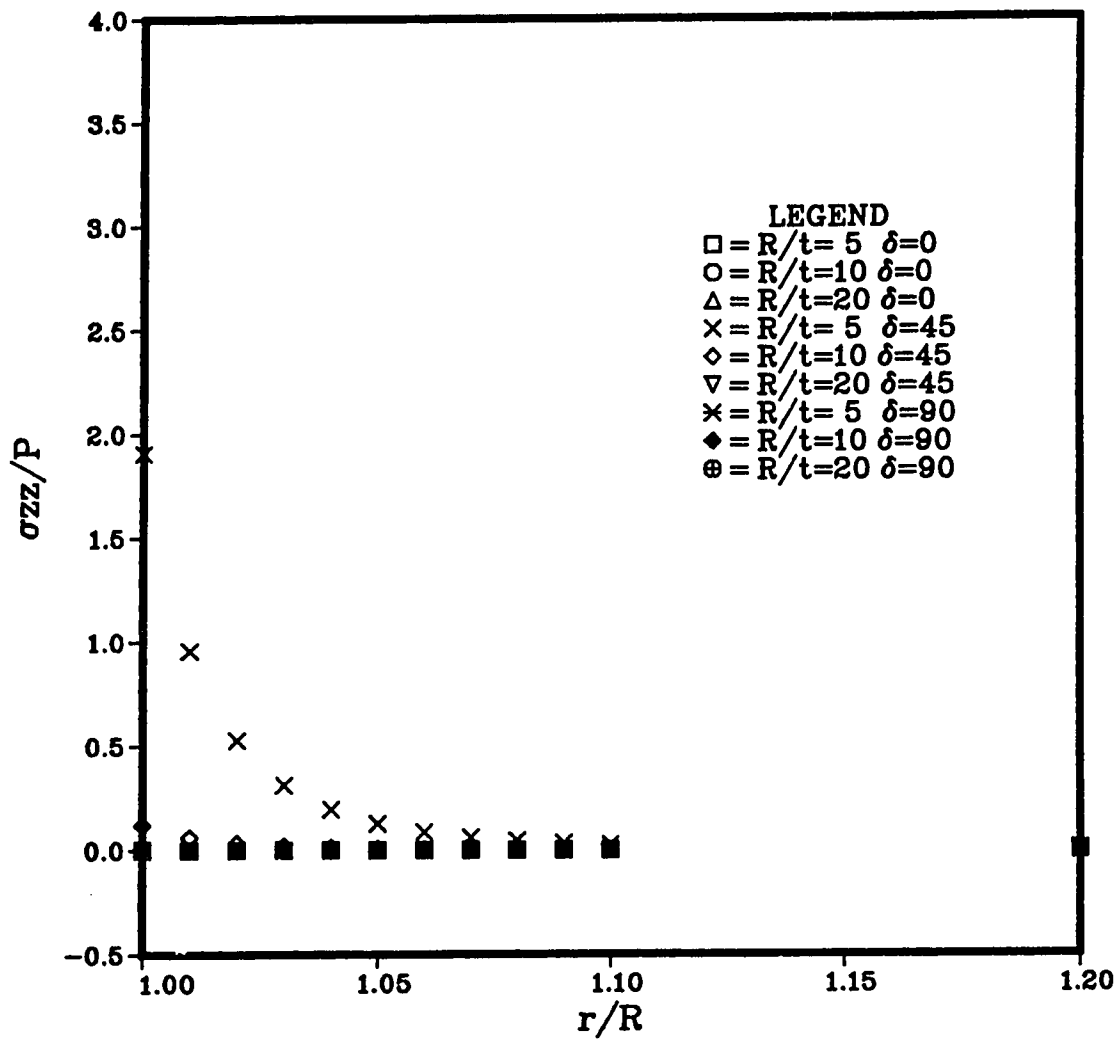


Figure 6.26: Radial Distribution of σ_{zz} at the Mid-Plane of the $[\pm 45]_s$ Laminate Around the Hole (Material B)

For comparison sake, Fig. 6.27 shows the normalized stress components (with respect to the applied load) obtained in a $[0/90]_s$ laminate made from *Material A* with an $R/t = 10$ at the position angle $\delta = 90^\circ$. The plane stresses and the interlaminar normal stress are calculated at the centerline of the laminate, while the interlaminar shear stresses are calculated at the interlaminar interface. The lines, once more, represent the results obtained using the classical laminate theory. From this figure it can be noticed that the values of the interlaminar stresses are much smaller compared to the plane stresses.

The solution obtained, as mentioned previously, satisfies edge boundary conditions only in an average sense. Therefore the results obtained might not be very reliable close to the hole. However the interior solution is also important since it can give some information about the magnitude of the stress components at the edge. To satisfy the edge conditions point by point, it might be necessary to superpose some sort of boundary layer solution. This solution would decay exponentially with the distance from the edge [84].

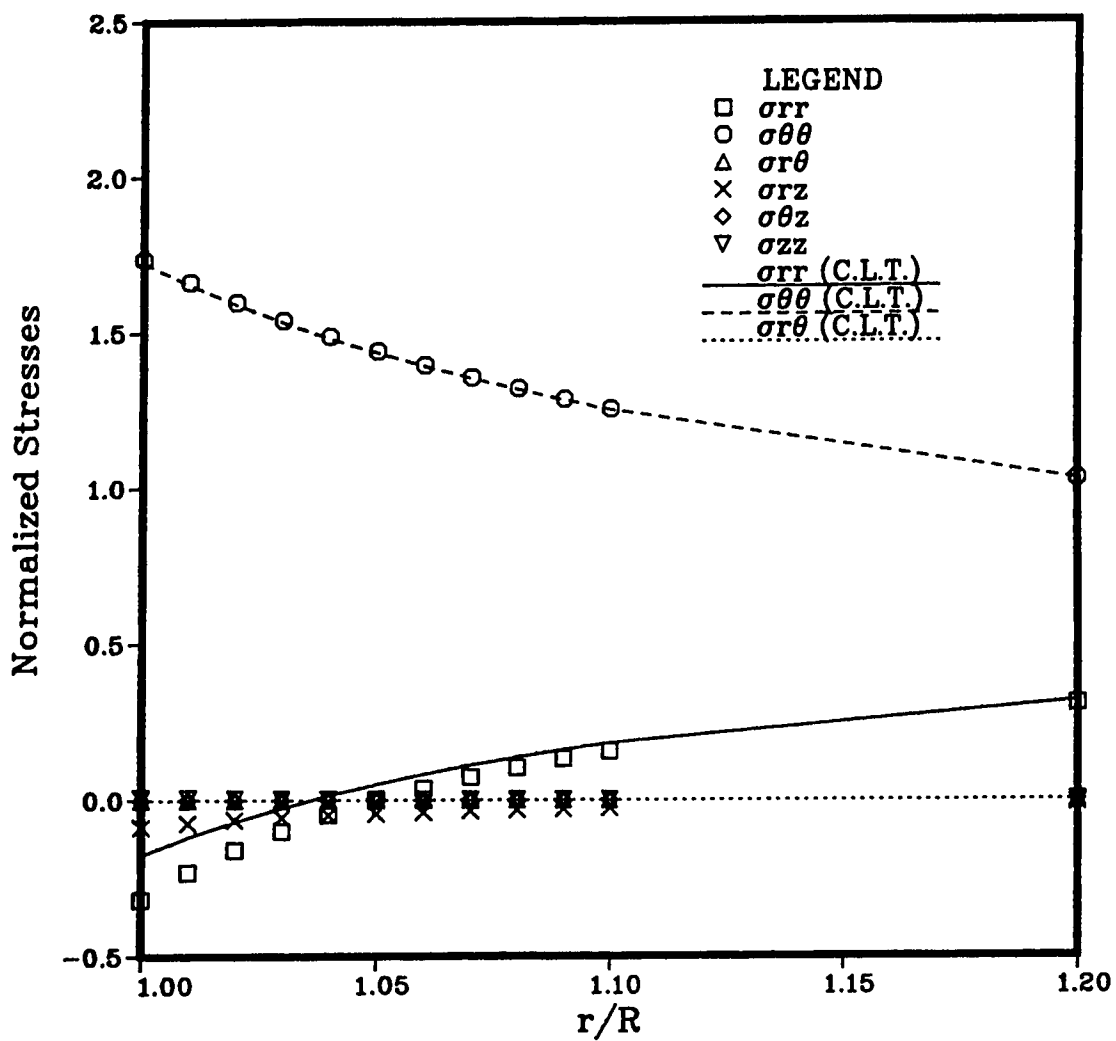


Figure 6.27: Normalized Stress Components for the $[0/90]$, Laminate ($R/t = 10$, $\delta = 90^\circ$, Material A)

Table 6.2: Material properties of the Graphite/Epoxy Composite Used by Lucking et al.

Properties	
E_{11} (GPa)	145
E_{22}, E_{33} (GPa)	10.7
G_{12}, G_{13} (GPa)	4.5
G_{23} (GPa)	3.6
ν_{12}, ν_{13}	0.31
ν_{23}	0.49

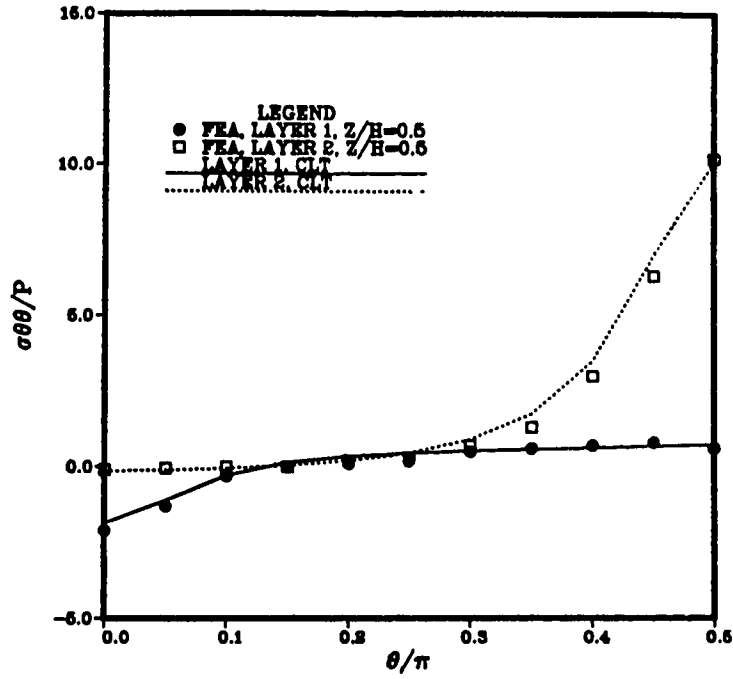
6.3.5 Comparison of the Present Solution and the Three-Dimensional Finite Elements Method Solution

From the previous section, it was determined that the present method will be more successful if the laminated plate is thin. The solution would seem to get even better if the anisotropy of the material was not very high.

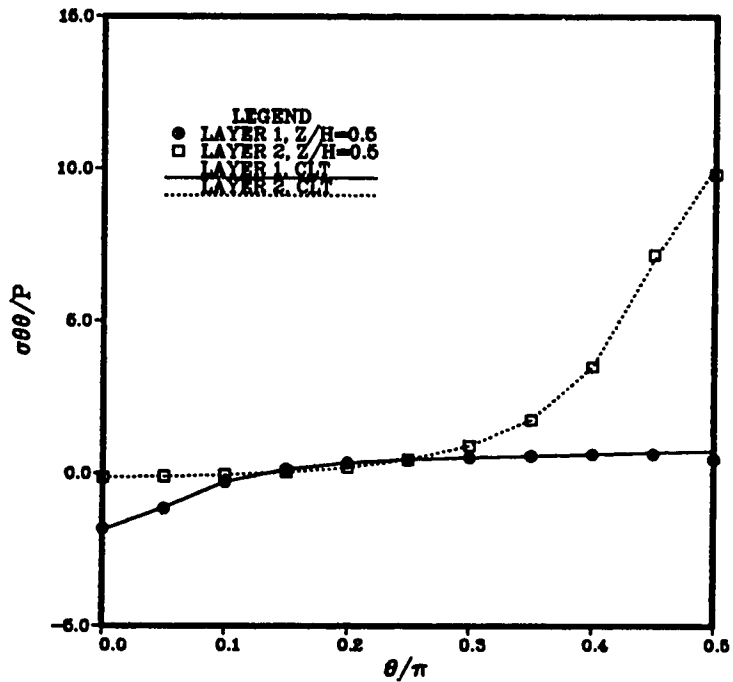
Lucking et al. [83] studied the effect of geometry on the interlaminar stresses of $[0/90]_s$ composite laminates with a traction-free circular hole. They used a *Graphite/Epoxy* with an *A.F.* of 13.55. The properties of the material they used is shown in Table 6.2. One of the laminates they considered had an R/t ratio of 12.5. The only reported in-plane stress component was the angular distribution of the tangential component, $\sigma_{\theta\theta}$ for each layer in the laminate. Figure 6.28 shows a comparison between the finite element analysis results and the results obtained using the present method, the CLT results are also included.

The normalized interlaminar stresses $\sigma_{rz}, \sigma_{\theta z}$ and σ_{zz} at various values of the position angle (δ) obtained using the present method, are compared to the finite element analysis results in Figs. 6.29-6.31. As expected, since the boundary

conditions are only satisfied on average, the values of the interlaminar stresses obtained at the hole are not accurate. It should also be noted that, near the hole, the solution does not converge. Therefore it does not satisfy the equilibrium equations for every lamina in the laminate (Fig. 6.31). Away from the hole, the results obtained are comparable to those obtained using the three dimensional FEM. In this case, the higher terms of the solution reduce to zero and the solution converges satisfying the equilibrium equations for each lamina.

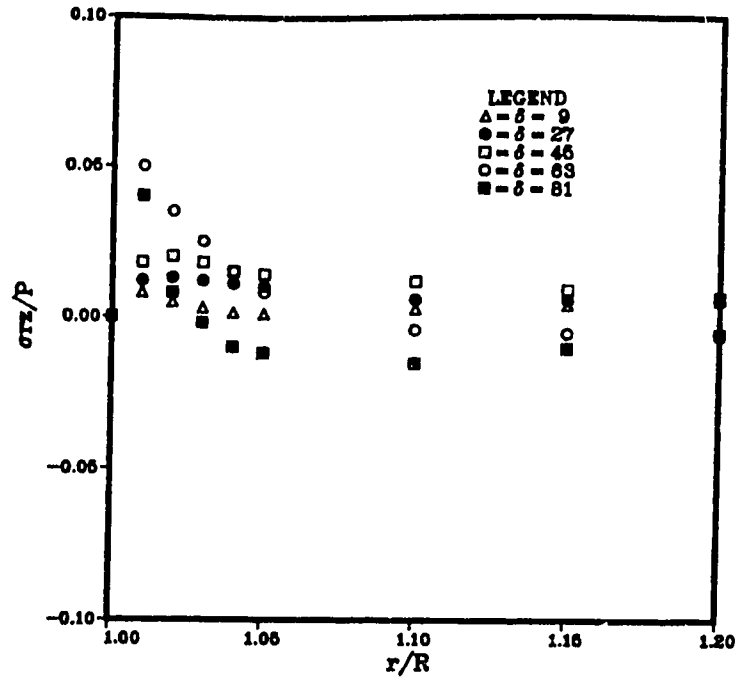


(a)

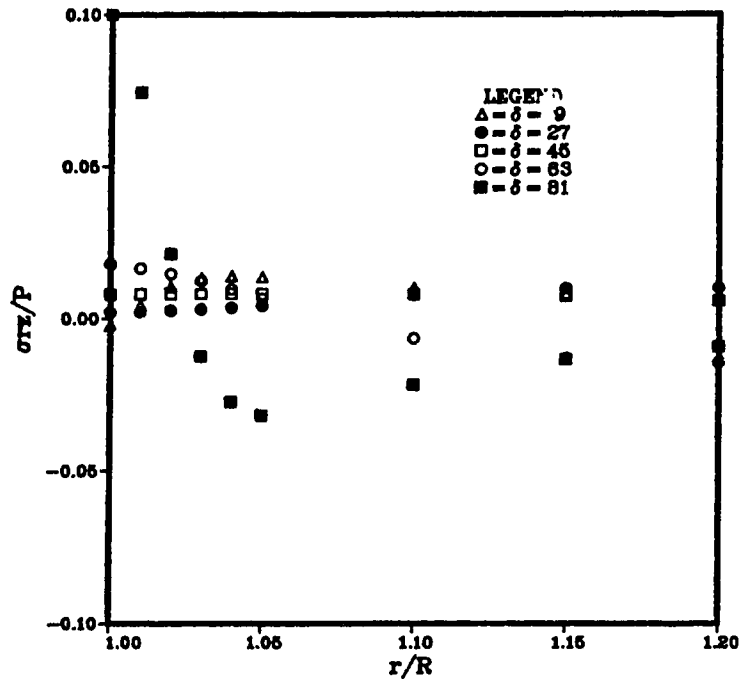


(b)

Figure 6.28: Angular Distribution of $\sigma_{\theta\theta}$ Around the Hole for Graphite/Epoxy
 (a) Finite Element Analysis
 (b) Present Method

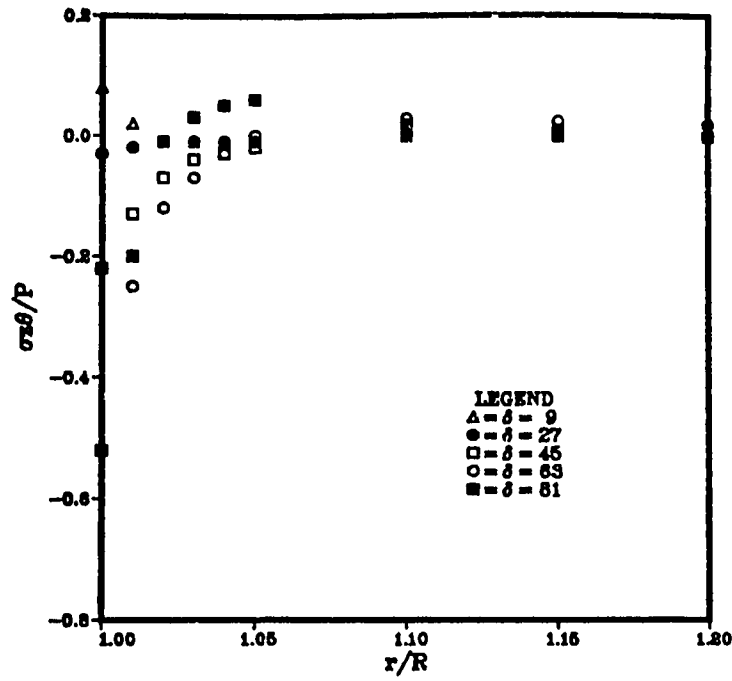


(a)

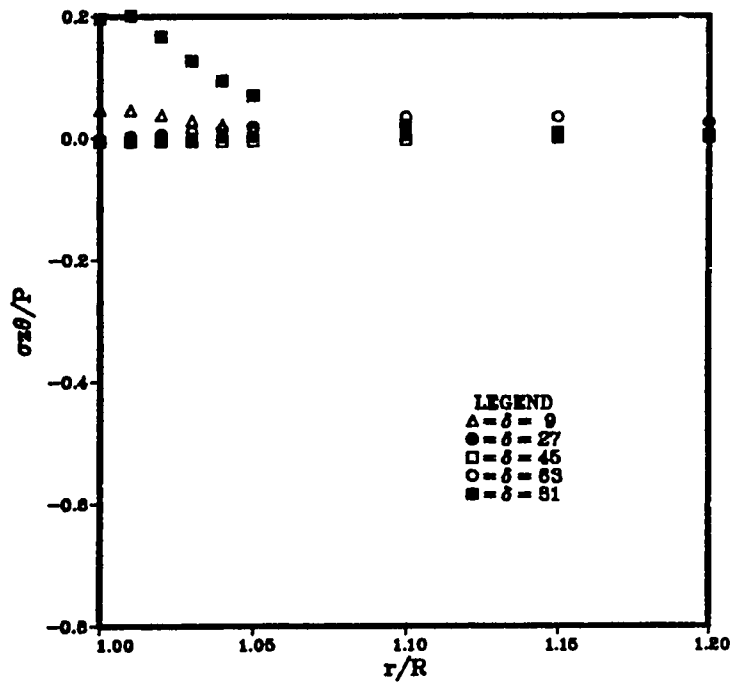


(b)

Figure 6.29: Radial Distribution of σ_{rz} on the Interface Plane Around the Hole for Graphite/Epoxy
 (a) Finite Element Analysis
 (b) Present Method

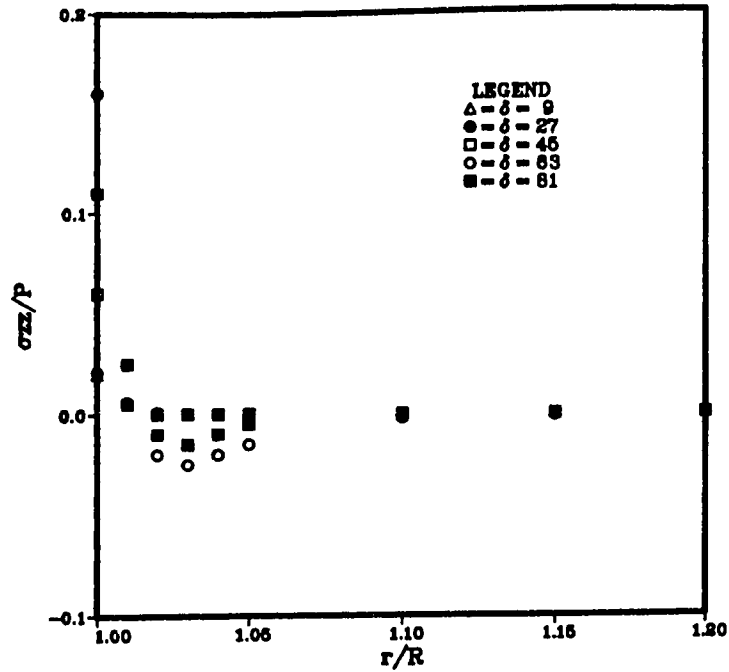


(a)

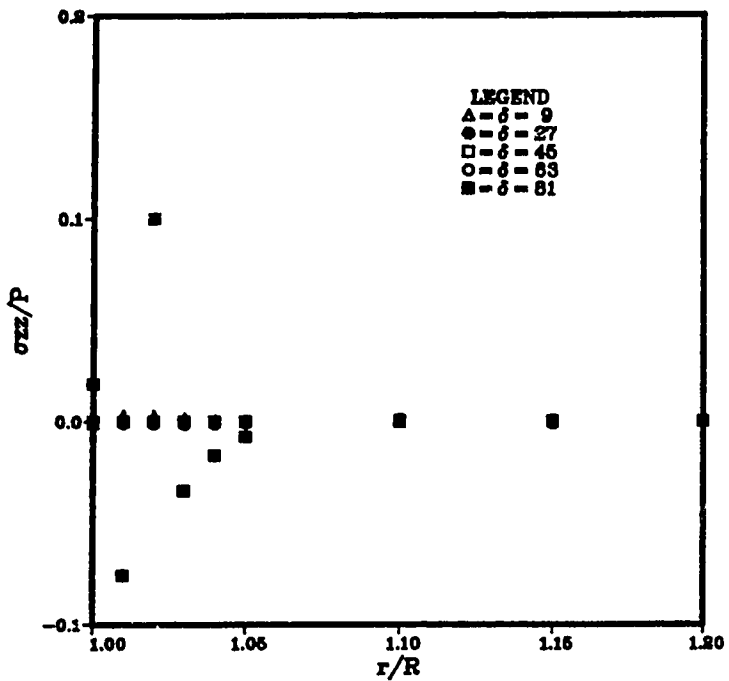


(b)

Figure 6.30: Radial Distribution of $\sigma_{z\theta}$ on the Interface Plane Around the Hole for Graphite/Epoxy
 (a) Finite Element Analysis
 (b) Present Method



(a)



(b)

Figure 6.31: Radial Distribution of σ_{zz} Near the Midplane Around the Hole for Graphite/Epoxy
 (a) Finite Element Analysis
 (b) Present Method

6.4 Concluding Remarks

The theory of symmetric anisotropic laminated elastic plates presented in chapter 5 was used to obtain the stress components for both an isotropic and an anisotropic laminated plate containing a traction-free circular hole subjected to a uniform tensile stress at infinity.

The results obtained for the isotropic case were the same as those reported in [78]. This method was found to give very reasonable results even in the cases where the properties of the isotropic materials forming the laminate were very different. The value of σ_{rr} obtained at the hole depends on the R/t ratio. If the laminate is thin enough ($R/t > 10$), this value is negligible but if a thicker plate was used, significant non-zero values result.

For the case of anisotropic laminated plates, the results were unacceptable for most of the cases considered. These results were found to depend on numerous factors such as anisotropy, thickness of the laminate, as well as the position considered. Close to the hole, the assumed form of the solution did not converge. Because of that, the equilibrium equations for the different layers were not satisfied. These results worsened when a thick laminate with a high anisotropy was considered.

Also, since the boundary conditions were only satisfied on average through the thickness of a laminate, the values of the stress components obtained at a specific point on or close to the boundary were not accurate. This is a serious problem since the main interest is the determination of the interlaminar stresses at the edges.

The natural recommendation for any further expansion of this work would be the use of a different form of series. This form should take into consideration the mismatch between the properties of the different layers in the laminate. This might lead to a better convergence even when the materials used are highly anisotropic.

Chapter 7

Conclusion

This work deals with damage of unidirectional fiber reinforced composite materials. A fatigue failure criterion for unidirectional coupons was presented. It is intended that the failure of a coupon represents the initiation of damage in a larger component. This fatigue criterion was based on the *Strain Energy*. The predictions obtained using this criterion were compared to published experimental results for different materials. In all cases the predictions were quite accurate. Since most of the available data was for a stress ratio of 0.1, a series of cyclic tests under different values of the stress ratio (0, 0.5 and -1) was conducted. The failure criterion was modified to include the effect of the stress ratio. The modified criterion was shown to accurately fit the experimental data.

The existing crack in the component will now start to propagate. The *Strain Energy Criterion* was also used to predict the direction of crack growth in unidirectional composites loaded monotonically under both uniaxial and general biaxial plane conditions. The predictions obtained using the present criterion were compared to those obtained using some other well-known criteria used for this purpose. The results obtained using the present theory were shown to consistently predict the direction of crack growth as well as or better than the other criteria.

The Classical Laminate Theory (CLT) is simple but is unable to predict the through-the-thickness components of the stress. To extend the use of the strain energy density criterion to the laminates, these stress components would have to be determined in order to calculate the value of the strain energy. The use of finite difference method and finite element analysis leads to accurate results. Unfortunately these methods often require high computing power.

A three dimensional anisotropic theory based on the easy-to-use CLT was developed. In this theory, the displacement and interlaminar stress continuity conditions through the interlaminar interfaces were satisfied. The zero traction condition on the lateral surfaces was also satisfied. The boundary conditions were satisfied in an average manner. When isotropic material properties were used, the present theory was seen to reduce to the isotropic form obtained by other researchers [78].

The problem of a symmetric laminate containing a traction-free circular hole and subjected to a tensile stress at infinity was investigated. For the isotropic case, the results obtained were identical to those obtained in [78]. The use of a thicker laminate resulted in a non-zero radial stress component at the hole. For the anisotropic case, the results obtained were unacceptable. These results were influenced by several factors such as the material properties and the thickness of the laminate. Close to the hole the solution did not converge and did not satisfy the equations of equilibrium for each layer.

The anisotropic results were then compared to those obtained using the three dimensional finite element analysis. Near the hole, where the interlaminar stresses are important, the present method gave erroneous results (due to the fact that the boundary conditions were only satisfied in an average sense). At a distance from the hole (equal to the laminate thickness), both methods gave comparable results.

The natural recommendation for improving the results obtained using the

present method, would be the use of a different form of solution. This new form would take into consideration the properties of the different layers in the laminate.

References

- [1] R.M. Jones
Mechanics of Composite Materials, McGraw-Hill, 1975.
- [2] M.M. Schwartz
Composite Materials Handbook, McGraw-Hill, 1992.
- [3] B.D. Agarwal, L.J. Broutman
Analysis and Performance of Fiber Composites, John Wiley & sons, 1980.
- [4] C.K.H. Dharan
Fracture Mechanics of Composite Materials
Journal of Engineering Materials and Technology, vol.100, pp.233-247, 1978.
- [5] H.T. Hahn and J.G. Williams
Compression Failure Mechanisms in Unidirectional Composites
In: *Composite Materials: Testing and Design, seventh conference*, ASTM STP 893, J.M. Whitney, ed., pp.115-139, 1986.
- [6] E.M. Odom and D.F. Adams
Failure Modes of Unidirectional Carbon/Epoxy Composite Compression Specimens
Composites, vol.21, no.4, pp.289-296, 1990.

- [7] L. Lorenzo and H.T. Hahn
Fatigue Failure Mechanisms in Unidirectional Composites
In: *Composite Materials: Fatigue and Fracture*, ASTM STP 907, H.T. Hahn, ed., pp.210-232, 1986.
- [8] M.J. Owen
Fatigue Damage in Glass Fiber Reinforced Plastics
In: *Composite Materials: Fracture and Fatigue*, L.J. Broutman, ed., vol.5, pp. 313-340, 1974.
- [9] J.R. Hancock
Fatigue of Metal-Matrix Composites
In: *Composite Materials: Fracture and Fatigue*, L.J. Broutman, ed., vol.5, pp. 371-414, 1974.
- [10] C.K.H. Dharan
Fatigue Failure in Graphite Fiber and Glass Fiber-Polymer Composites
Journal of Materials Science, vol.10, pp. 1665-1670, 1975.
- [11] J. Awerbuck and H.T. Hahn
Fatigue and Proof-Testing of Unidirectional Graphite/Epoxy Composite
In: *Fatigue of Filamentary Composite Materials*, ASTM STP 636, K.L. Reifsnider and K.N. Lauraitis, eds., American Society for Testing and Materials, pp. 248-266, 1977.
- [12] W.W. Stinchcomb, K.L. Reifsnider, P. Yeung, and T.K. O'Brien
Investigation and Characterization of Constraint Effects on Flaw Growth During Fatigue Loading of Composite Materials
Second Semi-Annual Status Report, NASA Grant NSG-1364, Virginia Polytechnic Institute and State University, Blacksburg, Va., Nov. 1977.

- [13] T. Tanimoto and S. Amijima
Progressive Nature of Fatigue Damage of Glass Fiber Reinforced Plastics
Journal of Composite Materials, vol.9, pp. 380-390, 1975.
- [14] D.O. Stalnaker and W.W. Stinchcomb
Load History-Edge Damage Studies in Two Quasi-Isotropic Graphite/Epoxy Laminates
In: *Composite Materials: Testing and Design (fifth conference)*, ASTM STP 674, American Society for Testing and Materials, pp. 620-641, 1978.
- [15] G.C. Grimes
Structural Design Significance of Tension-Tension Fatigue Data on Composites
In: *Composite Materials: Testing and Design (fourth conference)*, ASTM STP 617, American Society for Testing and Materials, pp. 106-119, 1977.
- [16] G.P. Sendeckyj and H.D. Stalnaker
Effect of Time at Load on Fatigue response of $[(0/\pm 45/90)_s]_2$ T300/5208 Graphite-Epoxy Laminates
In: *Composite Materials: Testing and Design (fourth conference)*, ASTM STP 617, American Society for Testing and Materials, pp. 39-52, 1977.
- [17] C.-G. Gustafson and M. Hojo
Delamination Fatigue Crack Growth in Unidirectional Graphite/Epoxy Laminates
Journal of Reinforced Plastics and Composites, vol. , pp.36-52, 1987.
- [18] K.L. Reifsnider, W.W. Stinchomb and T.K. O'Brien
Frequency Effects on a Stiffness-Based Fatigue Failure Criterion in Flawed Composite Specimens
In: *Fatigue of Filamentary Composite Materials*, ASTM STP 636, K.L. Reifsnider and K.N. Lauraitis, eds., pp.171-184, 1977.

- [19] G.C. Tsai, J.F. Doyle and C.T. Sun
Frequency Effects on the Fatigue Life and Damage of Graphite/Epoxy Composites
Journal of Composite Materials, vol.21, pp.2-13, 1987.
- [20] F. Ellyin and D. Kujawski
Frequency Effects on the Fatigue of Fiberglass-Epoxy Composite Laminates
Proceedings of the 1992 Annual Meeting of JSME/MMD Hokkaido University, Sapporo, Japan, pp.361-364, 1992.
- [21] F. Ellyin and D. Kujawski
Fatigue Testing and Life Prediction of Fiberglass-Reinforced Composites
Proceedings of the First Conference on Advanced Composite Materials in Bridges and Structures K.W. Neale and P. Labossière Eds., Sherbrooke, Quebec, Canada, pp.111-118, 1992.
- [22] L. Broutman and S. Sahu
Progressive Damage of Glass Reinforced Plastics During Fatigue
In: *Proceedings of the 24th Society of the Plastics Industry Conference*, pp. 1-12, 1969.
- [23] M.S. Salkind
Fatigue of Composites
In: *Composite Materials: Testing and Design (second conference)*, ASTM STP 497, American Society for Testing and Materials, pp. 143-169, 1972.
- [24] T.K. O'Brien and K.L. Reifsnider
Fatigue Damage: Stiffness/Strength Comparisons for Composite Materials
Journal of Testing and Evaluation, vol.5, no.5, pp.384-393, 1977.
- [25] J.T. Ryder and E.K. Walker
Effect of Compression on Fatigue Properties of Quasi-Isotropic

Graphite/Epoxy Composites

In: *Fatigue of Filamentary Composite Materials*, ST 636, K.L. Reifsneider and K.N. Lauraitis, eds., pp.3-26, 1977.

- [26] M.S. Rosenfeld and S.L. Huang
Fatigue Characteristics of Graphite/Epoxy Laminates Under Compression Loading
Journal of Aircraft, vol.15, no.15, pp.264-268, 1978.
- [27] A. Rotem and H.G. Nelson
Failure of a Laminated Composite Under Tension-Compression Fatigue Loading
Composites Science and Technology, vol.36, pp.45-62, 1989.
- [28] M.J. Owen and J.R. Griffiths
Evaluation of biaxial stress failure surfaces for a glass fabric reinforced polyester resin under static and fatigue loading
Journal of Materials Science, vol.13, pp.1521-1537, 1978.
- [29] Z. Fawaz
Étude Analytique, Numérique et Expérimentale Portant sur la Rupture et la Fatigue Biaxiale des Lamelles Renforcées de Fibres
Ph.D. thesis, University of Sherbrooke, Québec, Canada, 1992.
- [30] Z. Fawaz and K.W. Neale
A Parametric Criterion for Biaxial Fatigue Failure of Fiber-Reinforced Composite Laminae
Transactions of the Canadian Society for Mechanical Engineering, vol.14, pp.93-99, 1990.
- [31] E. Krempl and T.-M. Niu
Graphite/Epoxy [± 45]_s Tubes. Their Static Axial and Shear Properties and

- their Fatigue Behaviour Under Completely Reversed Load Controlled Loading
Journal of Composite Materials, vol.16, pp.172-187, 1982.
- [32] E. Krempl, D.M. Elzey, B.Z. Hong, T. Ayar and R.G. Loewy
Uniaxial and Biaxial Fatigue Properties of Thin-Walled Composite Tubes
Journal of the American Helicopter Society, vol.33, pp.3-10, 1988.
- [33] Z. Xia and F. Ellyin
Nonproportional Multiaxial Cyclic Loading: Experiments and Constitutive Modeling
Journal of Applied Mechanics, Transactions of the ASME, vol.58, pp.317-325, 1991.
- [34] K.E. Hofer, Jr., L.C. Bennet and M. Stander
Effects of Moisture and Fatigue on the Residual Mechanical Properties of S-Glass/Graphite Epoxy Hybrid Composites
In: *Fatigue of Filamentary Composite Materials*, ASTM STP 636, K.L. Reifsnider and K.N. Lauraitis, eds., pp. 103-122, 1977.
- [35] M.B. Kasen, R.E. Schramm and D.T. Read
Fatigue of Composites at Cryogenic Temperatures
In: *Fatigue of Filamentary Composite Materials*, ASTM STP 636, K.L. Reifsnider and K.N. Lauraitis, eds., pp. 141-151, 1977.
- [36] R.L. Tobler and D.T. Read
Fatigue Resistance of a Uniaxial S-Glass/Epoxy Composite at Room and Liquid Helium Temperatures
Journal of Composite Materials, vol.10, pp. 32-43, 1976.
- [37] H.T. Sumsion and D.P. Williams
Effects of Environment on the Fatigue of Graphite/Epoxy Composites
In: *Fatigue of Composite Materials*, ASTM STP 569, pp.226-247, 1975.

- [38] D.S. Mahulikar, Y.H. Park and H.L. Marcus
Environmental Influences on the Fracture and Fatigue Properties of Titanium Metal-Matrix continuous Fiber Composites
In: *Fracture Mechanics:Fourteen Symposium, vol II:Testing and Applications*, ASTM STP 791, J.C. Lewis and G. Sines, eds., pp.II-579-II- 597, 1983.
- [39] R.C. Tennyson, G.E. Wharram and G.E. Mabson
Final report on investigation of static failure and compressive fatigue of CF-18 graphite/epoxy laminates: part 1: experimental evaluation
Defence research establishment pacific, research and development branch, department of national defence, March 1986.
- [40] Z. Hashin
Theory of Composite Materials
In: *Mechanics of Composite Materials:Proceedings of the Fifth Symposium on Naval Structural Mechanics*, F.W. Wendt, H. Liebowitz and N. Perrone, eds., Pergamon Press, 1970
- [41] S.G Lekhnitskii
Theory of Elasticity of an Anisotropic Elastic Body Translated by Fern, P., Edited by Brandstatter, J.J., Holden-Day Inc., San Francisco, 1963.
- [42] P. Labossière and K.W. Neale
Macroscopic Failure Criteria for Fibre-Reinforced Composite Materials
SM Archives, vol. 12, No.2, pp.439-450, 1987.
- [43] S.W. Tsai and E.M. Wu
A General Theory of Strength for Anisotropic Materials
Journal of composite materials, vol. 5, pp. 58-80,1971.
- [44] R.C. Tennyson, D.MacDonald and A.P. Nanyaro

Evaluation of the Tensor Polynomial Failure Criterion for Composite Materials
Journal of Composite Materials, vol.12, pp.63-75, 1978.

- [45] S.Y. Zhang, L.W. Tsai and J.Q. Liu
Strain Energy Density Ratio Criterion for Fracture of Composite Materials
Engineering Fracture Mechanics, vol.37, pp.881-889, 1990.
- [46] V.D. Azzi and S.W. Tsai
Anisotropic Strength of Composites
Experimental Mechanics, vol.5, pp.283-288, 1965.
- [47] Green and Zerna
Theoretical Elasticity Oxford, Clarendon Press, 1954.
- [48] Z. Hashin and A. Rotem
A fatigue Failure Criterion for Fiber Reinforced Materials
Journal of composite materials, vol.7, pp.448-464, 1973.
- [49] Z. Hashin and A. Rotem
Fatigue Failure of Angle Ply Laminates
AIAA journal, vol.14, pp.868-872, 1976.
- [50] A. Rotem
Fatigue Failure of Multidirectional Laminates
AIAA journal, vol.17, pp.271-277, 1979.
- [51] I.J. Toth
Creep and Fatigue Behavior of Unidirectional and Cross-Plied Composites
In: *Composite materials: testing and design*, ASTM STP 460, American society
for testing and materials, pp.236-253, 1969.
- [52] I.J. Toth
Time Dependent Mechanical Behavior of Composite Materials

Annual technical report on contract AF33(615)-3062, TRW Inc., Cleveland, Ohio, Nov. 1968.

- [53] J. Awerbuch and H.T. Hahn
Off-axis Fatigue of Graphite/Epoxy Composite
In: *Fatigue of fibrous composite materials*, ASTM STP 723, American society for testing and materials, pp.243-273, 1981.
- [54] R.C. Tennyson
Strength and Fatigue Life Design Procedures for Composite Structures
Proceedings of the 8th symposium of engineering applications of mechanics, University of Sherbrooke, 1986.
- [55] R.C. Tennyson, G.E. Mabson, N. Napathanassis, G.E. Wharram
Spectrum Fatigue Model for Composite Laminates
Proceedings of the 15th international council of aeronautical sciences, London, U.K., 1986.
- [56] F. Ellyin and D. Kujawski
An Energy-Based Fatigue Failure Criterion
Proceedings of the international symposium of microstructures and mechanical behaviour of metals, eds. H. Gu and J. He, vol II, EAMS, U.K., pp.591-600, 1986.
- [57] F. Ellyin
Cyclic Strain Energy Density as a Criterion for Multiaxial Fatigue Failure
Proceedings Bi/multiaxial Fatigue, K.J. Miller and M.W. Brown (eds.), EGF publication, no.3, 1988.
- [58] F. Ellyin and K. Golos
Multiaxial Fatigue Damage Criterion

Journal of Engineering Materials and Technology, Trans. of the ASME, vol.110, pp.63-68, 1988.

[59] K. Golos and F. Ellyin

A Total Strain Energy Density Theory for Cumulative Fatigue Damage
Journal of Pressure Vessel Technology, Trans. of the ASME, vol.110, pp.36-41, 1988.

[60] G.C. Sih, E.P. Chen, S.L. Huang, E.J. McQuillen

Material Characterization on the Fracture of Filament-Reinforced Composites
Journal of Composite Materials, vol.9, pp.167-186, 1975.

[61] M.B. Buczek and C.T. Herakovich

Direction of Crack Growth in Fibrous Composites
Mechanics of Composite Materials, AMD. vol.58, pp.75-82, 1983.

[62] M.A. Gregory and C.T. Herakovich

Predicting Crack Growth Direction in Unidirectional Composites
Journal of Composite Materials, vol.20, pp.67-85, 1986.

[63] K. Golos and F. Ellyin

Generalization of Cumulative Damage Criterion to Multilevel Cyclic Loading
Theoretical and Applied Fracture Mechanics, vol.7, pp.169-176, 1987.

[64] S.Y. Zhang, L.W. Tsai, J.Q. Liu

Strain Energy Density Ratio Criterion for Fracture of Composite Materials
Engineering Fracture Mechanics, vol.37, pp.881-889, 1990.

[65] E.M. Wu

Fracture Mechanics of Anisotropic Plates
In *Composite Material Workshop*, Edited by Tsai, S.W., Halpin, J.C., Pagano, N.J., Technomic publishing Co., Inc, Lancaster, PA, pp.20-43, 1968.

- [66] G.C. Sih
A Special Theory of Crack Propagation
In: *Methods of Analysis and Solutions to Crack Problems*, Edited by Sih, G.C.,
Wolters-Noordhoff, pp.XXI-XLV, 1972.
- [67] G.C. Sih
Dynamics of Composites with Cracks
In: *Handbook of Composites, vol.3, Failure Mechanisms of Composites*, Edited
by Sih, G.C. and Skudra, A.M., North-Holland, pp.127-176, 1985.
- [68] M.A. Gregory, J.L. Beuth, Jr., A. Barbe, C.T. Herakovich
Application of the Normal Stress Ratio Theory for Predicting Crack Growth
Direction in Unidirectional Composites
Fracture of Fibrous Composites, AMD, vol.74, pp.33-42, 1985.
- [69] J.L. Beuth, Jr., M.A. Gregory, C.T. Herakovich
Crack Growth in Unidirectional Graphite-Epoxy under Biaxial Loading
Experimental Mechanics, vol.26, pp.245-253, 1986.
- [70] J.L. Beuth, Jr. and C.T. Herakovich
Analysis of Crack Extension in Anisotropic Materials Based on Local Normal
Stress
Theoretical and Applied Fracture Mechanics, vol.11, pp.27-46, 1989.
- [71] E.F. Rybicki
Approximate Three-Dimensional Solutions for Symmetric Laminates under
Inplane Loading
Journal of Composite Materials, vol.5, pp.354-360, 1971.
- [72] R. Byron Pipes and N.J. Pagano
Interlaminar Stresses in Composite Laminates under Uniform Axial Tension
Journal of Composite Materials, vol.4, pp.538-548, 1970.

- [73] K.H. Lo, R.M. Christensen and E.M. Wu
A Higher-Order Theory of Plate Deformation Part 1: Homogeneous Plates
Journal of Applied Mechanics, vol. pp.663-668, 1977.
- [74] K.H. Lo, R.M. Christensen and E.M. Wu
A Higher-Order Theory of Plate Deformation Part 2: Laminated Plates
Journal of Applied Mechanics, vol. pp.669-676, 1977.
- [75] K.H. Lo, R.M. Christensen and E.M. Wu
Stress Solution Determination for High Order Plate Theory
International Journal of Solids and Structures, vol.14, pp.655-662, 1978.
- [76] J.N. Reddy
A Simple Higher-Order Theory for Laminated Composite Plates
Journal of Applied Mechanics, vol.51, pp.745-752, 1984.
- [77] R.T.J. Bonser
Bending of Laminated Fibre Reinforced Plates with Applications to Interlaminar Cracks
Ph.D. thesis, University of Nottingham, 1984.
- [78] P.V. Kaprielian, T.G. Rogers and A.J.M. Spencer
Theory of Laminated Elastic Plates I. Isotropic Laminae
Philosophical Transactions of the Royal Society of London, series A, vol.324, pp.565-594, 1988.
- [79] A.J.M. Spencer
Developments in the Elastic Analysis of Laminated Plates
Proceedings of the 12th Canadian Congress of Applied Mechanics, Carleton University, Ottawa, pp.47-53, 1989.

- [80] E. Reissner
Reflections on the Theory of Elastic Plates
Applied Mechanics Review, vol.38, pp.1453-1464, 1985.
- [81] G. Savin
Stress Concentration Around Holes, International Series of Monographs in
Aeronautics and Astronautics, Translation Ed. W. Johnson, Pergamon press,
1961.
- [82] T.K. Tung
On Computation of Stresses Around Holes in Anisotropic Plates
Journal of Composite Materials, vol.21, pp.100-104, 1987.
- [83] W.M. Lucking, S.V. Hoa, T.S. Sankar
The Effect of Geometry on Interlaminar Stresses of [0/90]_n Composite
Laminates with Circular Holes
Journal of Composite Materials, vol.17, pp.188-198, 1984.
- [84] A.J.M. Spencer
Private Communications.
- [85] D.C. Curtis, D.R. Moore, B. Slater, N. Zahlan
Fatigue Testing of Multi-angle Laminates of CF/Peek
*Proceedings of the Second International Conference on Testing, Evaluation and
Quality Control of Composites*, ed. J. Herriot, University of Survey, Guildford,
UK, pp.40-50, 1987.

Appendix A

Experimental Investigation

A.1 Introduction

As mentioned in Chapter 3, due to the lack of published experimental data, tests were conducted to determine the effect of the stress ratio on the fatigue of unidirectional fiber reinforced composites. In this chapter, the material used, the different stages of the specimen development as well as the experimental apparatus used will be presented.

A.2 Material

The material used was “Scotchply Reinforced Plastic type 1003” which is a 3M product. This composite is a non-woven fiberglass reinforced epoxy resin material designed for high performance structural applications. This material was chosen because of its availability and its low cost. The fiberglass used has a continuous filament of “E” type. The uncured prepreg is supplied in rolls of unidirectional orientation of widths 150 mm (6 inches) to 300 mm (12 inches) with a standard roll length of 65.8 m (72 yards). The average uncured thickness of the prepreg is 0.275 mm (0.011 inches) and reduces to 0.25 mm (0.010 inches) after curing. Some of

Table A.1: Mechanical Properties at Various Stress Angles

	Stress Angle		
	0°	45°	90°
Flexural Strength (MPa)	1,150	145	75
Flexural Modulus (GPa)	38.6	13.8	11.1
Tensile Strength (MPa)	965	24	20
Tensile Modulus (GPa)	39.3	9.7	9.7
Compressive Strength (MPa)	880	240	195

the main mechanical properties of the material at various stress angles taken from the manufacturer's literature are shown in Table A.1. The experimental values of the monotonic strength as a function of the fibers orientation angle is presented in Fig. A.1.

A.3 Specimen

A.3.1 ASTM Standards

The ASTM standards for fatigue testing of fiber reinforced composites are only available for tension-tension fatigue specimens. No standards were found for tension-compression fatigue tests. The standard tension-tension was ruled inadequate since buckling would be expected under any compressive loads. Therefore different configurations were explored.

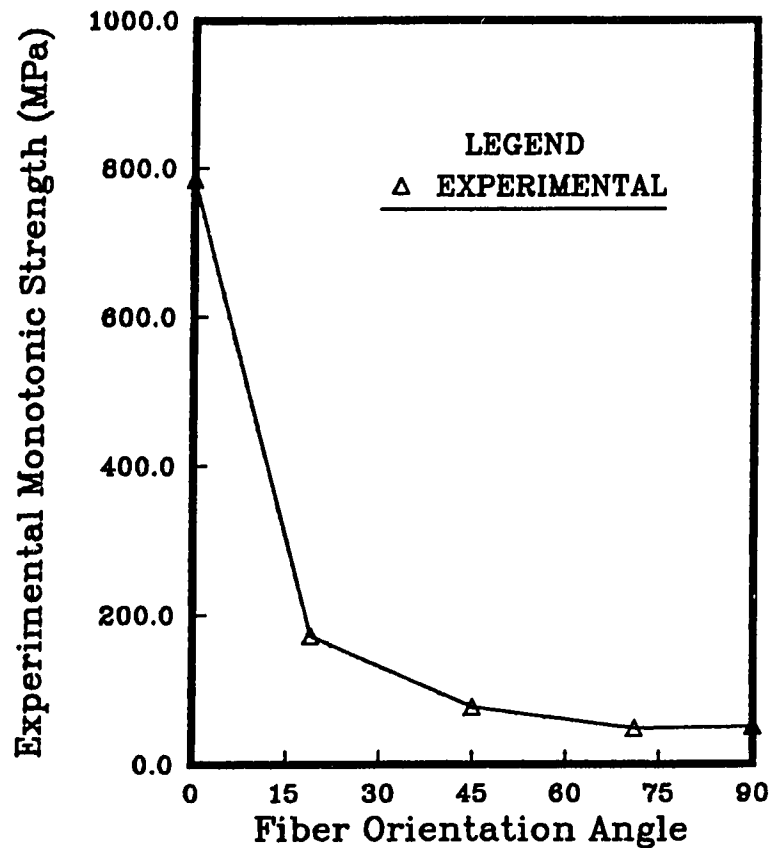


Figure A.1: Variation of Monotonic Strength with Fibers Orientation Angle

A.3.2 Specimen Design

Initial Design

The first specimen to be constructed (Fig. A.2) was a dogbone-type specimen with a reduced test section in the thickness direction. Twenty layers of prepreg were used to form the ends while ten layers were present in the test section. Two design configurations were attempted. Unfortunately both were not successful. Both configurations were built with enlarged ends containing a pin-hole permitting the use of the grips shown in Fig. A.3.

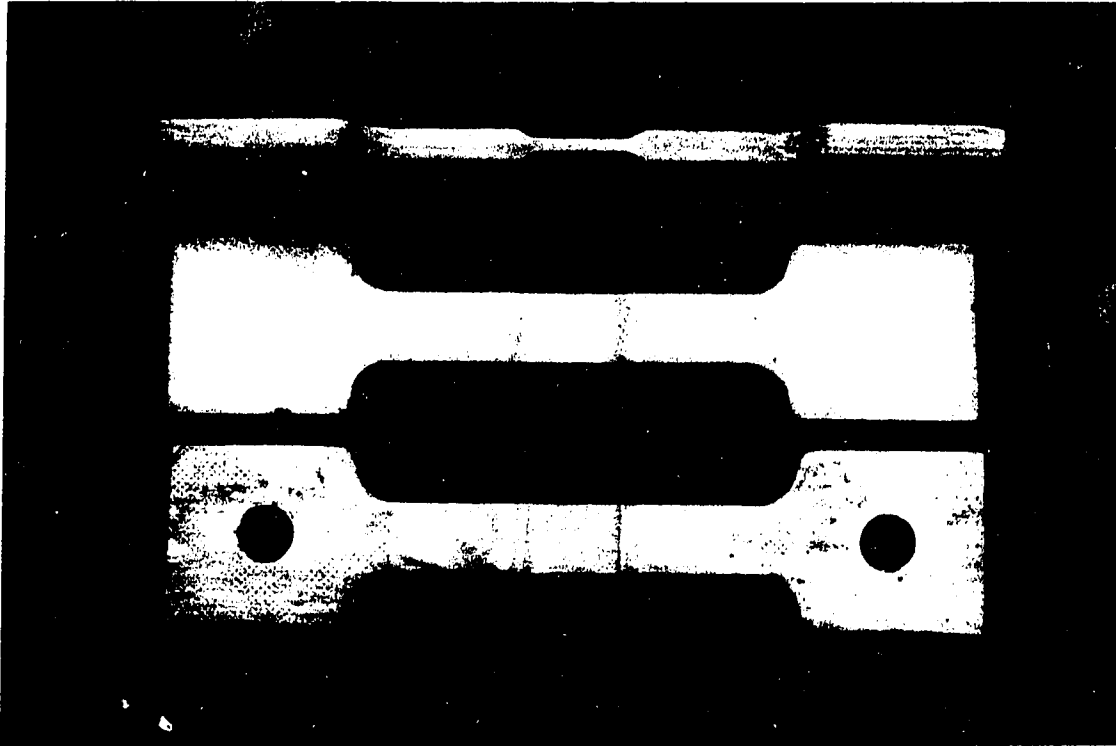


Figure A.2:Initial Specimen Design

Width Waisted Specimen

The specimen was next modified to a “width-waisted” [85] type as shown in Fig. A.4. Twenty layers were once more used with the test section having the same thickness but a smaller width than the specimen ends. The ends had once more pin-holes to grip the specimen using the same grips as before (Fig. A.3).

This specimen performed well for all off-axis specimens but not for the 0° specimens. In this case, higher loads were applied to the specimens creating premature failure. This configuration was also discarded.

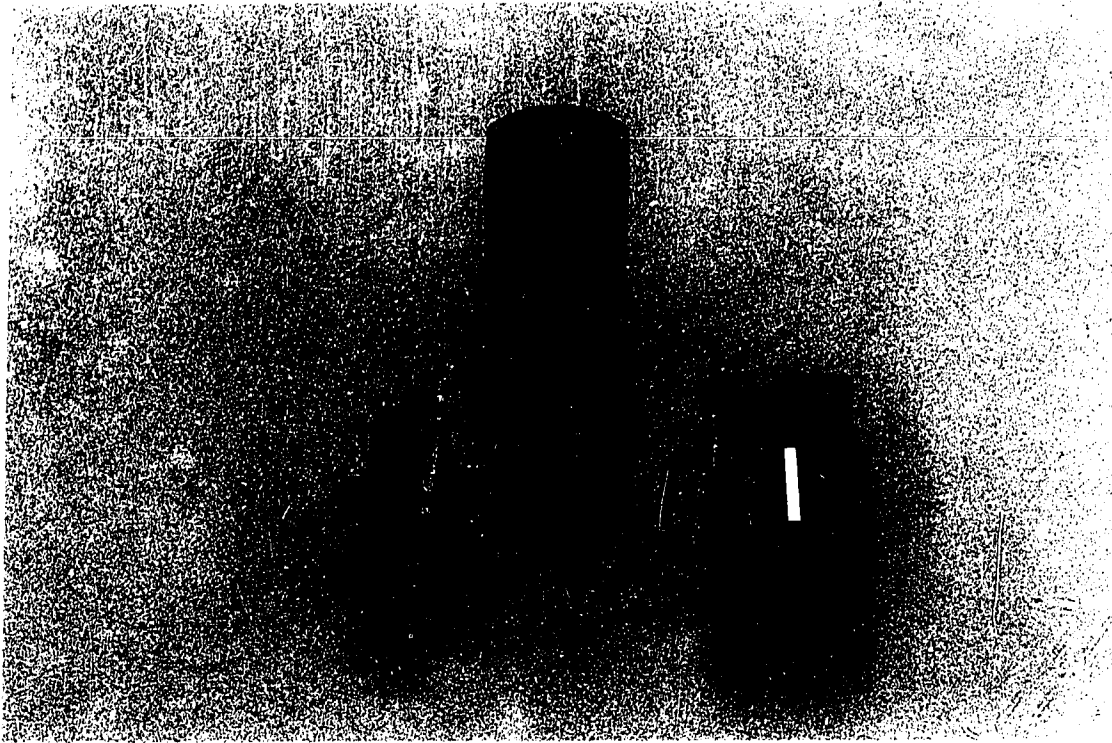


Figure A.3:Two-Part Grips

Final Configuration

Straight parallel sided specimens were finally chosen (Fig. A.5). These specimens had 20 layers for all the off-axis tests but only 10 layers for the 0° specimens where the required stresses to failure were considerably higher. According to Curtis et al. [85] this shape of specimen was not found to have any adverse influence on the properties obtained when compared to “width-waisted” specimens.

Due to the hardness of the composite material tested, tabs were found necessary for gripping purposes. Aluminum tabs were chosen because they are cheap, available in appropriate dimensions and needed only minor machining before being used.

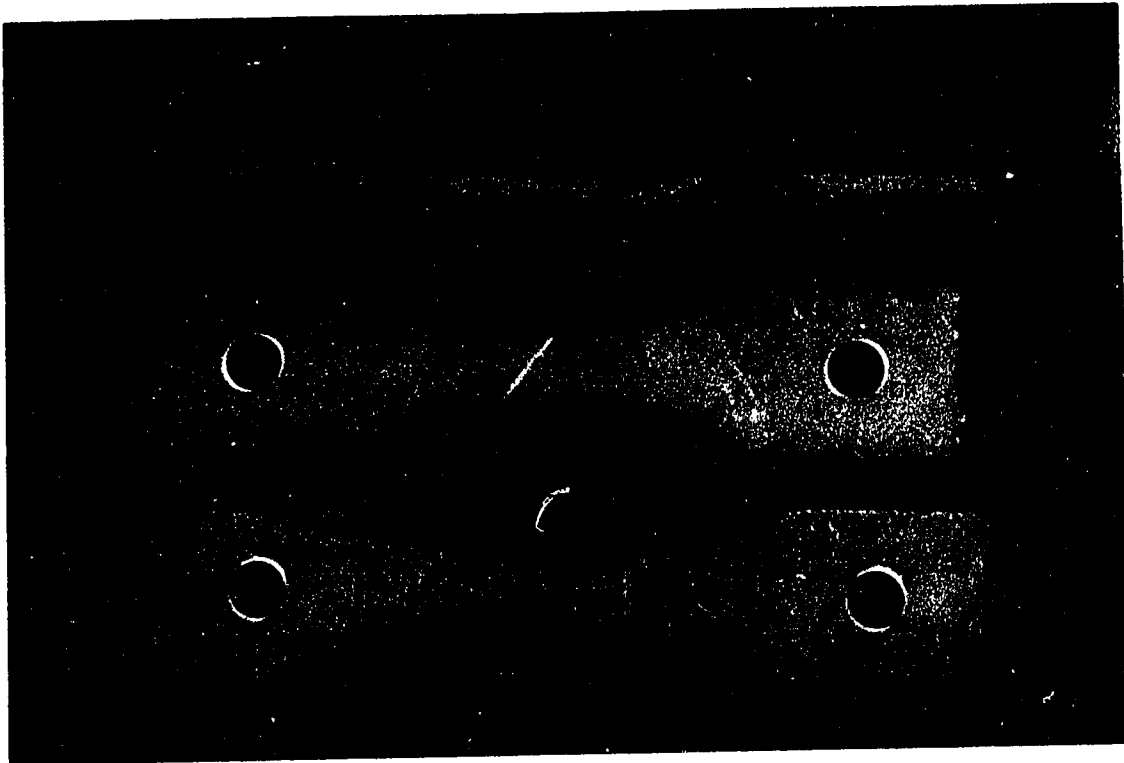


Figure A.4:Width Waisted Specimen

These tabs were glued on the specimen ends using “Loclite Black Max” a one-part room-temperature-curing adhesive. It reaches 80% of its maximum strength ($20.69\text{MPa}(3000\text{psi})$) after 24 hours and 100% of its maximum strength after 120 hours.

Although this glue proved effective with the off-axis specimens, it could not sustain the loads applied to the 0° specimens. So for these specimens an alternative glue, The “Fixmaster” twin weld adhesive was used. This Fiberglass Reinforced Epoxy adhesive reached its peak lap shear strength of $26.2\text{MPa}(3800\text{psi})$ after 3 hours at room temperature.

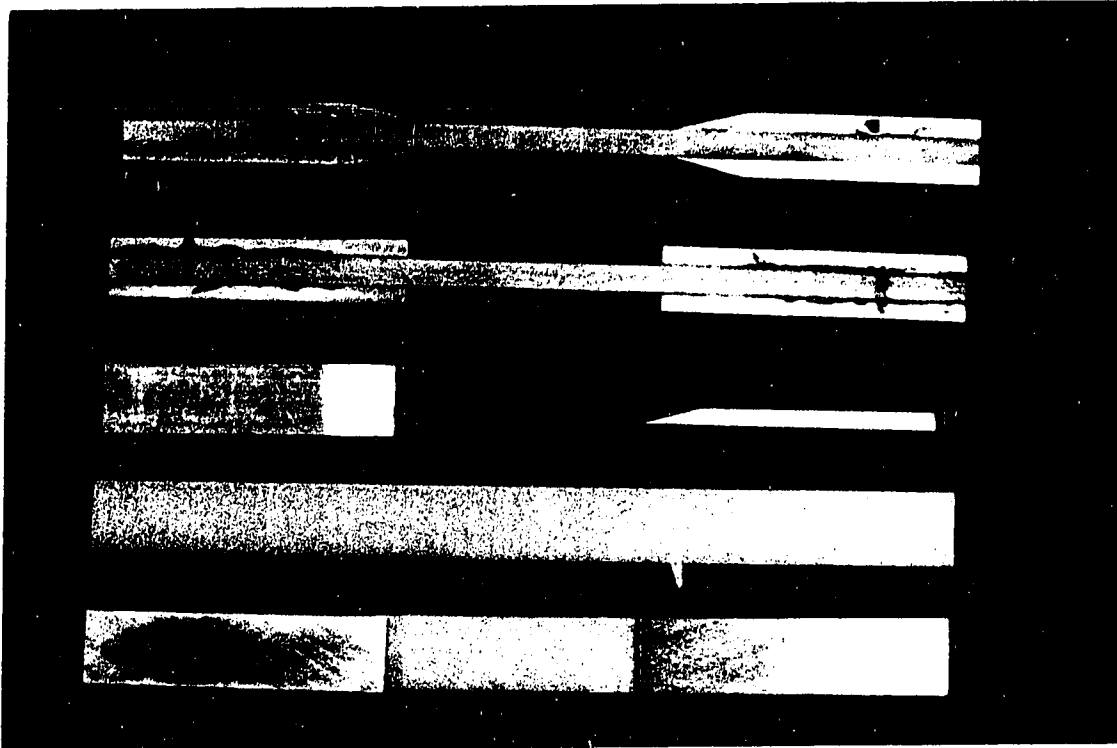


Figure A.5:Final specimen design

The final shape of the specimen used is shown in Fig. A.5.

A.4 Grips

Grips capable of withstanding both tensile and compressive loading were required. Two configurations were contemplated: the two-part grips and the modified tension grips.

A.4.1 Two-part Grips

The first type of grips tested were those mentioned in the previous section (Fig. A.3). These grips, although attractive for use with specimens with large ends, were not appropriate (the width of the specimen was reduced and so was the gripping area). The load carried by the bolts was sometimes too high. This caused a relative motion between the two parts of the grips causing a continuous movement of the specimen during the tests. The required grips should be in one piece, bulky and capable of carrying both tensile and compressive loads without any slip of the specimen.

A.4.2 Modified Tension Grips

Regular wedged tension grips would have been appropriate for this application in the absence of compressive loads. With the increase in tensile load, these grips tightened very well on the specimen, allowing no slippage, but under compressive loads the wedges would open and release the specimen.

A modification was implemented into these wedged tension grips allowing them to function in compression as well as in tension. Small steel plates were added inside the grips as shown in Fig. A.6. These plates prevented the wedged grips from opening when the specimen is subjected to compressive loads.

In the work done by Rosenfeld et al. [26] and by Rotem et al. [27], antibuckling devices were used to prevent buckling of the specimens under compressive loading. Here, for the off-axis testing, the specimens were designed with a minimal free length, thus, decreasing the possibility of buckling. For the 0° specimens, an antibuckling device had to be used, since in this case, the specimens were thinner and they were subjected to much higher loads than those of the off-axis specimens. Several configurations (Fig. A.7) were examined. The one that was finally used is shown in (Fig. A.8).

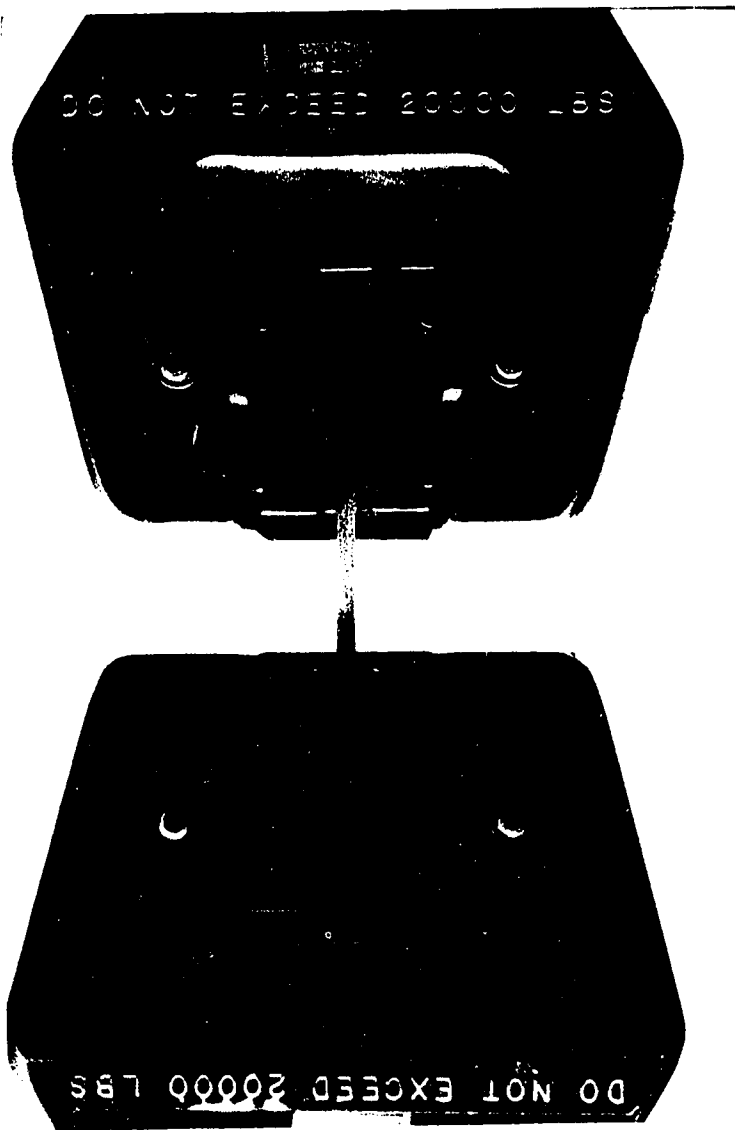


Figure A.6: Modified Tension Grips

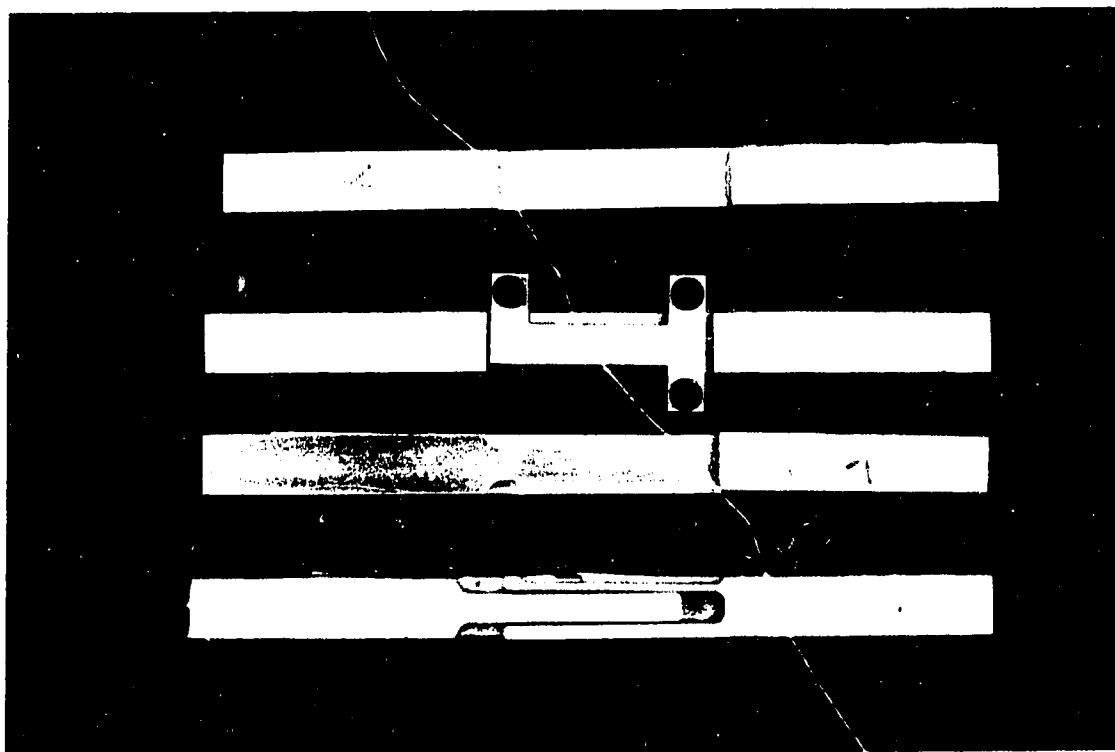


Figure A.7: Different Configurations for the Antibuckling Device

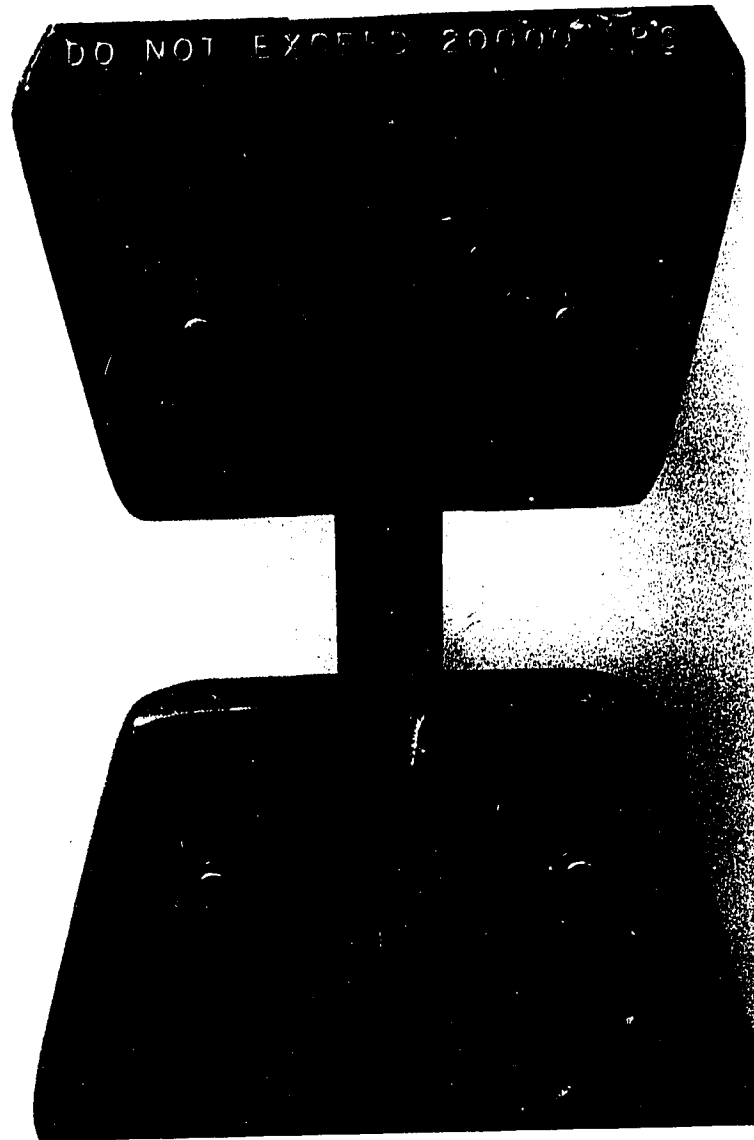


Figure A.8: Final Configuration for the Antibuckling Device

A.5 Specimen Manufacturing

The female part of the mould (Fig. A.9) was sprayed with “Sprayon” a heavy duty silicone mould release. A 0.5 mm (0.02 inches) thick layer of “Wrightlon 4600” release film was then placed inside each of the three cavities of the mould (The mould allows for the manufacturing of three specimens at the same time).

Prepreg strips with the required width, length and fiber orientation were then cut and carefully laid down on top of one another. Some pressure was consistently applied to assist in the removal of trapped air.

After reaching the required number of strips (twenty for the off-axis specimens and ten for the 0° ones), another sheet of release film was placed on top of the prepreg. The male part of the mould was then sprayed with the silicone mould release and placed on top of the female part. Pressure was applied on the prepreg by tightening the six bolts connecting the two parts of the mould.

The mould was then put in a time-regulated oven and the prepreg was cured according to the manufacturer’s specifications. Once the curing cycle was finished, the mould was left to cool inside the oven until it reached room temperature.

To take the specimen out of the mould, the male part was first removed by unscrewing the six bolts. Screws on the bottom of the female part of the mould were then used to uniformly push a stripper-bar under each of the cured specimens. This last step had to be done very carefully since any large difference between those screws’ displacement could result in a bent specimen. Any extra-resin was then cut and the whole specimen was filed. The tabs were finally glued onto the specimen which was now ready for testing

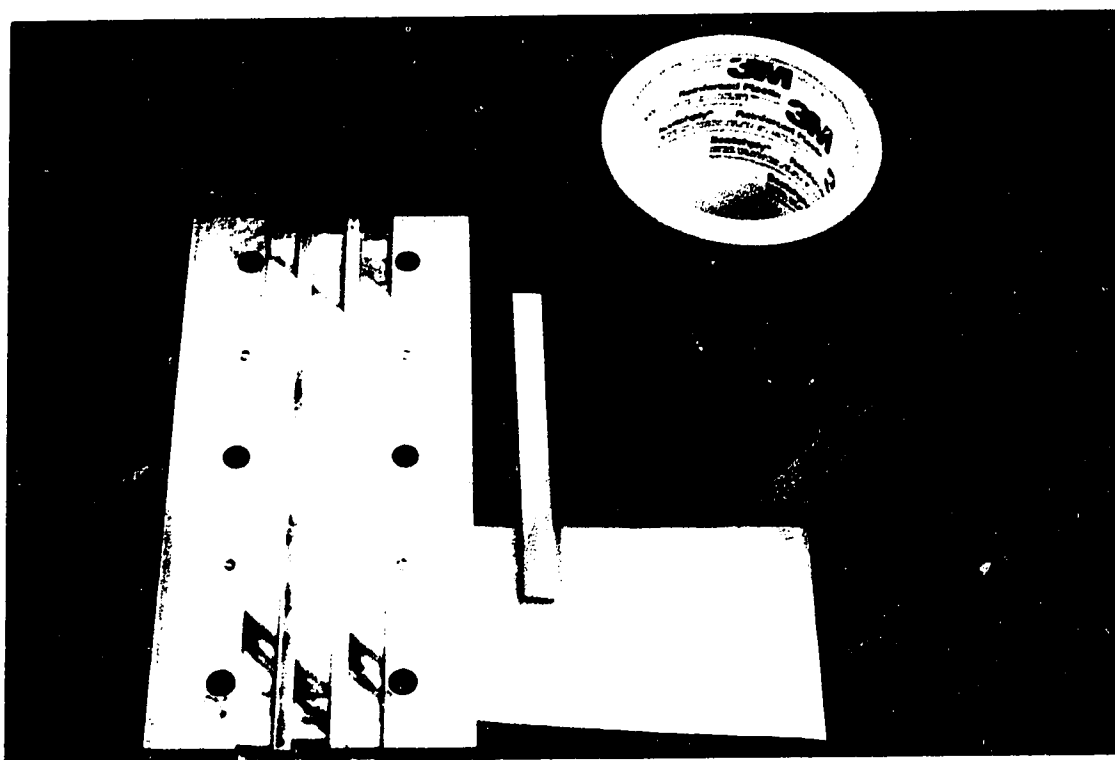


Figure A.9:Mould

A.6 Experimental Apparatus and Results

The apparatus used was an MTS testing machine controlled by an IBM PC. The entire test configuration is shown in Fig. A.10.

Unidirectional specimens with various fiber orientation angles were subjected to off-axis cyclic loading. Specimens used had fiber orientation angles of 0° , 19° , 45° , 71° and 90° with respect to the direction of loading. Tests were performed at room temperature for stress ratios of 0.5, 0.0 and -1.0 . Most of these tests have been conducted under a frequency of 3.33 Hz (200 CPM). The effect of loading frequency on the fatigue life of 45° off-axis specimens was considered by running tests under two frequencies (3.33 Hz and 0.426 Hz). The observed effect was minimal (see Fig. A.11).

Figs. A.12 - A.15 show the failed specimens in the case of the off-axis cyclic tests. All these specimens had an identical brittle failure mode. Fig. A.16 shows the different failures obtained when testing the 0° specimens; in this case the failure mode depended on the magnitude of the applied stress. At high stress levels (close to the monotonic strength), the failure mode was an abrupt broom-like shape failure accompanied by fiber breakage. At lower stress levels, delamination was observed and failure occurred over an extended period of time.

During the tests, both strain and stress were recorded. This allowed for the plotting of the hysteresis loops and monitoring the change of stiffness with time. Using Fig. A.17 as an example (71° off-axis, $R = 0$, $\sigma_{max} = 24.14 \text{ MPa}$, $N_f = 72,298 \text{ Cycles}$), it is seen that no significant modulus degradation was observed (a slight increase of 2.3% was observed in this case). In Fig. A.17, the solid line is a reference line with $E/E_o = 1$ and the dashed line is a possible extension to this relation until failure (since no readings were available in that range). The trend shown in Fig. A.17 was observed in all of the off-axis cases. The 0° specimens showed a maximum modulus drop of about 10% before the tests were stopped.

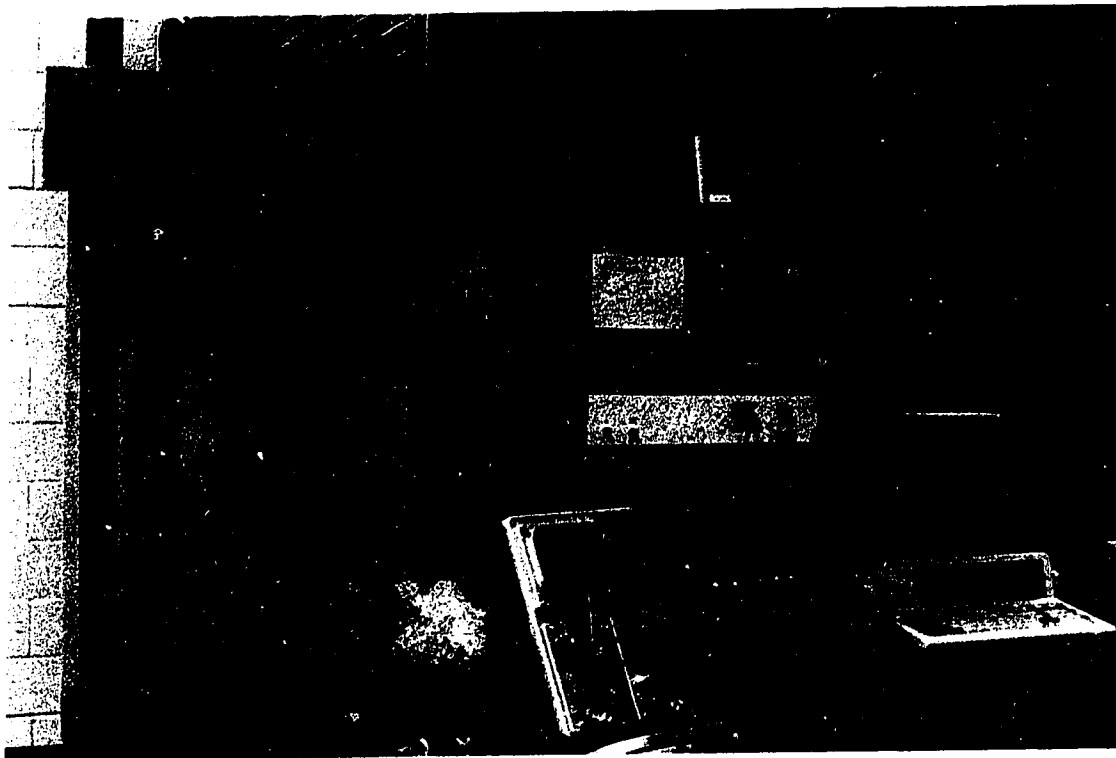


Figure A.10: Experimental Apparatus

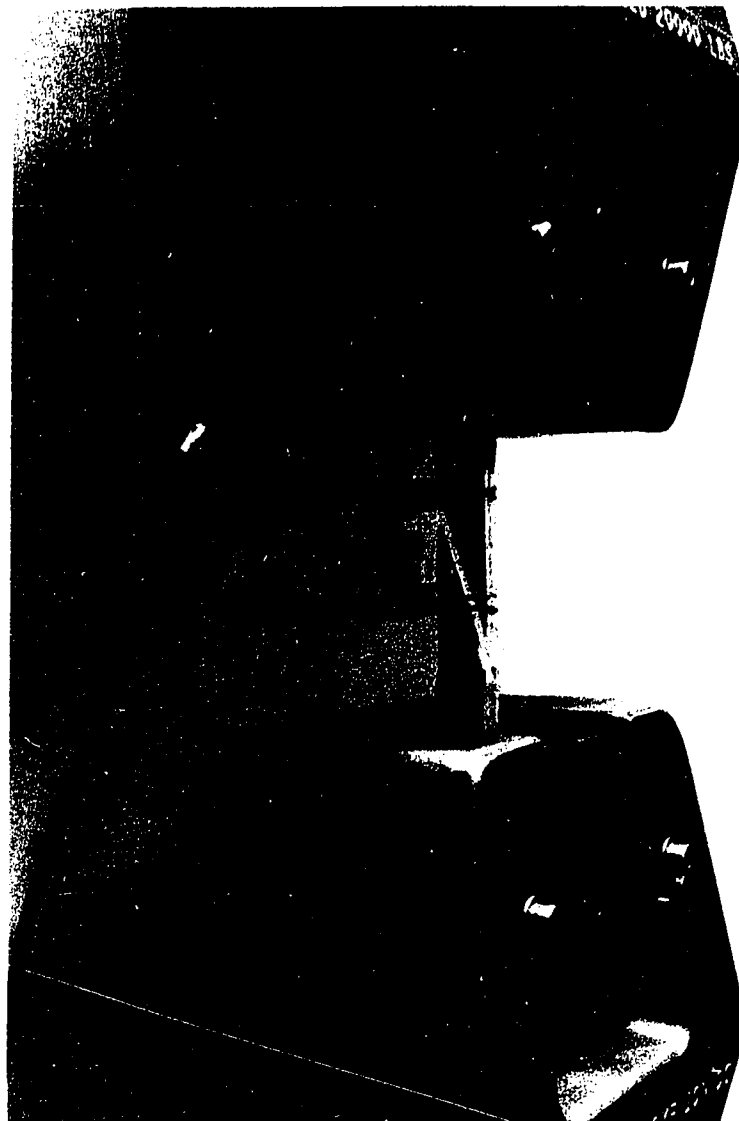


Figure A.12: Failure of a 19° Specimen under Cyclic Loading

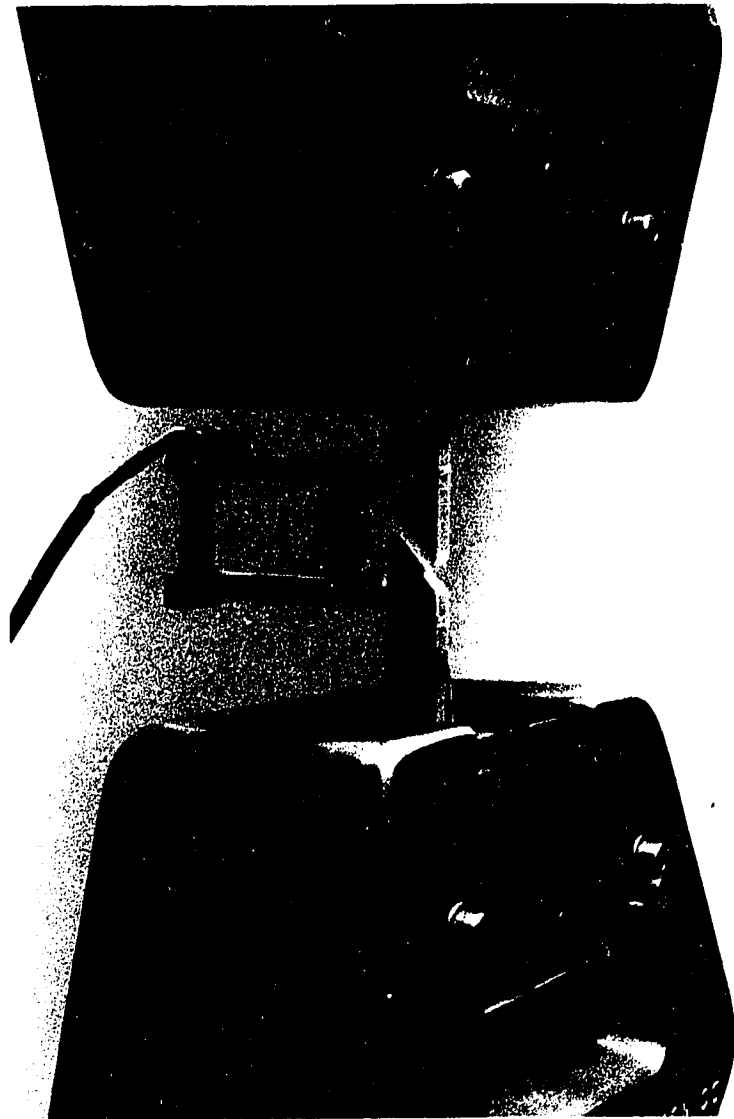


Figure A.13: Failure of a 45° Specimen under Cyclic Loading



Figure A.14: Failure of a 71° Specimen under Cyclic Loading

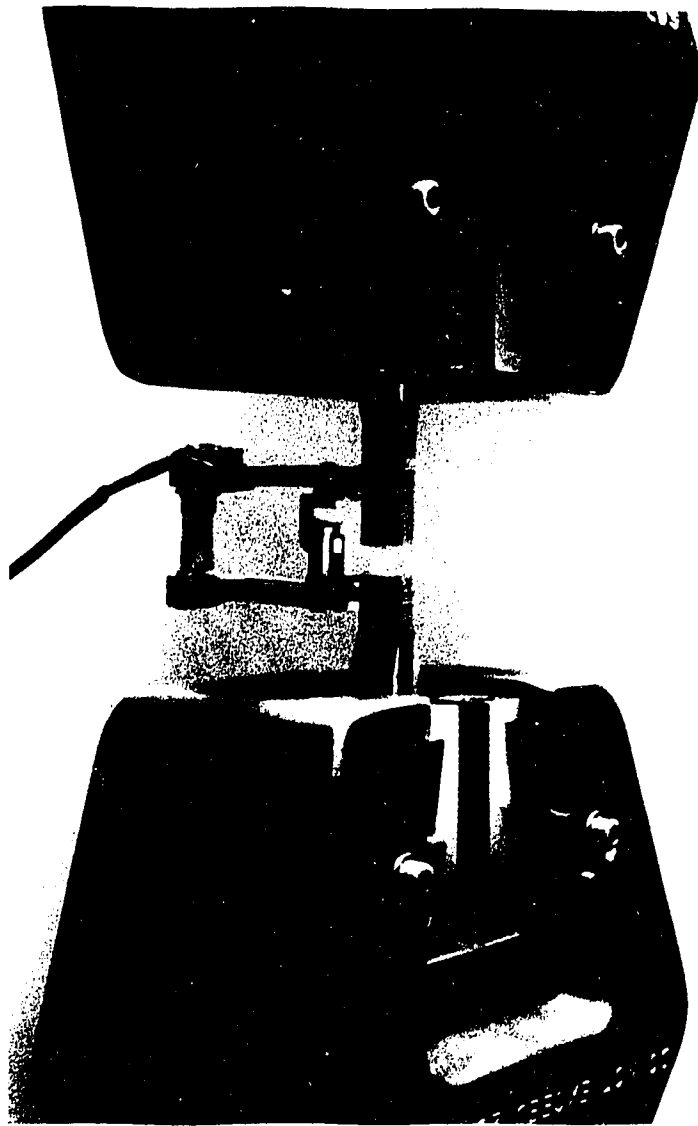


Figure A.15: Failure of a 90° Specimen under Cyclic Loading

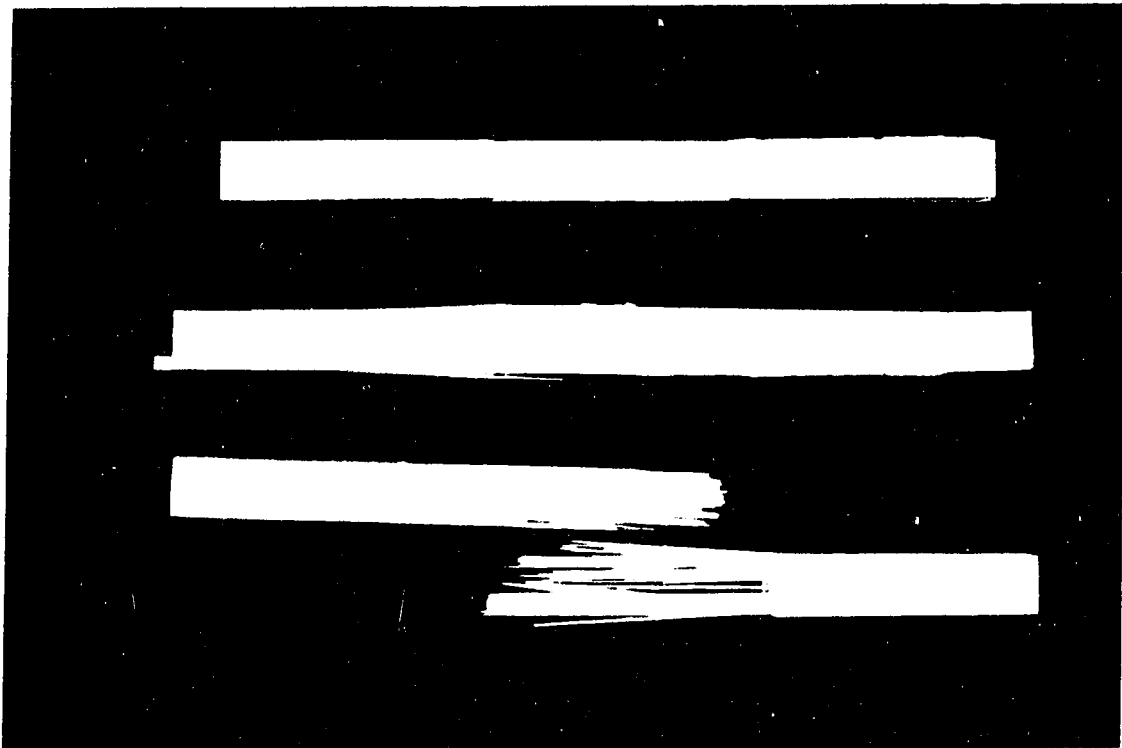


Figure A.16: Different Failure Modes of a 0° Specimen under Cyclic Loading.

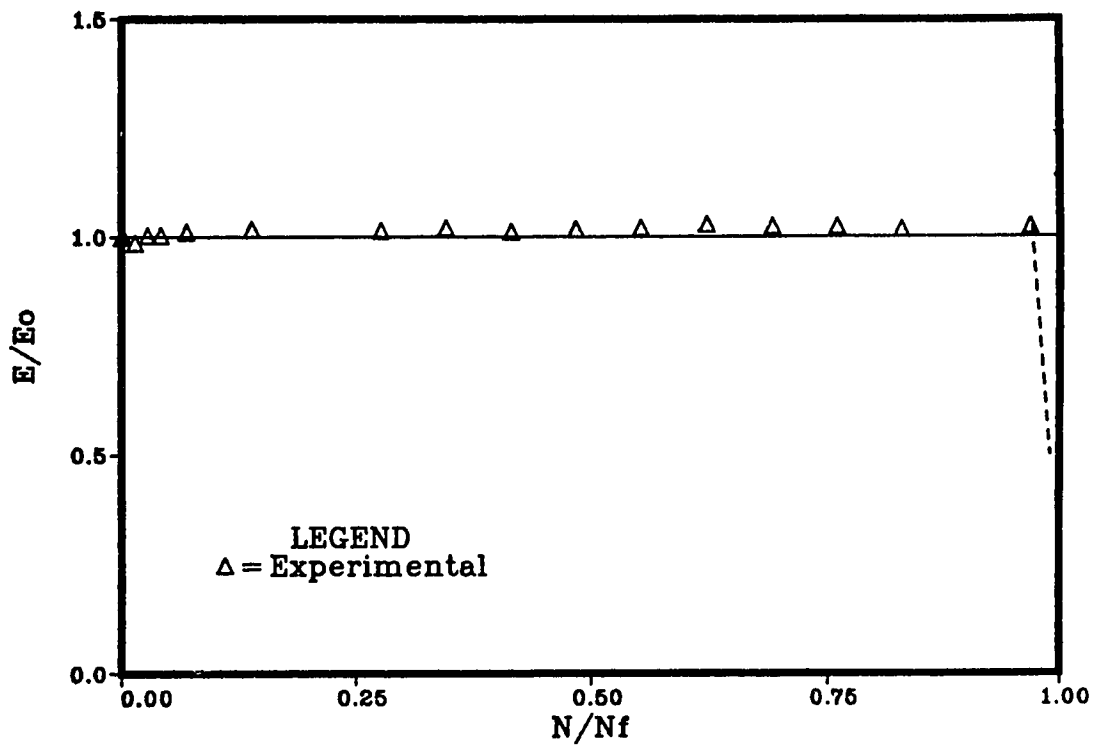


Figure A.17: Variation of Stiffness with Life for a 71° Specimen

For each value of the stress ratio, the maximum stress was plotted vs. the number of reversals to failure for the different fiber orientation angles as shown in Figs. A.18 - A.20. The complete tabulated values of stresses vs. number of cycles to failure as well as the individual plots of every fiber orientation angle and every stress ratio is shown in appendix B.

It should be noted here that although the failure of some specimens occurred close to or under the tab rather than in the middle of the specimen, the difference between the life of those specimen and the ones which failed in the mid-section was found to be within the expected scatter common to the fatigue tests.

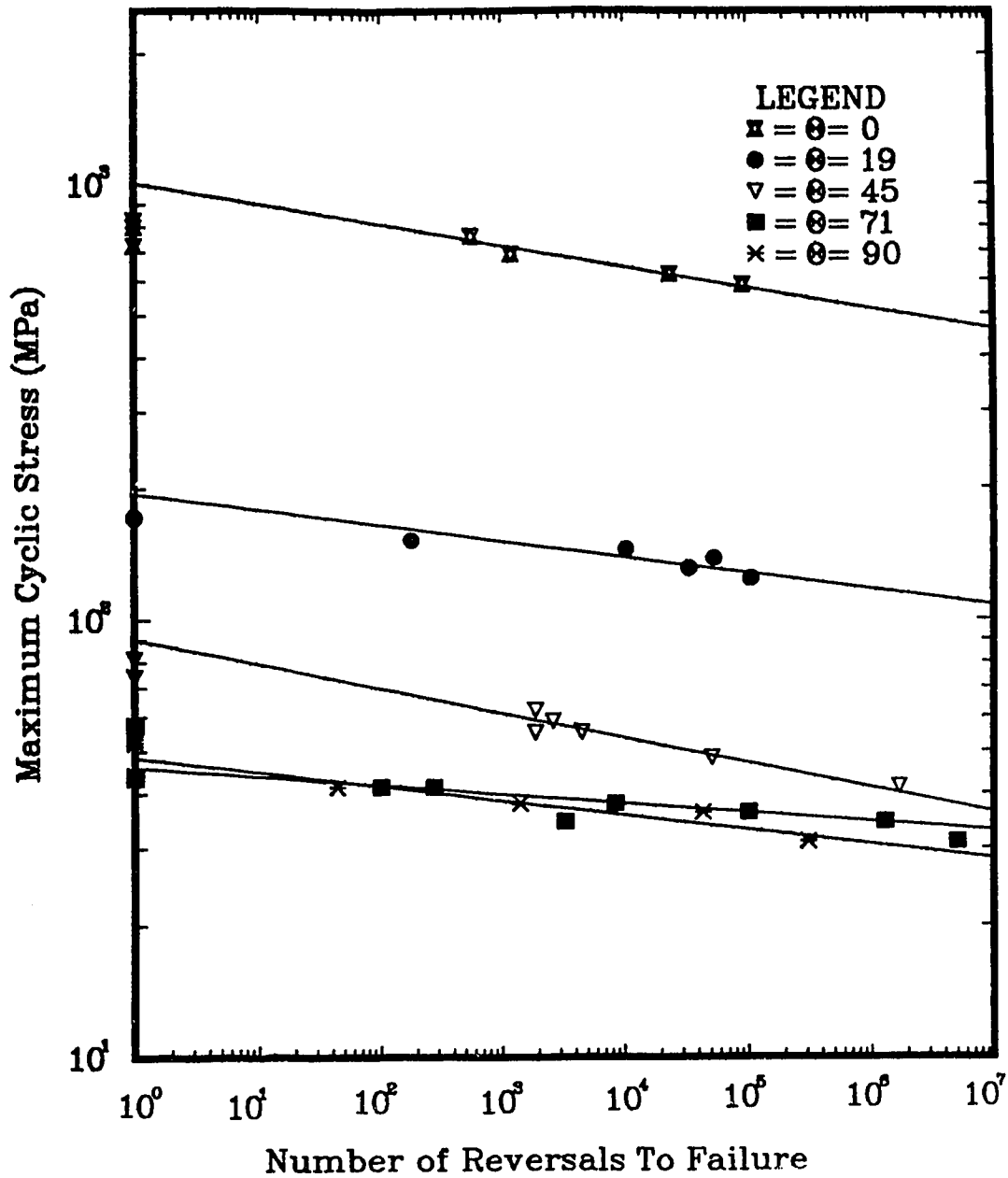


Figure A.18: Maximum Cyclic Stress vs. Number of Reversals to failure for Specimens with Different Fiber Orientation Angles at $R = 0.5$

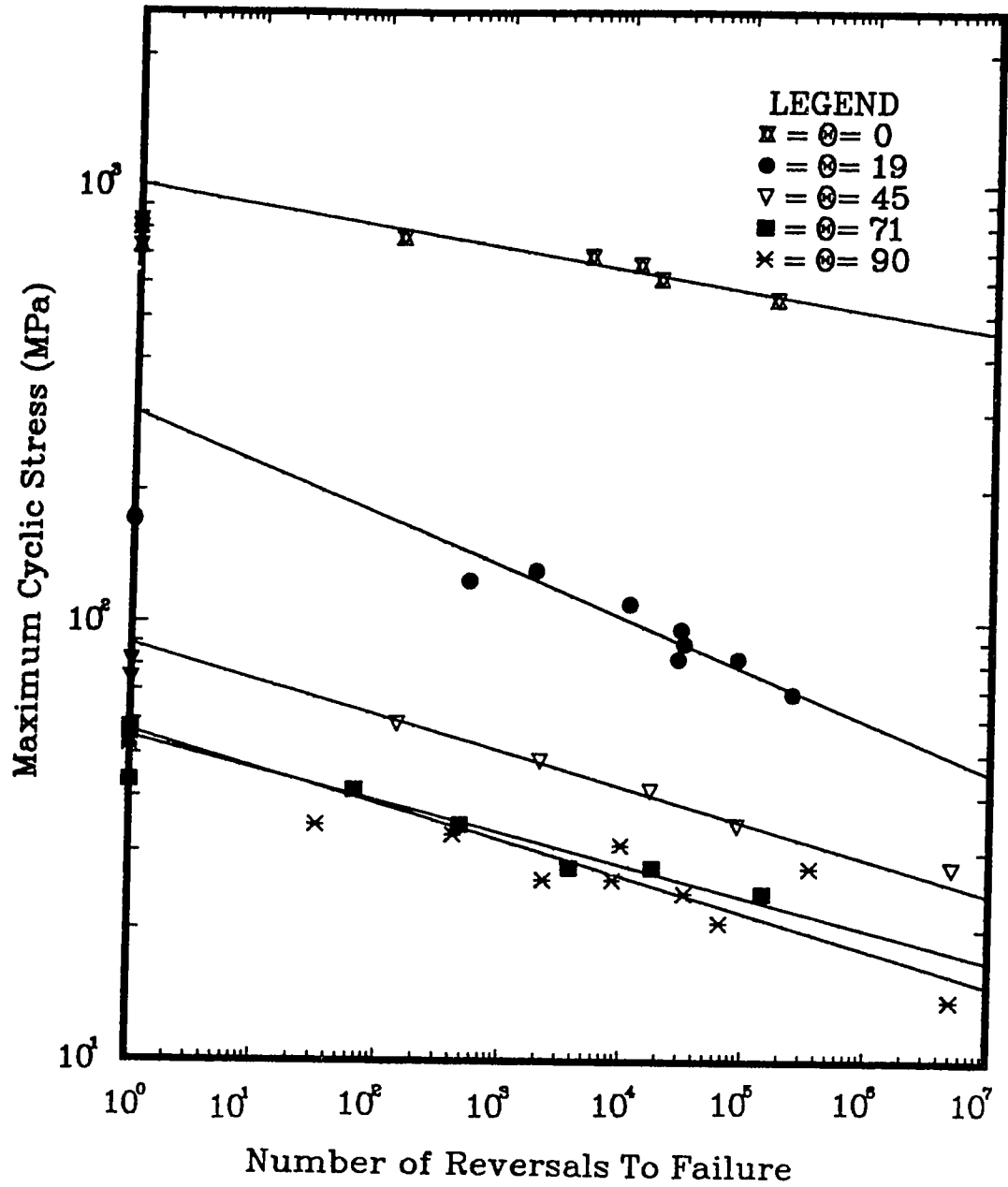


Figure A.19: Maximum Cyclic Stress vs. Number of Reversals to failure for Specimens with Different Fiber Orientation Angles at $R = 0$

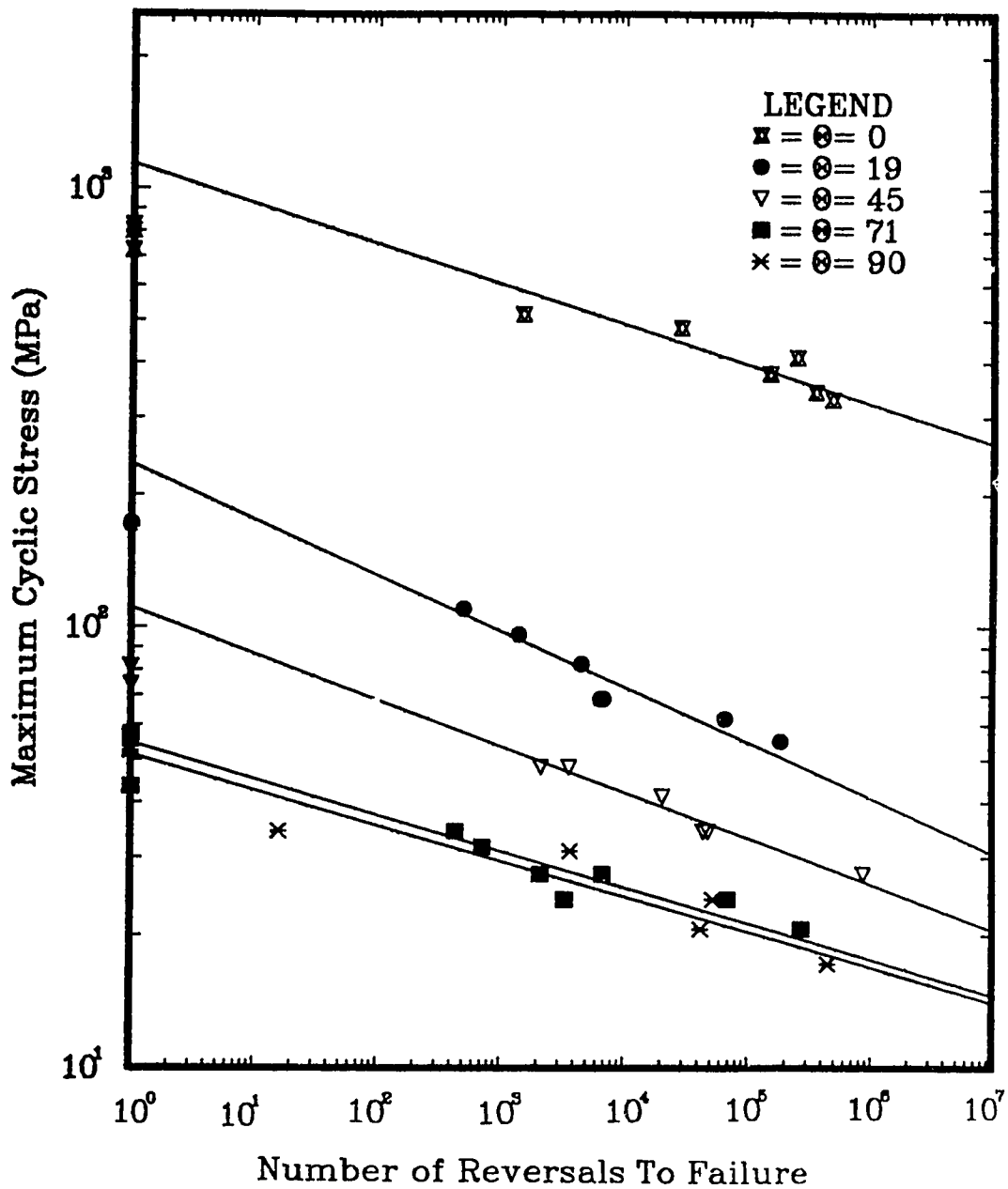


Figure A.20: Maximum Cyclic Stress vs. Number of Reversals to failure for Specimens with Different Fiber Orientation Angles at $R = -1$

Appendix B

Experimental Data

This appendix contains the experimental results obtained from the cyclic testing of laminae with different fiber orientation angles under various values of the stress ratio:

Table B.1: Uniaxial Fatigue Results for 0° Specimens at $R = 0.5$

Specimen Number	Frequency [CPM]	Stress (Maximum/Minimum) [MPa]	Cycles to Failure	Failure Mode
R05DG001	200	689.66/344.83	605	Fiber Breakage
R05DG002	200	620.70/310.35	12,018	Delamination
R05DG003	200	758.63/379.31	281	Delamination
R05DG004	200	586.21/293.11	46,939	Delamination

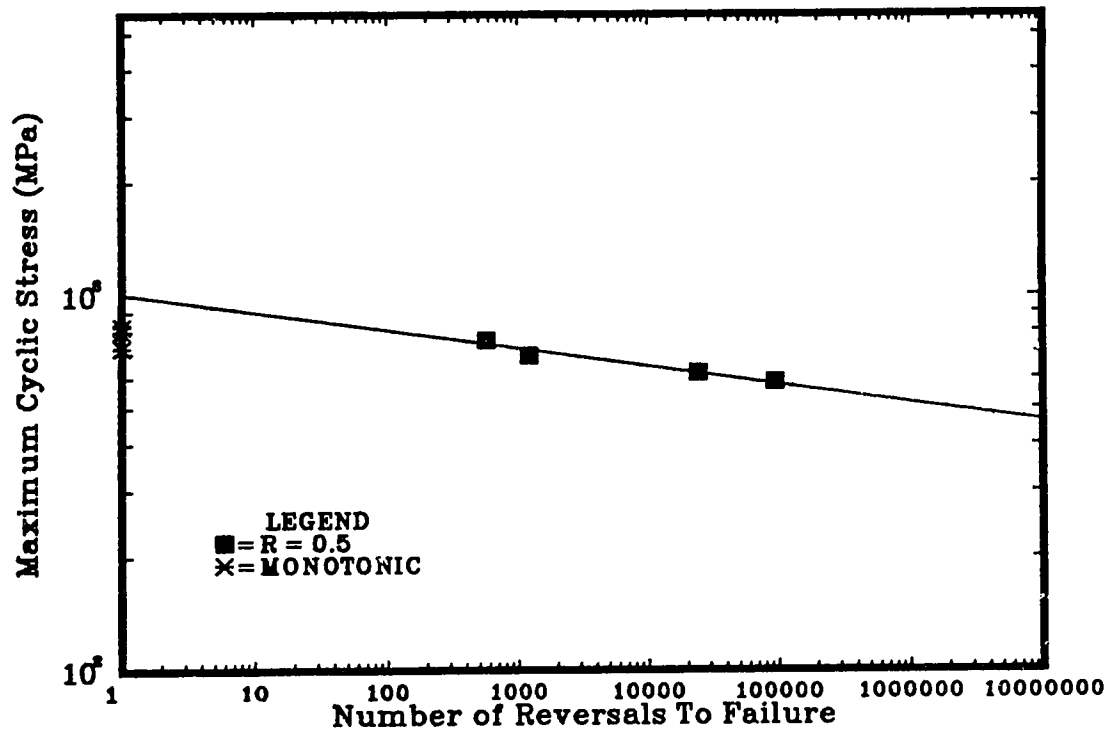


Figure B.1: Maximum Applied Stress vs. Number of Reversals to Failure for 0° Specimens at $R = 0.5$

Table B.2: Uniaxial Fatigue Results for 0° Specimens at $R = 0$

Specimen Number	Frequency [CPM]	Stress (Maximum/Minimum) [MPa]	Cycles to Failure	Failure Location
R0DG001	200	551.73/0	80,956	Delamination
R0DG002	200	613.80/0	8,964	Delamination
R0DG003	200	662.07/0	5,969	Delamination
R0DG004	200	689.66/0	2,372	Delamination
R0DG005	200	758.63/0	68	Fiber Breakage

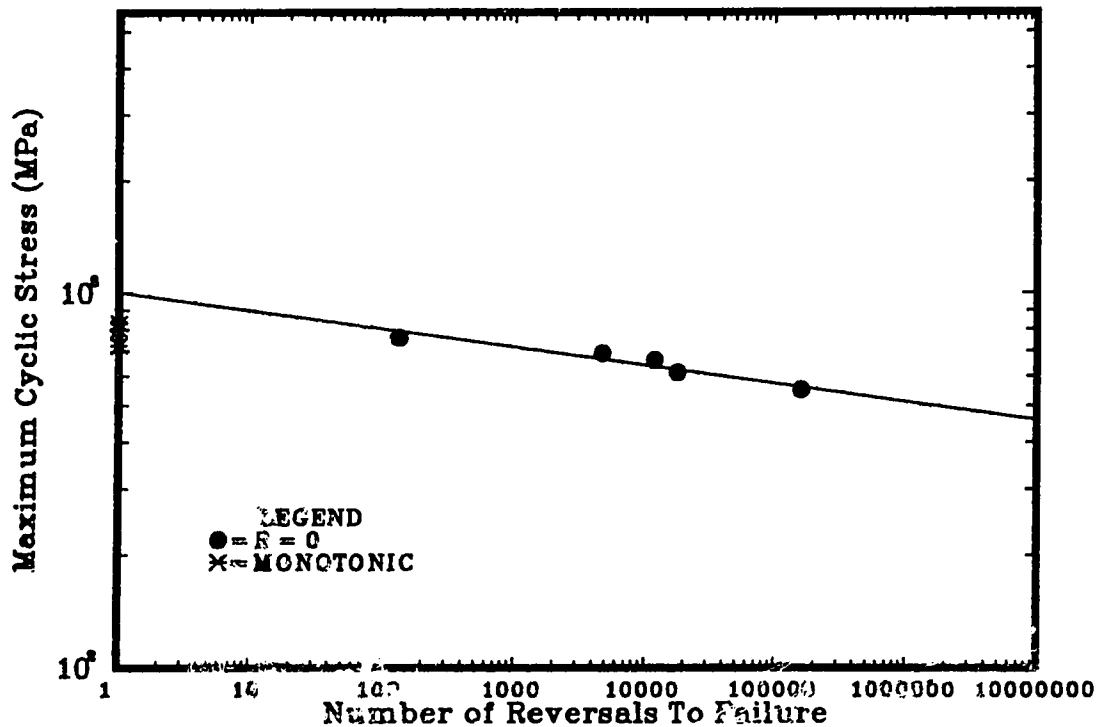


Figure B.2: Maximum Applied Stress vs. Number of Reversals to Failure for 0° Specimens at $R = 0$

Table B.3: Uniaxial Fatigue Results for 0° Specimens at $R = -1$

Specimen Number	Frequency [CPM]	Stress (Maximum/Minimum) [MPa]	Cycles to Failure	Failure Location
R-1DG001	200	344.83/-344.83	176,697	Delamination
R-1DG002	200	413.80/-413.80	125,000	Delamination
R-1DG003	200	482.76/-482.76	14,304	Delamination
R-1DG004	200	379.31/-379.31	75,000	Delamination
R-1DG005	200	517.25/-517.25	753	Buckling
R-1DG006	200	331.04/-331.04	240,451	Delamination

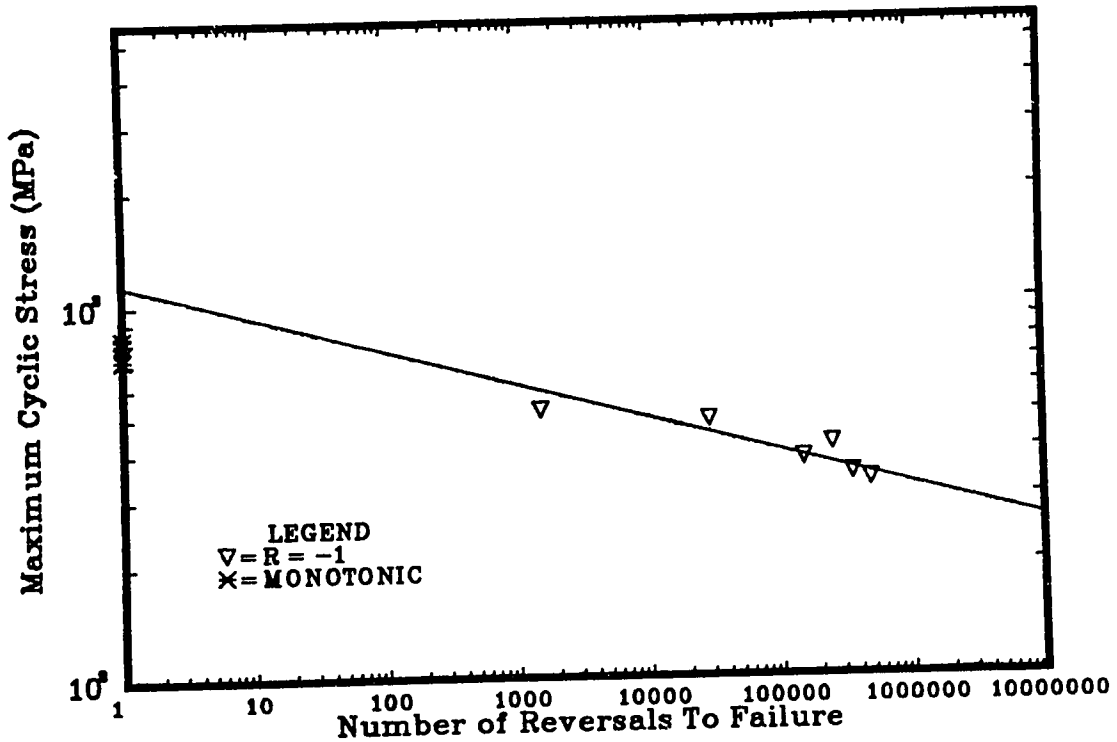


Figure B.3: Maximum Applied Stress vs. Number of Reversals to Failure for 0° Specimens at $R = -1$

Table B.4: Uniaxial Fatigue Results for 19° Specimens at $R = 0.5$

Specimen Number	Frequency [CPM]	Stress (Maximum/Minimum) [MPa]	Cycles to Failure	Failure Location
R05DG191	200	124.14/62.07	53,650	Partially Under Tab
R05DG192	200	137.93/68.97	26,978	Middle of Specimen
R05DG193	200	151.73/75.86	90	Middle of Specimen
R05DG194	200	144.83/72.41	5,209	Partially Under Tab
R05DG195	200	131.04/65.52	17,041	Partially Under Tab

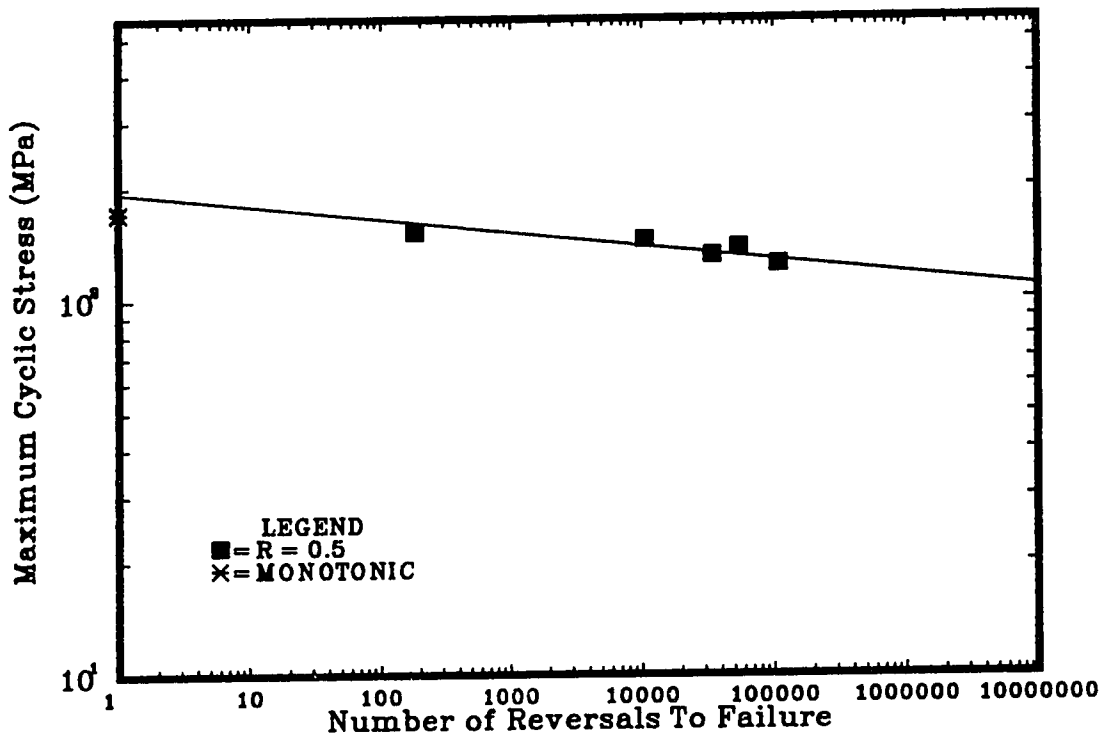
Figure B.4: Maximum Applied Stress vs. Number of Reversals to Failure for 19° Specimens at $R = 0.5$

Table B.5: Uniaxial Fatigue Results for 19° Specimens at $R = 0$

Specimen Number	Frequency [CPM]	Stress (Maximum/Minimum) [MPa]	Cycles to Failure	Failure Location
R0DG191	200	124.14/0	259	Partially Under Tab
R0DG192	200	110.35/0	5,469	Partially Under Tab
R0DG193	200	96.55/0	549	Inside Tab
R0DG194	200	96.55/0	14,710	Partially Under Tab
R0DG195	200	89.66/0	15,600	Middle of Specimen
R0DG196	200	82.76/0	14,906	Middle of Specimen
R0DG197	200	82.76/0	43,353	Partially Under Tab
R0DG198	200	131.04/0	907	Partially Under Tab

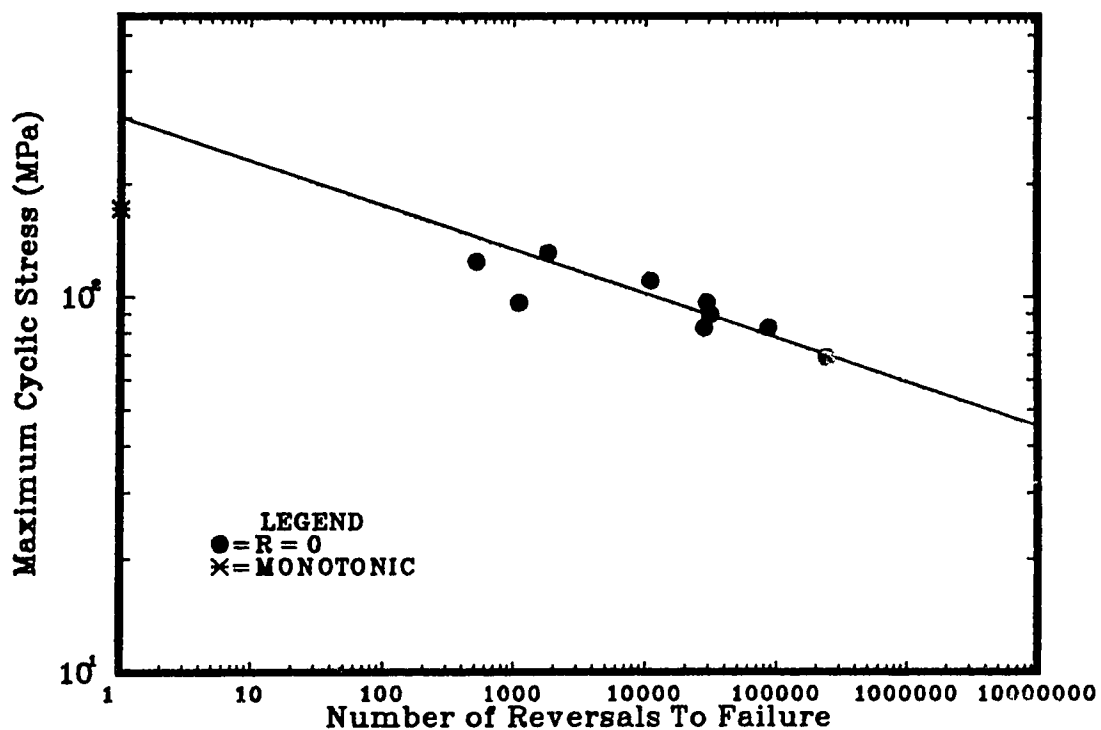
Figure B.5: Maximum Applied Stress vs. Number of Reversals to Failure for 19° Specimens at $R = 0$

Table B.6: Uniaxial Fatigue Results for 19° Specimens at $R = -1$

Specimen Number	Frequency [CPM]	Stress (Maximum/Minimum) [MPa]	Cycles to Failure	Failure Location
R-1DG191	200	110.35/-110.35	252	Partially Under Tab
R-1DG192	200	96.55/-96.55	713	Middle of Specimen
R-1DG193	200	82.76/-82.76	2,287	Partially Under Tab
R-1DG194	200	68.97/-68.97	3,257	Inside Tab
R-1DG195	200	68.97/-68.97	3,450	Middle of Specimen
R-1DG196	200	62.07/-62.07	32,860	Middle of Specimen
R-1DG197	200	55.17/-55.17	92,582	Middle of Specimen

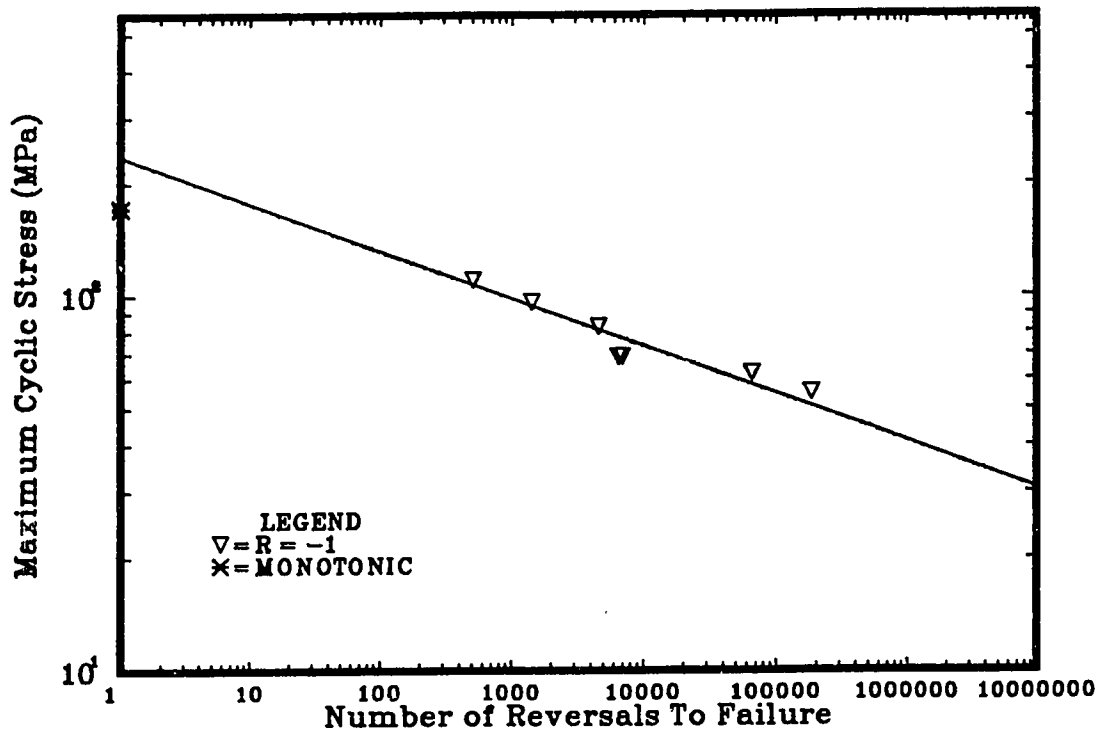
Figure B.6: Maximum Applied Stress vs. Number of Reversals to Failure for 19° Specimens at $R = -1$

Table B.7: Uniaxial Fatigue Results for 45° Specimens at $R = 0.5$

Specimen Number	Frequency [CPM]	Stress (Maximum/Minimum) [MPa]	Cycles to Failure	Failure Location
R05DG451	120	41.38/20.69	849,720	Middle of Specimen
R05DG452	200	55.17/27.59	2,256	Near Tab
R05DG453	120	55.17/27.59	940	Middle of Specimen
R05DG454	200	48.28/24.14	25,622	Near Tab
R05DG455	200	58.62/4250	1,313	Middle of Specimen
R05DG456	200	62.07/31.04	942	Near Tab

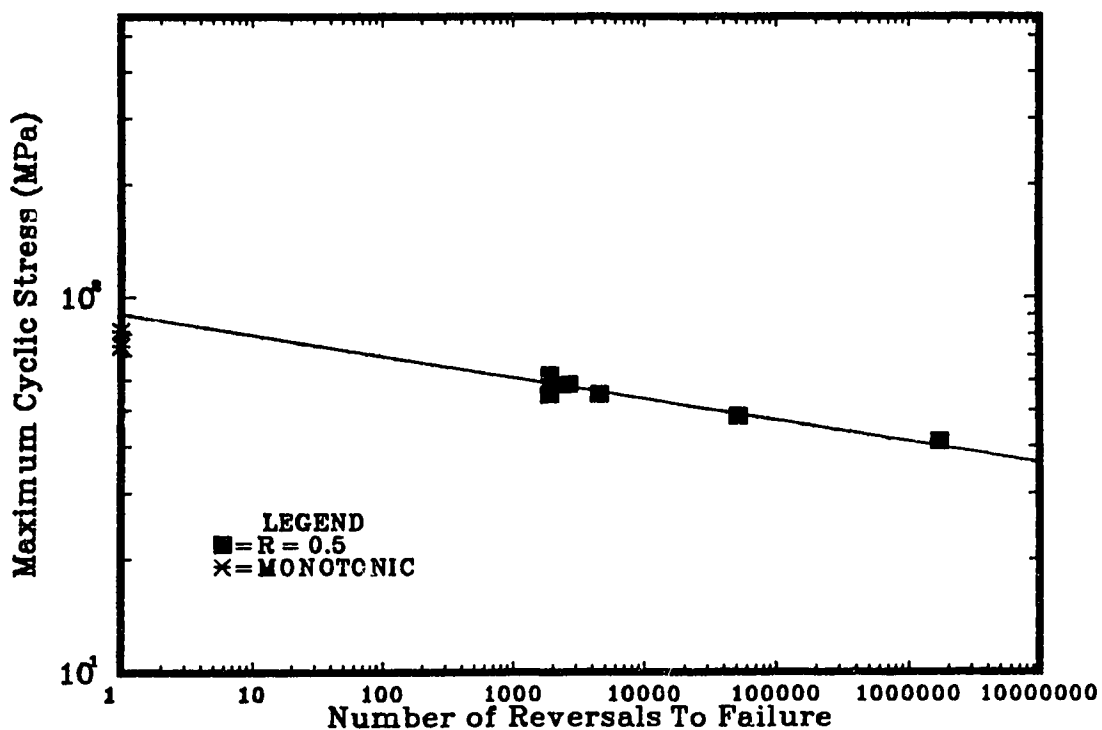
Figure B.7: Maximum Applied Stress vs. Number of Reversals to Failure for 45° Specimens at $R = 0.5$

Table B.8: Uniaxial Fatigue Results for 45° Specimens at $R = 0$

Specimen Number	Frequency [CPM]	Stress (Maximum/Minimum) [MPa]	Cycles to Failure	Failure Location
R0DG451	200	48.28/0	1,910	Near Tab
R0DG452	200	41.38/0	8,420	Near Tab
R0DG453	200	34.48/0	44,040	Near Tab
R0DG454	200	27.59/0	2,500,000	NO FAILURE
R0DG455	200	58.62/0	70	Middle of Specimen

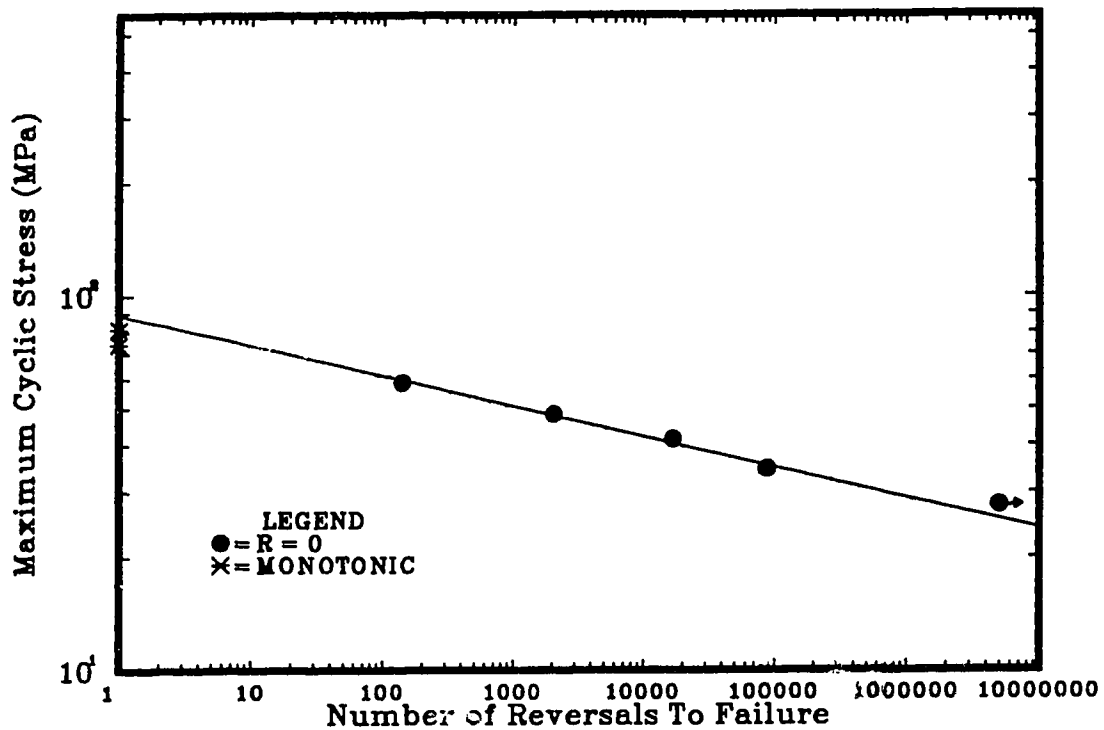
Figure B.8: Maximum Applied Stress vs. Number of Reversals to Failure for 45° Specimens at $R = 0$

Table B.9: Uniaxial Fatigue Results for 45° Specimens at $R = -1$

Specimen Number	Frequency [CPM]	Stress (Maximum/Minimum) [MPa]	Cycles to Failure	Failure Location
R-1DG451	120	48.28/-48.28	1,826	Middle of Specimen
R-1DG452	120	48.28/-48.28	1,073	Near Tab
R-1DG453	120	41.38/-41.38	10,300	Near Tab
R-1DG454	120	34.48/-34.48	22,200	Near Tab
R-1DG455	216	34.48/-34.48	24,170	Middle of Specimen
R-1DG456	200	27.59/-27.59	433,290	Near Tab

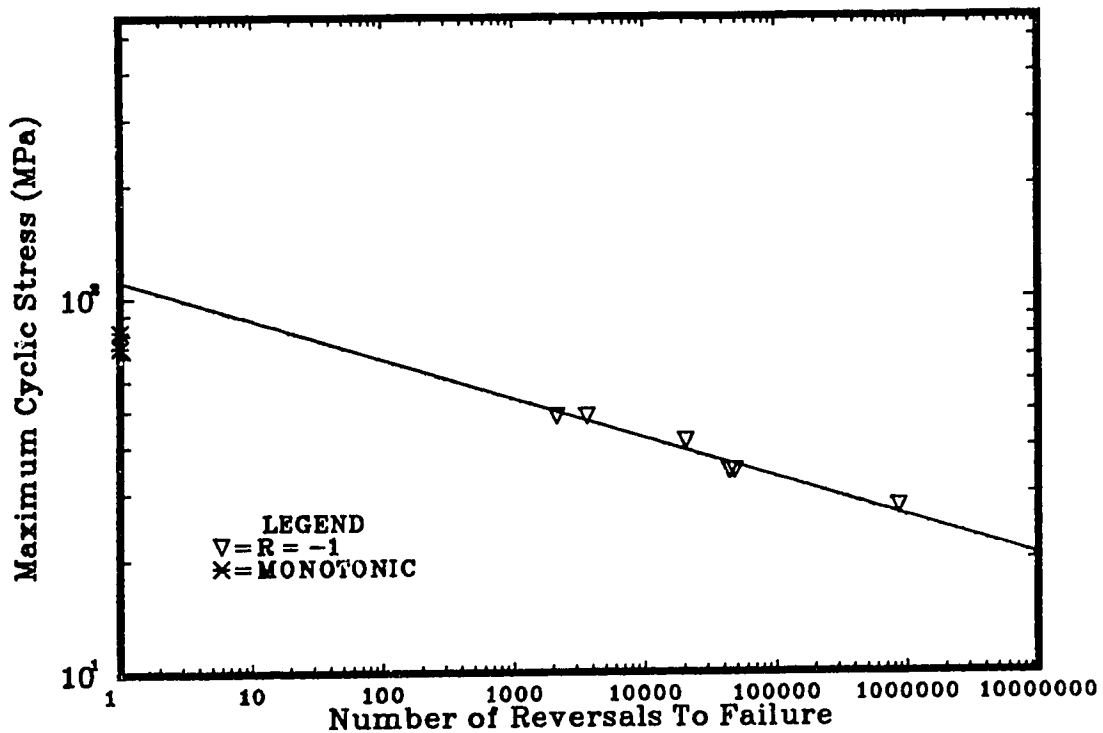
Figure B.9: Maximum Applied Stress vs. Number of Reversals to Failure for 45° Specimens at $R = -1$

Table B.10: Uniaxial Fatigue Results for 71° Specimens at $R = 0.5$

Specimen Number	Frequency [CPM]	Stress (Maximum/Minimum) [MPa]	Cycles to Failure	Failure Location
R05DG711	200	34.48/17.24	1,638	Middle of Specimen
R05DG712	200	31.04/15.52	2,500,000	NO FAILURE
R05DG713	200	41.38/20.69	50	Near Tab
R05DG714	200	37.93/18.97	4,218	Near Tab
R05DG715	200	34.48/17.24	645,846	Near Tab
R05DG716	200	36.21/18.10	50,265	Inside Tab
R05DG717	200	41.38/20.69	137	Middle of Specimen

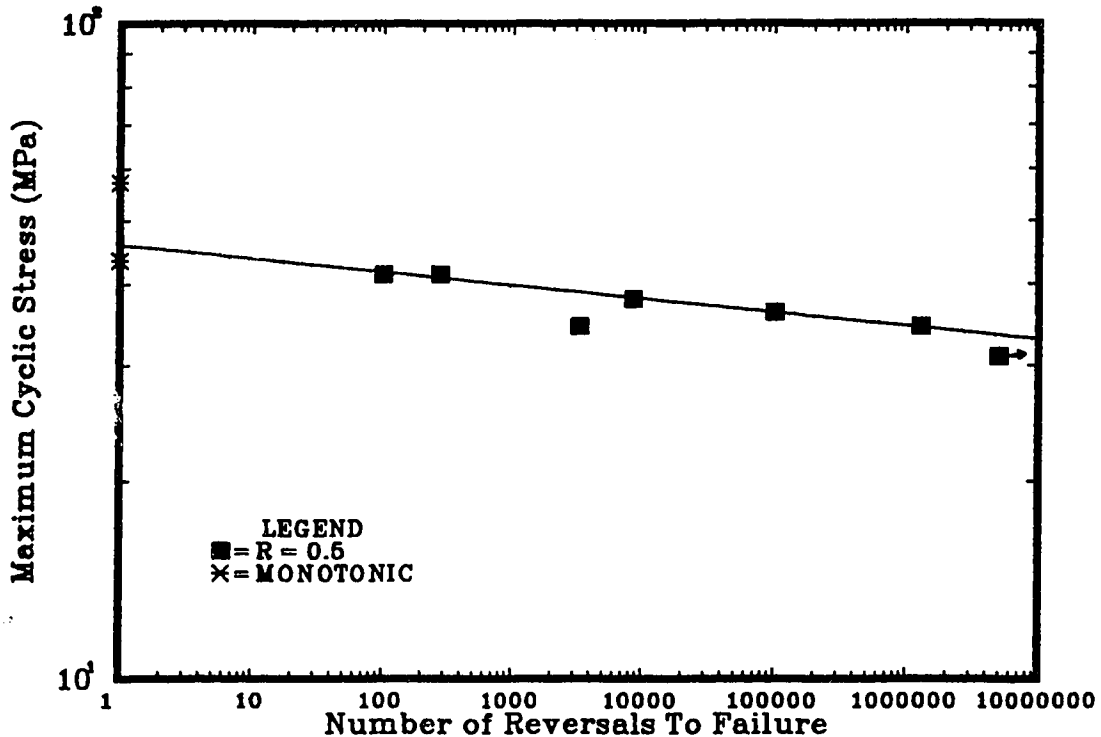
Figure B.10: Maximum Applied Stress vs. Number of Reversals to Failure for 71° Specimens at $R = 0.5$

Table B.11: Uniaxial Fatigue Results for 71° Specimens at $R = 0$

Specimen Number	Frequency [CPM]	Stress (Maximum/Minimum) [MPa]	Cycles to Failure	Failure Location
R0DG711	200	27.59/0	1,844	Middle of Specimen
R0DG712	200	41.38/0	32	Near Tab
R0DG713	200	34.48/0	231	Near Tab
R0DG714	200	27.59/0	8,863	Inside Tab
R0DG715	200	24.14/0	72,298	Near Tab

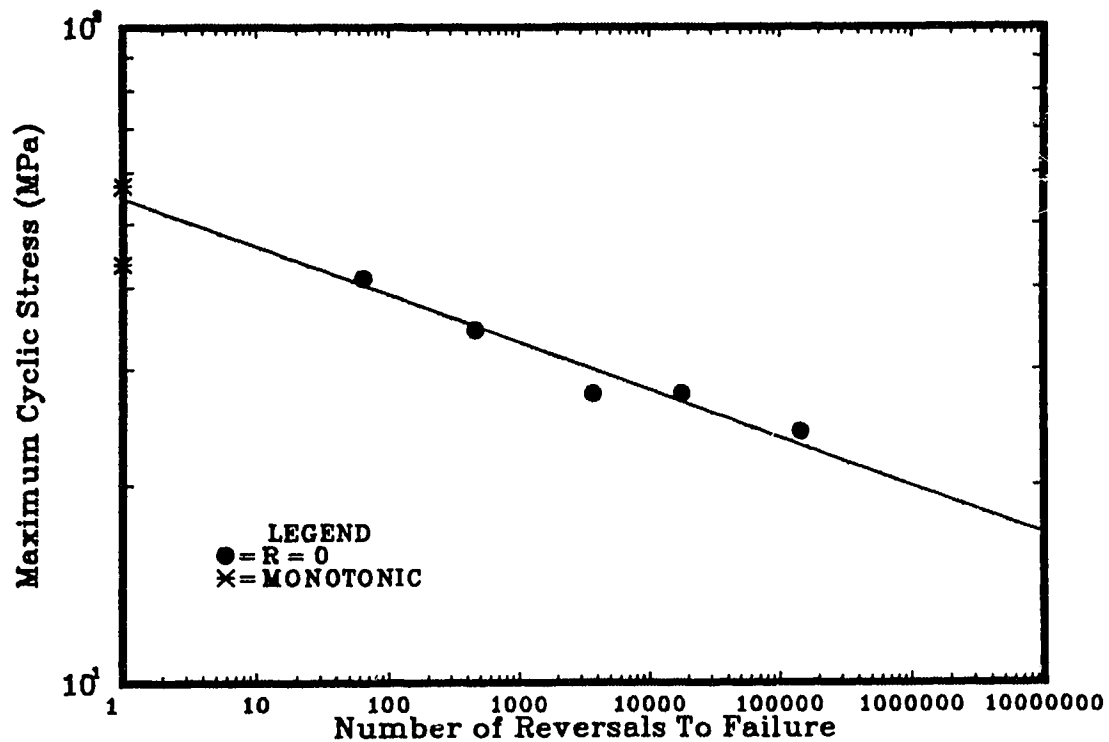
Figure B.11: Maximum Applied Stress vs. Number of Reversals to Failure for 71° Specimens at $R = 0$

Table B.12: Uniaxial Fatigue Results for 71° Specimens at $R = -1$

Specimen Number	Frequency [CPM]	Stress (Maximum/Minimum) [MPa]	Cycles to Failure	Failure Location
R-1DG711	200	31.72/-31.72	361	Middle of Specimen
R-1DG712	200	27.59/-27.59	1,069	Middle of Specimen
R-1DG713	200	24.14/-24.14	1,680	Middle of Specimen
R-1DG714	200	20.69/-20.69	130,490	Inside Tab
R-1DG715	200	24.14/-24.14	34,154	Middle of Specimen
R-1DG716	200	27.59/-27.59	3,368	Middle of Specimen
R-1DG717	200	34.48/-34.48	216	Middle of Specimen

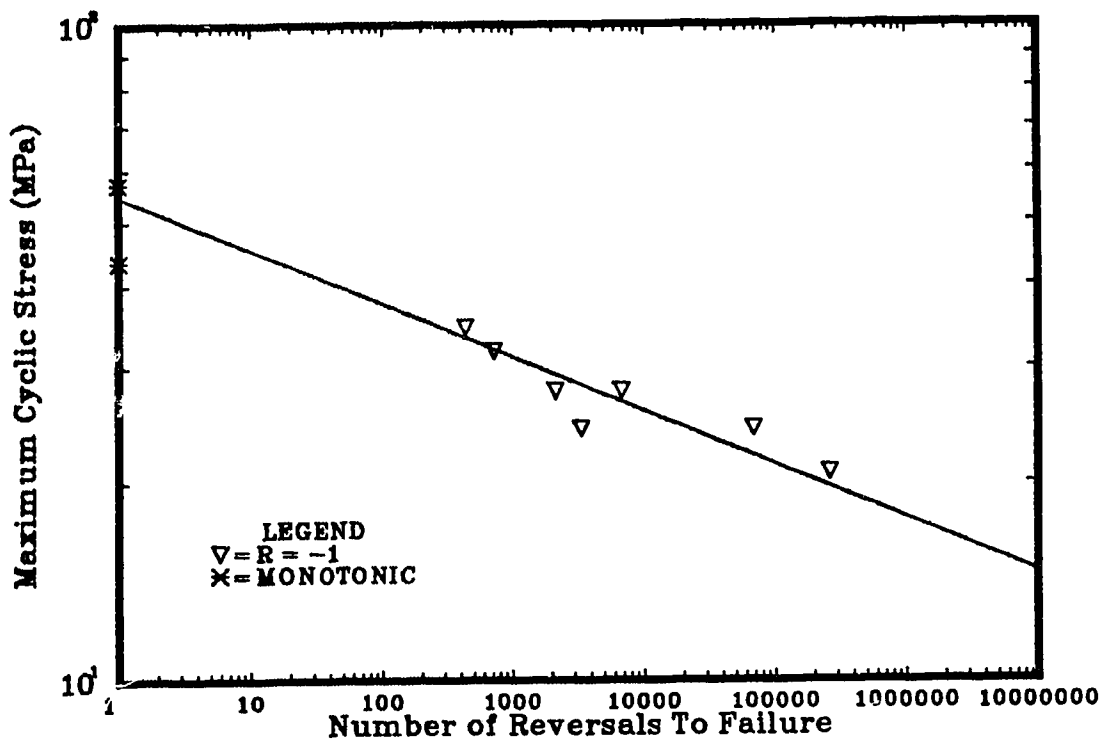
Figure B.12: Maximum Applied Stress vs. Number of Reversals to Failure for 71° Specimens at $R = -1$

Table B.13: Uniaxial Fatigue Results for 90° Specimens at $R = 0.5$

Specimen Number	Frequency [CPM]	Stress (Maximum/Minimum) [MPa]	Cycles to Failure	Failure Location
R05DG901	200	31.04/15.52	155,245	Middle of Specimen
R05DG902	200	41.38/20.69	22	Middle of Specimen
R05DG903	200	36.21/18.10	21,804	Near Tab
R05DG904	200	37.93/18.97	706	Near Tab

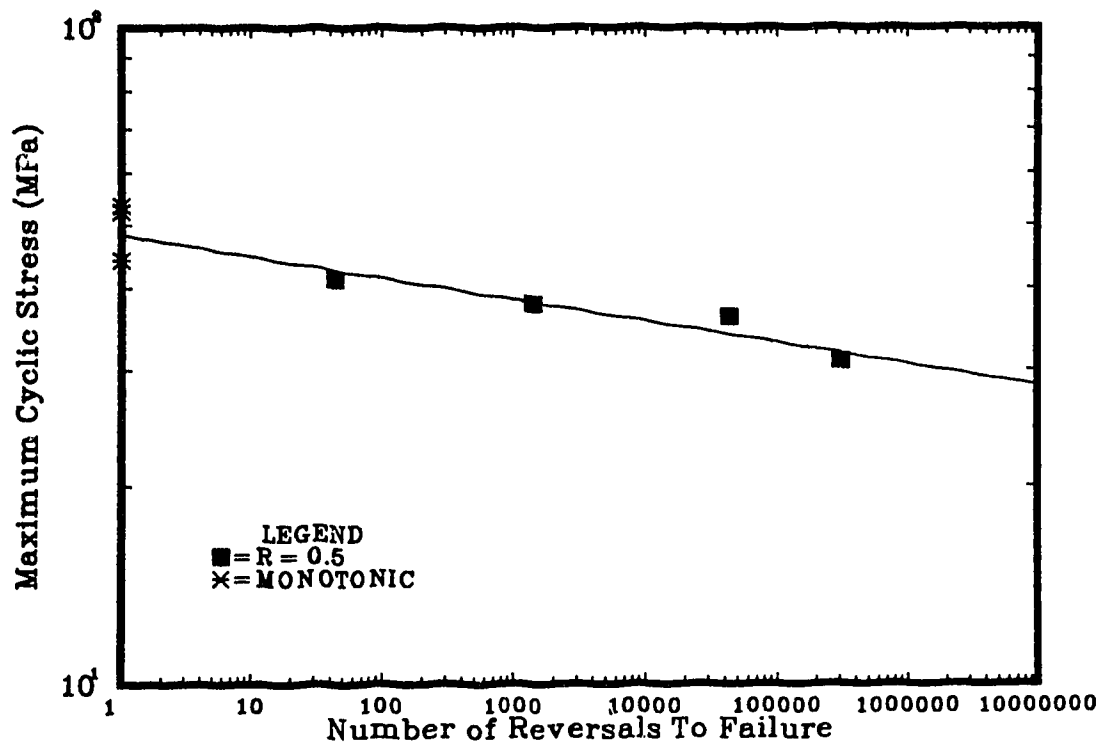


Figure B.13: Maximum Applied Stress vs. Number of Reversals to Failure for 90° Specimens at $R = 0.5$

Table B.14: Uniaxial Fatigue Results for 90° Specimens at $R = 0$

Specimen Number	Frequency [CPM]	Stress (Maximum/Minimum) [MPa]	Cycles to Failure	Failure Location
R0DG901	200	31.04/0	4,954	Near Tab
R0DG902	200	24.14/0	16,677	Near Tab
R0DG903	200	20.69/0	32,500	Middle of Specimen
R0DG904	200	13.79/0	2,500,000	NO FAILURE
R0DG905	200	34.48/0	16	Middle of Specimen
R0DG906	200	37.76/0	206	Near Tab
R0DG907	200	27.59/0	174,966	Near Tab
R0DG908	200	25.86/0	1,140	Middle of Specimen
R0DG909	200	25.86/0	4,265	Middle of Specimen

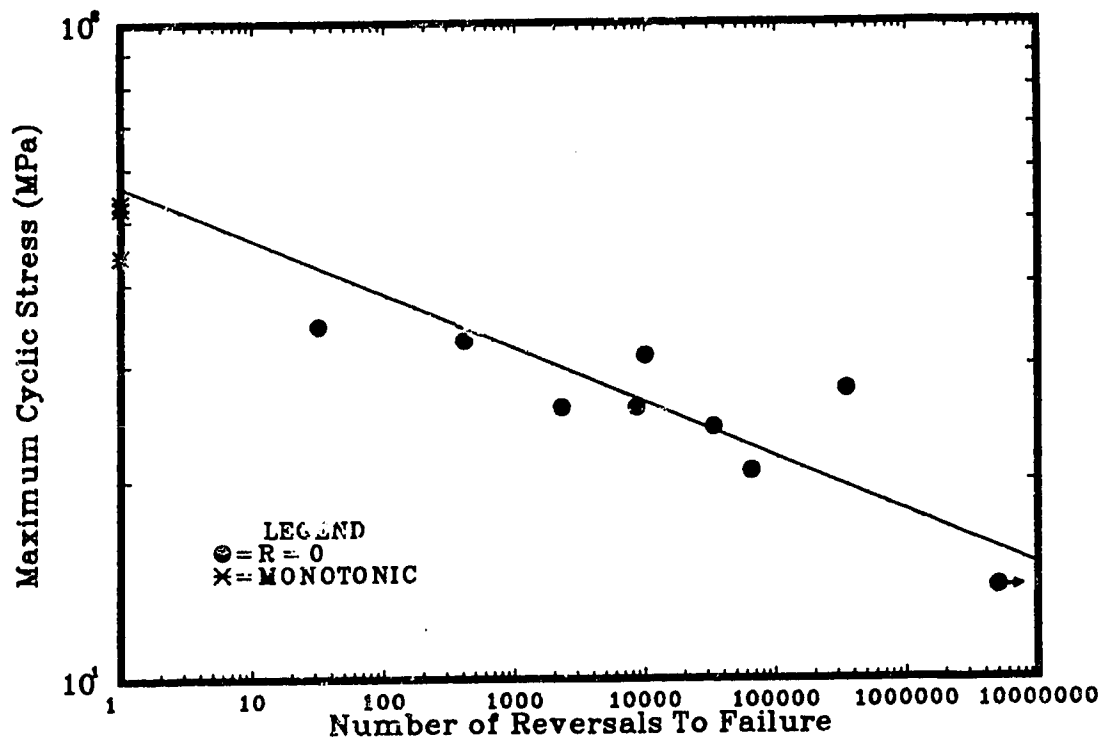
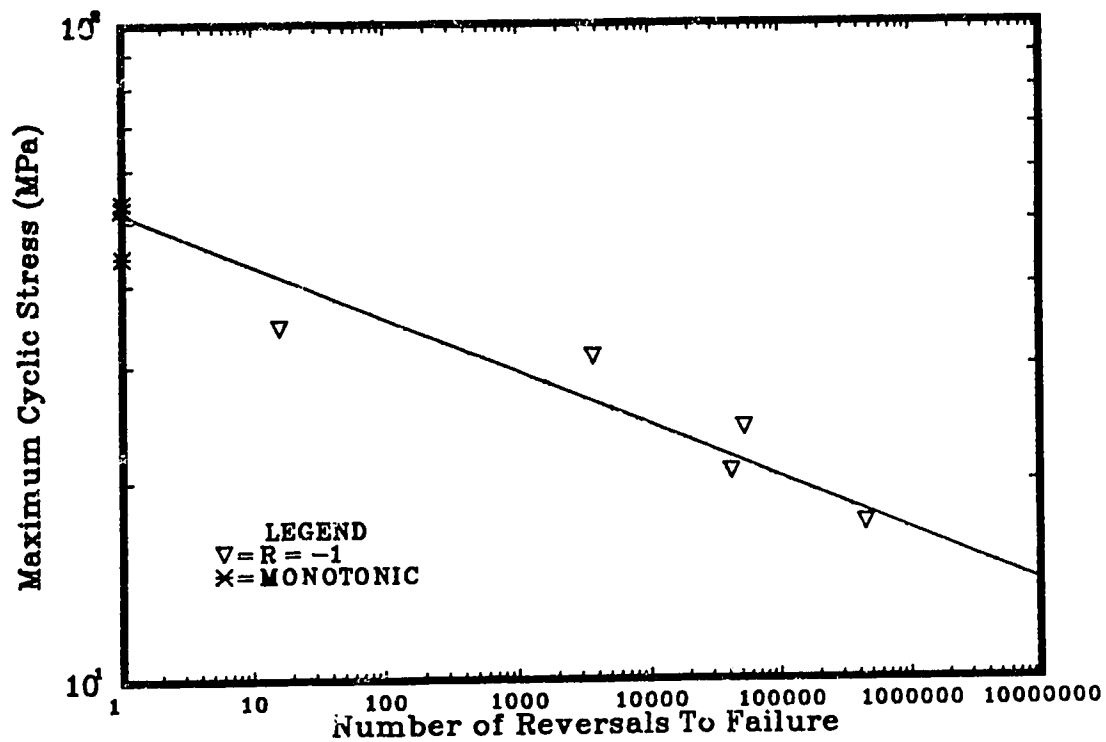
Figure B.14: Maximum Applied Stress vs. Number of Reversals to Failure for 90° Specimens at $R = 0$

Table B.15: Uniaxial Fatigue Results for 90° Specimens at $R = -1$

Specimen Number	Frequency [CPM]	Stress (Maximum/Minimum) [MPa]	Cycles to Failure	Failure Location
R-1DG901	200	31.04/-31.04	1,867	Middle of Specimen
R-1DG902	200	24.14/-24.14	26,448	Middle of Specimen
R-1DG903	200	20.69/-20.69	21,070	Near Tab
R-1DG904	200	17.24/-17.24	225,000	Near Tab
R-1DG905	200	34.43/-34.48	8	Near Tab

Figure B.15: Maximum Applied Stress vs. Number of Reversals to Failure for 90° Specimens at $R = -1$